Project Puente Rio Bio

NUEVO FERROVIARIO RIO BIOBÍO

Hydraulic and structural study for the new railway bridge to investigate the influence of river morphodynamics and tsunami impact on the structural stability of the bridge pier

PPRB
Project Puente Rio Bio

Disclaimer

Nuevo Ferroviario Rio Biobío

Hydraulic and structural study for the new railway bridge to investigate the influence of river morphodynamics and tsunami impact on the structural stability of the bridge pier

by

T. van der Voort (4288017)
T. Vrinds (4298608)
F.W. Wellen (4310241)
S. Winkel (4300165)

For the course CIE4061-09 Multidisciplinary Project,
Civil Engineering Consultancy Project,
at the Delft University of Technology

Date:	September 17, 2019
Project duration:	29th of April 2019 - 28st of June 2019
Website	www.pprb.nl

Faculty of Civil Engineering and Geosciences,
Delft University of Technology

Facultad de ingenieria,
Universidad Católica de la Santísima Concepción

Team

Civil Engineering: Msc. Hydraulic Engineering

Tjalie van der Voort
MSc. Civil Engineering
Tracks: Ports, River & Dredging Engineering

Fleur Wellen
MSc. Civil Engineering
Tracks: Coastal Engineering & Environmental Fluid Mechanics
Annotation: IDM, Integral Design Management

Sander Winkel
MSc. Civil Engineering
Tracks: Coastal, Dredging & River Engineering
Annotation: IDM, Integral Design Management

Civil Engineering: Msc. Structural Engineering

Thijs Vrinds
MSc. Civil Engineering
Track: Hydraulic Structures
Annotation: IDM, Integral Design Management

Supervisors

Delft University of Technology

Ir. Tjerk Zitman
Assistant Professor of Coastal and Hydraulic Engineering
T.J.Zitman@tudelft.nl

Ir. Sander Pasterkamp
Lecturer of Materials, Mechanics, Management and Design
S.Pasterkamp@tudelft.nl

Dr. Ir. Sander van Nederveen
Assistant Professor of Integral Design and Management
G.A.vanNederveen@tudelft.nl

UCSC, Universidad Católica de la Santísima Concepción

Dr. Diego Caamaño Avendaño
River Engineering
dcaamano@ucsc.cl

Dr. Rafael Aránguiz Muñoz
Coastal Engineering
raranguiz@ucsc.cl

Claudio Oyarzo Vera
Structural Engineering
coyarzov@ucsc.cl

Partners

Main Partners

Count & Cooper

Delft Deltas, Infrastructures & Mobility Initiative (DIMI)

TMF Mechanical Parts & Assemblies

Tessa Driessen Graphical Design and Critical Research

Knowledge Partners

TU Delft

Deltares

UCSC

Preface

This report is part of the Master Programme of the Delft, University of Technology. The Civil Engineering Consultancy Project is an elective course to broaden the expertise of the technical students. Our team consists of four students: three students following the Master track Hydraulic Engineering and one student following the Master track Structural Engineering. Our multi-disciplinary group has been given the opportunity to investigate the river morphodynamic and tsunami impact on bridge pillars of a new railway bridge, which is to be constructed in the Biobío River, Concepción, Chile. For nine weeks we have been guests of the UCSC, Universidad Católica de la Santísima Concepción in Chile, and have been working on this technical report, two hydraulic models and a preliminary bridge design.

This technical report is written mainly for engineers whom are interested in the morphological development of the Biobío river or interested in the design of the railway bridge. Conclusively, this report supplies more insight regarding the Biobío river system, the morphodynamic development of the river and the inherent connection between the hydraulic study and a structural design for the railway bridge.

Readers interested in the integral design part of the PPRB Project are advised to read chapters 2, 3, 4, 8, 9, 10 and 11. Parts for more hydraulic oriented readers are to be found in chapters 4, 5, 6 and 7, introducing the concept of river and tsunami modelling. Chapters concerning the structural aspects of the project are 8 and 11. Chapters including Integral Design Management aspects are 2, 3 and 11. Most figures are created by team members in ArcGIS, contributing to the integral design approach. The conclusion and recommendation of the project can be found in 12 and 14 respectively.

Many people have contributed either directly or indirectly to this project. First of all, we would like to thank our supervisors: Tjerk Zitman, Sander Pasterkamp and Sander van Nederveen for all their support. During our weekly updates, their quick answers were really welcoming and helpful. Secondly we would like to thank our Chilean supervisors. Firstly, Diego Caamaño, the river expert and excellent cook (salt bae), for his tips and tricks while setting up the Delft3D model and having the patience to answer all our questions. Secondly, Rafael Aránguiz, the tsunami expert, for introducing tsunami dynamics and NeoWave modelling to us and showing the importance of earthquake and tsunami knowledge. Thirdly, Claudio Oyarzo, for providing us with the necessary Chilean Building Codes and giving guidelines on how to apply these in the preliminary bridge design. We would also like to thank the entire UCSC crew for their welcoming attitude and their hospitality. Making us feel at home by providing office space (with heater!) and inviting us for a very nice Chilean BBQ. The help of Emiel Moerman and Kees Sloff from Deltares in the form of consultations via email was indispensable. Thank you both for answering our numerical Delft3D questions and showing us ways to work around inevitable errors (which we have learnt to accept). We would like to thank Dirk van Uffelen for coming all the way to Chile to give us a very helpful training about teamwork and leadership, this was truly inspirational. Another huge thank you to all our sponsors: DIMI, Count & Cooper, Deltares, TMF Mechanical Parts & Assemblies, Tessa Driessen and STIR. Without their help this Chilean adventure would not have been possible.

Tjalie van der Voort
Sander Winkel
Fleur Wellen
Thijs Vrinds
Concepción, Chile, June 2019

Table of Contents

Abstract

In Chile, the Biobío river separates the cities of Concepción and San Pedro de la Paz. Bridges crossing the Biobío river ensure a fast and dependable connection, which contributes to the transport options in the region. With the Biobío region being the second largest contributor to the country's GDP, an unreliable transport network is highly undesirable. However, this is exactly what happened since 2016. Some of the bridges crossing the river collapsed, excessive local pier scour near the foundation and negative effects of morphological dynamics were deemed to be one of the causes. Furthermore, Chile is prone to earthquakes and the resulting tsunamis, which can also damage the structural integrity of the bridge.

The Chilean Railroad Agency (EFE) wants to realise a new railroad bridge crossing the Biobío river in Concepción, replacing the existing century old railway bridge. To prevent the failure of the new railway bridge, which can result in unnecessary economic damages, the morphological influence and damages due to scour, earthquakes and tsunamis, must be thoroughly understood and modelled. This process of modelling the current and future situations of the Biobío river is part of this project, using Delft3D-FLOW and NeoWave as modelling agents. With the outcomes the programme of requirements and the preliminary design for the bridge are updated and presented.

Following the regional analysis, considering the Biobío river and its surroundings, it is found that the Biobío river is prone to changes and is therefore not in an equilibrium state. With a developing river bar on the inner southern band, the flow is constricted to the northern bank of the river. The recent growth of vegetation on the river bar decreases the erodability of the bar during a flood wave. Tidal analysis shows no skewness or asymmetry, making discharge the main cause of sediment transport. The location of the new railway bridge is sufficiently far from the river mouth to ignore wave and salinity effects. The results of the physical analysis are used as input parameters for the Delft3D-FLOW and Neowave Model. The Delft3D model is used to simulate hydro- and morphodynamics. Results of the 10 year period simulation, using the effective discharge as upstream boundary, show the bed level of the Biobío river changes significantly over time. Most changes occur during the first period, governing 5 years. Furthermore, it was observed that the location and dimensions of the main eroded channel do display the same variability as the Biobío river. However, due to simplifications in the Delft3D model and the natural variability, the precise locations and dimensions of different channels cannot be predicted. The EFE uses the 100 year return period of the discharge with a flow velocity of 2.5 m/s for their design. By running the short term simulation, using the same 100 year return period discharge, in the Delft3D model it is found that the flow velocity set by EFE, has a probability of exceedance of 48.75%. This indicates that the EFE is using a flow velocity which is too low. NeoWave is used to predict and analyse the effect of a tsunami travelling up the Biobío river. In most cases the Biobío river is protected by the submarine canyon situated in front of the river mouth, mostly due to the horizontal dimensions of the canyon and in lesser extent to the depth. Simulating a tsunami, resulting from an earthquake of M_W 9.0 forming at the most unfavourable location and therefore omitting the effect of the submarine canyon, in NeoWave results in a water level increase of 3.5 metres at the location of the new bridge. therefore it can be concluded that the effect of a tsunami should be accounted for in the bridge design.

The outcomes of the different analyses are implemented in the programme of requirements. These provide, next to the requirements, wishes and prerequisites, useful input and ensure the link between the hydraulic and structural aspect of the river and bridge design respectively. The programme of requirements is used to draw up different alternatives for the beam bridge design by EFE. These variants include an alternative beam, bowstring arch, suspension, truss with arch and cable-stayed bridge. Performing a multi-criteria analysis results in a new preferred design: the alternative beam bridge. This is an adaptation of the Hollandsch Diep bridge. This alternative scores highest due to its reduced amount of columns, leading to a better hydraulic performance, and the cost-effectiveness of this design. Although other variants score even higher, due to the decrease in the amount of columns. However, these designs require a significant increase in investment and are therefore not the preferred alternatives.

A preliminary design, based on the normative load combination of an earthquake, wind and train loading, for 2 columns supporting the superstructure is created. The resulting forces from these loads are significantly large and thus a 3.2m by 2.5m concrete column with a reinforcement percentage of 6% is needed to provide enough resistance. The subsoil, mostly consists of sand and a mixture of sand, silt and clay, beneath the designed columns is of a relatively good quality. The considered columns are supported by 14 to 17 foundation piles to a depth varying between 18 and 21 metres, respectively, in order to provide enough bearing capacity. Additionally, deep scour holes, up to approximately 9 metres, are predicted to be formed near the foundation columns and therefore bed protection might be needed. This can be investigated in a future study.

Concluding remarks include the importance of further hydraulic research concerning the Biobío river, as, for example, the maximum flow velocity used by EFE is proved to be too low. A more detailed Delft3D model is needed to investigate the influence of other factors, which are neglected in this research and further investigate to which extend external factors, such as the sand mining companies and tsunami propagation, influence the river morphodynamics. Furthermore, the alternative beam bridge is a serious option for the EFE and should be taken into account in future designs, instead of always resorting to the current beam bridge design.

1

Introduction

1.1 Background Information

The Río Biobío, the Biobío river, is the second largest river in Chile, and is well known due to its history and geographical features. The sources of the Biobío river can be found in the Andes, Laguna Galletué, Laguna Icalma and Laguna Laja (Nordbø, 2001). After a total length of 380 kilometres the river ends in the Pacific Ocean. The average width of the river is one kilometre, making it the widest river of Chile. (Ecoronel, Observatorio ecológico de Coronel, 2019) During the Spanish conquest of Latin America, the Biobío river marked the border between the Spanish troops on the northern river bank and the Mapuche people on the southern bank. Giving the river the nickname: 'La Frontera' (EcuRed, 2019). An overview of the Biobío river and its origin is presented in figure 1.1

In the past the river was used for nautical transportation. Continued deforestation in the 20th century resulted in heavy erosion, causing the Biobío river to silt up, making the river no longer suitable for larger (transportation) vessels. The construction of the Pangue Dam, used as hydropower plant, meant the regulation of the river was a fact.

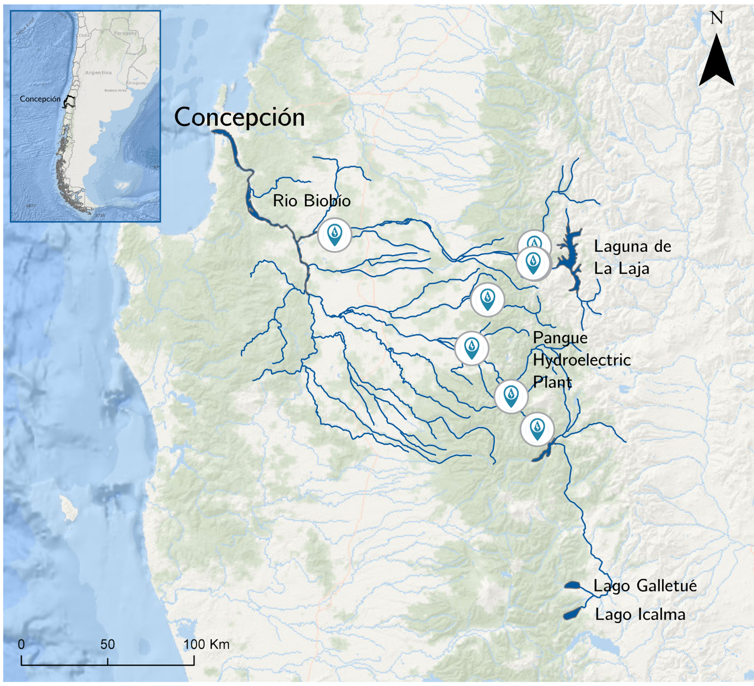

Figure 1.1: The Biobío river, its origin and its surroundings. Concepción is visible in the top left corner.

1.2 Problem Definition

Near the river mouth, the Biobío river separates the cities of Concepción and San Pedro de la Paz. Bridges crossing the Biobío river ensure a fast and dependable connection. The foundation pillars of these bridges crossing the river are prone to excessive local pier scour and effects of morphological dynamics. Furthermore, Chile is prone to earthquakes and resulting tsunamis, which can also play a role in the river morphology. The aforementioned aspects and their possible combinations can lead to different problems and the need for solutions.

Since 2016, some of the bridges crossing the Biobío river have collapsed. This caused damage to the economy and transportation routes for the inhabitants, as bridges are valuable assets in connecting Concepción with the city of San Pedro de la Paz and ensuring a train transportation to the mainland. The Chilean Railroad Agency (EFE) wants to realise a new railroad bridge crossing the river, replacing the existing railway bridge. To prevent failures of a new railway bridge, which can result in unnecessary economic damages after failure, the morphological influence and damages due to scour, earthquakes and tsunamis, must be thoroughly understood and modelled.

In association with the UCSC an analysis of the morphological changes and the effects of scour on bridge's foundations for the Biobío river is researched. The understanding of the morphology of the Biobío river is a prerequisite to prevent bridge collapses in the future by taking into account the morphology in the design of the bridge foundation, which has not been included in designs so far. The influence of the river and river bed changes are analysed with the help of a Delft3D model. The resulting data can indicate whether scour or morphological dynamics are occurring and to which degree. This information is taken into account when composing the programme of requirements for the railway bridge crossing the Biobío river. Following from the updated programme of requirements, an initial design for the bridge, with its supporting and foundation pillars, is proposed.

The above results in the following objective:

"Analyse and understand the morphological development in the Biobío river, and use the findings of the hydraulic research to update the programme of requirements for a railway bridge crossing the river. Furthermore, propose an initial design for this bridge, taking into account the effect of the morphodynamics of the Biobío river."

In order to reach the objective several tools are utilised. As a starting point, the surroundings of the Biobío river are mapped. This is done through a regional and stakeholder analysis. Data collected and obtained through these analyses are stored in a GIS (Geographical Information System) environment. This tool is utilised to increase project understanding and make data easily accessible and understandable. To investigate the morphodynamics of the river itself, a Delft3D model is created. This model is used to investigate the hydro- and morphodynamic changes of the river over time. By analysing the data from the computations performed in Delft3D, an insight in the development of the system over time can be achieved. With this insight the relevant physical processes in the Biobío river can be better understood. Furthermore, the Delft3D-suite can include river flood waves and tsunamis, which are both relevant natural disasters and their influence on the system can not be neglected. To specifically assess the influence of a tsunami on the river and thus the bridge, NeoWave is used. This model is developed for modelling long waves, such as tides and tsunamis. The accuracy of the model is within a few meters and thus a very safe estimation of forces on the bridge can be made.

With the understanding of the system, a preliminary bridge design is proposed, the design is supported with a 3D model of the bridge and is integrated into the landscape. The usage of the different tools, and the connection between these tools results in an integrated project approach. The effect this approach had on the project is evaluated at the end of the project.

1.3 Reading Guide

The report is split into four parts. Part I, Analysis, governs the regional, stakeholder and physical analysis. The information in these chapters is needed to lay a stable foundation for the rest of the project and be able to evaluate results in the future. This part includes the regional analysis, chapter 2, which describes Concepción and its surroundings. Moreover this chapter gives more hindsight of the initiation of the project. The stakeholders of the project are described and analysed in 3. Lastly, the physical analysis, chapter 4, describes the system of the Biobío river. This information is needed for the set-up of the models described in part II. This part II, Models, describes the two numerical models used to describe the river morphological changes and tsunami impact on the Biobío river. The Delft-3D FLOW model, used for the hydrodynamic and morphodynamic analysis, is described in chapter 5. The propagation of a tsunami up the Biobío river is simulated using NeoWave and described in chapter 6. Whereafter the results of both models are summarised in chapter 7. These results are used as input for the preliminary design of the new bridge, described in part III, Design. This part starts with the programme of requirements in chapter 8. With the programme of requirements as starting point, different variants are designed and presented in chapter 9. These variants are evaluated using a multi-criteria analysis, this process and its outcome is shown in chapter 10. One variant is chosen and further elaborated to create a preliminary design, summarised in chapter 11. Lastly, part IV, Conclusions, presents the conclusion, discussion and recommendations of the project.

I

Analysis

2

Regional Analysis

To be able to analyse the situation of the Biobío river correctly, it is important to understand the surrounding environment in a regional, historical, political and economical context. Additionally, to pinpoint the strategic relevance of the project, the transportation system in Chile and in Concepción must be understood.

In this chapter a regional analysis is performed. The region that is considered for this analysis is visible in the middle section of figure 2.1. The Biobío Region is one of sixteen regions in the country, thoroughly elaborated in section 2.1. The historical context is given in section 2.2. Whereafter, the political and economical aspects are discussed in section 2.3 and section 2.4 respectively. Finally, section 2.5 describes the transport and infrastructure systems in the region, leading to the aforementioned strategic relevance. Some facts and figures introducing the Biobío Region to the reader are presented in table 2.1, below.

Table 2.1: Facts and figures Biobío Region

Description	**Quantity**	**Source**
Total surface area	23,890.2 km^2	Gobierno de Chile (2019)
Population	1,557,414 inhabitants	Gobierno de Chile (2019)
Provinces in Region	3	Gobierno de Chile (2019)
Communes in Region	33	Gobierno de Chile (2019)
Regional capital	City of Concepción	Gobierno de Chile (2019)
Purchasing Power per Capita	6,887,363 CLP	Michael Bauer Research (2018)
Average temperature	13.0 °C	Climate-data.org (2019)
Average rainfall	1190 mm	Climate-data.org (2019)

2.1 Biobío Region

The country of Chile is divided into sixteen regions. Which are in turn divided into provinces, which are again subdivided into communes. The Regions are named and numbered from north to south. The Biobío Region marks the eighth region from the north, receiving the prefix VIII. The Biobío Region can be subdivided into three provinces: Arauco, Biobío and Concepción. As the name suggests, the city of Concepción is part of the Concepción province. This province consists of 13 communes, of which Concepción, San Pedro de la Paz and Hualpén are the communes surrounding the part of the Biobío river over which the new railway bridge is planned to be built. The region, province and communes are shown in figure 2.1, the yellow colours indicate the areas considered in this analysis.

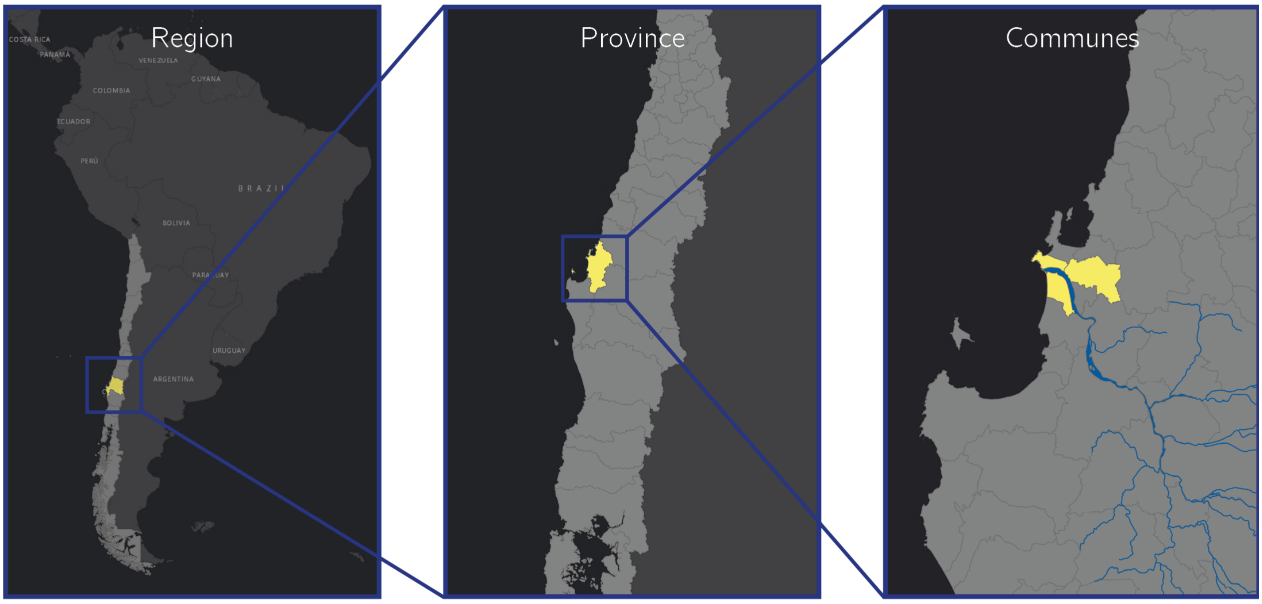

Figure 2.1: VIII Biobío Region with the province of Concepción, with the communes Concepción, San Pedro de la Paz and Hualpén

2.2 Historical Aspects

Pedro de Valdivia, a Spanish conquistador, undertook different expeditions in Latin America. From Mexico he travelled south to Chile via Peru. He founded the city of Santiago in 1541 and the city of Concepción in 1550. The latter, some kilometres north of the Biobío river, remained one of the most southern settlements of the Spanish. Since they were not able to defeat the Mapuche, an American Indian ethnic group, on the southern riverbank of the Biobío river. Therefore, this natural border marked the end of the Spanish conquest heading south for years to come and the river was nicknamed La Fronterra thereafter.

The original city of Concepción founded by Pedro de Valdivia in 1550 lies some kilometres north of the current city centre. The original location is known today as Penco. This is visualised in figure 2.2 in the top right corner. The current centre of Concepción is visible in the centre of the figure. The name given to the initial settlement reads: Concepción de María Purísima del Nuevo Extremo (Mary Immaculate Conception of the New End) (Herrera, 2018).

Penco was attacked and destroyed several times over since its establishment. This was not only due to violent attacks of the Mapuche people, but also several earthquakes and tsunamis. In the midst of the 18th century, the city of Concepción was relocated from the initial location to its present location, after a destructive tsunami hit the city once again. (Welcome Chile, 2019)

The city of Concepción in current times is described by McCarthy et al. (2018) as: 'an important and hardworking port city that is best known for its universities and music scene. There are a few plazas and museums worth checking out, and Spanish-speakers will be rewarded with an energetic and youthful arts, music and culture scene.'

Figure 2.2: The original city of Concepción, Penco, visible in top right corner.

2.3 Political Aspects

To be able to understand the different values and decisions of political stakeholders the political system in Chile is analysed. This analysis is performed from top, national level, to bottom, communal level, indicating who is in charge of decisions concerning the railroad bridge. The political structure is visualised in figure A.2 in the appendix.

2.3.1 *National level*

The Republic of Chile is a Presidential republic, the President is both chief of state and head of the government. The President is directly elected by the majority of the Chilean citizens every four years. The National Congress is the combination of the Senate and Chamber of Deputies, of both whose members are directly elected every eight and four years respectively. The President appoints the Cabinet and the Cabinet ministers are responsible for their own appointed Ministry (CIA, 2019). Considering the creation of a railway bridge, at least the following ministries are involved:

- Ministry of Finance
- Ministry of Economy, Development and Tourism
- Ministry of Public Works, discussed in the Stakeholder Analysis, section 3.1
- Ministry of Transport and Communications
- Ministry of Environment

The project concerns a single bridge and is therefore further supervised by the Biobío Region, which is discussed in the coming section.

2.3.2 *Regional level*

The regional government encloses the Ministerial Regional Secretaries, which coordinates public services in the region, and the Regional Council and its Intendant. The Intendant is appointed by the President and is his or her direct representative in the region. The Regional Council is elected by the Communal Councils.

The main functions of the regional government, according to OECD and The World Bank (2010), are limited to the functions of interest considering the creation of a railroad bridge, are:

- Design programmes and policies for regional development and productivity
- Approve the regional development plan
- Define and take investment decisions regarding use of resources from regionally defined public investments
- Advise municipalities
- Carry out various tasks related to infrastructure works

2.3.3 *Provincial level*

Within the province the Governor, appointed by the President, represents the Intendant. The Governor is head of the Provincial Economic Council, which acts as an advisory institution. One of their main functions is to oversee public services provided within the province. The construction of a new railway bridge is to be discussed by this governmental body (OECD and The World Bank, 2010).

2.3.4 *Communal level*

When considering an even more detailed governmental level, every commune in the province has its own Municipal/Communal council chaired by the Mayor. Both the Mayor and Municipal Council are elected by the inhabitants of the commune. Functions include promoting local development and developing the communal plans. The Economic and Social Council support the Municipal Council and is composed of representatives of civil organisations of the municipality (OECD and The World Bank, 2010). The commune is involved in the construction of the railroad bridge as it is part of local development plan.

2.4 Economical Aspects

In comparison with other Latin American countries Chile is a wealthy and growing nation (BBC, 2012). The main export goods include: copper, fruit, paper and pulp, fruit, fish products and wine. China is Chile's biggest export partner with a percentage of 27.5%, followed by the United States of America with 14.5%. Coincidentally, both countries are Chile's main import partners, due to imports from petroleum, electrical equipment and industrial machinery. The GDP per capita was 24,600 US dollars in 2017, marking the 82th place in the world ranking (CIA, 2019).

The city of Concepción and the surroundings of the Biobío river are both part of the Biobío Region. After Chilean independence this Region flourished as a result of the nearby lignite mine and the export of wheat for the Californian market. Improvement of the local infrastructure, railways and development of ports, further strengthened the economy of the Biobío Region (Lonely Planet, 2019). Currently, the main export products mostly consists out of provisioning: agriculture, forestry and fishing products (OECD and Bío Bío's Regional Steering Committee, 2009). The Region is the second largest contributor to the country's GDP. The economy in this region is characterised by a 'dual economy', part is comprised of large industrial companies in the forestry and steel sectors and the other part consists of a wide variety of small and medium-sized firms. The latter contributes for 80% to the of the employment rate. The bigger firms do not contribute significantly to employment rating via job creation or supply chain demand. Even though the amount of smaller firms is numerous, the rate of firm creation is low compared to the rest of the country (OECD and The World Bank, 2010).

The relative central location of the Biobío region and the city of Concepción, compared to the overall layout of Chile, creates opportunities for the transport sector. Goods going from north to south or vice-versa are likely to pass the Biobío region. Furthermore, the multiple harbours in this region provide excellent transportation possibilities via water. The transportation network is further elaborated in the next section, section 2.5.

The considerable higher wealth of this region, compared to the surrounding area, is visible in figure 2.3. The Purchasing Power per Capita in the communes: Concepción, San Pedro de la Paz and Hualpén, is on average 6,900,000 Chilean Pesos, see the zoomed window in figure 2.3, whereas the National Purchasing Power per Capita is approximately 6,350,000 Chilean Pesos (Michael Bauer Research, 2018). The local industries contribute highly to this difference. Besides the industries, it is important to note that these communes, also include several universities, raising the educational rate of the population.

In more detail the Biobío river contributes to the local economy by supplying the sand-mining companies, the water treatment plant, the oil refinery and the paper mill with its natural resources. The power, interest and attitude of these parties is taken into account in chapter 3.

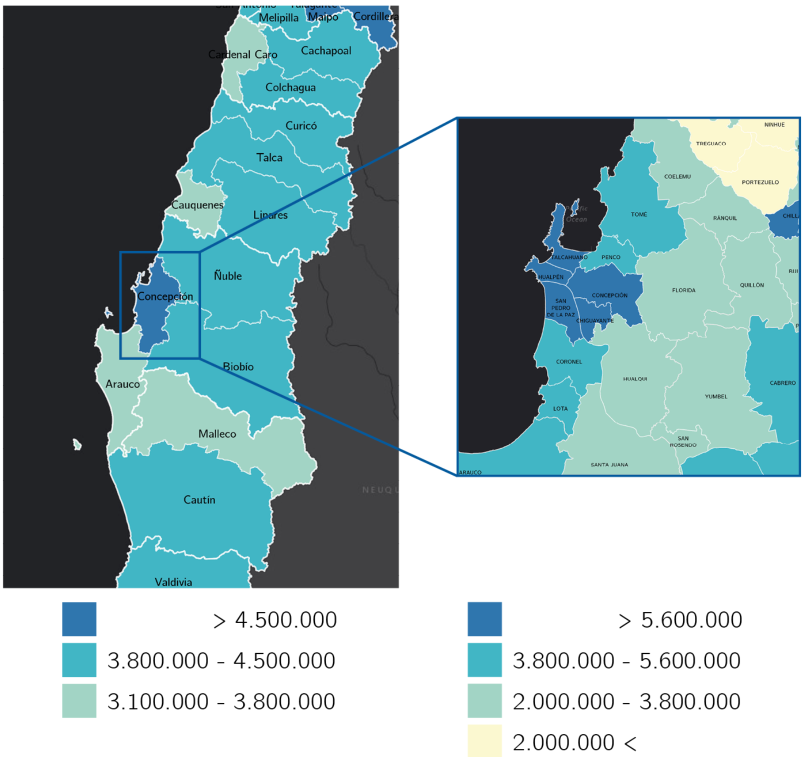

Figure 2.3: The Purchase Power per Capita of the three communes surrounding the mouth of the Biobío river and its surroundings. All values are in CLP.

2.5 Transport & Infrastructure

In a time period of 30 years, Chile has managed to greatly increase the connectivity of the country. Opening the door for economic growth and enabling companies and citizens alike to simplify their transport methods. This growth is the result of the establishment of a 'Concession System' in the form of a Public-Private Partnership (PPP), similar to the agreements utilised by 'Rijkswaterstaat' in the Netherlands, in 1993 (World Bank Group, nd). This has led, in combination with an attractive Risk/Reward Index (RRI), to growing interest from international companies, e.g. from Spain, Italy, France and Canada, to participate in these PPP's (Australian Government, nd).

2.5.1 *Infrastructure and economic prospects*

In the period 2011 to 2015 a total amount of US$ 42 billion, compared to an average of US$ 140 billion in western countries, has been invested into infrastructural projects (InfraCompass, nd). In a report, produced in 2017 by the 'World Economic Forum', the performance of infrastructures per country is analysed. Chile was awarded with a 4.7, on scale of 1-7, compared to an average of 5.5 for western countries (Swabb, 2017).

Ports
Ports play a vital role in Chile's import and export capacities. According to Ministry of Public Works (2009), roughly 90% of the country's foreign trade is handled by ports. As a result of a new law in 1997, the industry was largely privatised, resulting in an economic boost for governmental funds. Consequently, due to privatising, the efficiency of the ports was increased by 51%, in tonnes/hour, and charges decreased by 30%. Making it an attractive terminal for import and export (Ministry of Public Works, 2009).

This can clearly be seen in statistics produced by UNCTAD (2017), showing an increase of nearly 400% when comparing 2001 with 2017 [1]. The Ministry of Public Works, roughly similar to the Dutch 'Rijkswaterstaat', estimates that "by 2020, Chile's ports will need to be able to handle a throughput of 200 million tons, up from 30 million tons in the 1990s." (Ministry of Public Works, 2009)[p.53]

Aviation
The distances between the larger Chilean cities are rather spacious, making them time costly to undertake via road or rail. With global technological advances and investments made in the aviation sector, this led to an end of Chile's international geographical segregation and paving the way for domestic travel through air (Ministry of Public Works, 2009). The Ministry of Public Works published a record of total passengers using Chilean airports, seeing the number of passengers has increased from 6.4 million in 1998 to 10 million in 2008 (Ministry of Public Works, 2009). According to the The World Bank (2017), this number has steeply increased to 17.6 million in 2017. In contrast, the amount of cargo transported via air is decreasing, following from a peak in 2014 with 1,500 Mt*Km[2], to 1,200 Mt*Km.

Rail
Although the railway system was heavily neglected and nearly collapsed in the 1980s, the sector shows a healthy recovery. In figure 2.4, visible below, the number of passengers (multiplied with distance travelled) and total freight (multiplied with distance travelled) are shown. Comparing the year 1980 with 2008, an increase of 162% is visible in total tonnage transported via rail. Additionally, the freight tonnage multiplied with distance travelled has increased by 221% (Soto, 2008). It is expected that the total amount of cargo and passengers transported with the railway system will keep increasing (Soto, 2008). EFE itself estimates that cargo transport by rail will increase by 60% by 2022 compared to the value of 2017 and passengers transportation will have tripled relative to 2019. (Croquevielle, 2019)

[1] value for 2001: 1,080,000 TEU & 2017: 4,190,00 TEU, TEU is equal to 38.51 cubic meters
[2] Mt*Km is a million tons multiplied by kilometres

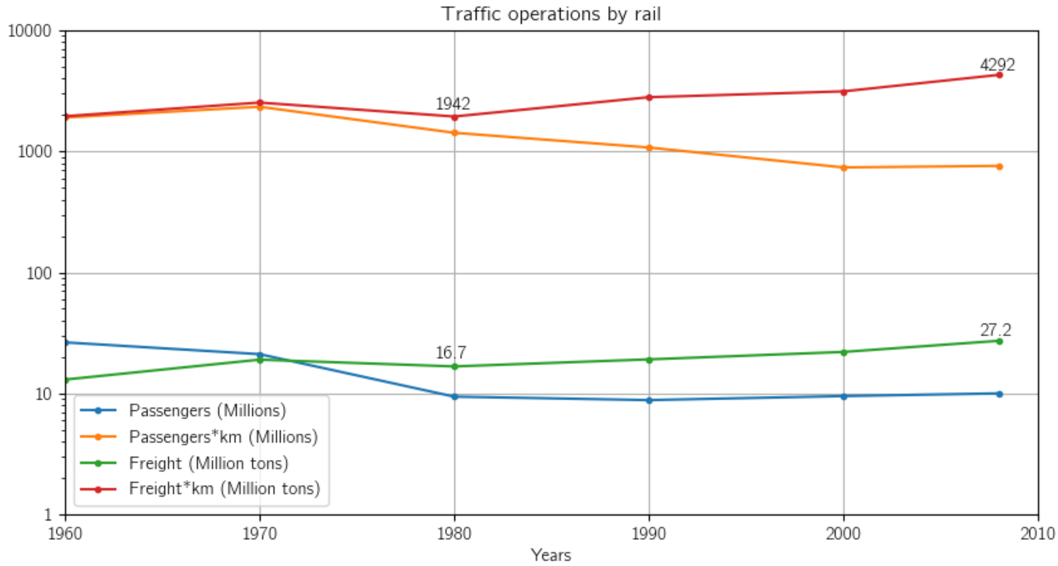

Figure 2.4: Transportation usage of the railway system utilised by EFE, Soto (2008).

2.5.2 *Infrastructure Concepción*

The capital of the region Biobío, Concepción, is surrounded by multiple ports, a relative large airport and connects the coast of northern Chile with the coastal areas in the south. In this subsection the infrastructural works of Concepción and surrounding urban areas are highlighted.

Existing and future Infrastructure
The regions north and south of the Biobío river are currently connected by two 2x2 highway bridges, Juan Pablo II and Llacolén, one single railway-track bridge and one 2x2 highway bridge, 'Chacabuco' which is close to finishing. The current situation can be viewed in figure 2.5. Additionally, the Ministry of Public Works is planning to construct an industrial bridge near the river mouth. (Puente Industrial, 2019). Connecting the industrial complexes in Talcahuano and Hualpén with infrastructure going to San Pedro de la Paz and Coronel, which will reduce industrial traffic going over the existing bridges. Furthermore, the new railway bridge, which is being considered in this advisory report, is visible in the figure. The new bridge will replace the current 130 years old railway bridge and is set to double the railway capacity of the current one. A schematic overview of the bridges and miscellaneous infrastructure can be viewed in figure 2.5

Figure 2.5: Schematic overview of existing and planned infrastructural works in the province Concepción.

The port of Talcahuano is connected to Concepción and the province via the highway- and railway system. As can be seen in figure 2.5, two additional ports are located north of Talcahuano, a recreational port and the largest military naval base. In addition, two more harbours in the region are connected to the provinces railway system, in the north-east the harbour of Penco and 25 km south of Concepción the harbour of Coronel. The ports in the Biobío region receive approximately 6.7% of the country's imports and exports, visualised in figure 2.6, excluding multi-region routes.

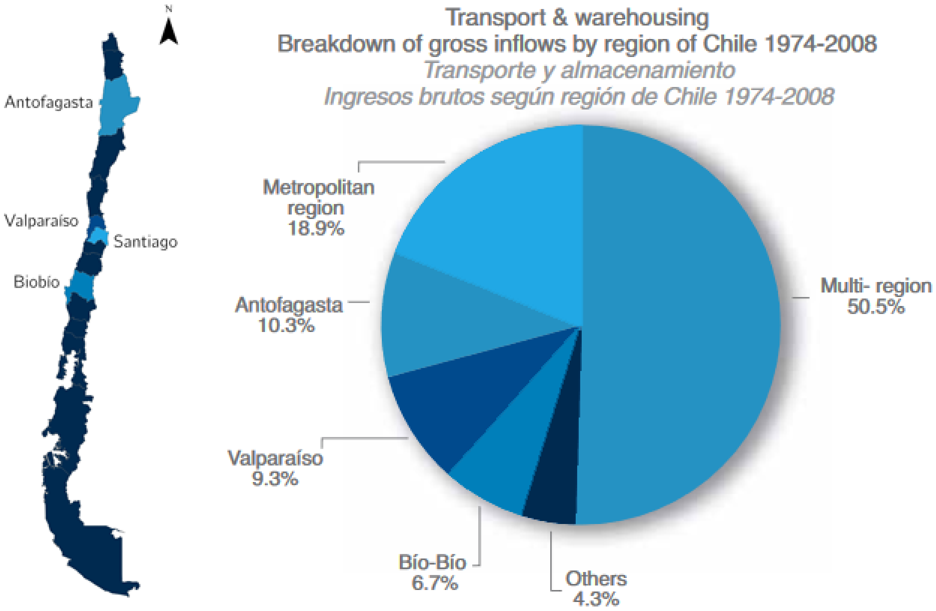

Figure 2.6: Pie chart of all inflows and warehousing from foreign trading of the most prominent regions (multi-region is domestic inflow & Metropolitan region equal 'Santiago' on the left side) (Ministry of Public Works, 2009)

3

Stakeholder Analysis

Every project includes stakeholders, over time their increasing diversity and power have increased project complexity (Winch, 2007). Furthermore, according to Pirozzi (2018) a project can be considered successful when it fulfils the requirements set by the stakeholders but can be considered to be really successful when the goals of the stakeholders are achieved. It is therefore important to investigate which stakeholders are relevant for the new railway bridge across the Biobío river, and assess the influence of each stakeholder on the project. This chapter starts with the identification of stakeholders in section 3.1, which contains a brief description of each stakeholder, followed by the mapping of the stakeholders in a 3D grid in section 3.2

3.1 Stakeholder Identification

Ministry of Public Works (MOP)

The Ministry of Public Works is the cabinet-level administrative office responsible and in charge of planning, studying, designing, constructing, operating and maintaining public infrastructure in Chile (Ministry of Public Works, 2019). However, the MOP is not responsible for rail infrastructure, this is the responsibility of the EFE and the ministry of transport. Despite the fact that the MOP is not directly involved in the project, it is planning to construct a new bridge further downstream, called the Puente Industrial (Puente Industrial, 2019). In the future this bridge is connected by a new highway at San Pedro de la Paz to the other bridges, thus crossing the new railway bridge.

Concepción and San Pedro de la Paz

These two communes do not share their boundaries via land but through bridge crossings only. Currently two highway and one railway bridge connect the two communities. Additionally, San Pedro de la Paz also shares one highway bridge and in the future the planned highway bridge (the Puente Industrial), aimed to be finished by 2022, with the commune Hualpén. Having only one relatively dated single-track railway bridge could prove to hinder the economic growth of the region and reduce the aspired growth of EFE, Croquevielle (2019).

Hualpén

Hualpén is a commune located west from Concepción, see figure 3.1. The municipalities' boundaries do not intersect with the planned railway bridge. However, it has its boundaries just downstream from the bridge, making it a stakeholder nonetheless. Furthermore, Hualpén houses one of the biggest regional economic powerhouses, ENAP Oil refinery.

Citizens of Concepción, San Pedro de la Paz and Hualpén

Citizens living in these two urban areas are not directly affected by the morphological changes of the Biobío river. However, since 2016 at least two bridges have collapsed due to the influence the river on the foundation blocks of the bridge. This caused economic damages and separated the two cities and the southern part of Chile from the northern part. This resulted in a negative impact on economic prospects of the inhabitants and hindered movement between the two communities.

EFE

The EFE is short for "Empresa de los Ferrocarriles del Estado". The EFE is Chile's national railroad company and was founded in 1884. The railway company bloomed during the early twentieth century, only to nearly collapse in the 1980s, due to an increase in competitors, like road transport and aviation, coalescent with a neglect in maintenance and a decrease in investments.(Croquevielle, 2019)

The state of Chile reignited interest, after a political administration change in the early 2000s, in the railway industry by heavy investments in the railway company. Paving the way for a growing railway industry. According to Fernández (2019), the year 2018 resulted in the highest number of passengers transported by railway and this number is likely to keep increasing.

In order to maintain this growth, the EFE is investing several projects throughout the country. Therefore, the planned railway bridge crossing the river Biobío plays a big part in the companies future. Furthermore, the construction of the bridge, in combination with other aspired project by the EFE, could result in an economic boost for the country. In particularly in the construction, tourism and transportation sectors.

ENAP - Oil Refinery
The oil refinery ENAP, situated in the commune Hualpén, was founded in 1950, five years after the first oil well was discovered. The plant situated in the Biobío region is the second of its kind for this company, and was constructed in 1966. Nowadays, the company provides roughly 80% of Chile's fuel consumption with a total capacity of 220.000 barrels a day, making it a major stakeholder in the region.(ENAP, nd)

Moreover, the ENAP has additional interests in the river, as it has constructed a pipeline, running from the refining plant to the Biobío river, which deposits its waste water into the lower stream of the river.

Harbours
Plentiful harbours are located in the vicinity of the region Biobío. Five harbours are located north of the river, three for logistical, one recreational and one for military usage. Three of these harbours are connected to the railway system. South of the river, and connected to the railway system that crosses the Biobío river, the harbour of Coronel is located.

As four out of six harbours in the vicinity are connected to the railway system, including the bridge crossing the Biobío, they are considered as important stakeholders.

Sand mining companies
Sand mining companies extract sand from the Biobío river, causing erosion of the river bed. Currently, five mining companies extract sediment from the river, four of them are situated on the northern river bank and one on the southern river bank. The main interest of these companies is to maintain and possibly increase the amount of sand they are allowed to extract from the river. However, this could potentially lead to further degradation of the riverbed, and thus increasing problems for the surrounding municipalities.

BO Paper Bio Bio - Paper mill company
The paper mill company extracts water from the river in order to produce its product, for this purpose a separate irrigation channel has been constructed. This irrigation channel crosses the planned bridge. The company has an interest in continuing its production during the construction phase.

Essbio Biobio - Water purification facility
The Essbio is the facility that purifies the water for the greater Concepcíon area, therefore the facility is interested in all changes of the river. However, since the bridge does not change the water quality, the interest of the facility is low.

Construction companies
Construction companies have a strong interest to win the tender for the construction contract of the new railway bridge.

Transportation companies
The aviation and trucking companies are natural competitors of the EFE in the logistics -and transportation industry. Although they do not directly influence the construction of the railway bridge, they do have interest in maintaining or increasing their stake in both markets.

UCSC
The UCSC, Catholic University of the Most Holy Conception, is one out of five universities situated in Concepción. The university is a private entity which receives some state support. The universities main focus is towards

the development of teaching, learning and research in the education it offers. (UCSC, nd) As a knowledge institute, with experience in engineering and specifically in hydraulic research, the university consults the EFE regularly on the planned railway bridge.

Nature Preservationists
In each construction project nature protection organisations are concerned with the impact of the project on the ecosystem. Although the organisations do not have a direct influence on the project they can lobby and gather support of the local community.

River Users
The river has no direct users, i.e. it is not used for inland waterway transport. River users will thus not be considered in the stakeholder analysis.

The location of the aforementioned stakeholders are visualised on a map, which can be seen in figure 3.1.

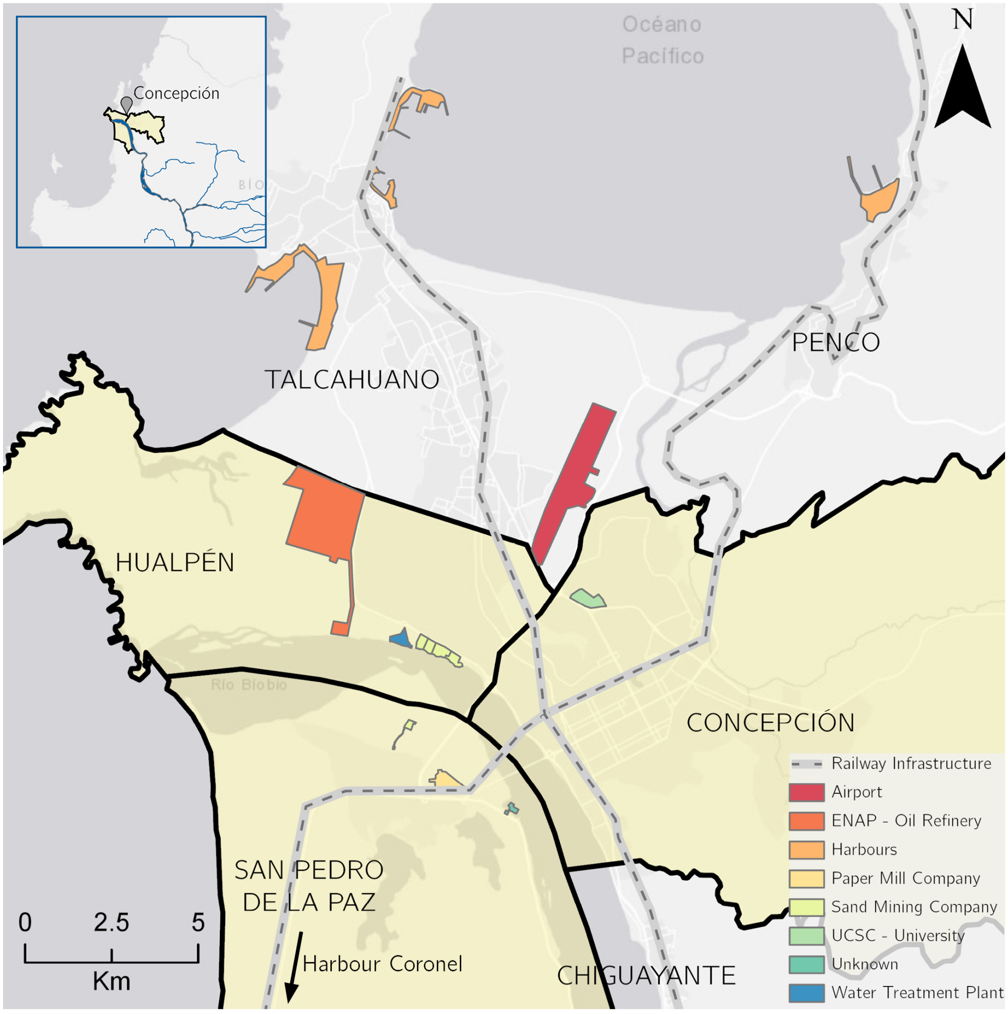

Figure 3.1: The location of the stakeholders

3.2 Mapping of stakeholders

This section is divided into two subsections, in the first subsection the method of stakeholder mapping is explained. After which the second subsection describes the method used to map the stakeholders identified in section 3.1.

3.2.1 *Technique*

There are several methods to map the identified stakeholders, the Project Management Institute (2013) has listed the following methods:

- Power/interest grid, grouping the stakeholders based on their level of authority ("power") and their level or concern ("interest") regarding the project outcomes.
- Power/influence grid, grouping the stakeholders based on their level of authority ("power") and their active involvement ("influence") in the project.
- Influence/impact grid, grouping the stakeholders based on their active involvement ("influence") in the project and their ability to effect changes to the project's planning or execution ("impact").

The similarity between described techniques is that they all use a 2D grid to map stakeholders. However, Murray-Webster and Simon (2007) have proposed the inclusion of a third dimension to make the technique even better. The proposed technique includes the following dimensions:

- Power, measured by the ability to influence the project organisation.
- Interest, measured by the extent to which they will be active or passive.
- Attitude, measured by the extend to which they will support or resist the project.

With these three dimensions a new grid to map stakeholders is created in 3D, this new grid can be seen in figure 3.2 with the different roles stakeholders can have in a project. This method of stakeholder mapping is used in the next subsection. For an elaborate description of the different roles one is referred to appendix A.

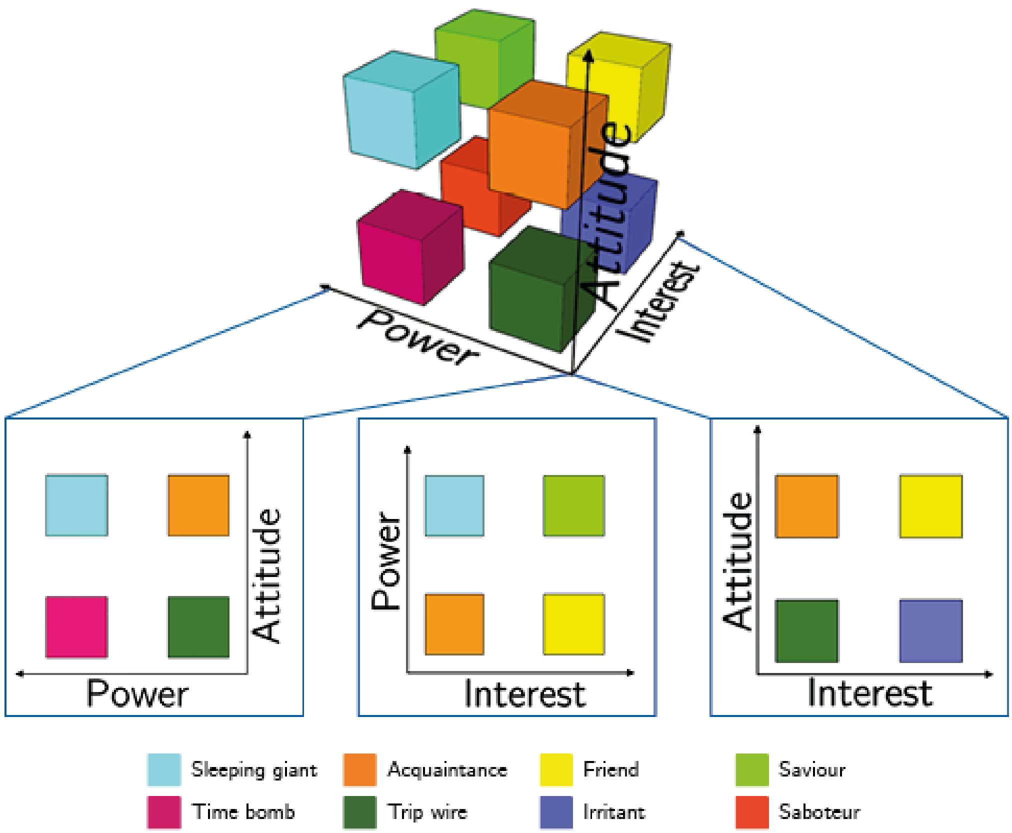

Figure 3.2: 3D Stakeholder mapping technique, redrawn from (Murray-Webster and Simon, 2007)

3.2.2 *Mapping*

Sleeping Giant

- ENAP: this company is a major economical player because they provide 80% of fuel consumption which makes them a powerful stakeholder. However, since they do not directly benefit from the new rail railway bridge, their interest in the project is low.
- Water purification plant: since no change in river flow is planned the water purification plant does not have an interest in the project. However, they are potentially a powerful party.

Time Bomb

- MOP: the MOP is planning to construct a bridge further downstream, a change in flow conditions or river behaviour which might change their interest in the project.

Acquaintance

- Hualpén: the commune is not directly affected by the construction works, as the planned building site is outside of its boundaries. However, Hualpén houses some big economic players: several sand mining companies and a water treatment plant. It therefore benefits most if said companies are not hindered in their daily production.
- Paper mill: the paper mill company does not directly gain nor lose from the construction works, provided that the company can continue extracting water from the river for its product.

Trip Wire

No trip wire stakeholders have been identified

Friend

- UCSC: during the design study the UCSC is involved to investigate the behaviour of the river, which increases their prestige in the region.
- Construction: construction companies have an interest in this project because if the tender is awarded to them they can earn money.

Irritant

- Citizens: citizens in the proximity of the construction site are often against the project because of the increase in nuisance during construction.
- Nature preservation: nature preservation are often against interventions in the river, as it could harm the local flora and fauna.
- Sand mining: these companies are keen on continuing their regular production. However, it is already noticeable that due to the sand extraction the riverbed is changing. From the hydraulic research it could be proven that sediment extraction has a negative effect on foundation pillars of bridges and therefor regulations on sediment extraction could be implemented, leading to a negative impact for said companies.

Saviour

- EFE: the client of the project, and are thus a powerful party with high interest and a positive attitude.
- Concepción: the bridge will start/end in the city of Concepción, making the municipality a powerful stakeholder.
- San Pedro de la Paz: the bridge will start/end in the city of San Pedro de la Paz, making the municipality a powerful stakeholder.
- Harbours: because the bridge will ensure an improved connection between harbours and the hinterland, the harbours in the Concepción area have a high interest and positive attitude towards the project. Combined

with the fact that they are important to the economy of the region they can also be regarded as a powerful stakeholder.

Saboteur

- Transportation sector: in Chile a lot of transport takes place over land via trucks, or by air with planes. The transportation sector is thus opposed towards any project which might compromise their market share.

4

Physical Analysis

As mentioned in the introduction the Biobío river system is a 380 kilometres long river, with along its course many interesting features to discuss. Although the main focus of this chapter is the analysis of the Biobío river from the mouth of the river to about 20 kilometres upstream, some features further away are analysed nevertheless in order to get a complete overview. The lower Biobío river system has been subject to considerable changes, such as a transition in the river course and the development of a river bar at the inner bend. These features, at this moment present near the mouth of the river, are visualised on a map in figure 4.1. Together with the relevant cities, which have already been mentioned in chapter 2 and 3.

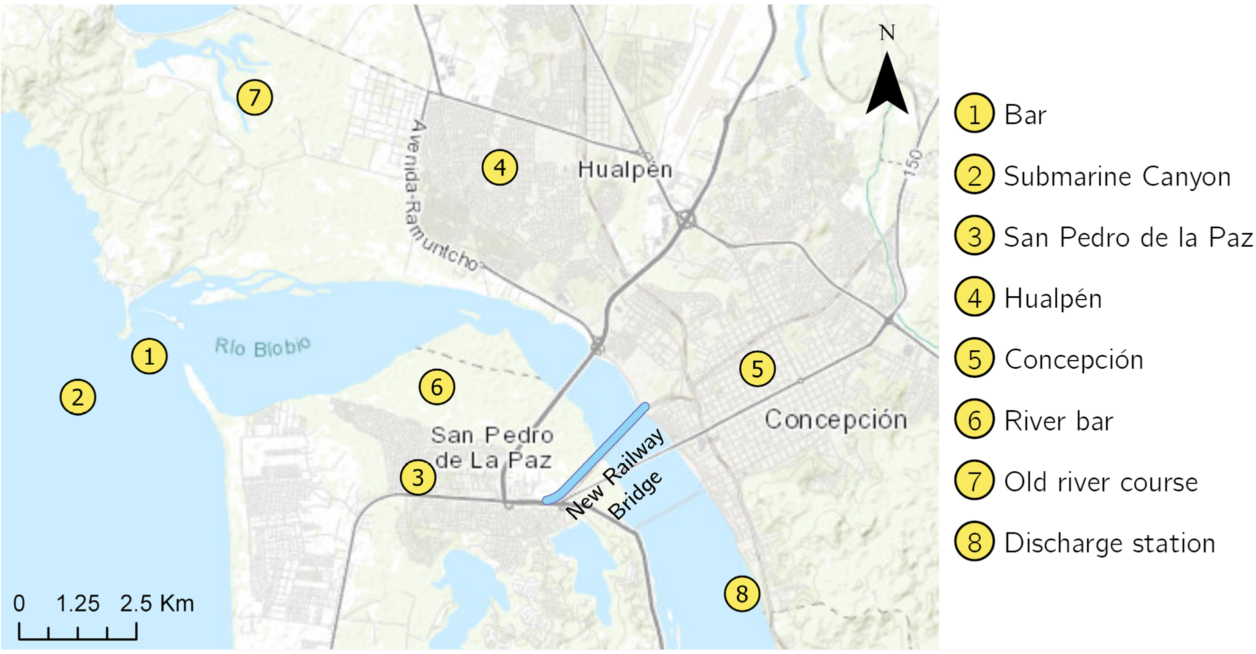

Figure 4.1: Features, at the moment of writing, present near the mouth of the Biobío river

The subject of the first section is the analysis of the Biobío river. Whereafter the available data is discussed in section 4.2, the goal of this section is to analyse the data and process it in such a way that it can be used as input for Delft3D. Besides the aforementioned features, the Biobío river is also in an area prone to natural disasters such as earthquakes and tsunamis, which have a profound influence on the system. Their understanding is thus a prerequisite. Finally, two case studies of recent natural disasters are analysed in the last section of this chapter.

4.1 Biobío River System

The river's origin is found in the Andes mountains. It originates from three lagoons: the Laja, the Icalma and the Galletué (Nordbø, 2001; Karrasch et al., 2006). Flowing from the mountains towards the Pacific Ocean, it forms a natural border as mentioned in section 2.2.

The main river Biobío originates from the latter two lagoons, while the Laja lagoon provides the Laja river. The Laja and the Biobío river merge at the town Laja. It is due to the fact that both rivers flow through a big part of the region, that the drainage basin of the river Biobío is largely similar to the region Biobío. This drainage basin is shown in figure 4.2 and consists of an area of approximately 24,260 km^2 (Gesche, 2018).

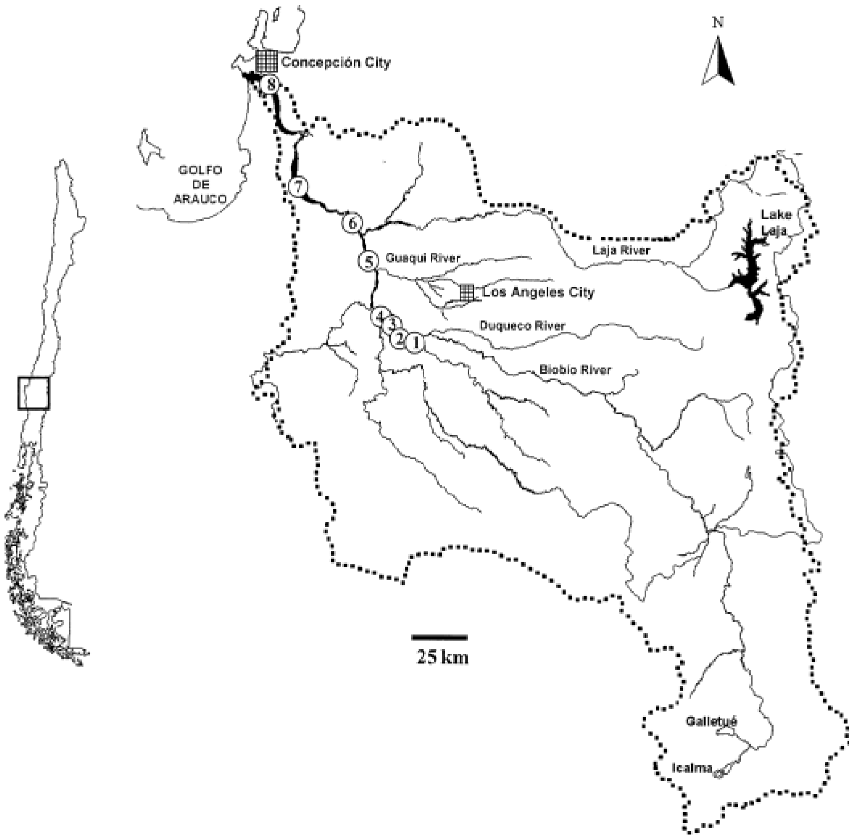

Figure 4.2: Drainage basin of the Biobío river from Habit et al. (2006)

Between 1962 and the mid 1980's, the Chilean government has been heavily investing in the construction of several (hydropower) dams. Which, after completion, nearly quadrupled the hydroelectric capacity for the country, according to Nelson (2013). Consequently, this has led to a mostly regulated river in the lower part of the river system. This regulation met some controversy and resistance, specifically for the Ralco dam. As the construction resulted in the need to relocate a whole native tribe (Nordbø, 2001).

4.1.1 *Old Courses*

The course of the river has changed significantly during the last century, albeit on a relatively small timescale. Therefore, the Biobío river cannot be assumed to be in an equilibrium state. As can be seen in figure 4.3, the bar is continuously changing over the course of the mid century.

Isla et al. (2012) assumes that the old path of the river was situated towards the Concepción bay, more to the north compared to the current westward location of the river mouth. The regions near Hualpén and Talcahuano were still islands in that time according the aforementioned paper. Concepción, San Vicente and Arauco were flooded quite often in these times. Since the maximum water level increased, the Concepción bay to started to fill with water. As a result an arm grew towards the islands of Talcahuano and Hualpén. This caused the outflow of the river to be re-situated more westward instead of northward, meaning its new location was in front of the submarine canyon, which is situated near the coast. Consequently this lead to a more efficient route of transporting the sand towards the sea (Isla et al., 2012).

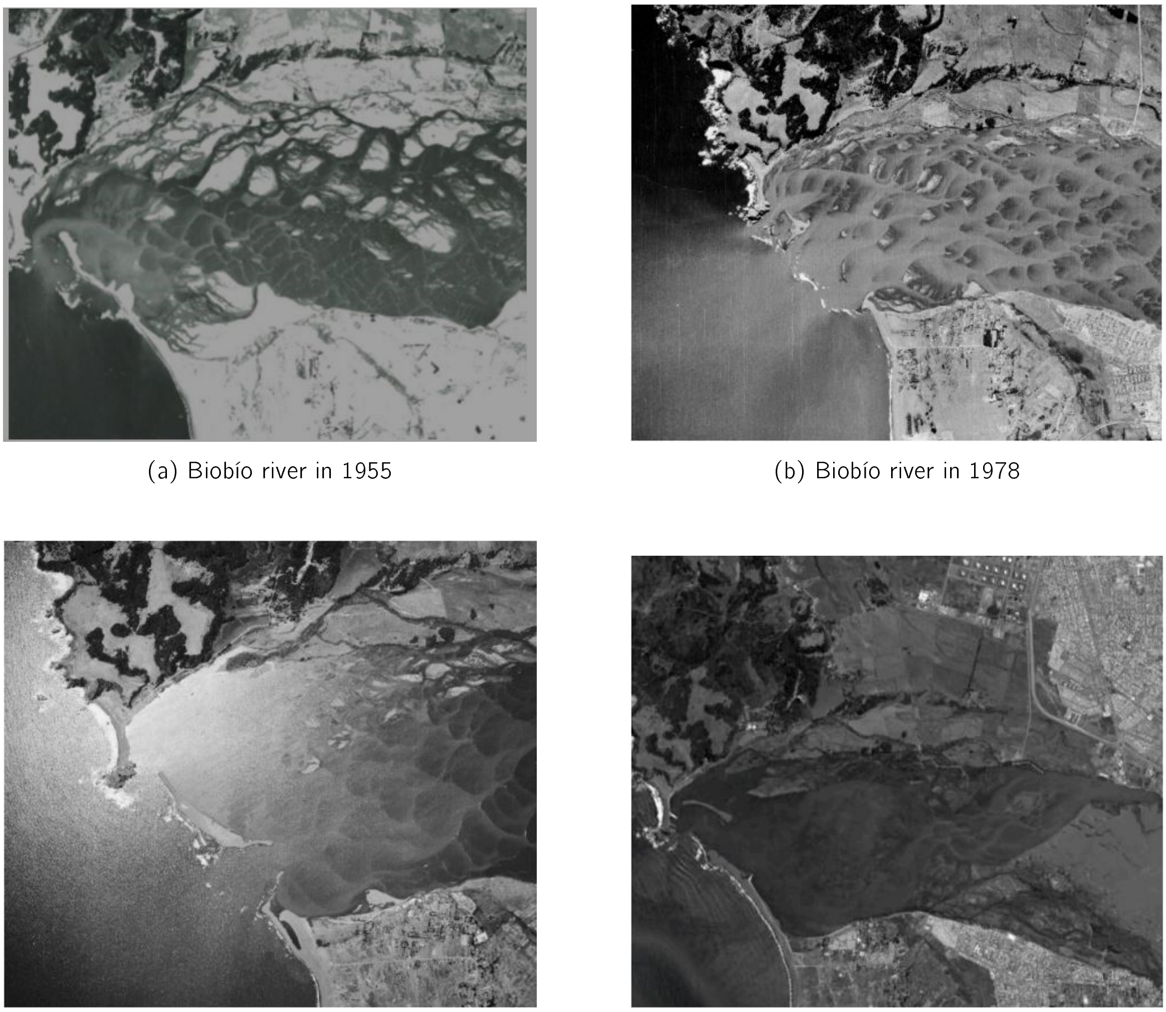

(a) Biobío river in 1955

(b) Biobío river in 1978

(c) Biobío river in 1992

(d) Biobío river in 2011

Figure 4.3: Changes of the bar at the river mouth of the Biobío river (Caamaño, 2010)

With the historical data supplied by the images from figure 4.3, it can be concluded that the bar in the river mouth is prone to be affected by currents, floods and waves. And thus, it can be considered as a dynamic bar that is present during low discharges, but is erased during high discharges.

In the paper of Caamaño (2010) the development of the lower part of the Biobío river is discussed, using measurements taken with a boat and GPS. Obtaining detailed measurements is difficult in the river, as discharges have to be sufficiently high enough to manoeuvre the boat. The measurements of the bed cannot be done during low discharges as the sand bed is not stable enough to withstand the pressure exerted by a person. When comparing the newly obtained data with cross-sectional measurements of 1992, it can be concluded that the cross-sectional profile of the river has decreased with approximately 3.17 metres in the last 40 kilometres of the river. Furthermore the river has shifted its path even more to the northern bank, as is also visible in figure 4.3.

Furthermore, a change from islands to small bars which than morph into sand dunes and ripples, can be seen on the southern bank over the duration of the century. This can be seen in figure4.3. Figure 4.3d shows a large sand bar in the lower right corner, which results in the concentration of the flow on the northern bank, as described in the previous paragraph. In order to mitigate erosion of the bank, a riprap, rock armour, protection has been applied. This bank protection is shown in figure 4.4.

Figure 4.4: Riprap protection at the north bank of the Biobío river

4.1.2 *River Profile*

The river has its origin in the mountains so different profiles for the upstream and downstream part are expected. Consequently, the grain size changes in the downstream direction, meaning smaller grain sizes are to be found in the lower part of the river and bigger grain sizes can be found in the mountain branches. The change of the river slope is shown in figure 4.5.

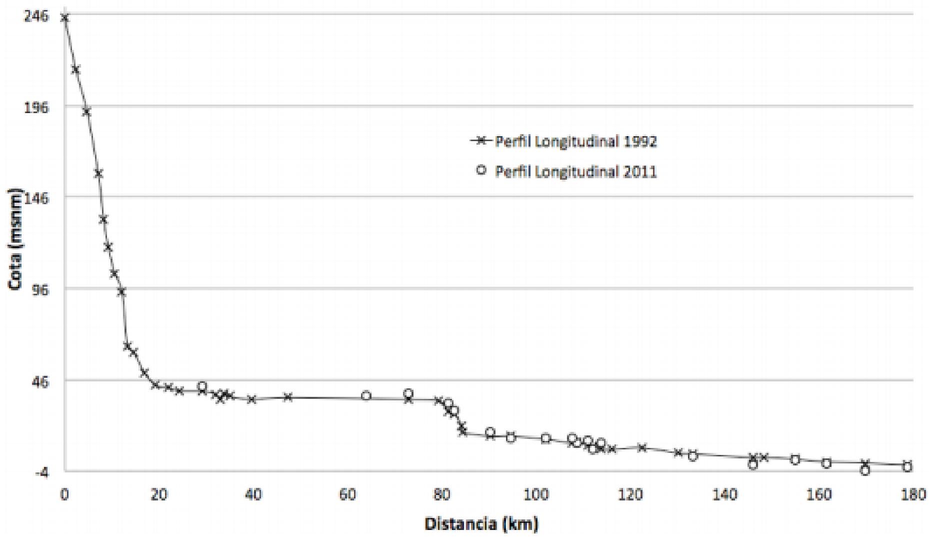

Figure 4.5: Longitudinal river profile from measures in 1992 and 2011 (Caamaño, 2010)

This profile can be described as an upward concave, For comparison a typical upward concave profile is shown in figure 4.6. The profile for the Biobío river and the typical profile show the same trend in downstream direction.

An upward concave profile means that the slope decreases when moving downstream. This is due to the effect of grain-size selective transport. As sediment particles collide they wear over time. This results in new smaller particles along the course of the river. As these finer grains require a less steep slope to be transported, since they are more mobile than coarser grains, the slope of the river decreases in the downstream direction (Blom, 2018).

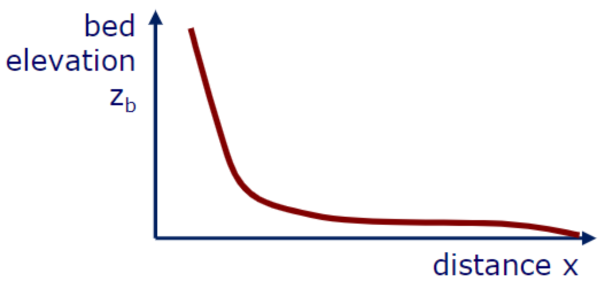

Figure 4.6: A typical upward concave profile (Blom, 2018)

Besides the fact that the river changes its profile, the flow pattern changes as well. Moving from the river mouth upstream, the river first has a meandering character. This meandering part increases the concavity due to the lengthening of the downstream part of the river. This leads to a more uniform distribution of the profile when flow increases downstream (Langbein and Leopold, 1970). Moving further upstream, the river shows a more anabranching character. Meaning that there are stable islands in the river which are relatively large compared to the width of the river (Blom, 2018).

4.1.3 *River Bar Development*

As mentioned before the bar in the river Biobío has been present since 2011. Though the outlines of the river bar are already visible in Google Earth from the early 90's. The changes to the river bar happen much faster than the changes of the course of the river. Since the absence of high discharges in the last years, the river bar had the opportunity to stabilise (Chiang et al., 2014), this process was increased by the growth of vegetation.

As the roots of the trees and plants on the river bar anchor the sand, making it more difficult for the river bar to erode in case of a high discharge flood. The development of the river bar over time is shown in figures 4.7a till 4.7d.

(a) River Biobío in 1991

(b) River Biobío in 2002

(c) River Biobío in 2014

(d) River Biobío in 2019

Figure 4.7: Changes of the bar near the river mouth of the River Biobío, photos from Google Earth using a zoom scale of 9 km

From figures 4.7a to 4.7d it can concluded that the bar has been growing upstream. While in 1991 it consisted of multiple smaller bars, the bar arised in 2002 as one big hump of sand. Furthermore, the narrowest part of the channel has become more narrow, leading to higher velocities and thus more erosion. Figure 4.7c shows vegetation is present on the bar. Following the remarks: the bar is stable and is more difficult to erode by higher discharges.

4.1.4 *Processes at River Mouth*

In most of the figures previously shown, figure 4.7 and 3.1, it can be seen that the new railway bridge is to be located near the mouth of the Biobío river. Hence, the sea influences the river system, by for instance the tide and stratification. Both have an effect on the morphological behaviour.

Depending on the skewness (horizontal asymmetry) of the tide the system either imports or exports sediment. In case of positive skewness, the system is flood dominant, which means that the rising period is shorter than the falling period. In this case the time between low and high tide is shorter than the time between high and low tide, due to the faster transition from low to high tide the velocities are faster. Averaged over the tidal period the system thus imports sediment. This is due to the fact that the maximum flood velocity exceeds the ebb velocity and the sediment transport responds non-linearly to the velocity (Bosboom and Stive, 2015).

In the river mouth the fresh water from the river and salt water from the sea meet, which can result in a stratified system. In a stratified system the flow velocity near the bottom is opposite to the flow velocity near the surface during the rising period, a so called salt wedge is then present in the river (see figure 4.8). The intrusion of the salt wedge into the river depends on the local system and daily conditions, for instance the discharge and tidal range.

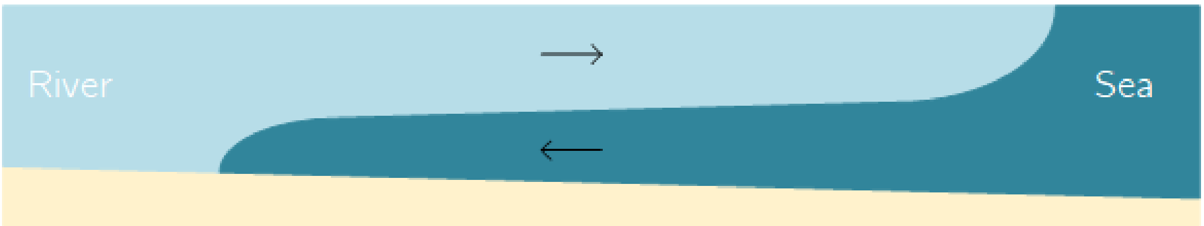

Figure 4.8: Visualisation of the salt wedge in a river mouth

Due to the change in the velocity profile the sediment transport also changes. As a result of the stratification, not all sediment is transported towards the sea, instead some sediment is transported near the bed as well. Geyer et al. (2004) stated that the sediment transport, in river influenced environments, is often influenced by the near-bed sediment transport, and that the understanding of sediment transport in the river mouth is a prerequisite for understanding the morphology. The reason salt wedge intrusion is important is because the stratification can shut down or decrease, the turbulence at the pycnocline which results in the deposition of suspended sediment (Pietrzak, 2016).

4.1.5 *Ecology*

Due to the Humboldt Current which is streaming from Antarctica towards the equator, cold nutrient-rich water is transported along the coast of Chile. When the current hits the shore a upwelling flow arises. This brings the nutrient-rich water to the surface driving a productive ecosystem, and thus providing excellent fishing grounds (Thiel et al., 2007; Strub et al., 2019).

The Biobío river is considered one of the rivers with the greatest richness in species by Vila et al. (1999). The river however, is suffering under the effects of human activities taking place in the river. Especially the paper and pulp industry (located near Concepción), which outputs its effluent water in the river. This effluent water has not been fully treated to meet the standards of the rest of the river water. Thus damaging the ecological system of the Biobío river (Karrasch et al., 2006). This is also the case for water treatment plants and has been leading to the absence of a lot of native species in the river nowadays (Habit et al., 2006).

Furthermore, the urbanisation and the shift in land use are putting a lot of pressure on the water bodies near cities (Aguayo et al., 2009). The expansion of the forest in the region of the Biobío river are associated with an increase of exotic forest industries, according to Chiang et al. (2014), oppressing the native nature. Above influences have caused the deterioration of the water quality over the recent years and thus having a negative influence on the ecological system.

4.2 Data

In this section the provided data is discussed and analysed, in the first section the bathymetry is discussed after which in subsection 4.2.2 the tidal information is analysed. Followed by the available discharge data of the Biobío river in subsection 4.2.3, And finally, in subsection 4.2.4, the sediment characteristics are discussed.

The stratification of the river mouth is not considered in this section due to the fact that the salt intrusion into the river is small (Bertran et al., 2001).

4.2.1 *Bathymetry*

In 2010 an extensive bathymetry survey has been carried out using LIDAR and a boat equipped with an echo sounder. The combined data from these sources is presented in figure 4.9.

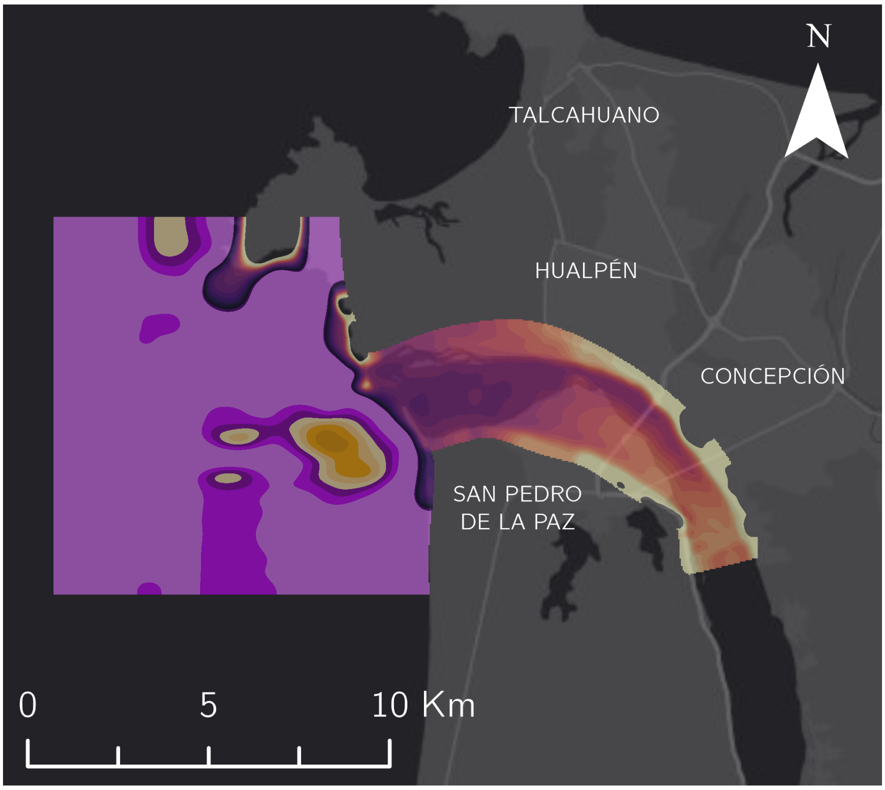

Figure 4.9: Bathymetry obtained in 2010

In the bathymetry, the river bar, located at the inner bend near San Pedro de la Paz, can clearly be seen. As mentioned in subsection 4.1.3 this river bar is currently growing. Another feature which is clearly visible in the bathymetry is the submarine canyon in front of the river mouth. The presence of this feature more or less protects the river against tsunamis, this is due to the fact that the tsunami refracts when approaching the coast (Aránguiz and Shibayama, 2013).

4.2.2 *Tide*

As mentioned in subsection 4.1.4 the influence of the tide is important for the morphological response of the river mouth, information about the tide is thus needed for morphological computations. No tidal station is located near the mouth of the river. However, three tidal stations are located in the proximity of the mouth. The location of these tidal stations are Coronel, Talcahuano and Coliumo, see figure 4.10.

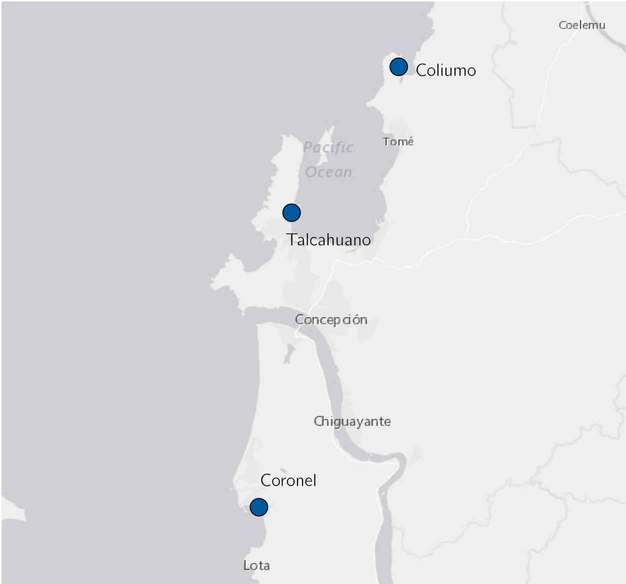

Figure 4.10: Location of the tidal stations near the mouth of the Biobío river

The tidal station located at Coronel is used as an input for the tidal data near the river mouth. The tidal signal from the period between the 8th of April and 8th of May is presented in figure 4.11.

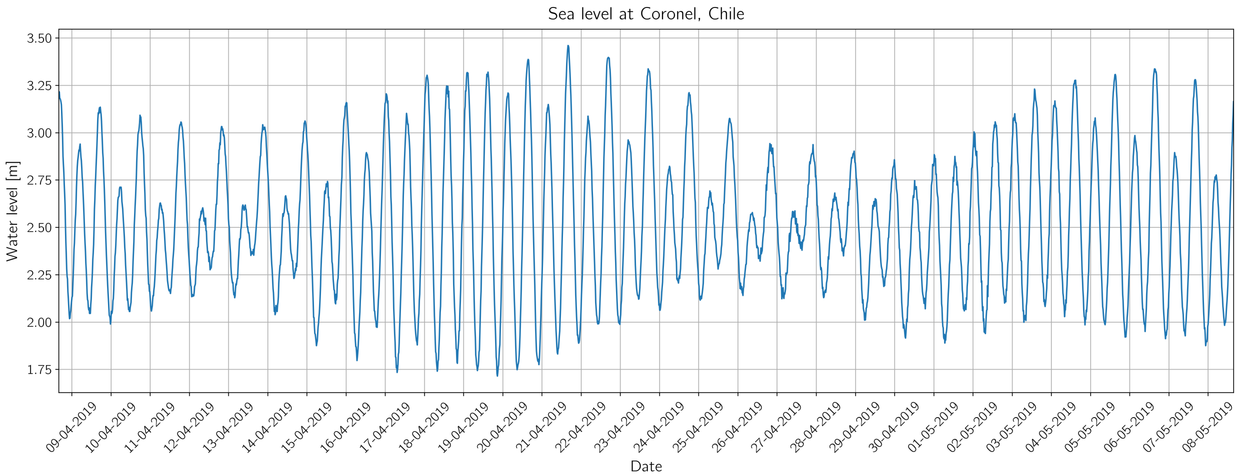

Figure 4.11: Tidal data at Coronel during the 8th of April and 8th of May, data from IOC Sea level monitoring (2019)

With this data it is possible to determine if there is a skewness or asymmetry in the system, this is be done by processing the raw data. From this analysis the following data is found:

- Average water level: 2.522 m
- Average rising period: 6 hours and 10 minutes

- Average falling period: 6 hours and 13 minutes
- Average height of the high tide: 0.492 m
- Average height of the low tide: 0.504 m

It can thus be concluded that there is no skewness or asymmetry in the system, and the system will, as a result, not import or export sediment averaged over a tidal period.

4.2.3 *Discharge*

The river is known to have seasonal variations, as stated by Saldías et al. (2012), a typical hydrograph could give more insight in the peak and minimum discharge. It is stated by van Heemst et al. (2012) that the discharge is mostly dependent on the precipitation accumulated in front of the dams in the river and only 10% is due to the melting of snow. In Chile there are multiple stations measuring the discharge in the rivers. In the Biobío river the most relevant station is located just upstream from the city of Concepción, and is called the Desembocadura gauge. The location is visualised in figure 4.1. On a yearly basis the discharge has a clear seasonal variation. As shown in figure 4.12 the discharge increases in the winter months. As mentioned before, the contribution of melt water to the discharge is only a small portion. The rest of the discharge is due to rainfall in the drainage basin.

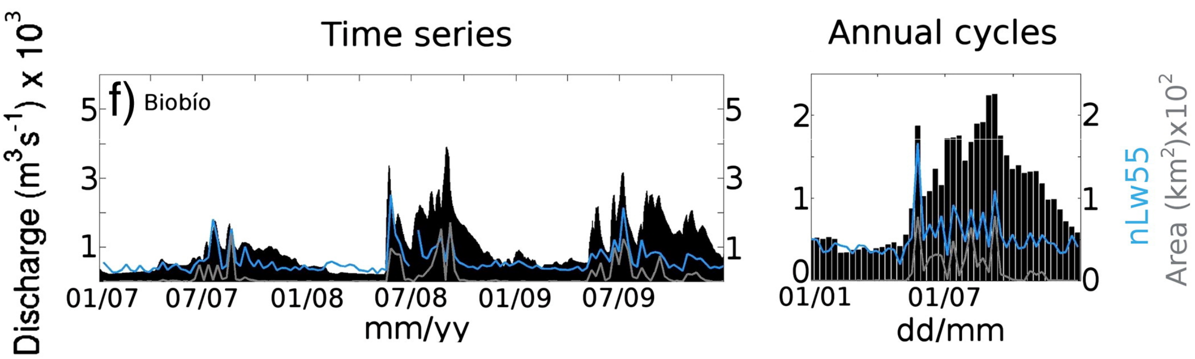

Figure 4.12: Seasonal variability of the Biobío river, modified from (Saldías et al., 2012)

In Chile the maintenance of gauge stations does not have the highest priority. As a result there are some gaps in the discharge data, presenting times the station was not operational. The annual average discharge of the Biobío river is set to 1000 m^3/s (Diego Caamaño Avendaño, 2019). However, according to Diego Caamaño Avendaño (2019) using the effective discharge provides a more accurate estimate of the influence of the discharge on river morphology. As described by Gordon Wolman and P. Miller (1960): 'the magnitude and frequency of river flows are responsible for the characteristic shape of a river channel'. This was further elaborated by Goodwin (2004), creating figure 4.13.

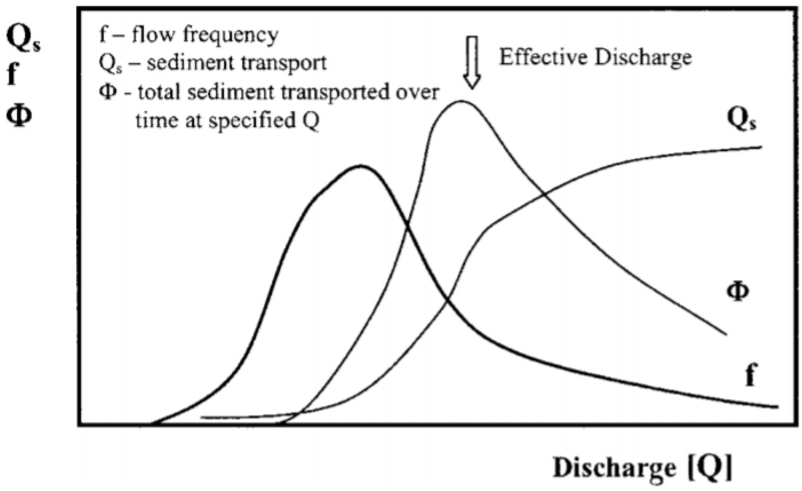

Figure 4.13: Identifying the effective discharge by Gordon Wolman and P. Miller (1960)

Here, both the magnitude and frequency influencing the total sediment transport over time, are taken into consideration. Diego Caamaño Avendaño (2019) has investigated this and the effective discharge of the Biobío river is: 1671 m^3/s.

The EFE has also estimated the 100 and 300 year return period discharges, these are 20,526 m^3/s and 23,861 m^3/s (Ingeniería Dolmen, 2015) respectively.

4.2.4 *Sediment Characteristics*

The sediment in the river mouth can be characterised using data available near Hualpén and Desembocadura. These stations are situated at a distance of 3 and 10 kilometres respectively, upstream from the river mouth. The measurements give the sieve curves, visualised in figures 4.14a and 4.14b. From the sieve curves the grain sizes (D_{85}, D_{50} etc.) can be determined to find the grading of the sand. This grading is of importance to be able to determine whether armouring and hiding effects play a role in the bed load transport. In case of a uniformly distributed sediment sample the effects of hiding and armouring are negligible, meaning the sediment is transported more easily.

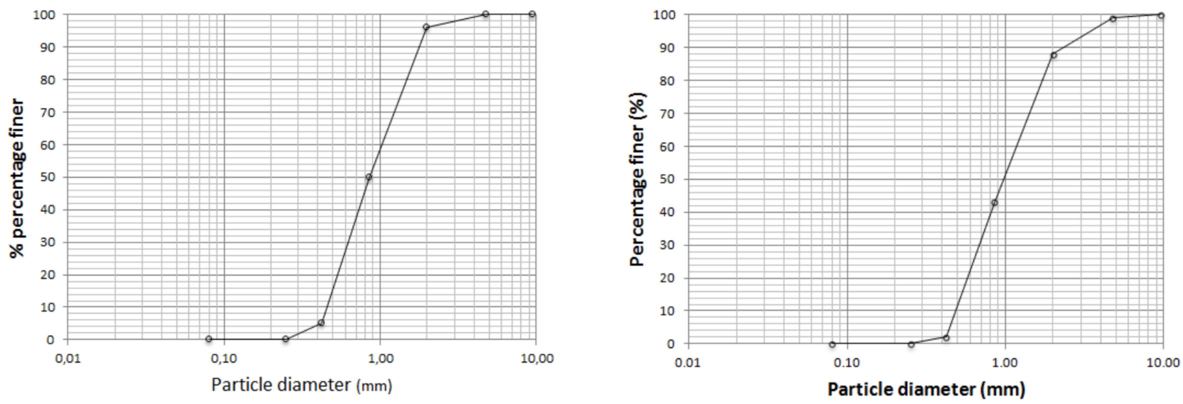

(a) Sieve curve of the sediment measured near Hualpén

(b) Sieve curve of the sediment near Desembocadura

Figure 4.14: Sieve curve of the sediment from the sample stations (van Heemst et al., 2012)

In the assessment of terrigenous (sediment deposited in the sea, originated from land) sediment samples by Lamy

(1998) it was found that most sediment available near Concepción is sandy mud or clayey silt. By assessing the sediment the following parameters have been obtained from the sieve curves: a D_{50} of 0.85 mm near Hualpén and a D_{50} of 1 mm near Desembocadura.

4.3 Case Studies

To be able to understand the behaviour of the Biobío river during extreme circumstances, two different events: the flood wave of 2006, and the earthquake and resulting tsunami in 2010, are described in this section. Both events caused serious damage in terms of human lives and economical loss in the Biobío Region. When modelling the river in a later stage, these two events can used as input data as to see how the model reacts to extreme events.

4.3.1 *Flood Wave of 2006*

In July of the year 2006, following a period of extreme precipitation, a large area near the mouth of the Biobío river flooded. Figure 4.15 shows the impact of the bad weather did not only influence the aforementioned area, but indicates the affected area was much larger. The red areas show the critical disaster areas, appointed by the Chilean President of the time. Here, most damage was caused, whereas the entire effected area is not only limited to the red areas, but also involves the green and yellow areas. Some facts to underline the severeness of the flood are presented in 4.1. Part of the affected population blamed the hydropower plants upstream, claiming the plants should not have opened the flood gates. These dams, however, are not built as flood defence although they have some buffer, but are mainly to generate power. The gates had to be opened to prevent damage to the dams.

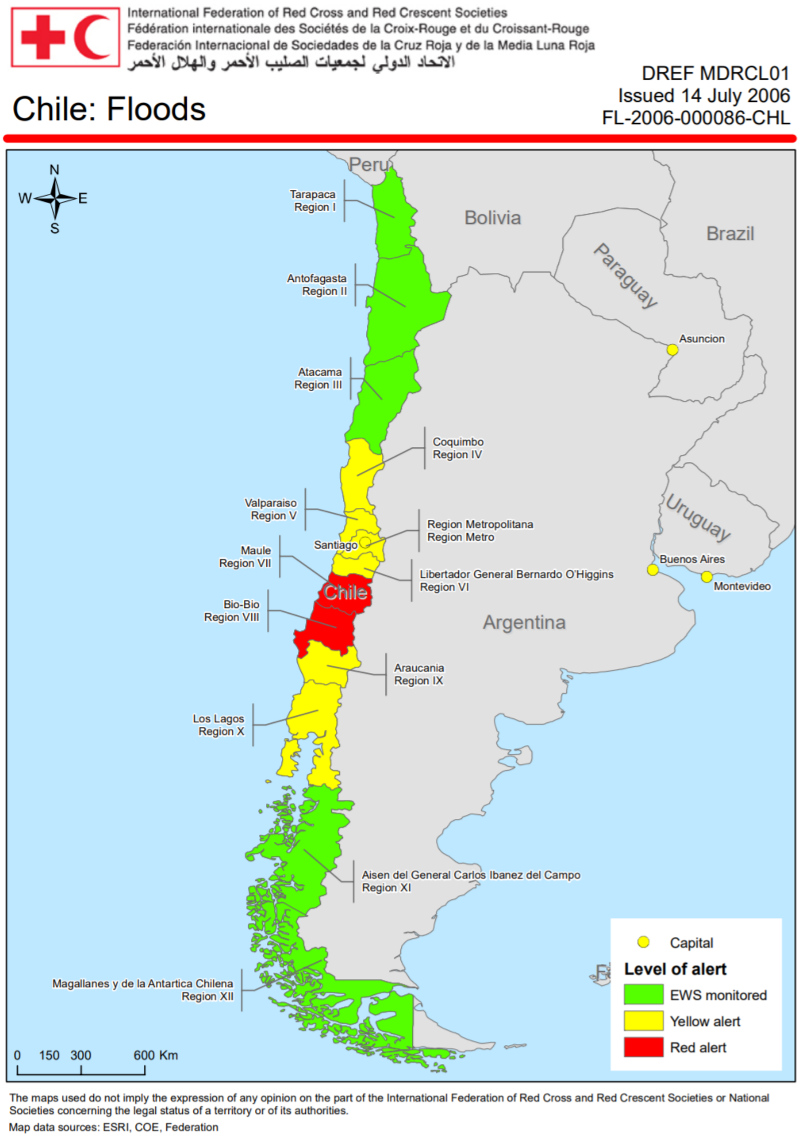

Figure 4.15: Showing the stretch of regions affected by the extreme weather of July 2006 by the International Federation of Red Cross And Red Crescent Societies (2006)

Table 4.1: Some facts of the flood from the International Federation of Red Cross And Red Crescent Societies (2009)

Description	**Number**
People affected	95,862
People killed	19
Damaged homes	14,024
Peak discharge Biobío river	15,000 m^3/s
Period flooding	11 days

Effected Area

As a result of the extreme rainfall, the discharge in the rivers increased rapidly. Due to this excessive discharge part of the Biobío river moved outside its natural borders, resulting in flooding of its surroundings. These 'hotspots' included the area west of Hualpén and Concepción, the northern and part of the southern embankment of the Biobío river. Furthermore, part of San Pedro de la Paz, situated on the southern river bank, and part of its coastal area flooded. The flooded areas are visible in figures 4.16a and 4.16b. The pictures show the mouth of the river is now located in a westward direction. During the flood the excessive water flowed into the low laying areas north of the river. Next to figure 4.16a, the height elevation of the same area is visible in figure 4.16b, from which can be concluded that the water outside the embankments of the Biobío river moved into the low laying regions, in this case the old location of the river as described in section 4.1.1.

A little right of the main flooding area on the northern riverbank, the flooding of the Biobío river has not reached the city of Concepción. However, taking into account the flooding of other river systems, such as the Andalién river, parts of the more northern regions of Concepción and Talcahuano were also partly submerged in the 2006 flood. (Rojas et al., 2018)

(a) Flooded areas near the mouth of the Biobío river

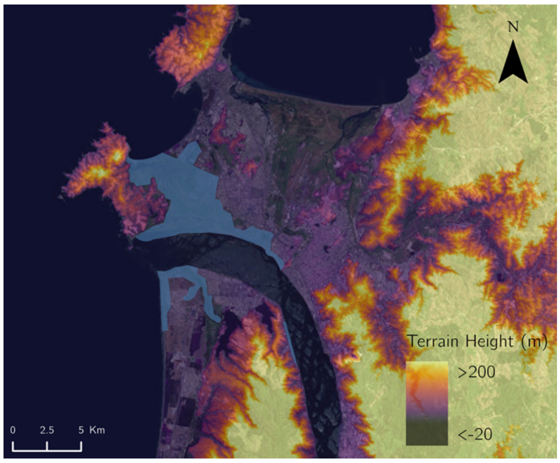

(b) Height elevation near the mouth of the Biobío river

Figure 4.16: Flooded areas visible in blue, shown next to the height elevation of the area (yellow is higher, purple is lower)

Increase in Sediment Transport

Looking at satellite images of NASA taken on the 26th of June 2006 and the 13th of July 2006, visible in figures 4.17a and 4.17b, more information about the flood can be deducted. Figure 4.17a shows the start of the flooding, whereas 4.17b shows the situation a month later. In this last satellite image, an increase in sediment transport is visible in the rivers and the coastal perimeter. Larger discharges are able to transport more sediment into the Pacific Ocean, visible as the brownish sweeps which have grown considerably from the 26th of June to the 13th of July. This increase is even more apparent near the river north of the Biobío river, a bigger brownish flume has formed next to the the river mouth. The sediment from the rivers is transported further south by the ocean currents, evident from the downward curving of the sweeps. Furthermore, the enlargement of the Biobío river due to the excessive water is noticeable.

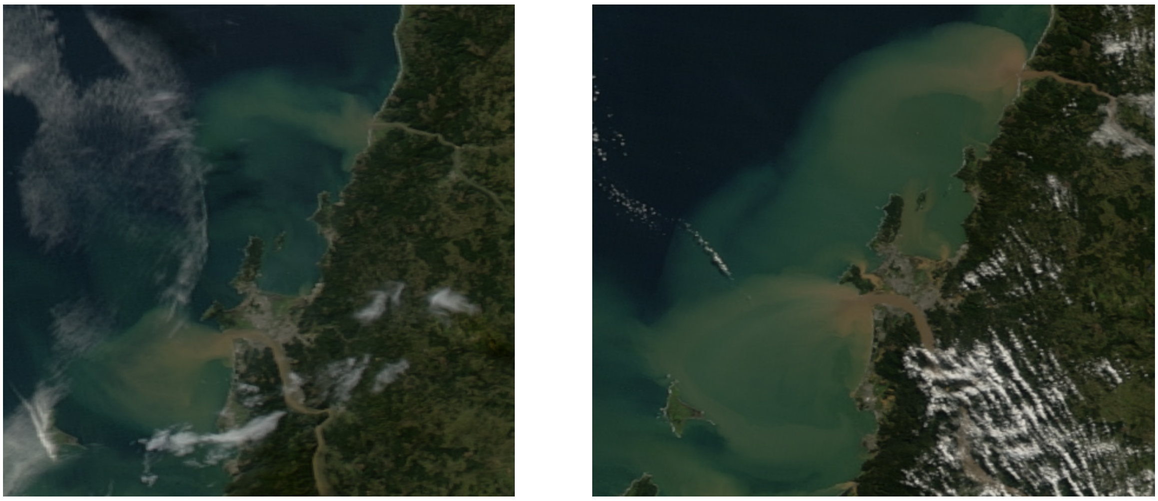

(a) 26th of June 2006 (b) 13th of July 2006

Figure 4.17: Satellite images of the Biobío Region from June and July 2006 (NASA, Earth Observatory, 2019)

More information on the analysis of floodwaves in general and in the Biobío river can be found in appendix B.

4.3.2 *Earthquake and Tsunami in 2010*

The next natural disaster hit Chile on the 27th of February 2010, and caused even more damage. At 03:34 in the morning an earthquake with a magnitude of 8.8 on the Richter scale with an epicentre in the Pacific Ocean woke the population. The epicentre in the ocean was close to the towns of Curanipe and Cobquecura, only 100 kilometres from Concepción, as can be seen in figure 4.18. Not only the earthquake destroyed several homes and important pieces of infrastructure, but also caused a tsunami, which was ruled out by authorities. Due to this miscommunication, parts of the population were not able to evacuate on time. This resulted in a huge loss of life (Montes, 2015). Some facts of the disaster, to underline the severeness, are presented in table 4.2.

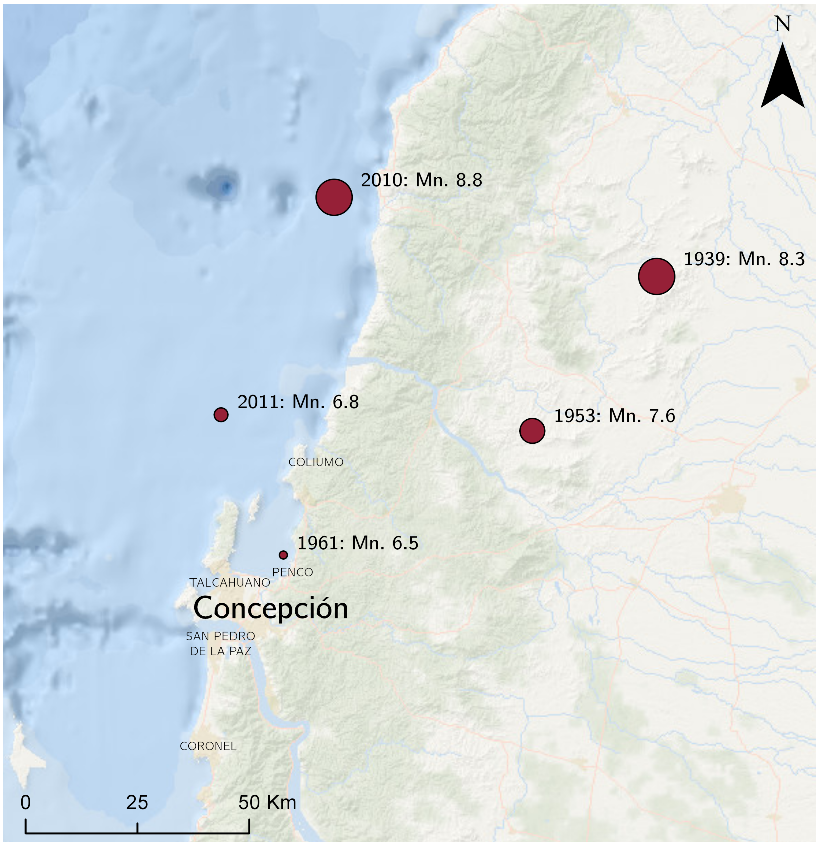

Figure 4.18: Concepción located in the left corner, the epicentre of the 2010 earthquake visible as the big red circle in the top right corner (other two smaller dots are earthquakes from 1961 and 2011)

Table 4.2: Some facts of the flood from the newspaper article Montes (2015), information from ArcGis, from NOAA, National Centers for Environmental Information (2018) and COPRI Chile Earthquake Investigation Team (2013)

Description	**Number**
People affected	>2,000,000
People killed	402
Damaged homes	>500,000
Magnitude on Richter scale	8.8
Distance Concepción moved to the west	3 metres
Tsunami height near Concepción	8 metres

Effects Earthquake

The earthquake with a magnitude of 8.8 on the Richter Scale is reported by COPRI Chile Earthquake Investigation Team (2013) as the fifth largest ever. The shock could be felt in Buenos Aires, Argentina, and São Paulo, Brazil. It even caused a seiche in lake Pontchartrain, Louisiana, approximately 7,000 kilometres from the epicentre. Peak accelerations exceeded 1g in both horizontal and vertical direction, in some locations the accelerations lasted more than 3 minutes (COPRI Chile Earthquake Investigation Team, 2013).

Research after the earthquake proved the inertial load failures caused by the earthquake were much less than expected. The primary cause of failure of coastal and infrastructure structures was soil failure. This included liquefaction, settlement and lateral spreading. Another unexpected result was the uplift and sideward displacement of entire regions. Concepción moved more than 3 metres westward and some areas were lifted upwards with more than 1 metre. These tectonic plate displacements are permanent (COPRI Chile Earthquake Investigation Team, 2013).

In the case of the Biobío river, up- or downlift can change the river characteristics. Uplift could result in flooding as the bed slope is no longer sufficient to force the water down, causing flooding of the surroundings as water cannot pass. Additional dredging is needed to ensure the flow of water through the original channels. Which can be a costly process. Dredging to ensure sufficient berthing depth was performed in the ports surrounding Concepción. Effects of uplift on the Biobío river were not noted, although further research has to show the effects of the earthquake on the bar development as described in section 4.1.3.

Effects Tsunami

The tsunami, of which the first waves hit the coast only 35 minutes after the earthquake, caused even more and more severe damage than the earthquake itself. The focal depth of the earthquake was approximately 30 kilometres (Boroschek et al., 2010). This depth might have limited the magnitude of the tsunami (COPRI Chile Earthquake Investigation Team, 2013). The energy of the earthquake was transferred to the oceanic water body and dispersed in every direction. This is clearly visible in figure 4.19. Not only the coast of Chile was subject to the resulting waves, but these waves were even monitored as far as the United States, Japan and Australia.

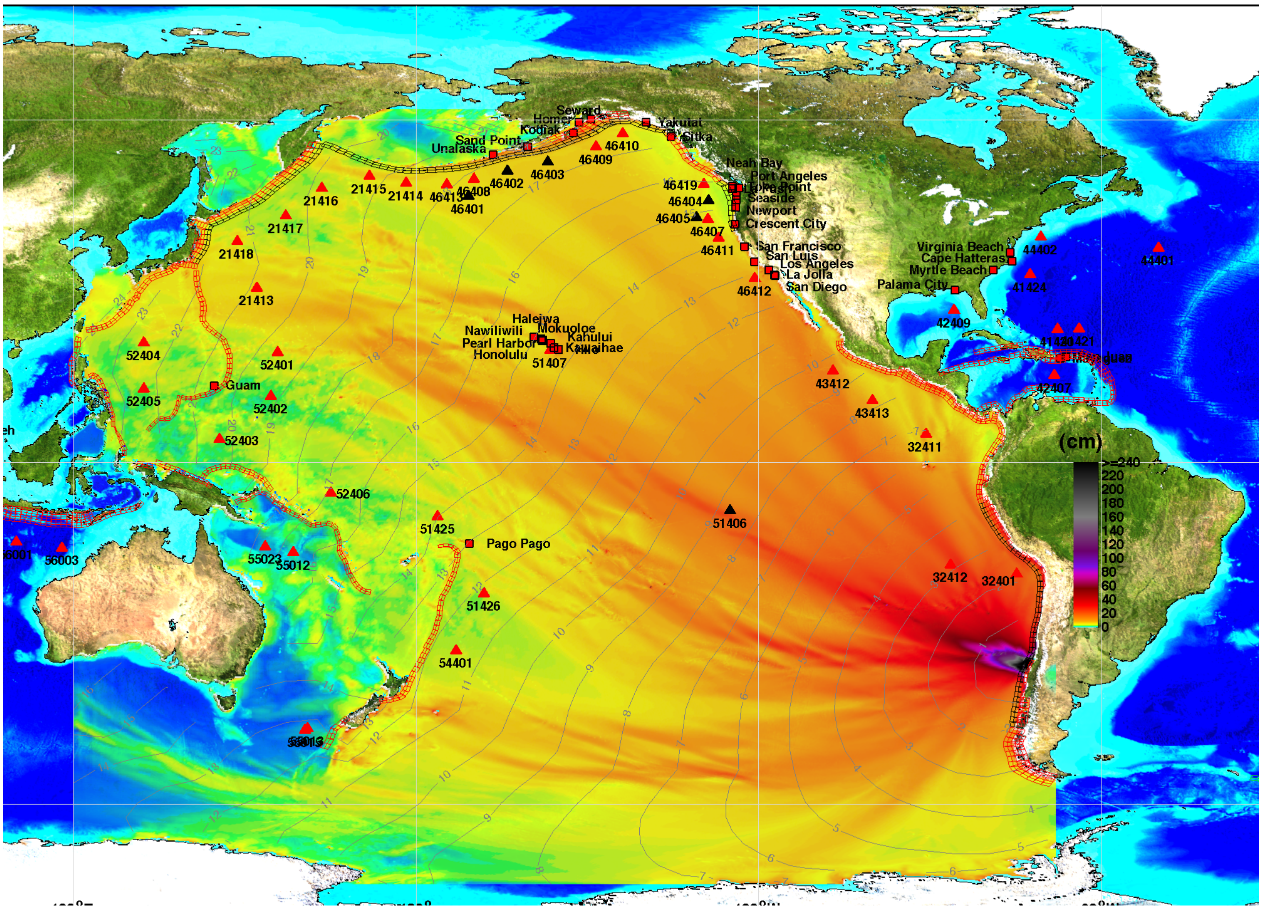

Figure 4.19: The impact of the earthquake and the reach of the tsunami from NOAA Center for Tsunami Research (2019)

The severeness of a tsunami is both caused by the wave height and its reach. The wave height is influenced by the available energy and the near shore bathymetry, as shoaling can lead to significantly higher waves. The reach land inwards is influenced by the wave height, the amount of waves in the tsunami and the topography of the land, as the waves are more prone to propagate in low-laying areas. Unlike most people think, a tsunami is composed of multiple waves, a wave train. The first wave reaching the shore is unlikely to be the highest of the coming waves. This causes significant danger, as people see a relative small first wave and do not expect additional and higher waves. In section 6.3 this is elaborated in more detail.

In the case of the 2010 tsunami four different waves reached the shore of Talcahuano. This port is situated some kilometres north of Concepción and gives the nearest data of the tsunami considering Concepción. The wave height reached between 3.3 to 6.3 metres. The first wave arrived at 3:54, within half an hour after the earthquake, the second at 5:30, the third at 6:00 and the fourth, and last, at 6:40. Of which the third and fourth waves were the largest. This meant there were approximately two to three hours to evacuate the surroundings before the highest waves hit the shore.

Important to note is the fact the earthquake occurred on a falling tide and the tidal waves diminished before the tide rose again, this limited the total wave run-up in the area. The tide and tsunami wave height are visible in figure 4.20. The blue line indicates the expected tidal motion, the red (and green) line show the measured water level. The tsunami reaches the measuring station during the low tide. The measurements stop at 09:00 as the measurement instrument stopped working as a result of the tsunami waves.

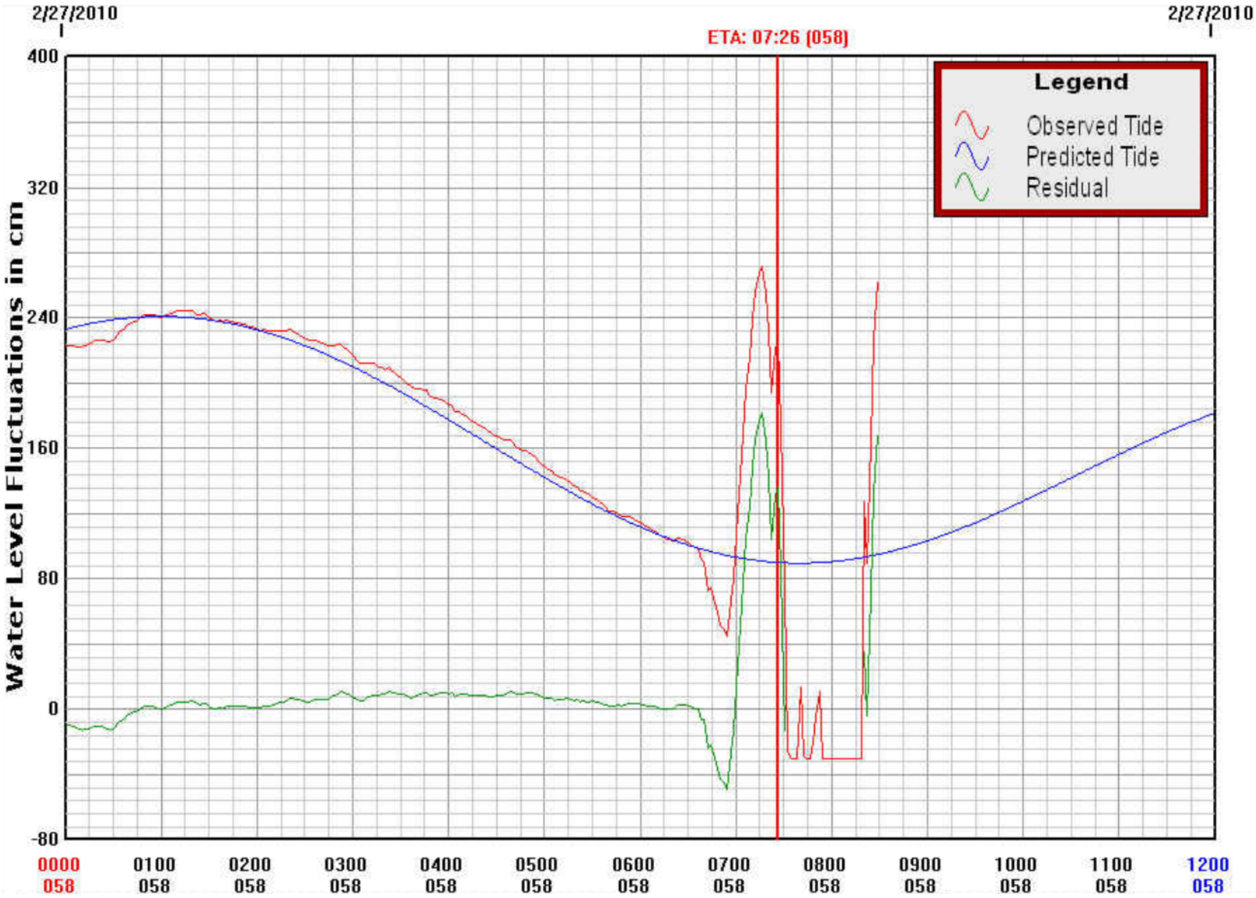

Figure 4.20: The expected tide in blue, the actual water level height in red, from NOAA Center for Tsunami Research and National Weather Service (2019a)

According COPRI Chile Earthquake Investigation Team (2013) the damage from the tsunami included structural failure from hydrodynamic loading, impact from floating objects and scour at foundations. The scour due to the receding flood waves was significant.

For a new railway bridge crossing the Biobío river not only the scour caused by river discharge should be taken into account, but also the scour caused by a receding tidal wave. However, in 2010 the effects of the tsunami in the Biobío river were not significant, but a direct cause for this is still part of research.

II

Models

5

Modelling River Morphodynamics

To study the influence of the river on the new railway bridge a Delft3D model is created of the lower section of the Biobío river. This chapter introduces the created Delft3D model. The area of interest is discussed in section 5.1, which includes the domain-decomposition system and the DD-boundaries. Three grids were created to be able to refine the results locally if desired. The boundary conditions and accounted processes, such as vegetation, sediment and morphology, are discussed in section 5.3 and section 5.4 respectively. Hereafter section 5.5 summarises the calibration and validation process, needed to create credible and usable output.

More detailed information about the set up of the model can be found in appendix C and the detailed input data is summarised in appendix D. Both can assist when altering or modifying the existing model or when creating a new model.

5.1 Area of Interest

Before the model can be created a decision must be made on the area of interest, i.e. the size of the model. The size of the model influences the computational time and if numerical errors can reach the domain of interest, in this project the location of the bridge. Another consideration to be made is the availability of data, in this case the availability of the bathymetry. In section 4.2.1 of the physical analysis the available data for the bathymetry, see figure 4.9, is discussed. From this analysis the observation was made that a large part of the bathymetry consists of offshore data, and that a somewhat smaller data set is available for the river.

One of the considerations, as mentioned above, is the computational time. The computational time depends on: the grid size, time step and the total grid area (in absolute size, not the size of the grid cells). Since the Pacific Ocean is not the main focus in this research, it can be partly omitted from the grid. The result is a smaller grid, and hence a faster model. However, the part of the grid located in the Pacific Ocean is important because of the tidal forcing at this boundary. As a result a certain distance to the river mouth has to be assured to ensure the correct inclusion of tidal forcing.

At the downstream boundary the limitation is the available bathymetry, as can be seen in figure 5.1. The bathymetry data is available upstream of the bridge, however compared to the sea there is less data further from the bridge. The end of the bathymetry data is thus used to mark the end of the area of interest.

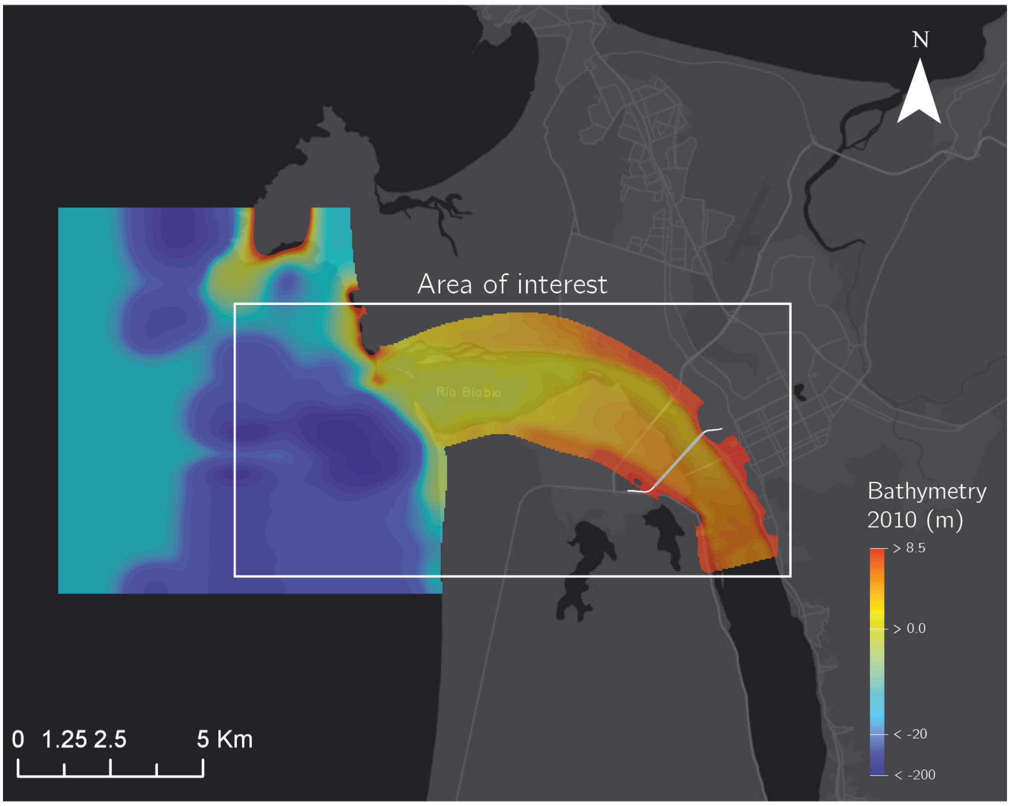

Figure 5.1: Location of the grid and available bathymetry

5.2 Domain-decomposition System

When considering the area of interest, this area is still rather large compared to the area directly surrounding the new railway bridge. This can result in large computation times as observed in the existing Delft3D model of the UCSC, analysed in appendix C, section C.1. However, when modelling systems in Hydraulic Engineering it is preferred to have a model which is as fast as possible, since a faster model can be used more often during the same period of time and hence more different simulations can be run. For an optimal model it is preferred to have grid cells which are as large as possible since this decreases the computational time. However, the size of the grid cells must be such that they can account the smallest features of interest. This means the grid cells cannot be increased freely, for example a channel with a width of 40 m cannot be modelled with grid cells of 100 m.

In this research the main focus is on the river, and to be precise the influence the Biobío river on the new railway bridge. Hence, finer grid cells are preferred in the area around the bridge, whereas at the ocean the use of larger grid cells is allowed. Unfortunately Delft3D-Flow does not allow the use of different resolutions in the same grid, refinement in one direction is possible but then the entire grid in this direction is refined as a result.

The solution for this problem in Delft3D-Flow is to use domain decomposition, which means that the entire domain is decomposed in different grids. This allows the use for different levels of refinement since every subgrid can then be adjusted and refined individually. By using domain decomposition and hence different resolutions for the grid, an optimum is reached in computational time. In this model the grid is divided into three parts, the difference of these three grids is described in table 5.1. Furthermore, in figure 5.2 the approximate size and location of the grids is depicted together with the bathymetry.

Table 5.1: 3 different grids to model part of the Biobío river

Grid name	Situation	Left boundary	Right boundary	Fine/coarse
Left	Sea and river mouth	Tide	DD-Middle	Coarse
Middle	Location of new railway bridge	DD-Left	DD-Right	Very fine
Right	Part of the river upstream from the bridge, location discharge station	DD-Middle	Total discharge	Fine

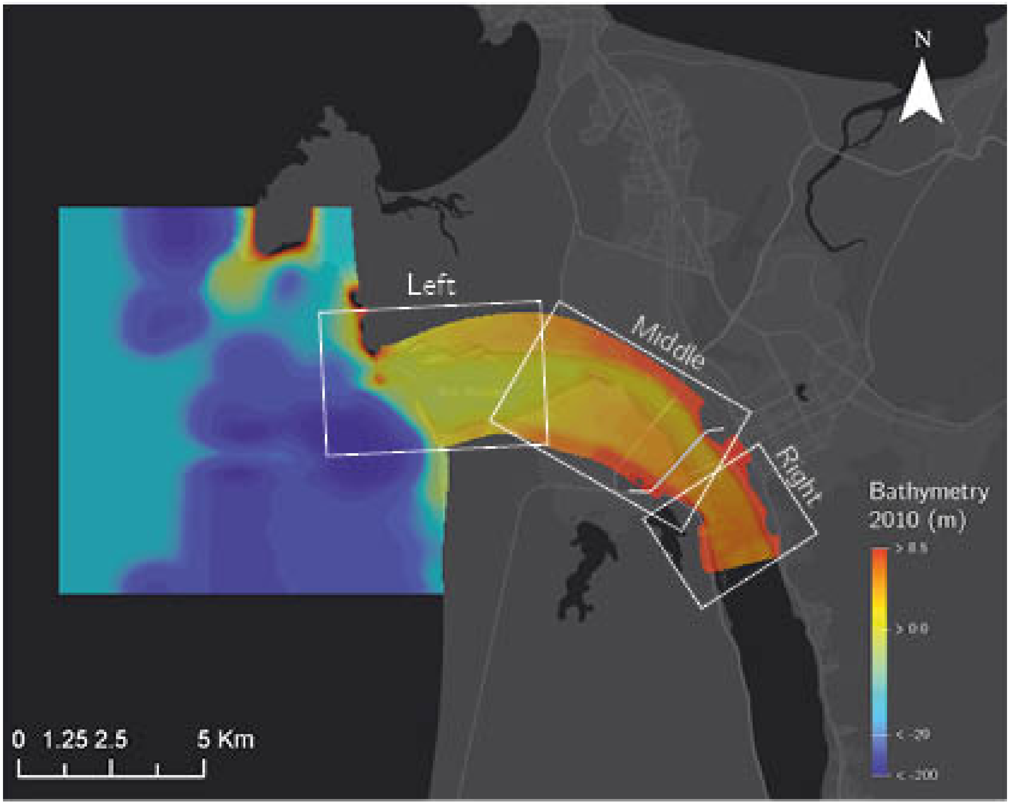

Figure 5.2: Size of the bathymetry and the decomposed grids

As mentioned, the separate grids are connected by a domain-decomposition system, or DD-boundaries for short. In table 5.1 the 'DD-' in the Left and Right boundary column mean a DD-boundary. More information on *Domain decomposition* can be found in section C.3 of the appendix and Appendix B.14 of Deltares (2019b).

In this model the three domains are connected with two DD-boundaries. Each domain requires its own .mdf file with input variables. The input variables of the .mdf are summarised in appendix D.

5.3 Boundary Conditions

For the model both an upstream and a downstream boundary condition are needed. For the upstream boundary condition the information of a discharge station is available, downstream the tidal information is used to create a boundary condition. More information on the boundary conditions can be found in section 4.2.2 and section 4.2.3.

5.3.1 *Discharge*

For longterm morphodynamics, in the order of decades, the upstream boundary condition is set to the effective discharge. This discharge is also used as a default setting for the model. For short term changes, for instance modelling the 2006 floodwave, the discharge is set to actual discharge data, obtained at the discharge station.

To summarise, the discharge in the base version of the model, is set to the effective discharge of: 1671 m^3/s.

5.3.2 *Tide*

The tidal information used to set the downstream boundary condition is summarised in 5.2. More information about the tidal forcing can be found in the previous chapter. For the model a downstream boundary condition is needed. The obtained data, described in section 4.2.2, considers only one month of measurements which is not sufficient to compute the tidal constituents and hence the annual morphodynamic changes. Therefore, this boundary condition is prescribed as an astronomical forcing which uses tidal constituents obtained from Aguirre et al. (2010) and summarised in table 5.2.

It should be noted that there are different methods to obtain the tidal constituents for the area of interest. This option uses the tidal constituents measured some kilometres North of Concepción as described by Aguirre et al. (2010). This method uses four constituents to prescribe the tidal motion. Another option, which could be used in the future, is to use data of more nearby buoy and find a better fit. For this report and model the four constituents are sufficient as the tides do not completely reach the location of the new railway bridge as discussed with Diego Caamaño Avendaño (2019).

Table 5.2: Tidal constituents for the Continental Shelf, which is North of Concepción (Aguirre et al., 2010)

Tidal Constituent	**Amplitude (m)**	**Phase (degrees)**
M_2	0.4100	108.92
S_2	0.1274	100.75
K_1	0.2364	54.58
O_1	0.1596	33.23

5.4 Accounted Processes

The accounted processes of Delft3D are the vegetation, sedimentation and morphology. These processes are of importance when describing the morphodynamics of the river. Processes as salinity and waves are not considered in this Delft3D model since the influence of these processes on the bridge are negligible. However, a more elaborate model can include processes such as salinity and waves. These processes are therefore discussed in the appendix, section C.5.

5.4.1 *Roughness*

The river bar has developed over the years as previously described in chapter 4, section 4.1.3. During the course of several years vegetation such as trees and bushes have started to grow on the river bar. This is also visible in the aerial photos of figure 4.7. This vegetation influences the Manning's Roughness Coefficient significantly.

The Delft3D model uses a uniform Manning's Roughness Coefficient of 0.03 as discussed and advised by our supervisor Diego Caamaño Avendaño (2019). This value is further fine-tuned in the calibration process, discussed in section 5.5.

5.4.2 *Sediment*

The available sediment data was discussed in section 4.2.4, for the modelling a non-cohesive sand with a median sediment diameter of 1000 μm is used.

The settings for the sediment are summarised in table 5.3.

Table 5.3: Sediment data used in morphological Delft3D model

Specific density (kg/m^3)	2650
Dry bed density (kg/m^3)	1600
Median sediment diameter (D50) (μm)	1000

The presence of sand and the absence of waves means the Van Rijn's transport formulas are used by Delft3D. More information about these formulas can be found on pages 332 till 336 of the Manual of Deltares (2019b) and in multiple papers, for instance formula 6 and 7 of Schuurman et al. (2013).

5.4.3 *Morphology*

Regarding the subject of this study and report, the morphology of the model is an important topic. Due to erosion and sedimentation all rivers change, so does the Biobío river. More importantly: how do these changes affect the river as a whole, for instance flow velocities and changing bathymetry? These questions need to be answered to be able to update the Programme of Requirements (POR) according the hydraulic findings.

Computing morphological processes in a numerical model rapidly increases the computation time compared to a 'simpler' hydrodynamic process, as the bed level is updated during the simulation. However, when comparing the timescales of both hydrodynamics and morphodynamics, the latter takes considerably longer to show changes.

This morphological process in the numerical model, can be sped up with the help of a morphological scale factor or for short: MorFac. Deltares (2019b) explains the MorFac as follows: 'The implementation of the Morphological time scale factor is achieved by simply multiplying the erosion and deposition fluxes form the bed to the flow and vice-versa by this scale factor, at each computational time-step. This allows accelerated bed-level changes to be incorporated dynamically into the hydrodynamic flow calculations.' Meaning the bed level is updated after each timestep, (Schuurman et al., 2013):

$$\frac{\delta z_b}{\delta t} = MorFac\left(\frac{\delta q_x}{\delta x} + \frac{\delta q_y}{\delta y}\right)$$

The maximum MorFac depends on the exact situation, a too large morphological acceleration factor can influence the accuracy of the model, whereas a too small factor unnecessarily increases computation time. According to Deltares (2019b) the interpretation of this factor depends on the specific situation: is the modelled area a river or coastal plain? In coastal applications the influence of the tide has to be considered, since the morphological changes during the simulation of one tidal cycle are enhanced by the MorFac. The increase is allowed if the morphodynamics do not significantly influence the hydrodynamics. If this is the case, one simulated tidal cycle is multiplied by the morphological acceleration to find the amount of real simulated tidal cycles in terms of morphological changes. For principally river models, tidal forcings are not present and not taken into account. This simplifies the usage of the MorFac somewhat, as a higher factor means speeding up the morphological changes.

Our area of interest is a combination of a river and coastal system. Downstream, there is a tidal forcing as boundary condition, whereas on upstream the river discharge provides the necessary other boundary. In this case the focus area in this area of interest is the riverbed around the new railway bridge. The influence of the tide at this location is minimal and therefore this part is treated as a river model. Considering the observations of Schuurman et al. (2016) the initial MorFac is set to: 24. This is below the maximum 25 as set by Schuurman et al. (2016) and is easy to work with. 1 Month of simulation represents 24 months of morphological change. As a result, to retrieve a decade of morphological data, a simulation time of $\frac{10 \cdot 12}{24} = 5$ months is needed. Resulting in an approximate running time of the model of 2.5 days. The impact of different morphological factors on the model is part of the sensitivity analysis, chapter 7, section 7.4.

Furthermore, the river morphodynamics are influenced by the bed slope. According to Walstra et al. (2007) the bed slope can affect the transport in the following ways.

1. 'the bed slope will influence the local near-bed flow velocity (hydrodynamic effect not considered here)'

2. 'the bed slope will change the threshold conditions for initiation of motion'
3. 'the bed slope may change the transport rate and/or direction, once the sediment is in motion'

Especially the last is of importance. As also explained by Schuurman and Kleinhans (2013): 'Without the bed slope effect unrealistically narrow bars with extremely steep rims arose. Bars have realistic width length ratios and height when bed slope effect and spiral flow are included. The effect of spiral flow is however much smaller than that of the bed slope effect.' This effect was visible in earlier versions of our model and resulted in errors, causing the model to crash. From our model and also according to Schuurman and Kleinhans (2013), the significance of the bed slope was visualised and could not be neglected. The bed slope effect is still one of the limiting factors of computations, even for programs as Delft3D. The influence of the bed slope effect has to be calibrated, tuning parameters yourself. This tunable parameters are the AlfaBn and AlfaBs values, and cannot be found in the Flow GUI, but in the .mor file (the file containing the morphological information). For the sloping bed load transport Delft3D uses the default Ikeda/Bagnold method, using the following equations (Walstra et al., 2007).

For a longitudinal sloping bed, following Bagnold (1966) and Ikeda (1988) as prescribed in the Flow Manual, Deltares (2019b):

$$\alpha_s = 1 + \epsilon_s \left(\frac{\tan\phi}{\cos(\tan\beta^{-1})(\tan\phi - \tan\beta)} - 1 \right) \tag{5.1}$$

In this equation ϵ_s is the tuning parameter. After the tuning parameters are found with equation 5.1, the adjusted bed-load transport components, $S'_{b,x}$ and $S'_{b,y}$, can be found using the following formulas:

$$S'_{b,x} = \alpha_s S_{b,s} \cos\alpha - S_{b,n} \sin\alpha \tag{5.2}$$
$$S'_{b,y} = \alpha_s S_{b,s} \sin\alpha + S_{b,n} \cos\alpha \tag{5.3}$$

The manual of Deltares (2019b) prescribes the Bagnold equation for the longitudinal slope and the Ikeda approach for the transverse slope. Equation 5.1 changes to:

$$\alpha_s = 1 + \alpha_{bs} \left(\frac{\tan\phi}{\cos(\tan\frac{\partial z}{\partial s}^{-1})(\tan\phi + \frac{\partial z}{\partial s})} - 1 \right) \tag{5.4}$$

In this equation the α_{bs} or AlfaBs, the manual tuning parameter, is evident. α_{bs} is the streamwise bed gradient factor for bed load transport. The transverse bed gradient factor for bed load transport, α_{bn} or AlfaBn, can also be tuned by the user, to calculate the additional bed load transport vector, $S_{b,n}$. This vector is directed normal to the unadjusted bed load transport vector, pointing downwards in regard to the slope.

$$S_{b,n} = |S'_b| \alpha_{bn} \frac{u_{b,cr}}{|\overrightarrow{u}_b|} \frac{\partial z_b}{\partial n} \tag{5.5}$$

More information on this matter can be found in chapter 11.4 of the Deltares (2019b) and Walstra et al. (2007).

As described above, during initial runs of the model, deep and narrow channels developed. After a consultation with Kees Sloff from Deltares, an improvement of the AlfaBn value was suggested: 'You may consider to increase the value of AlfaBn significantly (e.g. a value of 10) to see if narrow deep channels improve. This factor affects the transverse slope effect, which is the gravity component of sediment transport on a slope. With the Bagnold/Ikeda approach that you are using, in combination with Van Rijn transport (your default), very deep 1 grid-cell wide channels will develop unless you increase the AlfaBn. This is a numerical issue.' The AlfaBs value was left unchanged: default: 1.0, but the AlfaBn value was increased to 10.

The morphological information serving as input for the model, is summarised in table 5.4.

Table 5.4: Summary morphological information used as input in Delft3D model

Hydrodynamic time step (seconds)	0.1
Morphological scale factor (MorFac)	24
Morphological time step (seconds)	2.4
Streamwise bed gradient factor for bed load transport (AlfaBs)	1.0
Transverse bed gradient for bed-load transport vector magnitude (AlfaBn)	10.0

For further research, it could be interesting to run the morphodynamics using the 'online' approach as described by Roelvink (2006). This method includes running multiple simulations in parallel, using superpositioning of the results to find a combined and updated bathymetry. As a result short-term variations are taken into account more accurately.

5.5 Calibration

A working model does not necessarily mean the outcome of the model is correct and reliable. To be able to produce credible output, the model needs to be calibrated. First of all, calibration by forward regression can be used to analyse the initial outcomes of the model. The bathymetry of 2010 provides the necessary and detailed baseline. By running the model with a simulation period of 5 years (using an increased MorFac value), the outcomes can be compared with the bathymetry of 2015. Completing different simulations for this time period and changing only one variable at a time, produces (slightly) different outcomes. The results which match best with the real bathymetry of 2015, indicate fitting values for the variables.

The results from a simulation are compared to the measured bathymetry using three cross-sections, the location of the cross-sections are visible in figure 5.3. For each cross-section the bed level from a simulation is plotted against the measured bed level in 2015. As mentioned above the most optimal case is that these bed levels are the same and no differences are observed. However this is not realistic because there are always differences between measurements and simulations. The differences arise from the variability which is present in a natural system. Therefore the aim of the calibration is not to have an exact match between the simulation and measurements, but instead the aim is to represent the natural variability in a correct way. This is done by comparing a boxplot of the bed level from the simulation with the measured bathymetry.

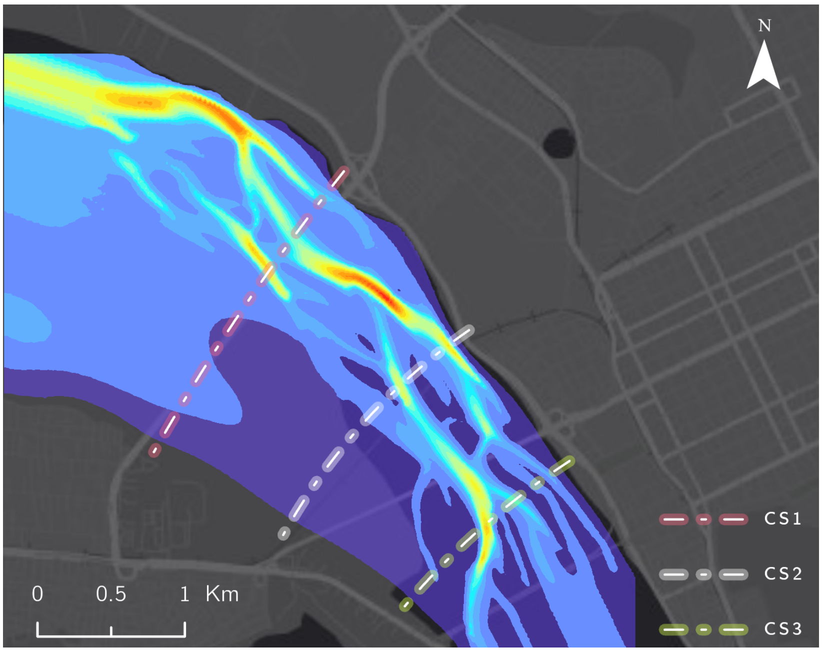

Figure 5.3: Locations of the cross-sections used in the calibration process, where CS2 is the location of the new railway bridge

The following parameters are calibrated for this model:

- Manning's Roughness Coefficient
- Horizontal eddy viscosity
- Transverse bed gradient factor for bed load transport (AlfaBn)

The iteration of these different variables is discussed in the coming sections. The Delft3D-FLOW incorporates numerous other variables, but there was no time to check the calibration and sensitivity of all variables, therefore the calibration is limited to the previous listed variables. The decision to work with these variables is based on discussions with our UCSC supervisor and consultations with Deltares.

All calibration runs were performed using input variables as described in appendix D, while changing one calibration variable at the time. All runs simulate a time period of 5 years, to be able to compare the development of the initial 2010 bathymetry with the surveyed bathymetry of 2015. To spare space only the results concerning the cross-section at the location of the new bridge, CS2, are shown. The graphical results from the other cross-sections can be examined in appendix E.

5.5.1 *Manning's Roughness Coefficient*

Initially the Manning's Roughness Coefficient in the entire model was set to a uniform value of: n = 0.03. However, this resulted in some channels forming on the river bar, which does not match the real situation. After a discussion with our supervisor the Manning's Roughness Coefficient was increased at the location of heavy vegetation on the river bar. This was accomplished by drawing a polygon in QUICKIN and changing the roughness values manually. This new .rgh file was loaded into the FLOW-GUI. The used polygon is visible in figure 5.4. As is visual in this figure, only part of the river bar received a higher roughness coefficient as not the entire bar is covered with vegetation. The area inside this polygon was given a value of n = 0.036 or n = 0.04, depending on the calibration run. These values were advised by Diego Caamaño Avendaño (2019), who used the book byHarry H. Barnes (1967) to come to these values. The Manning's Roughness Coefficient in the remainder of the river was left unchanged, and thus set equal to n = 0.03.

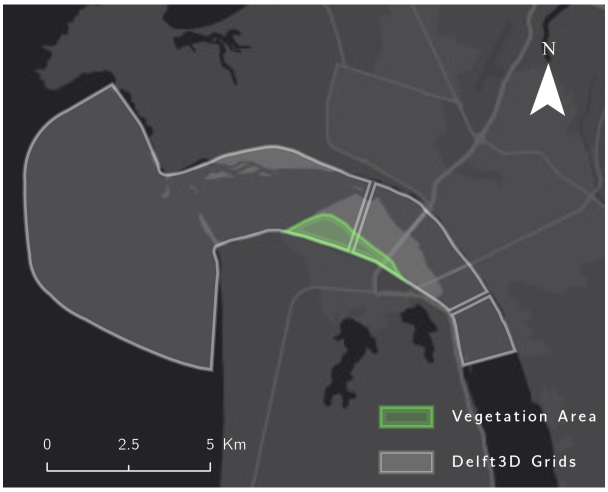

Figure 5.4: Vegetation area drawn as polygon in the Delft3D grids

The result of the calibration runs with the changing Manning's roughness coefficient is shown in figure 5.5.

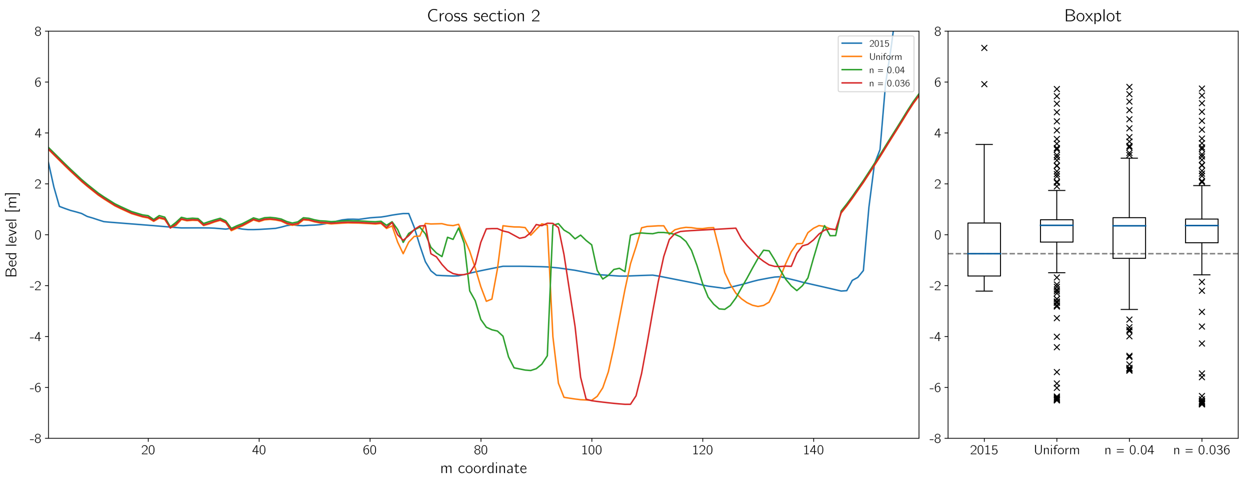

Figure 5.5: Results calibration run concerning the Manning's Roughness Coefficient

Considering figure 5.5, the median of the boxplot with a higher roughness coefficient better matches the real data. The shape of the boxplot of the variation of the roughness value of n = 0.04, matches the boxplot of the 2015 bathymetry variation better. Furthermore, this is also supported by the figures E.1 and E.3 in the appendix. All three cross-sections suggest the use of n = 0.04 for the vegetation on the river bar, as a result this value for the Manning's Roughness Coefficient was used for the polygon. The remainder of the river still has a roughness of n = 0.03.

5.5.2 *Horizontal Eddy Viscosity*

The horizontal eddy viscosity, ν_t, can be calculated with the help of the following formula from Vionnet et al. (2004).

$$\nu_t = \alpha U_* H \tag{5.6}$$

Where:

U_* = Average velocity magnitude

H = Average depth

The same paper states: 'The parameter α, which could be considered the dimensionless eddy viscosity, may range from approximately 0.07 to about 0.30.' This uncertainty prescribes the need of calibrating the horizontal eddy viscosity. Using preliminary numbers from earlier runs, the range for the correct horizontal eddy viscosity was set from 0.4 to 1.0 m^2/s. The latter has been used as upper boundary in the earlier model of the UCSC and was advised to use as a maximum by Diego Caamaño Avendaño (2019).

The result of the cross-section near the location of the bridge CS2, is shown in figure 5.6.

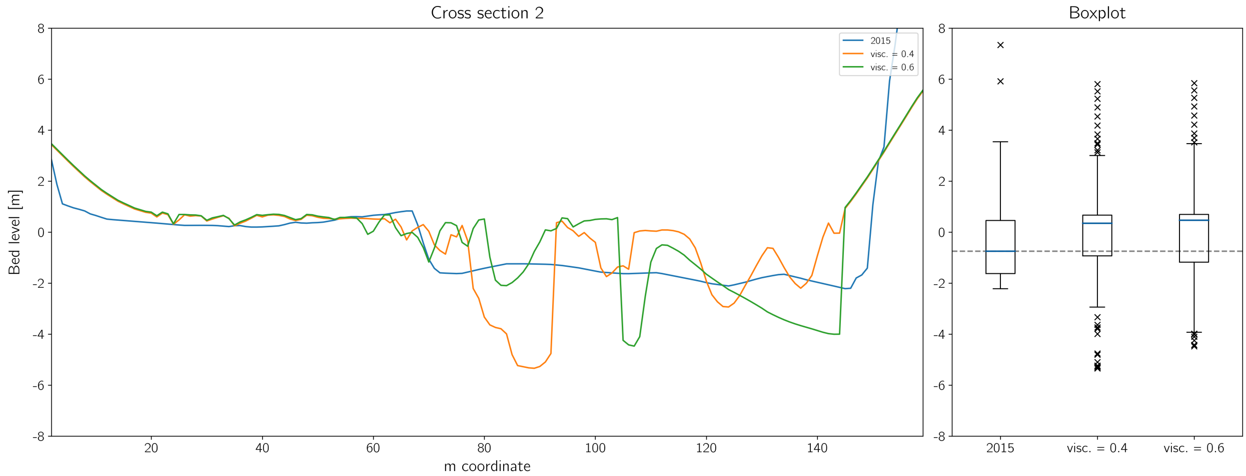

Figure 5.6: Results calibration run concerning the Horizontal Eddy Viscosity

From this figure one can deduce that the median of the boxplot created by the data with a horizontal eddy viscosity of 0.4 m^2/s is closer to the real data compared to a horizontal eddy viscosity of 0.6 or 1.0 m^2/s. Considering figure E.4 and E.6 the shape and values of boxplot concerning a smaller eddy viscosity value, better match the variation of the 2015 bathymetry. Therefore, a horizontal eddy viscosity of 0.4 m^2/s is chosen as calibrated parameter.

5.5.3 *Transverse Bed Gradient Factor for Bed Load Transport*

As discussed before, after a consultation with Deltares, the transverse bed gradient factor for bed load transport (α_{bn} or AlfaBn) was increased from the default setting of 1 to 10. When further calibrating the model, this value was increased slightly more to 15. This value of 15 was used in similar models such as a model of the Columbia River by Moerman (2011). The result at the location of the bridge is visible in figure 5.7.

Although the results at the cross-section of the bridge, figure 5.7, do not show a real difference between an AlfaBn value of 10 or 15, the other cross-sections, CS1 and CS3, show a little difference. Concerning CS1, figure E.7, both medians are close to the median of the 2015 bathymetry boxplot, although the variation following an AlfaBn factor of 10 looks more similar to the variation of the original data. Figure E.9 shows the shape of the boxplot of the AlfaBn of 10 better matches the shape of the boxplot of the real data. Considering the above, an AlfaBn factor of 10 was chosen for the model. However, as differences are limited and both values are not a perfect approach of the real situation, it is recommended to investigate the influence of the AlfaBn on the model in later research.

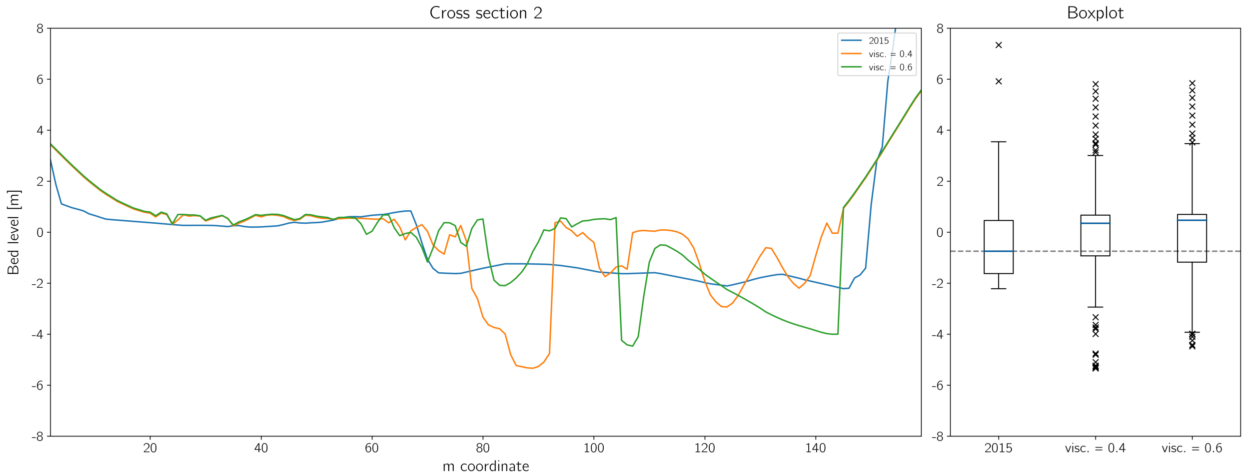

Figure 5.7: Results calibration run concerning the Transverse Bed Gradient Factor for Bed Load Transport (α_{bn} or AlfaBn)

5.5.4 *Streamwise Bed Gradient Factor for Bed Load Transport*

In addition to the transverse bed gradient factor, also a calibration run with a changed streamwise bed gradient factor for bed load transport (α_{bs} or AlfaBs) was performed out of curiosity. The default setting of AlfaBs was changed from 1 to 10, to see how this would influence the morphodynamics. The result near the location of the new bridge is visualised in figure 5.8.

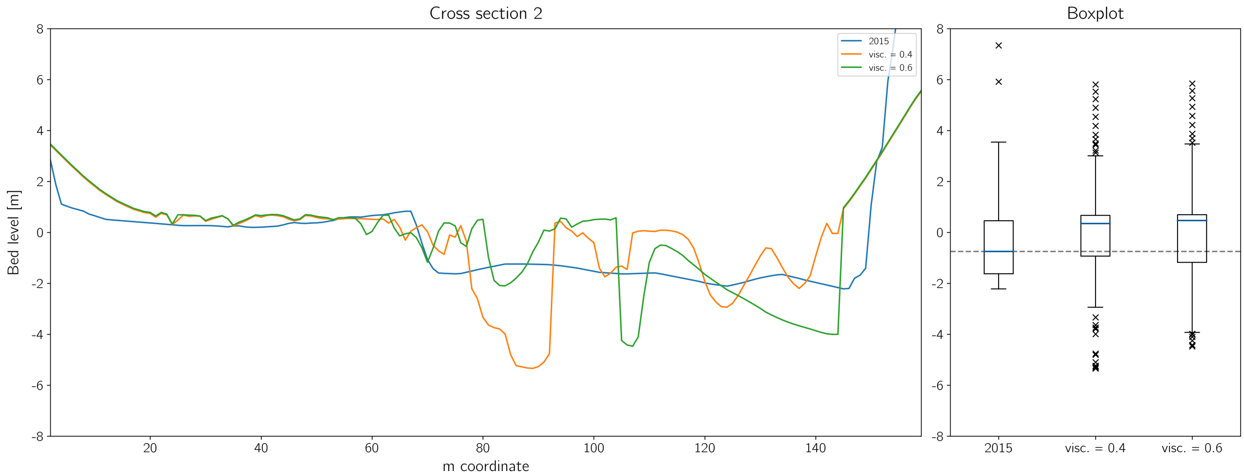

Figure 5.8: Results calibration run concerning the Streamwise Bed Gradient Factor for Bed Load Transport (α_{bs} or AlfaBs)

Considering figure E.10, the variation obtained by an AlfaBs factor of 1 better matches the variation obtained from the 2015 bathymetry. The same can be said for the results visible in figure 5.8, however the differences are negligible. When analysing figure E.12, the differences are also limited, although the median of the data concerning the AlfaBs factor of 1 is closer to the median of the real data. For the calibration of the Streamwise Bed Gradient Factor no definite conclusions can be formed based upon these results. As a result, the default factor of 1 for AlfaBs is used. More research concerning this topic is recommended for the future.

5.5.5 *Chosen Calibration Parameters*

The chosen parameters from the calibration process are summarised below:

- Manning's Roughness Coefficient: n= 0.03 river and n= 0.04 river bar
- Horizontal Eddy Viscosity: 0.4 m^2/s
- AlfaBn (α_{bn}): 10
- AlfaBs (α_{bs}): 1

6

Modelling Tsunami Influence in a River

Tsunamis are one of the most infamous natural disasters nowadays and for Chile a quite important one as well, as described in section 4.3.2. The name comes from the Japanese word 'harbour wave' and are mostly caused by a fault event in the Earth's crust (Stuhlmeier, 2009). However, tsunamis can have other origins, e.g. landslides or volcanic activity.

Concepción, the Biobío river and the new railway bridge are all located near tectonic plates that show movements of about 72 mm/year, figure 6.2. A tsunami can originate from moving tectonic plates and is likely to reach great height when entering the coastal zone, it is therefore necessary to assess the influence, e.g. hydraulic pressure and sedimentation/erosion, a tsunami could possibly have on the river and the bridge.

Properly modelling a tsunami is not an easy task. However, with the development of multiple numerical models over time this is becoming easier, one of this models is the NeoWave software, which can approximate tsunamis.

In this chapter the most relevant information is described regarding the origin of a tsunami, this to stay within the scope of the project. More background information is described in F.

In section 6.1 the fault movement mechanism which may cause a tsunami is described. Followed by the dynamics and processes that take place for a tsunami wave in the coastal and deep water zone in section 6.2. The link between the magnitude of an earthquake and the model are elaborated in section 6.3. At last, the NeoWave model is described in section 6.4.

6.1 Origin of a Tsunami: Fault Movement on the Seafloor

The most well known source of a tsunami is an earthquake. Though technically speaking this is not fully correct. Since an earthquake and tsunami are generated by a fault movement of the seafloor, the earthquake is not the actual source, but the fault movement is. In this description a fault is defined as a weak spot in a planar zone passing through the earths crust (ITIC, nd). An example of this mechanism is shown in figure 6.1.

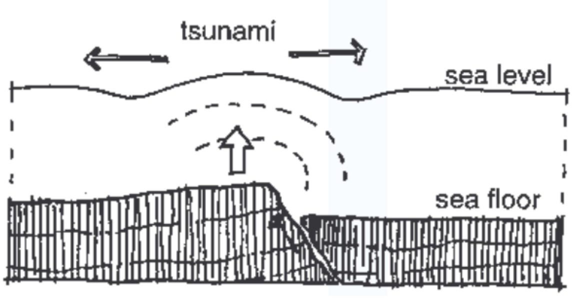

Figure 6.1: Example of a tsunami caused by a fault movement of the seafloor, from ITIC (nd)

In general, earthquakes have three failure modes to induce a tsunami, either by strike-slip, dip-slip or thrust-slip (Bryant, 2014). These failure modes depend on the kind of fault zone. In Chile the dip-slip failure is primarily present, as the fault zone is characterised by an oceanic plate diving under a continental plate (National Geographic, 2019).

Plate Tectonics near Chile

Since the origin of most tsunamis can be related to the earths' tectonic plates, it is needed to elucidate the theory. However, as the earth is a complex system and the domain of the project is in Chile, the focus from this point is towards the mechanisms that take place in front of the Chilean coast.

At the coast of Chile, the system can be described as a submerging oceanic plate (the Nazca Plate) and a drifting continental plate (South-American Plate) (ESRI, 2019; USGC, 2019). This mechanism is also known as a convergent plate movement, or subduction zone. The movement of the plates is visualised in figure 6.2.

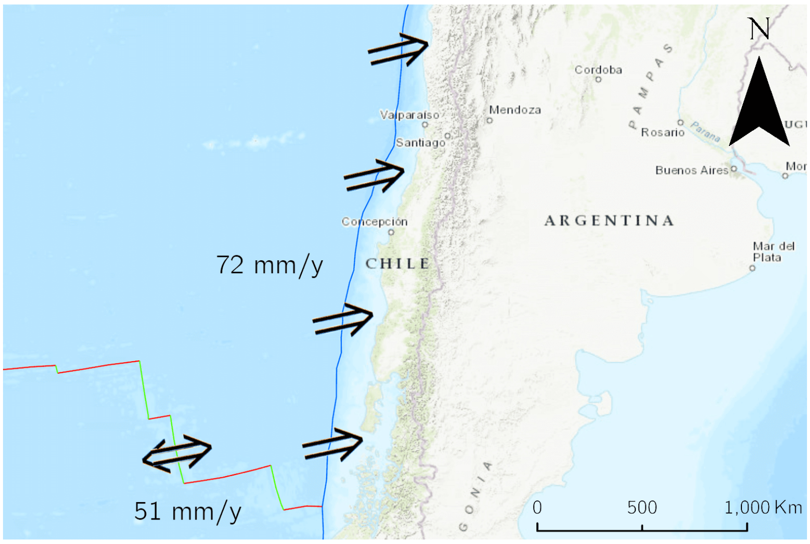

Figure 6.2: Movement of the tectonic plates near Chile relatively to each other (USGC, 2019)

Displacement of the Water Body

As a consequence of the oceanic plate diving underneath the continental plate, a lot of tension is stored. Since the continental plate is unable to slide over the oceanic crust due to friction its tip is taken along. If the stress reaches a certain threshold in the oceanic crust, the continental plate slips back to its original position. This results in an earthquake, which could possible lead to a tsunami. Generally speaking a tsunami is triggered if the earthquake is larger than 7.0 M_s (Bryant, 2014). This process is visualised in figure 6.3.

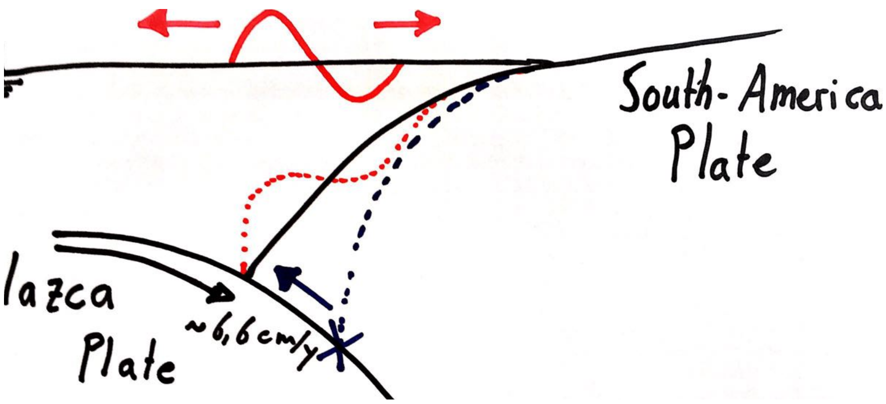

Figure 6.3: Sketch of the process in the subduction zone in front of the coast of Chile

As the continental plate slips back with violent force, the crust creates a wave like pattern in its displacement.

In case of a dip-slip mechanism, the side where uplift occurs, generates a wave with a leading edge. On the side of subsidence a trailing edge travels up front (Murata et al., 2009).

Subsidence or Elevation of Land
As mentioned before, an earthquake in a subduction zone leads to an uplifted and subsidence area. In a hypothetical case that the river mouth is subsided, the tsunami wave train has an easier way of entering the river and travelling further upstream. As this is a worst case scenario it is interesting to review the effect on the loads close to the planned location of the bridge bridge.

Quite some literature elaborate on seismic cycles theories (Bryant, 2014; McGuire, 2008; Zöller et al., 2006). A seismic cycle can be described as a period in which a crucial amount of stress has built up at the plate margins and is released in a large earthquake. This cycle also results in the periodic subsidence and elevation of landmass near the plate borders of converging plates. The predictability of these seismic cycles are still inaccurate. McGuire (2008) tried to find a correlation between large events, though he was not very successful in finding a strong correlation between the moment ratio and the interevent interval.

6.2 Tsunami Dynamics

A tsunami wave can be considered a long wave in shallow water as soon as it is generated. This is due to the fact that a tsunami has a sizeable wavelength, in the order of hundreds of kilometres, compared to the average water depth of 4 kilometres in the Pacific. As soon as the wave is generated, the energy spectrum of the wave is affected by processes that are accounted for in shallow water (Holthuijsen, 2007):

- Quadruplet wave-wave interactions
- Triad wave-wave interactions
- White-capping
- Bottom friction
- Depth-induced surf breaking

As a wave enters shallower water, the wave undergoes the basic processes of shoaling, refraction and diffraction. These processes are described in more detail in F.2. However, in coastal zones a tsunami wave most often does not break. Therefore, other (non-linear) processes are taking place to ensure the structurability of the wave. Some assumptions in the shallow water wave theory are thus no longer applicable for the wave propagation near the shore Bryant (2014).

Non-linear Behaviour of Tsunamis
If the tsunami is located in deep water, its behaviour resembles that of linear waves in deep water. Yet a tsunami is a very long wave, which can be stable in very shallow water. Therefore the non-linear effects of waves are expected to play a more significant role when describing this waveform. Pelinovsky et al. (2001, 2006) concluded that the linear wave equations describe the tsunami wave well enough, yet an exception should be made for the resonance waves and tsunami waves with a wave length in the order of 100 m to 10 km. These resonance waves can be described by the Korteweg de Vries (KdV) equations. As for the relatively short tsunami waves, the non-linear dispersive effects become important as well (Pelinovsky et al., 2006) and can be described by the KdV equations too.

The KdV equation describes a balance between the dispersion and non-linearity, which is a very interesting derivation, but beyond the scope of this report. Therefore, for more information a reference is made to Stuhlmeier (2009) or Pelinovsky et al. (2006).

The Influence of a Submarine Canyon
After the 2010 earthquake near Concepción the tsunami that was generated propagated into the many rivers in the Biobío region. Except for the Biobío river. It is thought to be due to the influence of the submarine canyon in front of the river mouth of the Biobío river. To assess this influence Aránguiz and Shibayama (2013) used a numerical model with an idealised and simplified bathymetry to explore the effects of the submarine canyon.

Aránguiz and Shibayama (2013) concluded that submarine canyons have a strong influence on both the propagation and run-up of a tsunami. Mostly due to the influence of the length and width of the submarine canyon and in lesser extent the depth. A submarine canyon primarily induces a diffraction effect on the wave front. Leading to a refraction effect as well since the wave turns even more normal to the canyon edge.

Due to these processes the wave front enters the Gulf of Arauco in the same direction, regardless of the origin of the tsunami. Besides the effect of the submarine canyon, the island of Santa María is an important factor as well since it causes a diffraction pattern (Aranguiz, 2012; Aránguiz and Shibayama, 2013). This effect is shown in figure 6.4.

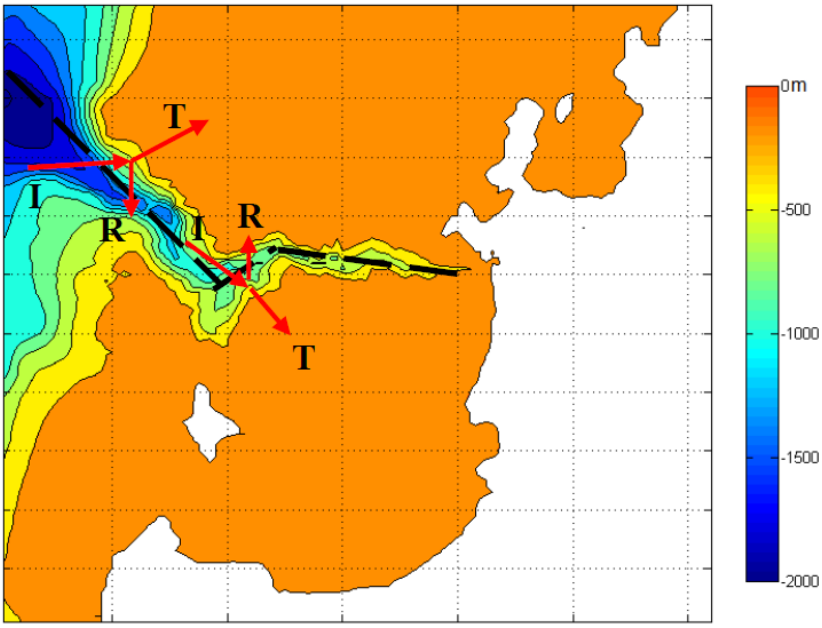

Figure 6.4: Bathymetry of the Biobío canyon, with contour lines every 200 m. The dashed lines represent the main segments of the canyon and the red arrows shows incident (I), reflected (R) and transmitted (T) tsunami waves (Aranguiz, 2012)

6.3 Magnitude of an Earthquake and Resulting Tsunami

The potential of an earthquake and subsequently of a tsunami both depend on the magnitude of the earthquake. The magnitude can be expressed on many different scales (Kanamori, 1983). For example, the moment magnitude scale (M_W), the Richter scale (M_L) and the Mercalli scale. Nowadays, the moment magnitude is most common to use, as it can be applied globally and is more accurate for large scale events (UPSeis, 2007).

The moment magnitude is a physical quantity that is related to the slip on the fault, multiplied by the total area of the fault. This gives the relation to the total amount of energy that is released during an earthquake. To calculate the moment magnitude one first needs to determine the seismic magnitude (M_0), from Martínez and Aránguiz (2016):

$$M_0 = \mu L w D \tag{6.1}$$

The seismic magnitude is considered reliable as it depends on the length and width of the fault, L and w respectively, as well as the displacement, D. The moment magnitude is an empirical relation based on the seismic magnitude. The moment magnitude shows uniform behaviour for all magnitude ranges as it has a directly proportional relation to the logarithm of the seismic moment (Scordilis, 2006). This relation is composed by Kanamori (1977); Hanks and Kanamori (1979) as:

$$M_W = \frac{2}{3} \log M_0 - 10.7 \tag{6.2}$$

Some remarks about the moment magnitude are of importance. Since it is primarily derived for earthquakes with a $M_S \geq 7.5$ (surface wave magnitude scale), it is interesting to see how the relation resembles smaller magnitude earthquakes Scordilis (2006). As the full derivation of the moment magnitude goes beyond the scope of this project, a reference is made to Kanamori (1977) and Hanks and Kanamori (1979) for further elaboration.

6.3.1 *The Okada Model*

By computing the magnitude of the earthquake, one does not exactly know how the sea floor has deformed. However, this deformation is needed to compute the resulting tsunami. To approach the deformation of the sea floor, and subsequently the tsunami, Okada (1985) derived an analytical model for this purpose. This model is also known as the Okada model and is applied in many numerical simulations as Delft Dashboard and NeoWave.

This model translates the slip of the fault plane onto the seafloor deformation, assuming a flat homogeneous isotropic elastic sea bottom. Therein distinguishing the difference between a single point source and a finite rectangle fault sources (Okada, 1985). A more realistic view is given by the finite rectangle fault source, this uses an uniform displacement over the area.

The deformation is derived by using the length and width of the fault plane (Okada, 1985, 1992). Besides this, also the strike, dip and rake angle are of importance, as well as the actual slip and centroid depth of the fault. Where the slip can be seen as the displacement of the fault, the strike is defined as the orientation of the top edge in relation to the North. Okada (1985) defined the dip as the angle normal to the fault plane and the plane where it dips downward. The rake is defined as the angle in which the slip occurs, also known as the slip angle (Clawpack, 2019). For a clear overview, the parameters needed for the Okada model are shown in figure 6.5.

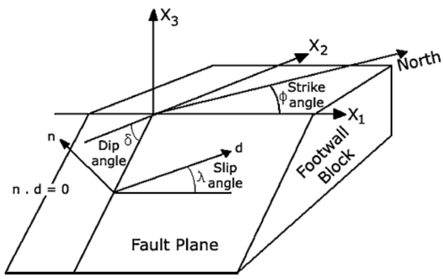

Figure 6.5: Visualisation of the parameters used in the model of Okada (1985), retrieved from Khan (2011)

Using numerical simulations Okada (1992) visualised the deformation of a cube subjected to strike-slip, dip-slip and tensile fault. This visualisation is shown in figure 6.6. These numerical simulations are based on an adjustment of the previous analytical expressions derived by Okada (1985) to better resemble the finite rectangle fault plane for all kind of faults. The Okada model is considered as a fairly accurate tool determining the deformation of the seafloor and thus the subsequent tsunami.

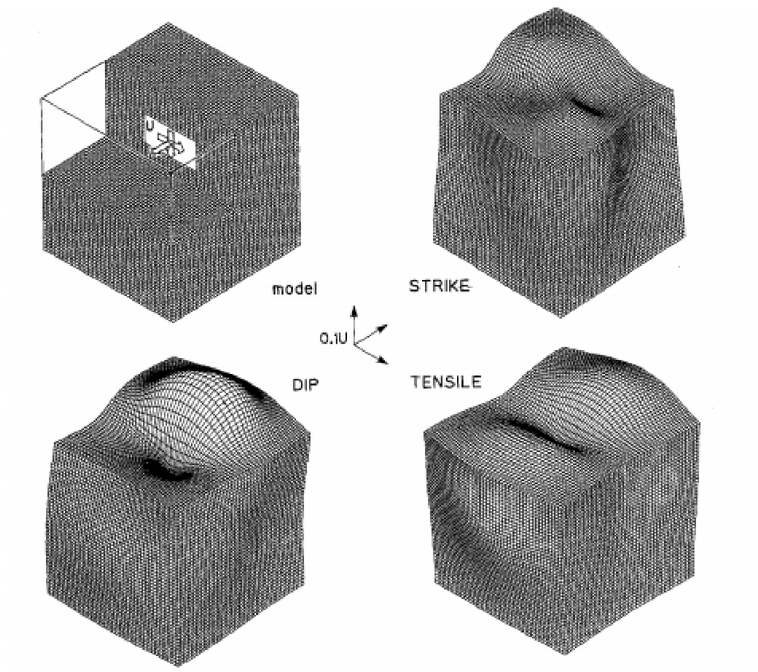

Figure 6.6: Deformation of a cube subjected to a strike-slip, dip-slip or tensile fault (Okada, 1992)

6.3.2 *Resonance Modes*

As a tsunami wave train approaches the shore the shoaling and refraction processes cause the waves to grow. It is a popular belief that the first wave is the highest wave in the wave train. Although, depending on the bathymetry and topography, the second or third wave can be even higher. This is due to the fact that a bay has a certain eigenfrequency. This eigenfrequency can be excited as the period of the waves are in the order of $T = \frac{4L_b}{\sqrt{gd}}$. Where L_b is the length of the basin (Bryant, 2014). This type of resonance is described as seiches.

Other occurrences of resonance at shores after a tsunami, can be described as captured waves in the coastal zone. This is due to the fact that part of the incoming wave energy is reflected back seawards. Although the waves are still in shallow water, the wave refracts back towards the shore. At a different location this can lead to two positive amplitudes arriving at the same time, coinciding and giving rise to an even higher amplitude wave. This is called shelf resonance and can lead to even bigger wave heights than the initial wave height of the tsunami. Yamazaki and Cheung (2011) studied the propagation of the nodes and anti-nodes of the 2010 earthquake in Chile, of which the slow direction of the standing waves varies. Leading to onshore waves origination from different directions at different times.

6.4 Introduction to NeoWave

NeoWave stands for Non-hydrostatic Evolution of Ocean WAVE and was developed to increase the possibilities of modelling long-wave propagation, run-up and transformation (Yamazaki et al., 2009). In numerical models, explicit schemes are often used and sufficient for the application in modelling of tsunamis and their associated flood hazard. However, these explicit schemes have problems modelling wave breaking and dispersion. These schemes are based on the non-linear shallow water equations (NLSWE) by applying a finite difference method to make it easier to implement the schemes into a model. Another issue that arises, is the fact that finite difference schemes for the NLSWE are non-conservative, resulting in loss of volume and energy dissipation at increasing wave steepness and flow approaches a discontinuity. This becomes very significant when modelling a tsunami (Yamazaki et al., 2009).

6.4.1 *Description of the Model*

For the NeoWave model Yamazaki et al. (2009) derived the non-hydrostatic depth-integrated free surface flow from the incompressible Navier-Stokes equations and the continuity equation. The NeoWave model uses the momentum-conserved advection scheme and the non-hydrostatic formulation to the non-linear shallow water model created by Kowalik et al. (2005). The program has been written in FORTRAN and has a modular structure that allows the selection of various numerical schemes. This way, one is able to use the model for specific applications (Yamazaki et al., 2009). These applications include tidal waves and tsunamis.

When modelling a tsunami, a smart way to decrease computing time, while keeping a large spatial domain, is grid nesting. As NeoWave is developed to model long-waves a large spatial domain is needed to properly visualise the propagation, transformation and run-up. This means that grids of different sizes and resolutions are used: increasing the resolution in areas where an exact solution is needed (Yamazaki et al., 2011). To prevent instabilities and errors in the grids one should ensure that the starting nodes of the smaller grids are on the same location as a node of the bigger grid.

6.4.2 *Numerical Model*

The numerical formulation of the NeoWave model is divided into a hydrostatic part and a non-hydrostatic part. The hydrostatic model consist of an explicit scheme characterised as the upwind scheme. The upwind scheme in NeoWave can either be first or second order in which the latter accounts for non-linearities. Many non-linear shallow water modes, are not able to capture flow disruptions associated with breaking waves or hydraulic jumps. For this Stelling and Duinmeijer (2003) derived an alternative discretisation which can be used in the NeoWave model.

6.4.3 *Comparing to Other Models*

NeoWave is not the only numerical model that is able to compute the propagation and flooding of non-linear waves. Another model is Delft 3D - Dashboard. Whereas Dashboard is a standalone Matlab based program which uses online sources for for instance the bathymetry and locations of tide stations. With this model the wave propagation of a tsunami can be modelled fairly easily. One must bear in mind large areas of interest mean large grids and nesting is not implemented easily. As a result for high resolution, large output files are expected, making it difficult for QUICKPLOT to process the outcomes smoothly. As Dashboard is a model maker programme and Delft3D is the computing core, one can set up a model in Dashboard and load it into the Delft3D shell to run the model.

On the basis of numerical schemes the difference between Dashboard and NeoWave can be clearly distinguished. Where NeoWave uses a upwind (hyperbolic) scheme, Delft 3D uses an Alternating Direction-Implicit (ADI) method. This means that one time step is split into two, leading to second order accuracy in space. Depending on the choice for the order of the upwind scheme used in NeoWave, the order of accuracy can be the same.

The spatial discretisation of horizontal advection terms has three options in Delft3D: the WAQUA-scheme, the cyclic method and the flooding scheme. The latter can be used for hydraulic jumps and bores. For more technical elaboration about the schemes a reference is made to the user manual of Deltares (2019b).

The use of the different schemes clearly distinguishes the use of modelling possibilities for each model. As Delft3D is used for a broad spectrum of modelling cases it is a robust model, though losing some significance in specific cases of for example a tsunami. Which can be modelled in more detail with NeoWave.

6.5 Setting up the NeoWave Model

To be able to model a tsunami properly, one has to have the basis of the model well thought out. This is done by placing the grids of different resolutions at the correct locations and simulate an earthquake which is hypothetically possible. In this section the steps for setting up the model used to assess the hydraulic influence on the bridge are elaborated. The set up follows the same steps as was done by Aránguiz et al. (2015) and Martínez and Aránguiz (2016) for the Illapel earthquake and tsunami in 2015 and a tsunami risk assessment near San Pedro respectively.

6.5.1 *Staggered Grid*

Based on the source of the earthquake multiple level grids are created to assess the tsunami wave. For the creation of the grids an excel sheet was used to compute the necessary locations of the corner grid cells. Then by applying a certain grid size, one can create a rectangular grid. The smaller grid, with a higher resolution can, by using the same steps as before, be created within the bigger grid. Repeating these steps once more gives the final grid for the Biobío river. The resulting grids are shown in figure 6.7.

The different grid levels require different resolutions. For stability reasons this means that the time steps are different for each grid, these values are summarised in table 6.1

Table 6.1: Summary of grid characteristics

Level	**Resolution**	**Time step** (Δt) [s]
Grid 1	120"	1
Grid 2	30"	0.5
Grid 3	6"	0.25
Grid 4	1"	0.0625

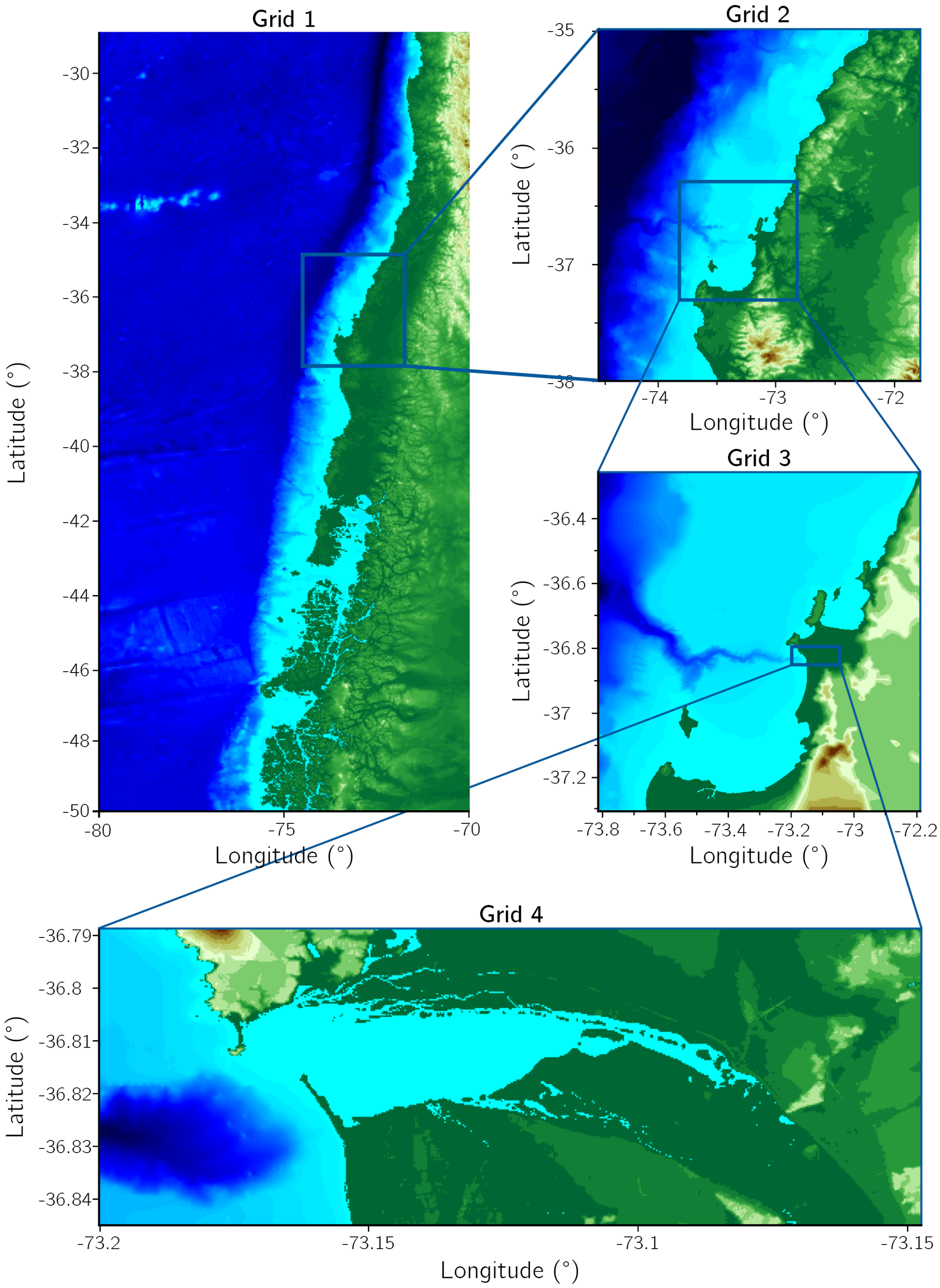

Figure 6.7: Grids used in the NeoWave simulation

6.5.2 *Bathymetry in the Grids*

To assess shoaling, refraction, diffraction processes the bathymetry is needed. The bathymetry of the different grids does not differ, though on a smaller scale, one is able to see more differences in depth. This processing is carried out with Globemapper.

The first, second and third grid contain a combination of the bathymetry data of GEBCO and nautical charts of SHOA. The level 4 grid requires more adjustments, the bathymetry of the river in Globemapper is not very accurate and a lot of information is missing. By adding the bathymetry of 2010 used for the Delft3D into the program, a high resolution bathymetry is created for the Biobío river. This data is accurate enough to be used for the level 4 grid.

6.5.3 *Location of Observation Points*

To visualise the data created in the model a few observation points need to be placed. In the NeoWave model this is done by placing tide gauges. Though these points can be seen as observation points for this assessment.

To see whether the tsunami wave reaches the location of the new bridge some points are placed on the location of the old bridge. As this bridge is located around 50 meters downstream of the new one, this will be sufficient for the assessment.

Three points along this bridge are placed, the first one in one of the main channels, the second in a shallower channel (transition zone) and the third on the sand bar. By doing this a clear distinction can be made on what forces act on what part of the bridge. This is needed for the design, chapters 9 and 11. In figure 6.8 the location of the observation points is shown.

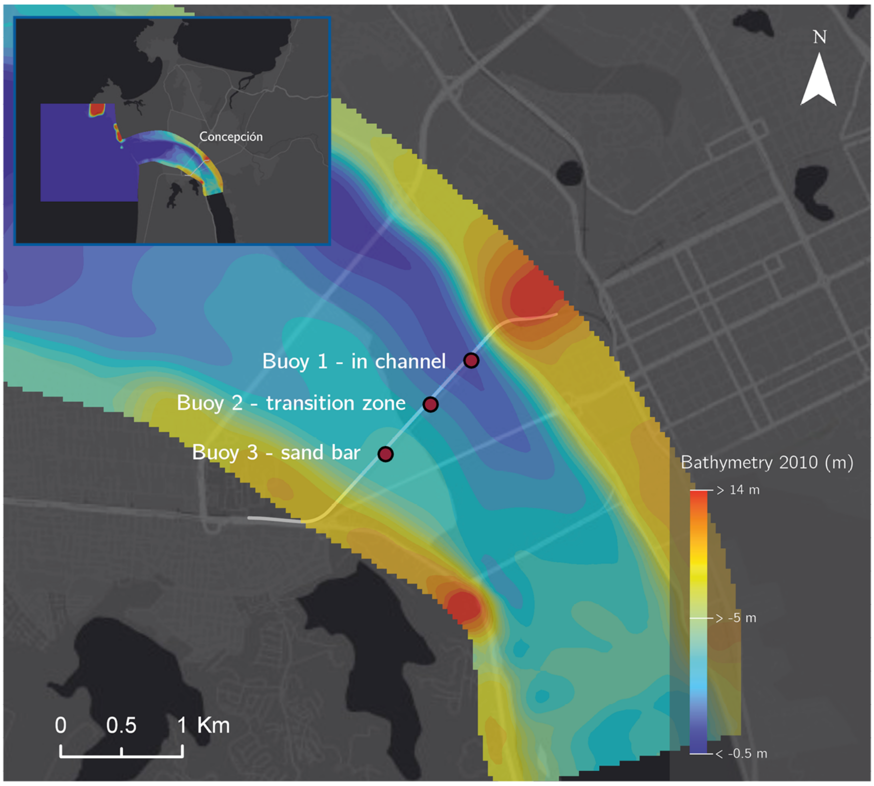

Figure 6.8: Location of the observation points in the smallest grid of the Biobío river tsunami model

7
Results

In this chapter the results of both models, the Delft3D (section 7.1) and NeoWave model (section 7.2), are summarised. Based on these results a recommendation for the hydraulic aspects of the Programme of Requirements (POR) can be formed in section 7.3, the POR is further discussed in chapter 8. Lastly, a sensitivity analysis for the Delft3D model is performed, to investigate the sensitivity of certain parameters on the model.

7.1 Delft3D - Modelling River Morphodynamics

This section is split into two subsections, first the different scenarios are elaborated after which the results of these scenarios are presented in the second subsection.

7.1.1 *Scenarios*

Three different scenarios are simulated using the calibrated Delft3D model: one long-term scenario and two short-term scenarios. Each scenario is briefly discussed in the coming paragraphs.

Long-term - 10 years
For the long-term morphodynamic changes of the Biobío river the calibrated model is used and run for a simulated period of time of 10 years. The collected data provides the morphological changes for a decade. Both the tidal constituents and the effective discharge, as discussed in section 5.3 are used in this simulation. The input information, differing from the original model as described in chapter 5 and appendix D, is summarised in table 7.1.

Table 7.1: Input Parameters Delft3D Model - long-term simulation, 10 years

Description	**Value**
Simulation start time	28 06 2019 00 00 00
Simulation stop time	15 11 2019 00 00 00
MorFac	24 [-]
Simulated time	10 [years]
Discharge	Effective: 1671 [m^3/s]

Short-term - 2006 Floodwave
As discussed in section 4.3.1 in 2006 a floodwave flood the Biobío river system, this floodwave is simulated with the Delft3D model. The input information, differing from the original model as described in chapter 5 and appendix D, is summarised in table 7.2. This short-term model differs in MorFac value and thus simulated time.

Table 7.2: Input Parameters Delft3D Model - short-term simulation, 2006 Floodwave

Description	**Value**
Simulation start time	28 06 2019 00 00 00
Simulation stop time	12 07 2019 00 00 00
MorFac	1 [-]
Simulated time	14 [days]
Discharge	Input from table 7.3

Table 7.3: Discharge during the 2006 flood from Gobierno de Chile (2019)

Date (dd-mm-yyyy)[1]	**Discharge (m^3/s)**
06-07-2006	1656
07-07-2006	1741
08-07-2006	2626
09-07-2006	2696
10-07-2006	2647
11-07-2006	5271
12-07-2006	13746
13-07-2006	9771
14-07-2006	6115
15-07-2006	4450
16-07-2006	3631
17-07-2006	3209
18-07-2006	2882
19-07-2006	2912

Short-term - 100 year return period

The EFE uses a 100 year return period discharge in their designs, as discussed in section 4.2.3, the discharge coupled to this return period, is also simulated in Delft3D. As a result, the 2006 floodwave and this return period discharge can be compared. The input information, differing from the original model as described in chapter 5 and appendix D, is summarised in table 7.4.

The report of Ingeniería Dolmen (2015) only describes the peak discharge of the 100 year return period, not the evolution of this discharge. Therefore the discharge data of the 2006 flood is scaled and adapted to meet the peak discharge of the 100 year return period.

Note: Because of the larger discharge and thus the higher flow velocities the timestep was reduced from 0.1 seconds to 0.05 seconds to prevent Courant warnings and crashes of the Delft3D Model.

Table 7.4: Input Parameters Delft3D Model - short-term simulation, 100 year return period

Description	**Value**
Simulation start time	28 06 2019 00 00 00
Simulation stop time	11 07 2019 00 00 00
MorFac	1 [-]
Simulated time	14 [days]
Discharge	Input from table 7.5

Table 7.5: Discharge evolution during 100 year return period from Ingeniería Dolmen (2015) and scaled to meet the evolution of 7.3

Date (dd-mm-yyyy)	Discharge (m^3/s)
28-06-2019	2000
29-06-2019	2600
30-06-2019	3921
01-07-2019	4800
02-07-2019	5700
03-07-2019	8400
04-07-2019	20526
05-07-2019	14590
06-07-2019	9131
07-07-2019	6645
08-07-2019	5222
09-07-2019	4092
10-07-2019	2500
11-07-2019	2000

7.1.2 *Results*

Long-term - 10 years

The results of the long-term Delft3D simulation with a simulated time of 10 years are visualised in figures 7.1 to 7.6.

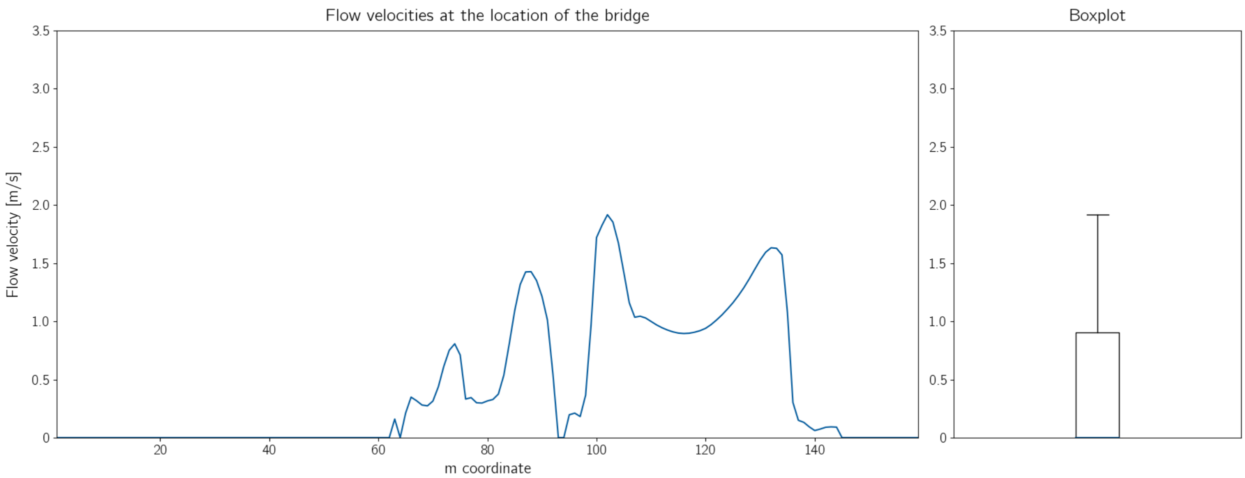

Figure 7.1: Maximum flow velocities at the location of the bridge on 13-08-2019 (corresponding to a simulated period of 1112 days)

The maximum flow velocity occurs 1112 days, approximately 3 years, after the start of the simulation (time step t = 557, using MorFac 24). The value of the maximum flow velocity is equal to 1.9 m/s. The flow velocities at the location of the channels are higher compared to the flow velocities at the location of the river bar. The median of the boxplot, visible on the right of figure 7.1, is zero as half of the points are dry and by definition have no flow velocity. From the boxplot it can be deduced that there is a 25% chance for a flow velocity between approximately 0.9 and 1.9 m/s at that point in time. Figure 7.1 only shows the flow velocities at the cross-section of the bridge at the time the maximum flow velocity occurs. This means at other points in time the flow velocities are lower.

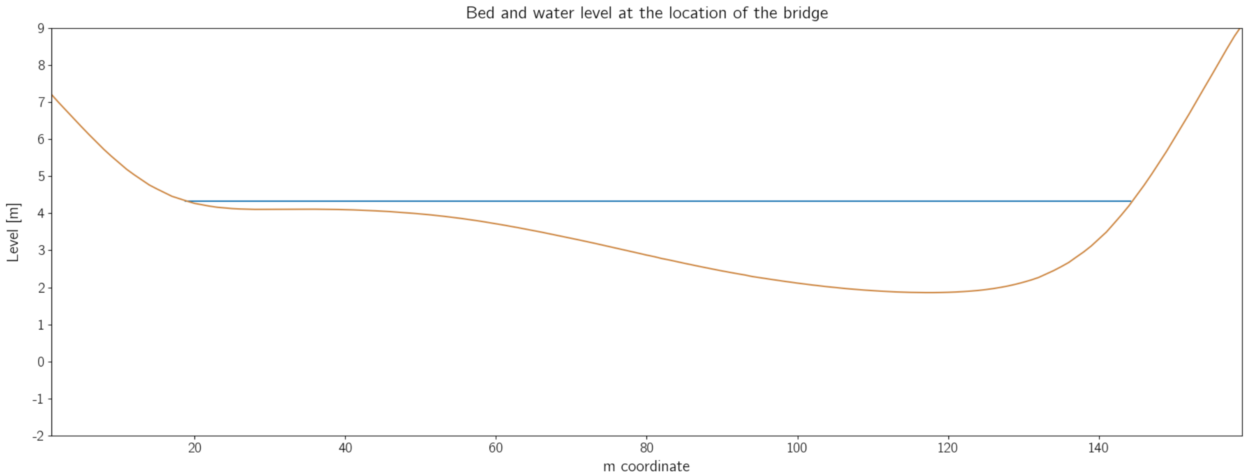

Figure 7.2: Water level at the location of the bridge on 28-06-2019 (start simulation)

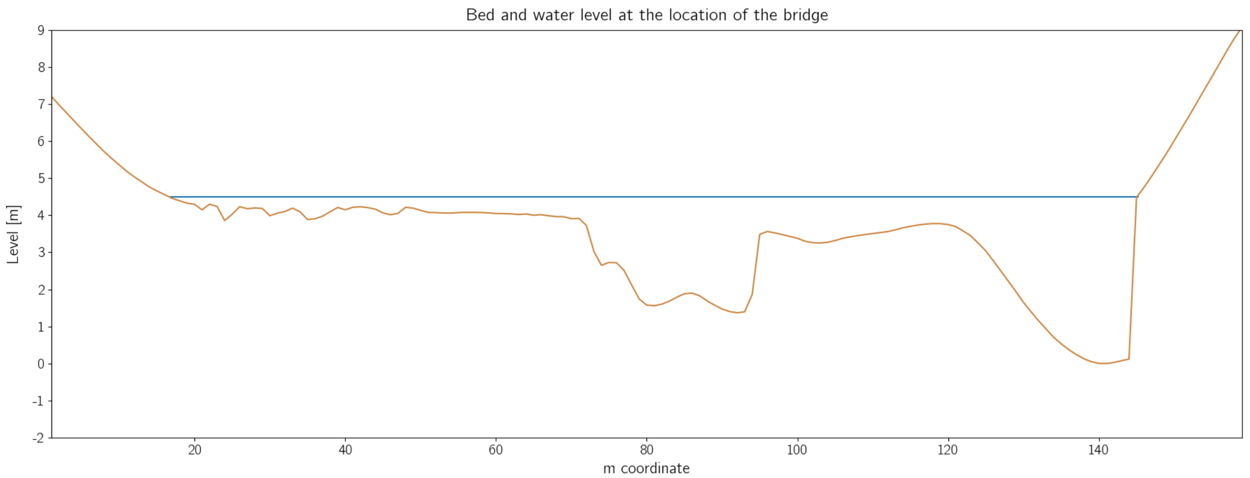

Figure 7.3: Maximum water level at the location of the bridge on 05-07-2019 (corresponding to a simulated period of 170 days after the start)

The maximum water level occurs 170 days, approximately half a year, after the start of the simulation (time step t = 86, using MorFac 24). The value of the maximum water level is equal to 4.5 m. Comparing figures 7.2 and 7.3, it is visible that the water level does not change significantly. This is explained by the fact that the discharge is constant for the entire simulated period of time, as a result the water level seeks equilibrium and remains constant. However, the river morphodynamics, such as the bed level do change. This is visible when comparing the orange lines, representing bed level, in figures 7.2 and 7.3. The development of channels is visible, on both the river bar and next to the river bar (closer to the northern embankment).

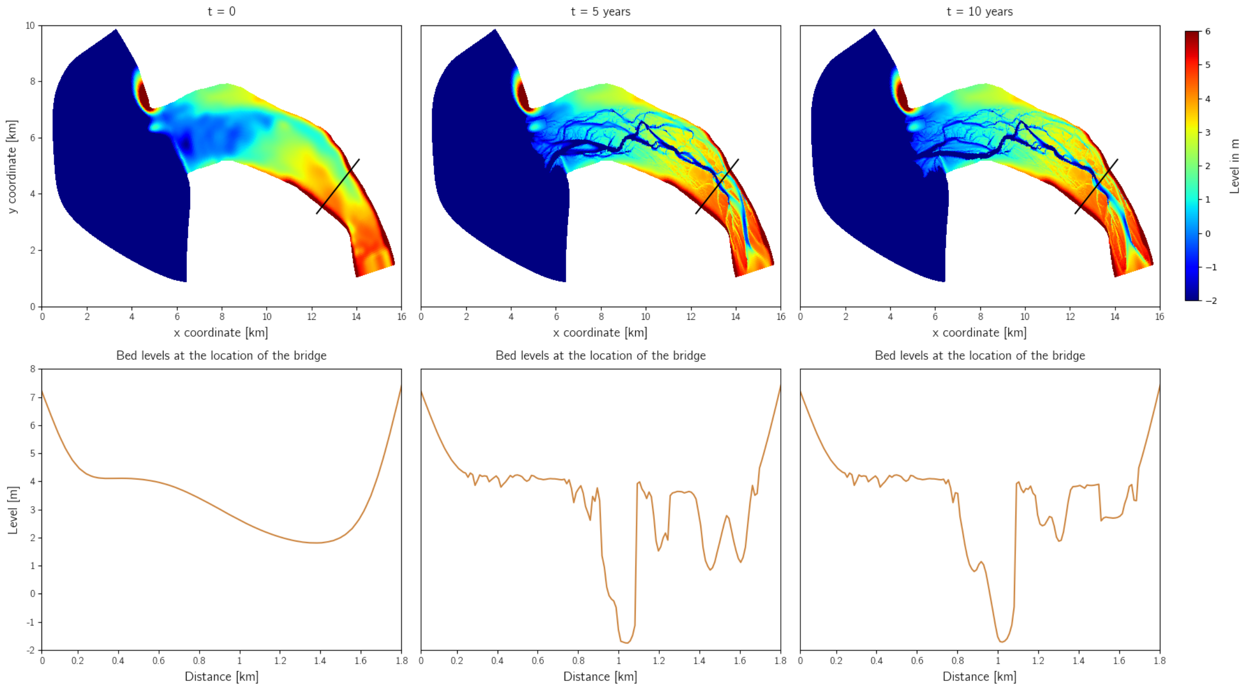

Figure 7.4: Comparing bed levels after 0, 5 and 10 years of morphodynamic simulation

In figure 7.4 the morphological development of the modelled part of the Biobío river is visualised. It is evident that the bed level changes significantly during the first 5 years as multiple channels are subject to erosion and sedimentation. In the last 5 years of the simulation the bed level changes are more subtle. The deepest channel, already clearly visible at t = 5 years, is still present but has widened a little. The channel in the outer bend, present at t = 5 years, has experienced sedimentation in the following five years and is, at the end of the simulation, less deep and less wide.

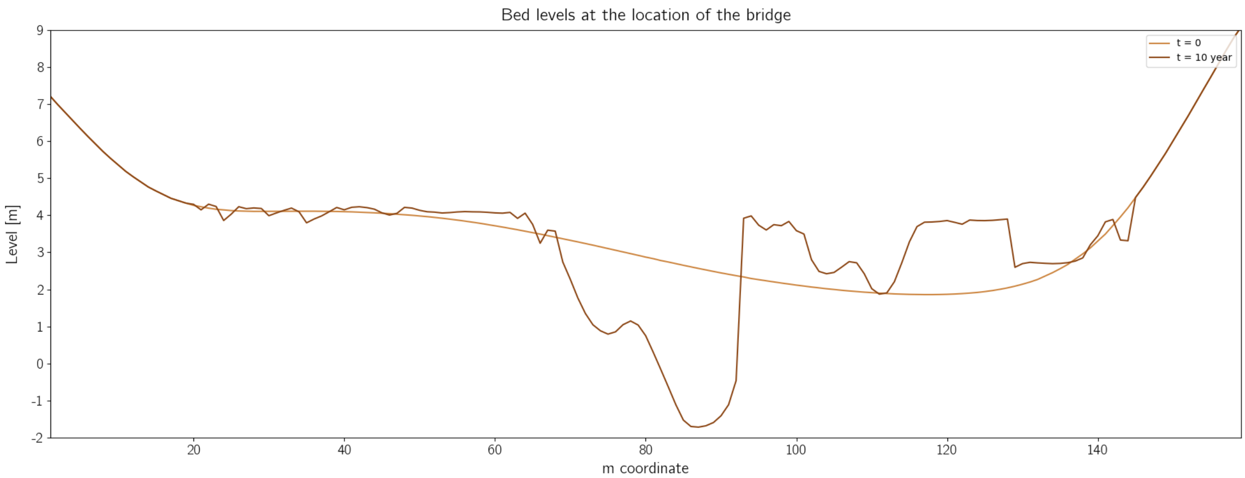

Figure 7.5: Comparing bed level at start of the simulation and after 10 years

Figure 7.5 shows the developed bed level after a simulated period of 10 years, using the effective discharge as a constant upstream boundary and the tidal constituents as a downstream boundary. The figure shows the evolution of various channels. At both the left and right part of the plot, the outlines of the bed levels remains unchanged as these are the southern and northern embankment respectively. Furthermore, it can be observed that the sand bar present at the inner bend (left in the figures, between 0 and 0.8 km) is quite stable and does not show large variations in time.

As this is a model and is used to approximate the real life situation, the locations of the development channels cannot be taken as governing. A clear-cut conclusion about the location of the channels cannot be given, but something can be said about the variation in bed level. This is visualised as a boxplot in figure 7.6, below.

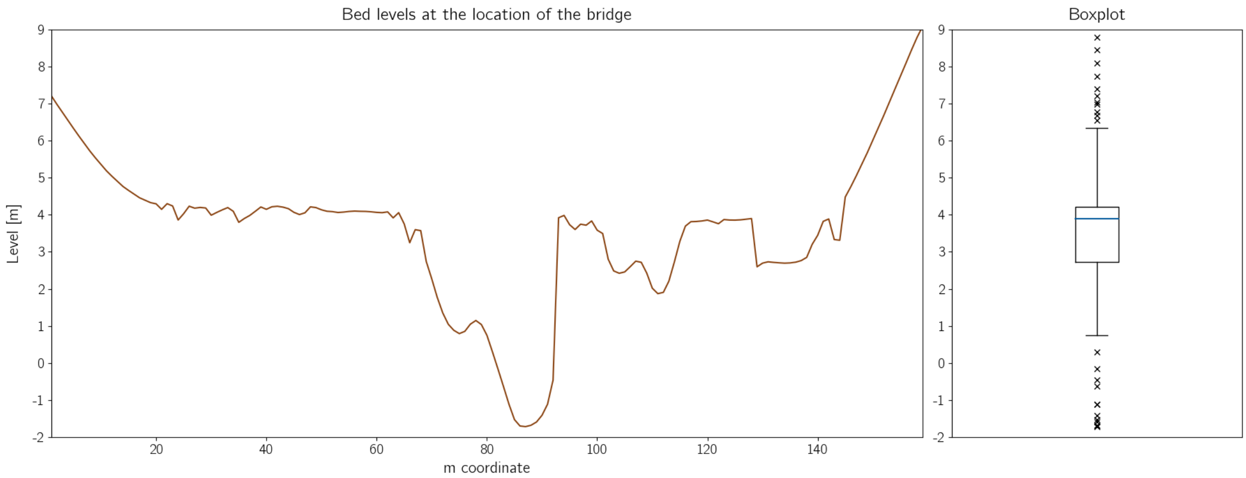

Figure 7.6: Bed level after 10 years of morphodynamics

Figure 7.6 shows the bed level after 10 years of morphodynamics, plus the boxplot of the variation on the right. The median of this boxplot is situated at approximately 4 metres. There is a 50% chance of a bed level variation between 4 and 0.9 metres. The change of the bed level being lower than 2.6 metres is 25%.

Short-term - 2006 Floodwave

The results of the short-term Delft3D simulation of the 2006 floodwave are visualised in figures 7.7 to 7.9.

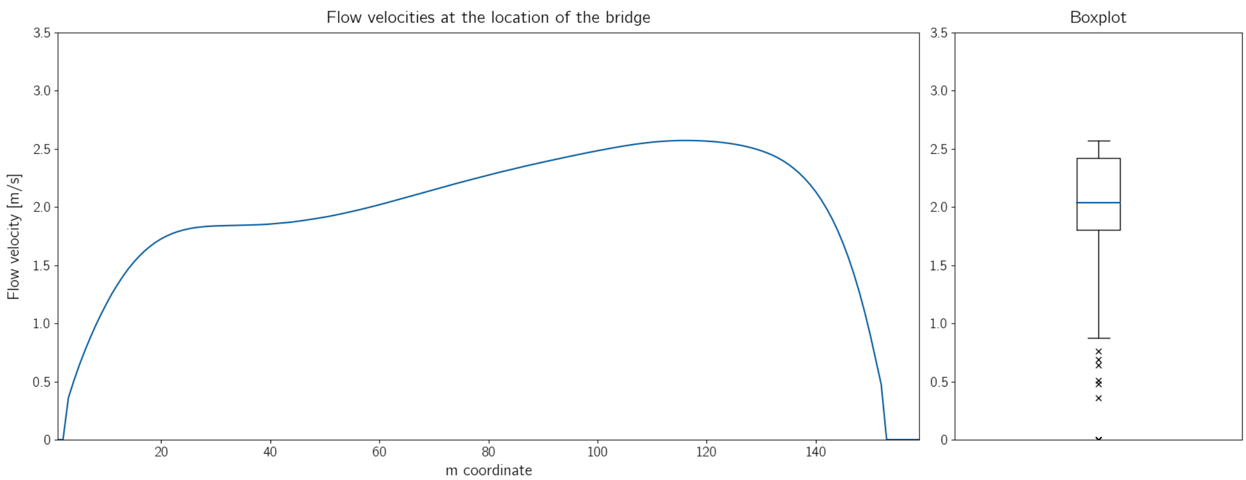

Figure 7.7: Maximum flow velocities at the location of the bridge on 04-07-2019 (after simulated time of 7 days, representing 12-07-2006)

The maximum flow velocity occurs on the same day as the maximum discharge, namely the 4th of July 2019 (being the 12th of July in the 2006 dataset). The value of the maximum flow velocity is equal to 2.6 m/s. The flow velocities at the location of the channels are higher compared to the flow velocities at the location of the river bar. From the boxplot, visible on the right of figure 7.7, it can be deducted that there is a 50% chance for a flow velocity between approximately 1.8 and 2.4 m/s. An even greater value up until 2.6 m/s has a possibility of 25%.

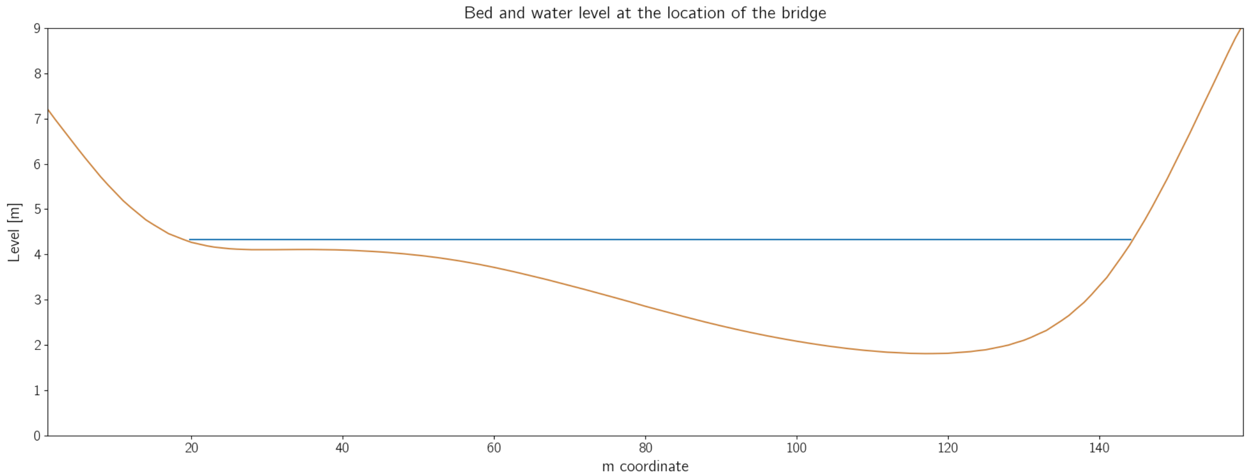

Figure 7.8: Maximum water level at the location of the bridge on 28-06-2019 (start simulation, representing 06-07-2006)

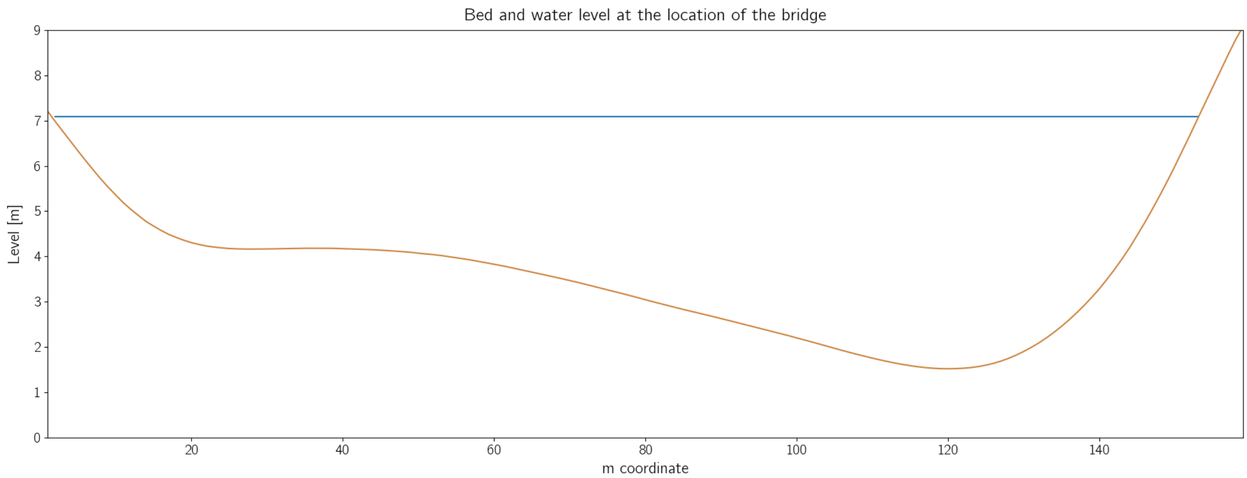

Figure 7.9: Maximum water level at the location of the bridge on 04-07-2019 (after simulated time of 7 days, representing 12-07-2006)

The maximum water level occurs on the same day as the maximum discharge, namely the 4th of July 2019 (being the 12th of July in the 2006 dataset). The value of the maximum water level is equal to 7.1 m. Comparing figures 7.8 and 7.9, it is visible that the water level has increased from approximately 4.2 metres to 7.1 metres in just six days. The increase of discharge, leading to an increase in water level of 2.9 metres, also influences the river morphodynamics as the bed level has changed, visible when comparing the orange lines, representing bed level, in figures 7.8 and 7.9.

Short-term - 100 year return period

The results of the short-term Delft3D simulation for the 100 year return period discharge are visualised in figures 7.10 to 7.12.

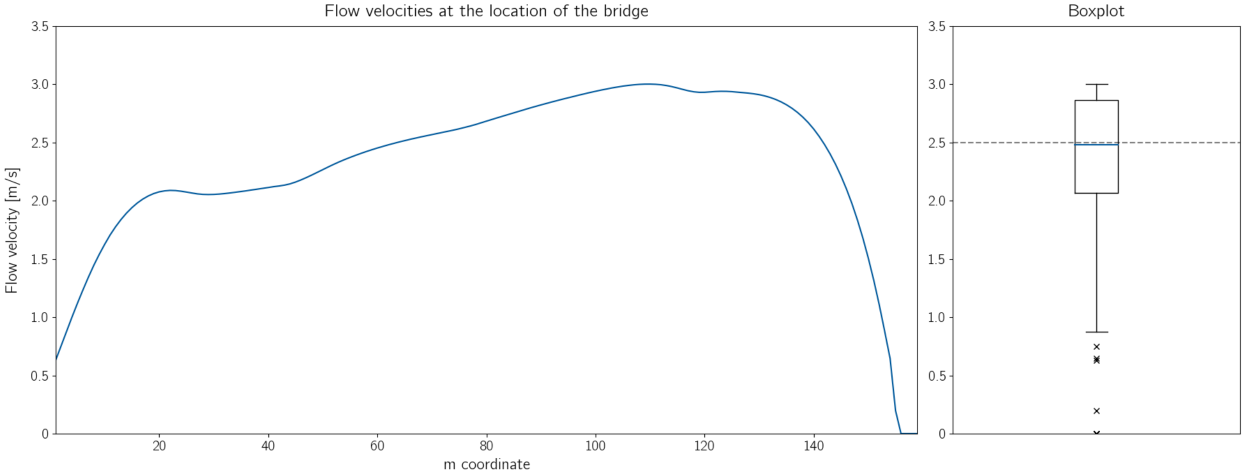

Figure 7.10: Maximum flow velocities at the location of the bridge on 04-07-2019 (after simulated time of 7 days)

The maximum flow velocity occurs on the same day as the maximum discharge, namely the 4th of July 2019, and is equal to 3.0 m/s. The flow velocities at the location of the channels are higher compared to the flow velocities at the location of the river bar. From the boxplot, visible on the right of figure 7.10, it can be deducted that there is a 50% chance for a flow velocity between approximately 2.1 and 2.8 m/s. An even greater value up until 3.0 m/s has a possibility of 25%.

The dotted line in the boxplot indicates the maximum flow velocity derived by EFE for this scenario (the 100 year return period discharge). This value of 2.5 m/s is close to the median of the flow velocity variation of the Delft3D model with the 100 year return period discharge meaning that there is a relatively large chance this flow velocity is exceeded. To be exact, the chance that the flow velocity is higher than the maximum flow velocity set by EFE, 2.5 m/s, is 48.75%.

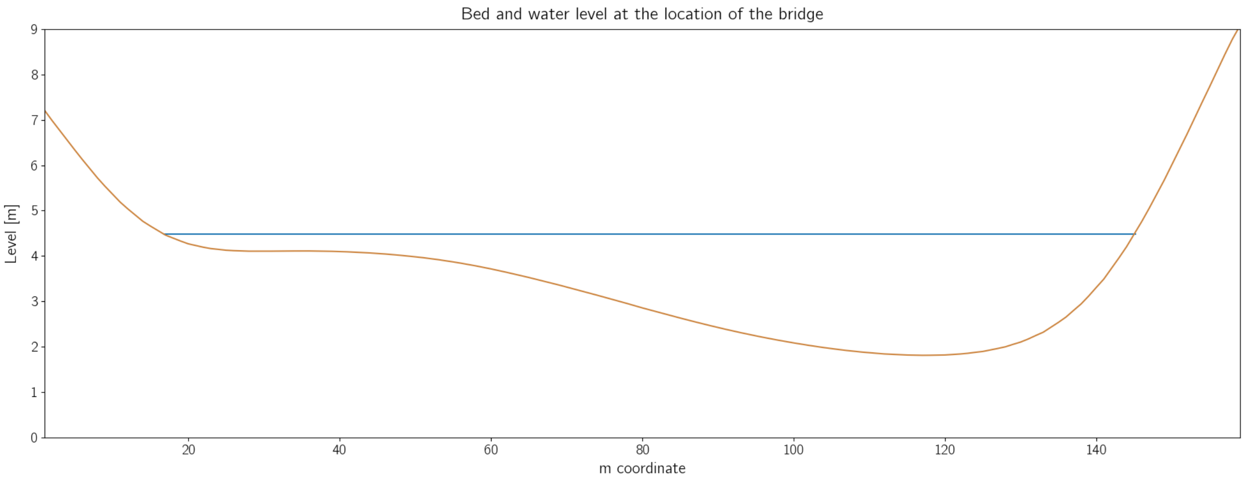

Figure 7.11: Maximum water level at the location of the bridge on 28-06-2019 (start simulation)

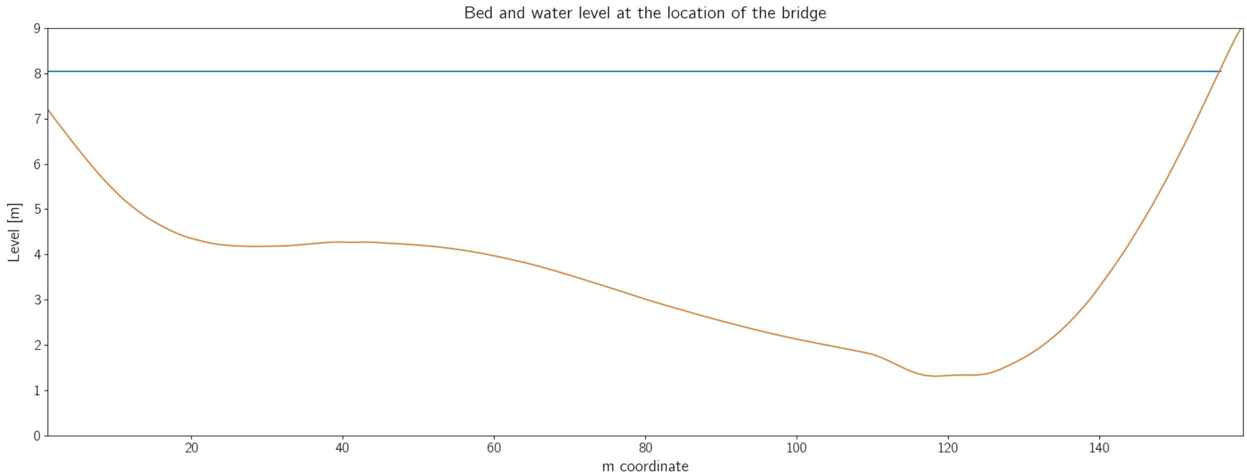

Figure 7.12: Maximum water level at the location of the bridge on 04-07-2019 (after simulated time of 7 days)

The maximum water level occurs on the same day as the maximum discharge, namely the 4th of July 2019, and is equal to 8.0 m. Comparing figures 7.11 and 7.12, it is visible that the water level has increased from approximately 4.2 metres to 8.0 metres in just six days. The increase of discharge, results in an increase in water level of in 3.8 metres, and also again influences the river morphodynamics as the bed level has changed, visible when comparing the orange lines, representing bed level, of figures 7.11 and 7.12. Furthermore, it can be observed on the left side of figure 7.12, the water level is so high, it is no longer kept between the embankments, meaning nearby areas could flood.

7.2 NeoWave - Modelling Tsunami Influence in a River

The NeoWave model has been used to assess the influence of a tsunami on the river and how it may affect the design of the new railway bridge. By using the results of this simulation a better design can be achieved for the railway bridge.

7.2.1 *Scenario: Simulated Earthquake*

The NeoWave simulation is based on an earthquake right in front of the river mouth of the Biobío river, Concepción. This to negate the effect of the submarine canyon (as described in section 6.2) as much as possible as this might decrease the run up of a tsunami on the Biobío river. It is important to note that the earthquake simulation is only hypothetical. Meaning that the probability of occurrence of an earthquake exactly the same as the simulated earthquake is very small. Though for a preliminary design of the bridge it is interesting to check whether the bridge is subject to tsunami loads. This can be shown best by assessing a 'worst case' scenario.

The simulated earthquake is modelled based on the Okada (1985) model, using the finite fault model of the rupture area with variable slip. For this situation, a distribution with three areas is assumed. This non-homogeneous distribution resembles a real earthquake more accurately than a homogeneous distribution. The earthquake has been created in such a way that the moment magnitude (M_W) is equal to 9.0. This non-homogeneous slip distribution can be visualised in a figure by plotting the values of the segments used for the creation of the earthquake. The slip distribution is shown in figure 7.13.

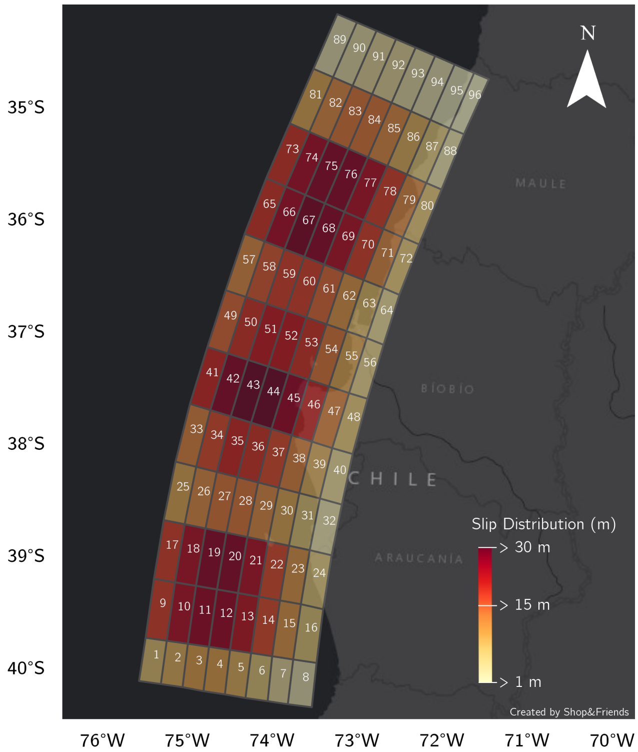

Figure 7.13: Slip distribution used for the simulation of an earthquake in NeoWave

Based on the slip distribution in figure 7.13, a visualisation can be made of the initial condition of the tsunami wave. This visualisation is shown in figure 7.14, wherein the three higher slip areas are clearly visible. As these areas show a higher initial water level.

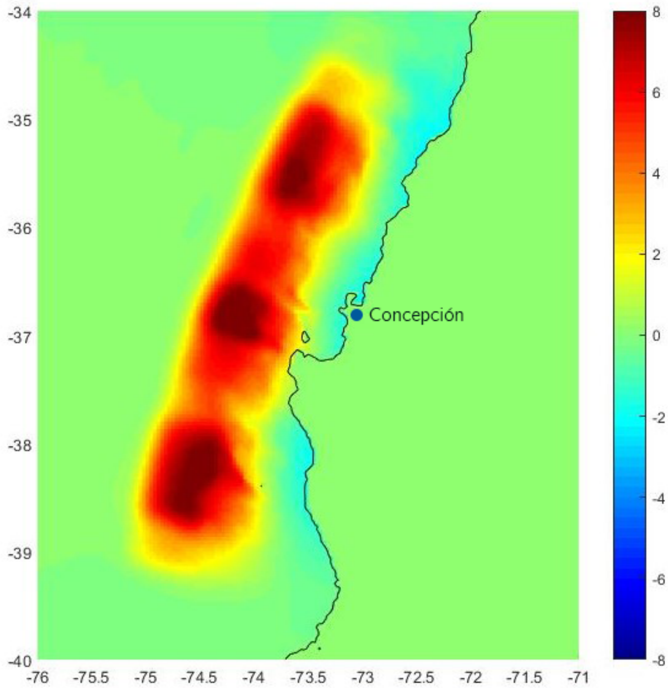

Figure 7.14: Initial conditions used in the simulated earthquake in NeoWave, with the water level in m

7.2.2 *Results*

The results of the NeoWave model can be used to determine whether the tsunami influences the bridge, and whether or not the tsunami effects need to be taken into account when designing the new bridge. The results can be compared to the high discharges (flood waves), to check which process is normative. The waves that enter the Biobío river are quite heavily influenced by the submarine canyon in front of the river mouth, see section 6.2. Leading to a relatively small inundation at the river mouth. According to the simulation surrounding areas can experience greater waves.

Processing the results from the NeoWave simulation gives the water level inundation and flow velocities. The water level inundation is shown in figure 7.15 and the flow velocities are visible in figure 7.16. By computing the momentum of the flow, one is able to determine the resulting forces due to the tsunami. Here only the results of buoy 1 are shown as these represented the normative values.

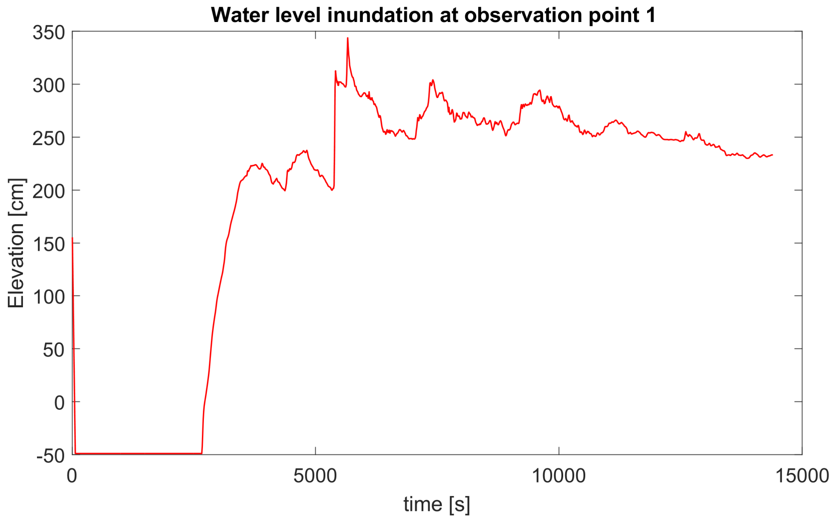

Figure 7.15: Water level inundation ζ, at buoy 1, retrieved from the NeoWave simulation

From figure 7.15 it can be concluded that the maximum water level inundation is close to 3.5 meters. Thus, this means the tsunami scenario has an influence on the bridge, and consequently the tsunami effects have to be accounted for in the bridge design. Furthermore, figure 7.16 shows the maximum flow velocity occurs in the first wave that reaches the observation point. This wave has a celerity of 2.37 m/s.

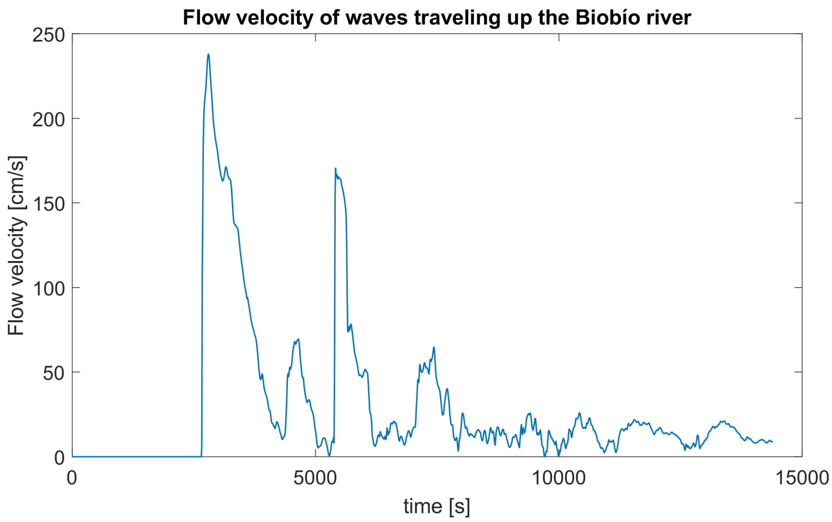

Figure 7.16: Flow velocity, at buoy 1, retrieved from the NeoWave simulation

As mentioned before, the momentum can be computed with the flow velocity and water level inundation by $Momentum = \zeta * U^2$. The calculated momentum is plotted in figure 7.17. By comparing the flow velocity, water level inundation and the momentum one can see that peaks occur at slightly different points in time. The highest peak of the momentum in the river is present in the second tsunami wave.

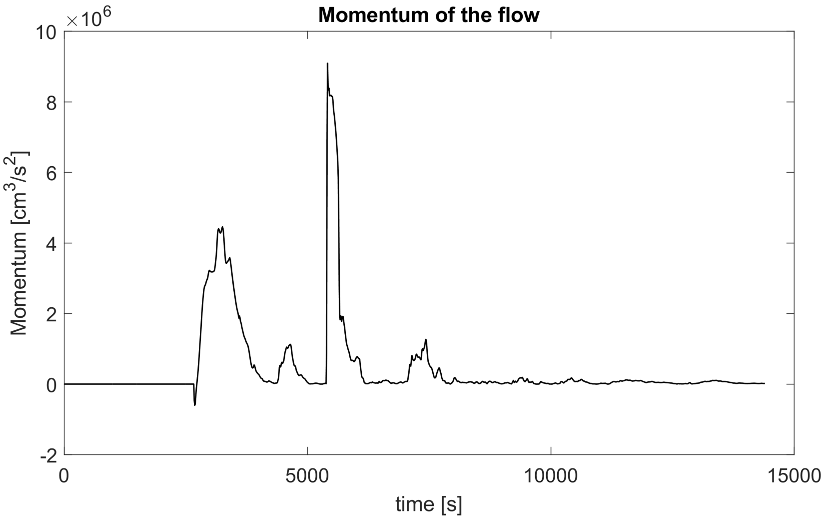

Figure 7.17: Flow momentum, at buoy 1, determined from the NeoWave simulation

Using the momentum, the required tsunami forces can be determined. These forces are needed for the design, according to NCh3363:2015 (2015) two situations need to be considered. These situations are elaborated in more detail in section 8.6.4. The hydrodynamic forces are shown in figure 7.18. These are needed to assess the influence of the hydrodynamic part of a tsunami wave on a structure.

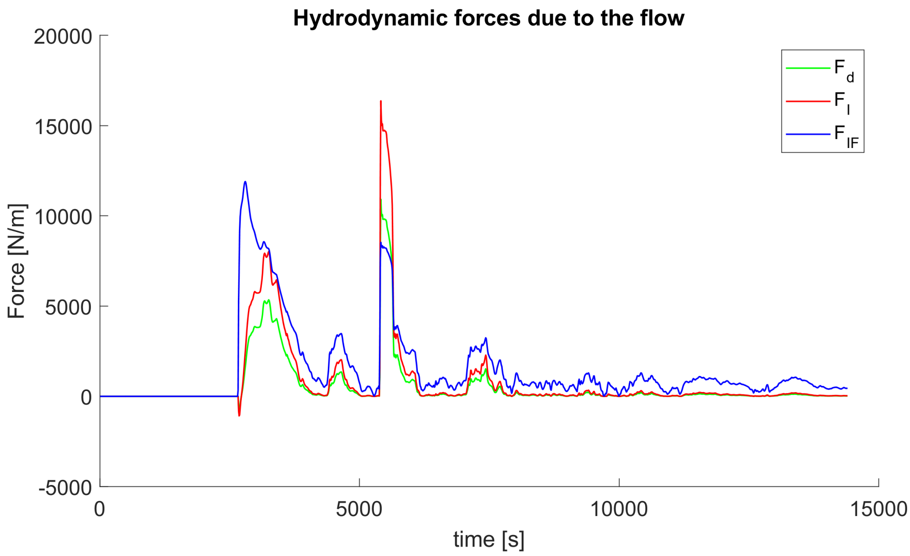

Figure 7.18: Hydrodynamic forces, determined from the NeoWave simulation

Note that in figure 7.18 only 3 different forces are presented. The accumulation force due to floating objects (F_{dd}) is not computed separately as this force has the same value as F_d if calculated per unit width. The calculation of the forces is based on a different density of water, to account for the amount of sediment a tsunami carries. To account for the sediment the density (ρ) is therefore set to 1200 kg/m^3, in accordance with NCh3363:2015 (2015). The equations used for the computations can be found in appendix F.3, the following maximum forces were found:

- Drag force: $F_{d,max} = 11.2$ kN/m
- Wave impact Force: $F_{I,max} = 16.9$ kN/m
- Impact force due to floating objects: $F_{IF,max} = 9.8$ kN/m

Besides the hydrodynamic loads, the hydrostatic loads are important too. These loads act as compression forces on the bridge's components. The evolution of the hydrostatic force in time is given in figure 7.19. From this figure it can be concluded that the maximum hydrostatic force is equal to 68.5 kN/m.

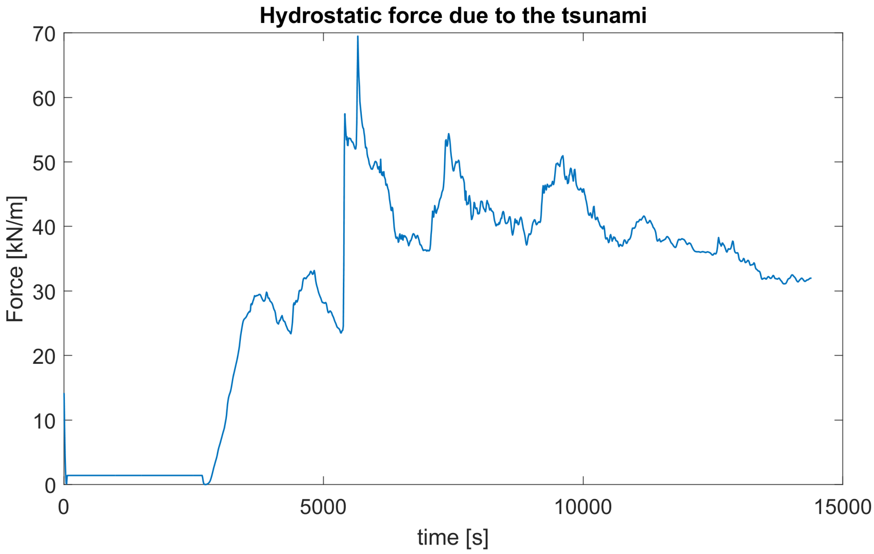

Figure 7.19: Hydrostatic force, determined from the NeoWave simulation

For the bridge design it can be of interest to assess different load combinations of the tsunami loads to see whether the bridge design is sufficiently strong.

7.3 Recommendations for Design

The results of the hydraulic analysis are used in the programme of requirements for the new railway bridge. The most important hydraulic aspects are summarised in table 7.6.

Table 7.6: Hydraulic aspects for the programme of requirements

Hydraulic Aspect	**Result of Scenario**	**Value**
Maximum flow velocity	Delft3D River simulation: short-term - 100 year return period discharge	3.0 m/s
Maximum bed level variation	Delft3D River simulation: long-term - 10 years	6.0 m
Maximum water level change from upstream	Delft3D River simulation: short-term - 100 year return period discharge	3.8 m
Maximum water level change from downstream	NeoWave Tsunami simulation	3.5 m
Maximum hydrostatic force	NeoWave Tsunami simulation	68.5 kN/m
Maximum drag force tsunami	NeoWave Tsunami simulation	11.2 kN/m
Maximum wave impact force tsunami	NeoWave Tsunami simulation	16.9 kN/m
Maximum impact force due to floating objects tsunami	NeoWave Tsunami simulation	9.8 kN/m

7.4 Sensitivity Analysis of Delft3D Model

In the sensitivity analysis of the Delft3D model two variables are investigated, the median sediment diameter (D50) and the morphological scale factor (MorFac). The influence of the parameter is examined by doing the same simulation with an increased and decreased value of the parameter. Subsequently the changes in the results are compared to examine the influence of the parameter in the model.

7.4.1 *Median Sediment Diameter - D50*

For the sensitivity analysis of the D50, the original median sediment diameter of 1000 μm is increased with 20% to 1200 μm and decreased with 20% to 800 μm. The results of these simulations are presented in figure 7.20.

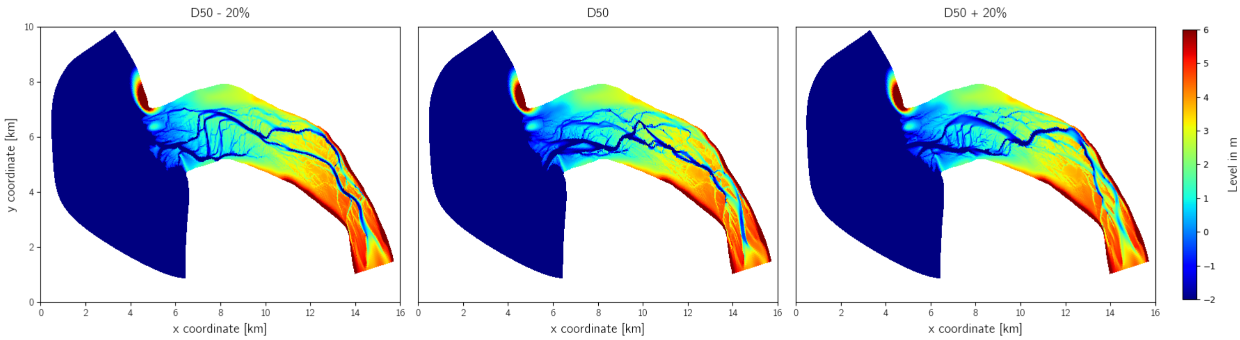

Figure 7.20: Results on the last time step, after a simulated time of 5 years, of the sensitivity run for the D50

The results from the sensitivity simulation are interesting as both the decreased and increased D50-value have a large channel located in the outer bend, which is consistent with the real Biobío river. The difference between the decreased and increased value is the second channel at the location of the bar. The existence of this specific channel can be explained by the lower median sand diameter, as a lower diameter is easier to erode than a larger one. In the real Biobío river the second channel is not present, instead one channel exist in the outer bend. However, near the mouth of the river the default D50 and decreased D50 appear to be a better fit for the real Biobío river.

From these simulations it can thus be concluded that more research is required to determine the median sediment diameter because the solution is sensitive to this parameter. Furthermore, the need to incorporate a spatially varying D50 is supported by these simulations and should therefore be investigated. It is recommended to include this variability in a later version of the Delft3D model.

7.4.2 *Morphological Scale Factor - MorFac*

For the sensitivity analysis of the MorFac, the original morphological scale factor of 24 is increased and decreased to 48 and 12 respectively. The results are presented in figure 7.21.

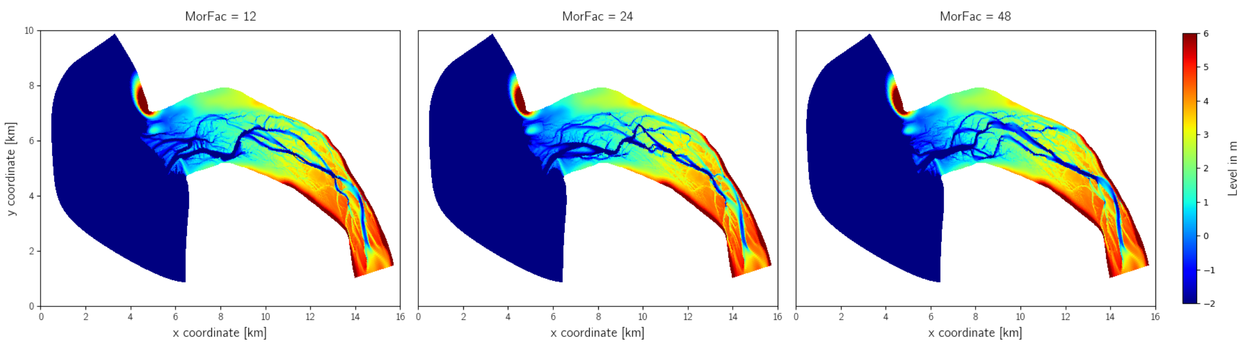

Figure 7.21: Results on the last time step, after a simulated time of 5 years, of the sensitivity run for the morphological scale factor

If the three figures are compared it can be seen that the general behaviour of the river is the same for all, i.e. all simulations display channels and near the mouth of the river more small channels are present. As previously mentioned, there is a large channel present in the outer bend of the authentic Biobío river which neither of the simulations predict. However, the lower MorFac value shows a channel located closer to the outer bend of the river.

A conclusion that can be drawn from the sensitivity results, is that the solution is sensitive to the morphological scale factor and that increasing the value could result in an incorrect solution. Hence, the solutions which higher morphological scale factors should be compared to the solution with no morphological scale factor. The simulation which then displays the smallest error is the optimal morphological scale factor to be used in forthcoming simulations.

III

Design

8

Programme of Requirements

This chapter includes the programme of requirements for the new railway bridge, named 'Neuvo Ferroviario Bio Bio', proposed by EFE. The programme of requirements serves as a basis in order to correctly assess the initial design supplied by EFE and the design variants which are established in chapter 9. In addition, the surrounding landscape is thoroughly mapped.

It is important to note that this chapter is based upon logical and realistic assumptions, because the official programme of requirements from the EFE was not available.

The programme of requirements is built up as follows: the main description of the project is given in section 8.1, which is followed by the project requirements in section 8.2. The prerequisites and wishes of the client are discussed in sections 8.3 and 8.4 respectively. Lastly, the initial designing points, including amongst other things technical regulations and loads, are discussed in section 8.5.

8.1 Project Description

The EFE, aforementioned in chapters 1, 2 & 3, is planning to replace the current 130 years old railway bridge, named 'Puente Ferroviario Rio Bio Bio'. The new bridge, named 'Nuevo Ferroviario Rio Bio Bio', is going to be located roughly 60 metres (centre to centre) downstream compared to the old Ferroviario bridge. The approximate length of the new bridge is close to 1.9 kilometres.

8.1.1 *Location and Highlights*

The planned location of the bridge has been provided for by the EFE in the form of initial AutoCAD drawings. These drawings have been integrated into the GIS environment. Initially, the location proposed by EFE is assumed as the basis for the variant study in chapter 9.

A short description of the POI's, Points Of Interest, is supplied below. In Appendix G the POI's are more thoroughly highlighted. The POI's described below can be found in figure 8.1.

- A: A mountain is situated at POI − C, the current and planned bridge both go through the mountain. It is therefore needed to construct a tunnel. This POI also includes the Northern Abutment of the bridge.
- B: Southern Abutment, the bridge physically ends at this point and continues on land.
- C: A mountain with its highest point of 76 metres. Several water storage tanks are constructed on top of the mountain, supplying the city with potable water.
- D: Exit of the tunnel through the mountain.
- E: An artificial irritation canal was dug by the paper mill company. The canal flows beneath the superstructure of the bridges.
- F: The river Biobío, as thoroughly analysed in chapter 4.

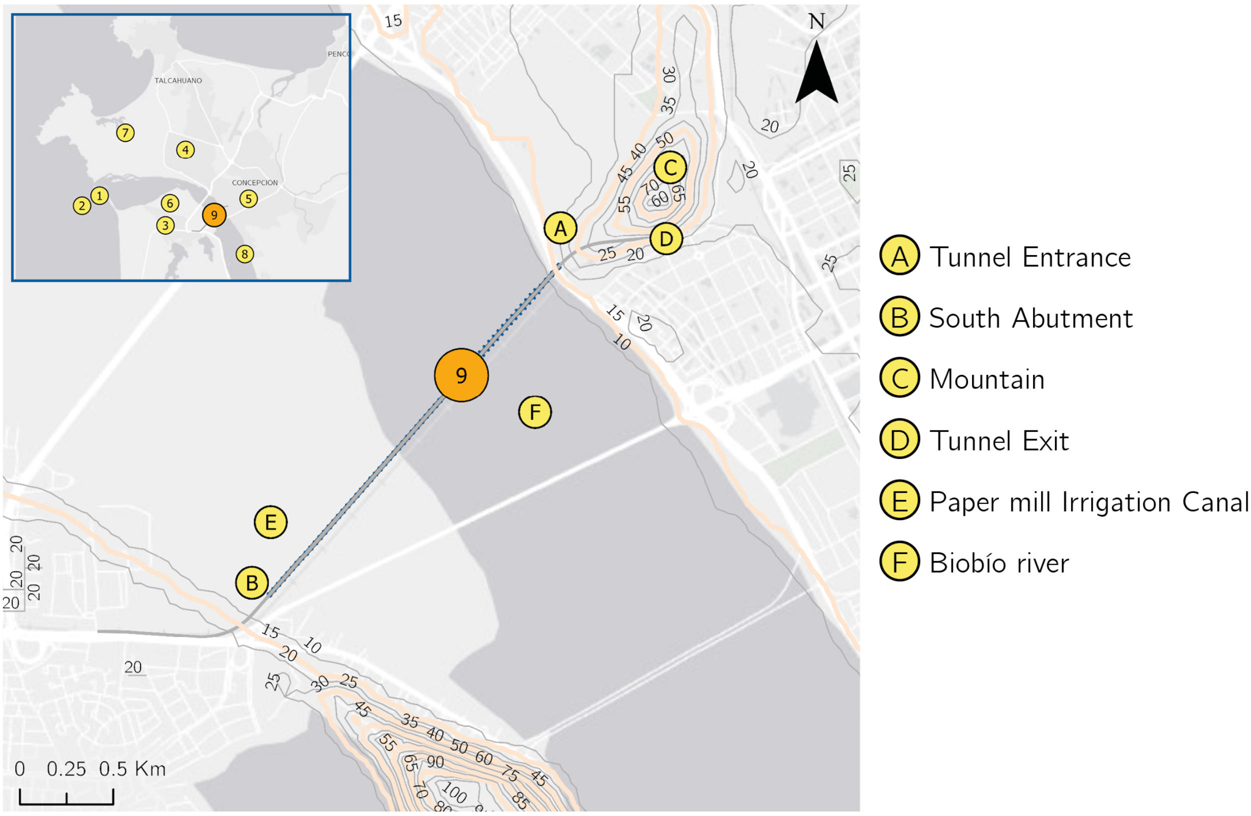

Figure 8.1: Location of the railway bridge with additional points of interests (POI). The image in the top left corner refers to figure 4.1. The terrain elevation has been added and numbered in metres.

8.1.2 *Scope*

Within this consultancy report only the new railway bridge, its features and natural boundary conditions are considered. The river morphodynamic and tsunami influence are taken into account, as these influence the bridge design. The old railway bridge and any adjacent roads are neglected for this preliminary design.

8.1.3 *Geological Survey*

The soil has a great impact on the stability and substructure of the bridge. The EFE has conducted several soil penetration tests along the longitudinal axis of the bridge. These figures are used for calculations performed in this report. The exact location and characteristics of the substances found can be viewed in appendix G.2 figure G.11. Most common soil types are summarised below:

- Sand
- Silt
- Granite

8.1.4 *Hydraulic Survey*

In the Physical Analysis, chapter 4, an elaborate analysis of the Biobío river system has been made. It can be shown that, amongst other things, near the location of the bridge a river bar is developing at the inner bend. On this bar vegetation is growing which increases the roughness, as explained in section 5.5. This increase results in the flow diverging around the river bar which has the effect that about half of the river is dry during normal flow conditions. This is confirmed by the Delft3D model since the long term simulation shows that the flow velocity is equal to 0 m/s in approximately half of the cross section, see figure 7.1.

Furthermore, due to the increase in vegetation the erosion of the channels in the flow part could be expected to increase due to the reduced conveyance width. The deeper channels could prove to be a threat to the structural stability of the bridge since the foundation pillars are more exposed, this is further elaborated in section 8.6.

However, the vegetation is not the only process which has an influence on the bridge. As the bridge is located near the mouth of the river there might also be an influence of the tide. In section 4.2.2 the tidal variation during one month is plotted in figure 4.11. Nonetheless, the values of interest from a design point of view are not the daily, or hourly, variations but the long term average of the extreme water levels. To receive these values a long term tidal analysis must be made, such an analysis has been made by van Heemst et al. (2012). In their analysis van Heemst et al. (2012) found the values as presented in table 8.1. The values presented in the centre column are with respect to NRS (Nivel Reduccion de Sondas), which is the reference level used in Chile. In the last column the water levels are with respect to MSL (Mean Sea Level), which is equal to 0.92 m NRS.

Lastly, the river system is influenced by extreme natural forcings such as tsunamis and flood waves. Both of these natural disasters occurred in the past 15 years and expected to occur again during the life time of the bridge, they are therefore considered as special load cases in the design.

Table 8.1: Tidal ranges from the port of Talcahuano

	Water level [m NRS]	**Water level [m MSL]**
HAT	+2.01	+1.09
MHWS	+1.88	+0.96
MLWS	*unknown*	*unknown*
LAT	+0.23	-0.69

The hydraulic design points, covering the results found in the hydraulic analysis of the river, are discussed in section 8.6.

8.2 Requirements

8.2.1 *Utilisation*

- Provide dependable cargo transport route from Concepción and Coronel
- Provide commune transportation, connecting Concepción and Coronel, see figure 8.2

Figure 8.2: Train transportation routes in the Biobío region. Retrieved from 1994bus (2017).

8.2.2 *Future & Adaptability*

- The economic lifetime has to be 100 years for the constructional parts
- The structure should be relatively easy to maintain, e.g. withhold erosion and easy to re-paint
- The structure should fit into the landscape
- The bottom of the bridge deck should be 12 m above sea level
- The structure should be able to withstand:
  - Soil subsidence
  - Tsunamis, including debris
  - Extreme river discharges (flood waves)
  - Earthquakes
  - Dynamic train loading

8.2.3 *Finance*

- Create added economical value to EFE and the community
- Maintenance is cost effective
- Overall project costs should be kept low
- Increase cargo transportation between Coronel and Concepción
- Increase civilian transportation between Coronel and Concepción

8.3 Prerequisites

- Project is limited to proposed location set up by the EFE, as this provides the best connection with the existing infrastructure

- Topographical characteristics are according to the analysis in appendix G
- The geological properties are according to appendix G
- Hydraulic data utilised for structural calculations are according to chapter 7, based on three scenarios: long-term river morphological changes, short-term flood wave impact and tsunami-impact as result of an earthquake

8.4 Wishes

- Project should be finished by 2023
- Aesthetics should fit in the environment and be appealing to local residents
- Aesthetics should be according to the identity of EFE
- During constructional works:
  - Delaying deadlines should be avoided
  - Minimise noise nuisance
  - Minimise the negative effects on accessibility of nearby infrastructures

8.5 Initial Designing Points

8.5.1 *Standards and Regulations*

Bridge design in Chile should be conform Chilean Building Codes. However, in some applications the Chilean codes are insufficient, and as the American codes (AASTHO) are not retrievable, Dutch or European building codes are applied instead.

The following standards apply:

- Chilean Standard - NCH2369 of 2003 - Earthquake-Resistant Design
- Chilean Standard - NCH3363 of 2015 - Buildings in risk areas of flooding due tsunami or seiche
- Chilean Standard - NCH433 of 1996 & modification 2010 - Seismic Design
- Dutch Standard - NEN-EN 1990 - Basis of structural design
- Dutch Standard - NEN-EN 1991 - Actions on structures
- Dutch Standard - NEN-EN 1992 - Design of concrete structures
- Dutch Standard - NEN-EN 1993 - Design of steel structures
- Dutch Standard - NEN-EN 1994 - Design of composite steel and concrete structures
- Dutch Standard - NEN-EN 1997 - Geotechnical Design
- Dutch Standard - NEN-EN 1998 - Design of structures for earthquakes resistance
- Dutch Standard - NEN-EN 3215 - Drainage system inside and outside buildings
- Dutch Standard - NEN-EN 9997 - Geotechnical design of structures

8.5.2 *Consequence Class, Design Life and Exposure Classes*

According to NEN-EN 1990+A1+A1/C2:2011 and NEN-EN 1992-1-1

- Consequence Class - CC2
  - Cargo and commuter railway bridge
  - No urban or civilian activities in the vicinity, consequence of structural failure low for loss of life
  - Economic loss for EFE in case of structural failure of bridge is considerable
- Design Life - Class 5 (100 years)
- Exposure Class
  - Superstructure: XC4, XS1
  - Substructure: XC1, XC2, XS1

Ultimate Limit State

The Ultimate Limit State (ULS) When determining the ultimate limit state (ULS) the following partial factors have to be used, according to NEN-EN 1990/A1, in combination with the Ψ-factors visible in appendix section G.3:

Table 8.2: Design values of actions (EQU) (Set A). Retrieved and revised from NEN-EN 1990/A1 (1995, p.18).

Persistent and transient design situation	**Permanent actions**		**Prestress**	**Leading variable action (*)**	**Accompanying variable actions (*)**	
	Unfavourable	Favourable			Main (if any)	Others
Eq. 6.10	$\gamma_{Gj,sup} G_{kj,sup}$	$\gamma_{Gj,inf} G_{kj,inf}$	$\gamma_P P$	$\gamma_{Q,1} Q_{k,1}$	-	$\gamma_{Q,i} \Psi_{0,i} Q_{k,i}$
(*) Variable actions are those considered in Tables A2.1 to A2.3.						
	$\gamma_{G,sup}$	= 1.05				
	$\gamma_{G,inf}$	= 0.95 (1)				
	γ_Q	= 1.45 for rail traffic actions, where unfavourable (0 where favourable) = 1.50 for all other variable actions for persistent design situations, where unfavourable (0 where favourable).				
	γ_P	= recommended values defined in the relevant design Eurocode.				

Table 8.3: Design values of actions (STR/GEO) (Set B). Retrieved and revised from NEN-EN 1990/A1 (1995, p.19).

Persistent and transient design situation	**Permanent actions**		**Prestress**	**Leading variable action (*)**	**Accompanying variable actions (*)**	
	Unfavourable	Favourable			Main (if any)	Others
Eq. 6.10	$\gamma_{Gj,sup} G_{kj,sup}$	$\gamma_{Gj,inf} G_{kj,inf}$	$\gamma_P P$	$\gamma_{Q,1} Q_{k,1}$	-	$\gamma_{Q,i} \Psi_{0,i} Q_{k,i}$
Eq. 6.10a	$\gamma_{Gj,sup} G_{kj,sup}$	$\gamma_{Gj,inf} G_{kj,inf}$	$\gamma_P P$	-	$\gamma_{Q,1} \Psi_{0,1} Q_{k,1}$	$\gamma_{Q,i} \Psi_{0,i} Q_{k,i}$
Eq. 6.10b	$\xi \gamma_{Gj,sup} G_{kj,sup}$	$\gamma_{Gj,inf} G_{kj,inf}$	$\gamma_P P$	$\gamma_{Q,1} Q_{k,1}$	-	$\gamma_{Q,i} \Psi_{0,i} Q_{k,i}$
(*) Variable actions are those considered in Tables A2.1 to A2.3. *NOTE 1 The choice between 6.10, or 6.10a and 6.10b will be in the National Annex. In the case of 6.10a and 6.10b, the National Annex may in addition modify 6.10a to include permanent actions only.* *NOTE 2 The γ and ξ values may be set by the National Annex. The following values for γ and ξ are recommended when using expressions 6.10, or 6.10a and 6.10b:*						
	$\gamma_{G,sup}$	= 1.35 (1)				
	$\gamma_{G,inf}$	= 1.00				
	γ_Q	γ_Q = 1.45 when Q represents unfavourable actions due to rail traffic, for groups of loads 11 to 31 (except 16, 17, 263) and 273)), load models LM71, SW/0 and HSLM and real trains, when considered as individual leading traffic actions (0 when favourable) γ_Q = 1.20 when Q represents unfavourable actions due to rail traffic, for groups of loads 16 and 17 and SW/2 (0 when favourable) γ_Q = 1.50 for other traffic actions and other variable actions				
	ξ	= 0.85				
	γ_{Gset}	= 1.20 when linear elastic analysis and 1.35 in case of non-linear analysis				
	γ_P	= recommended values defined in the relevant design Eurocode.				
Comments:	1)This value covers: self-weight of structural and non structural elements, ballast, soil, ground water and free water, removable loads, etc. 2)This value covers: variable horizontal earth pressure from soil, ground water, free water and ballast, traffic load surcharge earth pressure, traffic aerodynamic actions, wind and thermal actions, etc. 3) For rail traffic actions for groups of loads 26 and 27 γ_Q = 1.20 may be applied to individual components of traffic actions associated with SW/2 and γ_Q = 1.45 may be applied to individual components of traffic actions associated with load models LM71, SW/0 and HSLM, etc.					

Table 8.4: Design values of actions (STR/GEO) (Set C). Retrieved and revised from NEN-EN 1990/A1 (1995, p.20).

Persistent and transient design situation	**Permanent actions**		**Prestress**	**Leading variable action (*)**	**Accompanying variable actions (*)**	
	Unfavourable	Favourable			Main (if any)	Others
Eq. 6.10	$\gamma_{Gj,sup}G_{kj,sup}$	$\gamma_{Gj,inf}G_{kj,inf}$	γ_PP	$\gamma_{Q,1}Q_{k,1}$	-	$\gamma_{Q,i}\Psi_{0,i}Q_{k,i}$
(*) Variable actions are those considered in Tables A2.1 to A2.3.						
	$\gamma_{G,sup}$	= 1.00				
	$\gamma_{G,inf}$	= 1.00				
	γ_Q	= 1.25 for rail traffic actions where unfavourable (0 where favourable) = 1.30 for the variable part of horizontal earth pressure from soil, ground water, free water and ballast, for traffic load surcharge horizontal earth pressure, where unfavourable (0 where favourable) = 1.30 for all other variable actions where unfavourable (0 where favourable)				
	γ_{Gset}	= 1.00 in the case of linear elastic or non linear analysis, for design situations where actions due to uneven settlements may have unfavourable effects. For design situations where actions due to uneven settlements may have favourable effects, these actions are not to be taken into account.				
	γ_P	= recommended values defined in the relevant design Eurocode.				

Each respective group should be checked when the following applies for the respective definitions:

- EQU (Equilibrium): loss of static equilibrium of the construction
- STR (Structural): internal collapse or deformations of the construction or constructive elements
- GEO (Geological): collapse or deformations of the soil where the strength of the soil or rock is normative for the resistance

For seismic and accidental actions in the ULS, according to NEN-EN 1990/A1 table A2.5:

Table 8.5: "Design values of actions for use in accidental and seismic combinations of actions." Retrieved and revised from NEN-EN 1990/A1 (1995, p. 22).

Persistent and transient design situation	**Permanent actions**		**Prestress**	**Leading variable action (*)**	**Accompanying variable actions (*)**	
	Unfavourable	Favourable			Main (if any)	Others
Accidental Eq. 6.11a/b	$G_{kj,sup}$	$G_{kj,inf}$	P	A_d	$\Psi_{1,1}Q_{k,1}$ or $\Psi_{2,1}Q_{k,1}$	$\Psi_{2,i}Q_{k,i}$
Seismic Accidental Eq. 6.12a/b	$G_{kj,sup}$	$G_{kj,inf}$	P	$A_{Ed} = \gamma_I A_{Ek}$	$\Psi_{2,i}Q_{k,i}$	
NOTE The design values in this Table A2.5 may be changed in the National Annex. The recommended values are γ = 1.0 for all non seismic actions.						

Serviceability Limit State

For the serviceability limit state (SLS) table A2.6 from NEN-EN 1990/A1 with partial factor γ = 1.0 is used.

Table 8.6: Design values of actions for use in the combination of actions. Retrieved and revised from NEN-EN 1990/A1 (1995, p.23).

Combination	**Permanent actions G_d**		**Prestress**	**Leading variable action (*)**	**Accompanying variable actions (*)**
	Unfavourable	Favourable		Leading	Others
Characteristic	$\gamma_{Gj,sup}G_{kj,sup}$	$\gamma_{Gj,inf}G_{kj,inf}$	P	$Q_{k,1}$	$\Psi 0, iQ_{k,i}$
Frequent	$\gamma_{Gj,sup}G_{kj,sup}$	$\gamma_{Gj,inf}G_{kj,inf}$	P	$\Psi 1, 1Q_{k,1}$	$\Psi 2, iQ_{k,i}$
Quasi-permanent	$\Psi\gamma_{Gj,sup}G_{kj,sup}$	$\gamma_{Gj,inf}G_{kj,inf}$	P	$\Psi 2, 1Q_{k,1}$	$\Psi 2, iQ_{k,i}$

Load Combinations Rules

The load combinations rules are according to:

$$E_d = E \cdot (G_{k,j}; \Psi_{1,infq}Q_{k,1}; \Psi_{1,i}Q_{k,i})$$

With the combination inside brackets can be expressed as:

$$\Sigma G_{k,j} + P + \Psi_{1,infq}Q_{k,1} + \Sigma\Psi_{1,i}Q_{k,i}$$

In addition, for the railway bridge specific combinations rules are applied, these can be found in appendix section G.3 or in NEN-EN 1990/A1 page 11.

8.5.3 *Strength in Case of Fire*

The risk and potential of a fire is considered to be very low. In addition, as this railway bridge is utilised as for cargo transport, loss of life is very low. Depending on the material of the bridge the following building codes should be considered:

- NEN-EN 1992-1-2 Design of Concrete Structures - Structural Fire Design
- NEN-EN 1993-1-2 Design of Steel Structures - Structural Fire Design
- NEN-EN 1994-1-2 Design of Composite steel and Concrete Structures - Structural Fire Design

8.5.4 *Seismic Loads*

Seismic loading of the structures can be calculated using the Chilean Building codes, namely NCH2369-2003 (2003); NCH433-96 (1996); NCH433-96-2010 (2003). Although these building codes do not govern the seismic loading of bridges. Therefore, the Eurocode is used in this preliminary design, in more detail NEN-EN 1998-1 (2005); NEN-EN 1998-2 (2006), as these do focus on seismic loading of bridges. For site specific information concerning the area of Concepción, the governing peak ground acceleration and the load combination rules the aforementioned Chilean building codes are used as these are not described by the Eurocode.

8.5.5 *Snow Loads*

According to Eurocode NEN-EN 1990+A1+A1/C2 (1990) snow loads are not needed to be taken into account in any load combination after completion of the bridge. In addition, snow loads can most certainly be neglected, as Concepción has a relatively warm climate showing no sign of snowing temperatures during winters (Climate-Data.org, 2018).

8.5.6 *Rain Loads*

The rain loads are based on data regarding rain and the NEN 3215+C1+A1 (2018). As heavy rain is expected from time to time in Concepción, the railway bridge needs to be able to drain the rain water sufficiently. Based on Pizarro et al. (2012), who estimated the rainfall intensity for different return periods at different locations in Chile, the required bridge drain capacity is determined. The nearest measurement was in Chillán Viejo. The rainfall intensities for different return periods are shown in table 8.7. For this bridge it is deemed acceptable that the rainfall drainage system overflows once in a hundred years. As the drainage system is therefore able to suffice in the lower rainfall intensities, all the water is drained from the bridge deck and thus no additional load is expected, so ψ is equal to zero. The design of this drainage system is outside of the scope of this report, and is therefore neglected in the design.

Table 8.7: Rainfall intensity, estimated at Chillán Viejo, from Pizarro et al. (2012)

Return period [years]	**Rainfall intensity [mm/hr]**
R = 5	18.33
R = 100	29.02

8.5.7 *Wind Loads*

The wind loads are determined according to NEN-EN 1991-1-4+A1+C2 (2011). In chapter 8 of this standard, the methods to determine all coefficients regarding wind loads on bridges are described. This standard is only viable for bridges with a simple deck. For now the assumption is made that this is the case. For the force coefficient ($c_{f,x}$) the width to height ratio of the bridge deck is of importance. In the case of a bridge deck, the end effect coefficient is negligible as the wind streams above and beneath the deck.

The reference surfaces for railway bridges, which is needed for the calculation of the total wind force, has to include the combination of the wind load and traffic at the same time. This can be accounted for by using a height of 4 meters above the topside of the tracks to compute the reference area. This has to be applied over the full length of the bridge, as stated in NEN-EN 1991-1-4+A1+C2 (2011). The wind loads should be accounted for with accompanying reduction factors, as given in table 8.8. In case the wind loads are acting simultaneously with the traffic loads, the wind force $\psi_0 F_{wk}$ should be smaller than F^{**}_{wk}, according to NEN-EN 1990+A1+A1/C2 (1990).

Table 8.8: Summary forces and ψ values for wind loads NEN-EN 1990+A1+A1/C2 (1990)

	ψ_0	ψ_1
F_{wk}	0.75	0.5
F^{**}_{wk}	1.00	0

To calculate the vertical force component of the wind load, the eccentricity of the force and the area ($A_{ref,z}$) are of importance. The force coefficient in z-direction ($c_{f,z}$) again depends on the ratio of width to bridge deck height. The force coefficient can assumed to be 0.9, though this might result in a more conservative design. In the case that a dynamic response calculation is unnecessary one can easily determine the wind force using a relatively simple expression 8.1.

$$F_w = \frac{1}{2}\rho g v_b^2 C A_{ref,x} \tag{8.1}$$

Where C and $A_{ref,x}$ depend on the dimensions of the bridge deck.

8.5.8 *Train Loads*

The train loads are divided into two categories: static and dynamic train loading. Both are discussing in the coming two paragraphs.

Static
The loading model for the trains is determined according to NEN-EN 1991-2+C1 (2015), assuming both cargo and civilian transportation, the loading models in table 8.9 apply. For unloaded cargo trains a distributed load of 10 kN/m suffices.

Table 8.9: Characteristic values for vertical loading of loading models SW/0 and SW/2, retrieved and edited from NEN-EN 1991-2+C1 (2015)(p.75)

Loadingmodel	**q,vk [kN/m]**	**a [m]**	**c [m]**
SW/0	133	15.0	5.3
SW/2	150	25.0	7.0

Besides the SW/0 and and SW/2 load models, the LM71 load model should be verified as well NEN-EN 1991-2+C1 (2015). This load model has fixed values for the forces which have to be accounted for:

- $q_{vk} = 80\ kN/m$
- $Q_{vk} = 250\ kN$

Since the expected trains are larger than "regular train traffic" an extra measure needs to be taken, to account for the larger forces. This is done by applying an α value. Which needs to be multiplied with the characteristic values.

Dynamic
Moving train traffic can weaken and strengthen certain static stress and shape altercations, (NEN-EN 1991-2+C1, 2015). This is mostly due to the following effects:

- Fast changes in loading due to the speed at which the train passes over the bridge
- Passing of several following loads with roughly the same heart-to-heart distance, which could lead to a resonating effect
- Changes in the size of the wheel loading caused due to track and train deviations

Depending on the bridge design, a dynamic or static calculation for the loading has to be made. This is determined according to NEN-EN 1991-2+C1 (2015), see figure G.13 in the appendix.

8.5.9 *Deflections and Accelerations for Serviceability Assessments*

Maximum Seismic Deformations
In accordance with NCH2369-2003 (2003) chapter 6.3 the maximum allowable deformations for this bridge is:

$$\begin{aligned} d^{max} &= 0.015 \cdot \mathrm{h} \text{ where:} \\ h &= \text{height between two point located on the same vertical} \end{aligned} \tag{8.2}$$

Maximum Vertical Deformations
In accordance with NEN-EN 1990/A1 "the maximal total vertical deflection along the track due to rail traffic actions should not exceed L/600."

Passenger Comfort
For passenger comfort the following values apply. For the preliminary design, created in this report, the passenger comfort is neglected as other forces are considered normative.

Table 8.10: Recommended levels for vertical acceleration to ensure passenger comfort. Retrieved and revised from NEN-EN 1990/A1 (1995, p.29).

Level of comfort	Vertical acceleration b_v (m/s^2)
Very good	1.0
Good	1.3
Acceptable	2.0

8.5.10 *Settlements*

The design should be verified according to NEN-EN 1997-1 (2005).

8.5.11 *Noise Reduction*

The railway bridge is not located in an urban area. Therefore it is deemed unnecessary to apply noise reduction applications.

8.5.12 *Accidental Actions from Specified Causes*

Ship Collision
The Biobío river is not available for any kinds of shipping or recreational usage. Therefore, ship collision protection does not need to be applied.

Accidents with Cranes
Near the bridges in the Biobío river excavators on a pontoon are sometimes used to dig out sediment between the bridge pillars. As this is a operation in water under a bridge an accident can happen. This in the form of a collision of the pontoon with the bridge or by an accidental strike of the bucket against the bridge. This can

be accounted for with an impact load conform NEN-EN 1991-1-7+C1+A1 (2015). Though for the preliminary design this can be neglected, as other loads are expected to be normative.

Train Accident
In case of a train accident where the train gets derailed on the bridge extra loads need to be resisted by the bridge. To account for such loads a special load combination has to be checked. This has to be conform NEN-EN 1991-2+C1 (2015). In paragraph 6.7 the loads are described which need to be accounted for in case a train is derailed. For the design two derailed load combinations have to be accounted for in the detailed design. The train derailing loads are neglected for the preliminary design stage as other loads are assumed normative.

8.5.13 *Pile Stiffness*

Type of pile usage is unknown at this stage.

8.5.14 *Abutments*

The abutments of the bridge is beyond the scope of this project

8.6 Hydraulic Design Points

The important hydraulic aspects found in the hydraulic analysis performed in chapters 5, 6 and 7 are used as hydraulic design points, for the preliminary design of the new railway bridge.

8.6.1 *River Development*

In section 7.1 a long term (10 year) morphological simulation has been performed. This long term simulation is used as input for the design of the bridge. A simulated bed level is needed because the deep channels can be formed in the Biobío river and large scour holes around the foundation pillars due to the high flow velocities in these channels could be the result. In the most extreme case this scour hole becomes so deep that the foundation could collapse. However, the exact location of the channels cannot be given with certainty, this due to the omission of certain processes and the natural variability of the river system. But the variation of the channel depth and a possible configuration of the river can be simulated with the Delft3D model, a possible configuration in the year 2020 together with the current bridge design is presented in figure 8.3.

Figure 8.3 shows a deep channel in the middle of the river and a few smaller channels near the northern bank of the river. Whereas the southern bank is less active and shows no clear channels, the river bar present at the start of the simulation is thus still present after a simulation of 10 year. The river is therefore divided into two segments, a 'wet' segment and a 'dry' segment. The wet segment is the more active part of the river and thus more prone to erosion and sedimentation whereas the dry segment is the less active segment of the river. This dry segment only becomes active during extreme conditions, for example in case of a flood wave.

The deep channel in the middle of the river has a depth of approximately 6.0 metres, see also 7.6. This channel therefore transports most of the water during normal flow conditions which results in higher flow velocities and thus scour holes around the pillars located in this channel. However, as previously mentioned the exact location of the channels cannot be predicted and the configuration shown in figure 8.3 is only a possibility. As a result it is desirable to limit the amount of foundation pillars as much as possible to decrease the chance of a foundation pillar located in the middle of deep channel. This consideration shall thus be taken into account for each of the proposed design variants.

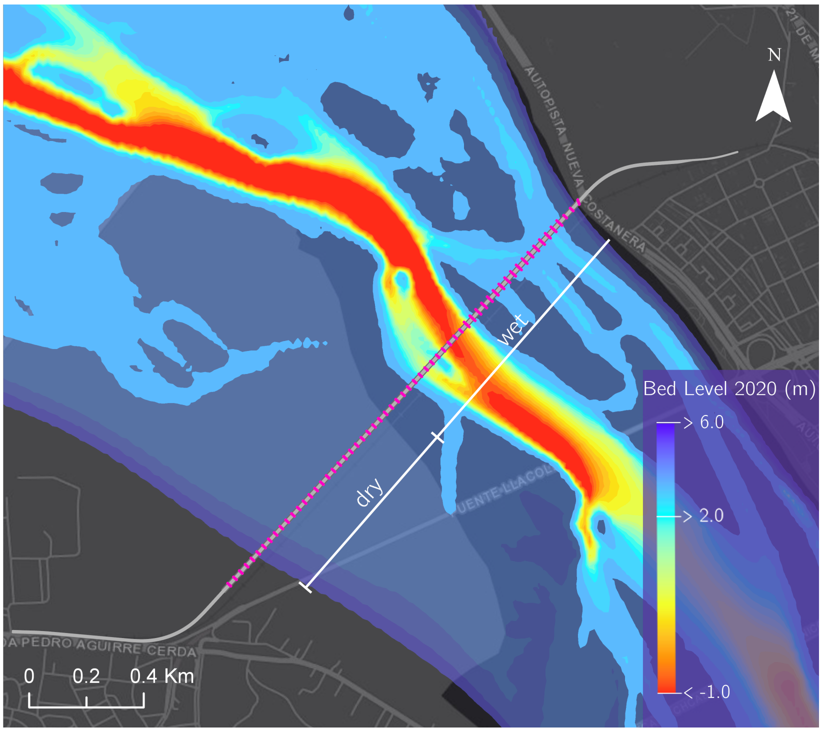

Figure 8.3: EFE's bridge design over the Biobío river with the simulated bed level of 2020

8.6.2 *Discharge & Flow Velocities*

The discharge loads were firstly based on a earlier survey performed by Ingeniería Dolmen (2015) for EFE. They calculated the return periods to be used for the design of a new railway bridge. According to this survey two return periods are important, which are summarised in table 8.11. In the report of Ingeniería Dolmen (2015) the water surface elevation is depicted in Meters Above Mean Sea Level (MAMSL), as is the bottom level. Subtracting these values results in the depth of the river, at a given discharge. Therefore the depth resulting from this discharge is taken as design depth for the hydrostatic load and can assumed to be a permanent action. The hydrostatic force is computed in accordance with NEN-EN1991-1-6 (2005) section 4.9. For this design it is assumed that the railway bridge is designed for the 100 year return period.

Table 8.11: Hydraulic parameters based on the findings of Ingeniería Dolmen (2015)

Return period [years]	**Discharge [m^3/s]**	**Flow velocity [m/s]**	**Depth [m]**
R = 100	20,526	2.5	6.51
R = 300	23,861	2.7	6.91

For this design it is assumed that the railway bridge is designed for the 100 year return period. The data used by EFE is verified by running the 100 year return period discharge scenario in the Delft3D model, as described in chapter 7. The governing values are used in the preliminary design, these are summarised in table 8.12. The most important finding of this simulation is the maximum flow velocity which is not equal to 2.5 m/s as proposed by EFE, but 3.0 m/s according the Delft3D model. The chance of exceeding 2.5 m/s has a probability of 48.75% in the scenario of the 100 year return period and is therefore likely. Hence, in the preliminary design the computed 3.0 m/s is used as maximum flow velocity.

Table 8.12: Important parameters for design concerning river discharge and flow velocities

Hydraulic Aspect	**Source**	**Value**
Maximum flow velocity	Delft3D River simulation: short-term - 100 year return period discharge	3.0 m/s
Maximum water level change from upstream	Flood wave with a 100 year return period (section 7.1)	3.8 m

8.6.3 *Scour*

Due to the velocities around the foundation pillar a scour hole around the foundation pillar is formed, which could endanger the stability of one or several foundation pillars. A scour hole is formed due to the fact that the flow 'attacks' the foundation pillar, due to the pillar the flow is deflected downwards attacking the bed and causing erosion of the bed. In order to determine if protection against a scour hole is necessary one wants to know the depth of the scour hole. However, to compute the depth several parameters must be determined, these are:

- Depth
- Dimensions of the foundation pillar
- K_S = shape factor and thus depends on the shape of the foundation pillar, a more streamlined foundation pillar results in a smaller and shallower scour hole
- K_α = angle of attack, this factor depends on the angle of attack of the flow. The larger the angle of attack, the larger the factor is and a larger scour hole is formed as a result
- K_u = velocity factor, this factor is dependent on the flow velocity and the critical velocity, i.e. the velocity for which sediment transport occurs

The scour depth can then be computed using formula 8.3 (Schiereck and Verhagen, 2016):

$$h_s = 2\, D\, K_S\, K_\alpha\, K_u\, \tanh\left(\frac{h_0}{D}\right) \tag{8.3}$$

8.6.4 *Tsunami Loads*

In case of an earthquake a tsunami might be the result. The bridge needs to be able to withstand this type of loading. To properly account for this type of loading the results from the NeoWave simulation in section 7.2 are used here. According to the NCh3363:2015 (2015) two situations need to be checked. The first situation is the combination of the impact force, and the impact of floating objects. The second situation is after the impact of the wave: and it accounts for the drag force, impact of floating object, stacking of floating objects, and the buoyancy. Additionally the loads may need to be checked at certain times. Meaning that at a certain time a high water is present, though not accompanied with the highest velocity. These combinations are important for the normative strength of the bridge as well. Though for the preliminary design this is not considered.

Taking into account the information above, the important parameters resulting from the tsunami scenario as described in chapter 7, to be used in the preliminary design, are summarised in table 8.13.

Table 8.13: Important parameters for design concerning a tsunami

Hydraulic Aspect	**Source**	**Value**
Maximum water level change from downstream	NeoWave Tsunami simulation (section 7.2)	3.5 m
Maximum hydrostatic force	NeoWave Tsunami simulation	68.5 kN/m
Maximum drag force tsunami	NeoWave Tsunami simulation	11.2 kN/m
Maximum wave impact force tsunami	NeoWave Tsunami simulation	16.9 kN/m
Maximum impact force due to floating objects tsunami	NeoWave Tsunami simulation	9.8 kN/m

9

Bridge Type Variants

To correctly determine a design for EFE's railway bridge, multiple different design concept types should first be considered. "Types" are named according to the principal load carrying structure. (Policy Advisory Group, 2007) Each differing in certain aspects, giving a broad spectrum of types to choose from and the possibility to combine between. The programme of requirements from chapter 8 serves as a basis for the 'Multi-Criteria Analysis' or MCA, chapter 10, in short. The MCA gives the proposed variants from section 9.2 each a certain score, based upon specific aspects, each with a relative weight. The variants are created with inspiration from reference projects throughout the world in section 9.1 and appendix H.2.

9.1 Reference Projects

In order to gain insight for the design variance study, different railroad bridge types that have been constructed are consulted. These reference projects need to adhere to four criteria:

1. the bridge must be a railway bridge
2. the bridge should cross a water body or river
3. the total length must be larger than 500 m
4. the bridge should not be older than 50 years

In addition, other non-railroad bridges have been taken into account as well, these are listed in the appendix H.2. Conclusively, rail- and non-rail bridges are summarised in subsection 9.1.2

9.1.1 *Reference Railway Projects*

Brug Hollandsch Diep – The Netherlands
This railway bridge crosses the Hollandsch Diep and its construction, finalised in 2005, was part of the extension of the HSL-network (the network of high-speed rail connections between different parts of Europe). With its length of approximately 2 kilometres this bridge is the longest in the route from Amsterdam to Paris. Composite materials, mainly concrete and steel, were needed to withstand vibrations generated by the high-speed trains. Due to the location of the bridge, several metres above an open body of water, it is prone to high wind velocities. In 2020 windscreens are going to be installed, to protect passing trains from these winds. However, preliminary investigations have shown the structure of the bridge might not be able to carry the additional loads of these screens (Kruidhof, 2018).

Figure 9.1: Bridge "Hollandsch Diep", retrieved from Hans Hendriksen (2017)

- Type: Rigid frame bridge with V-shaped legs
- Length: 1,992 m
- Width: 14.2 m
- Main span: 105 m
- Clearance: 20 m (Wols, 2009)
- Costs: €141,000,000.-[1] (Cobouw, 1996)

Hamm Railway Bridge – Germany
The Hamm railway bridge in Germany was constructed in 1987. The bridge is a combination of a truss system with an integrated steel arch and allows for train transportation over one of the largest rivers in Germany, the Rhine.

Figure 9.2: Hamm railway bridge, retrieved from Starossek Engineering (nd)

[1]Original costs are in Dutch 'guilders', approximated at f200 million', with on average a inflation of 2% over 20 years will result in 141 million euros.

- Type: Steel truss with integrated arch
- Length: 813 m
- Width: 26.5 m
- Main span: 250 m
- Clearance: Unknown
- Costs: €61,400,000.- (Endmann, 1989)

Almonte HSR Viaduct
This bridge forms part of the Madrid-Portuguese Border High Speed Rail link. The construction started in 2011 and the bridge was finished in 2016. The bridge is made of concrete parts and has a arch with an octagonal section. The bridge can be classified as a deck arch bridge (Pereda, nd)

Figure 9.3: Almonte High Speed Rail Viaduct, retrieved from Pereda (nd)

- Type: Deck arch
- Length: 995 m
- Width: 14 m
- Main span: 384 m
- Clearance: 65 m
- Costs: €41,000,000.- (IABSE, nd)

Vembanad Lake bridge
The longest railway bridge in India with a length of more than 4.6 km. The bridge was constructed in 2007 and finished in 2010 (PTI, 2009). The bridge consists of pre-stressed concrete beams. It forms the link between Edeppally and the site of the International Container Transshipment Terminal on Vallarpadam Island (The Hindu, 2010) and it was designed for the transport of material in bulk form.

Figure 9.4: Vembanad Lake bridge, retrieved from Balachandran (2012)

- Type: Beam
- Length: 4,620 m
- Width: 5 m
- Main span: 40 m
- Clearance: 7.5 m
- Costs: €37,700,000.- (PTI, 2009)

9.1.2 *Summary Bridge Projects*

The reference projects from section 9.1 and miscellaneous projects from appendix H.2 are combined, with their respective characteristics, in table 9.1.

Table 9.1: Summary of referenced projects used for the bridge type variance study, including both rail- and non-railway bridges.

Name	Country	Type ((non-)rail)	Construction Year	Total Span/Main span (m)	Costs (Euros)
Hollandsch Diep	The Netherlands	Rigid Steel Frame (Rail)	2005	1,992 m / 105 m	141,000,000.-
Hamm Railway Bridge	Germany	Steel Truss with Arch (Rail)	1987	813 m / 250 m	61,400,000.-
Almonte HSR Viaduct	Portugal	Steel Deck Arch (Rail)	2016	995 m / 384 m	41,000,000.-
Venbadad Lake Bridge	India	Concrete Beam Bridge (Rail)	2010	4,650 m / 40 m	37,700,00.-
Stord	Norway	Suspension (Non-rail)	2000	1,077 m / 667 m	45,000,000.-
Blue water	USA/Canada	Bowstring and Arch (Non-rail)	1997	1,862 m / 281 m	67,700,000.-
Chacabuco	Chile	Concrete Beam (Non-rail)	Present	1,465 m / 40 m	76,000,000.-
Øresund	Denmark/Sweden	Cable-Stayed (Non-rail)	2000	7,845 m / 490 m	-

9.2 Favouring Process

Each of the alternative type designs should fulfil or live up to the standards from the programme of requirements in chapter 8. In combination with the reference projects from the previous paragraph 9.1, six type variants, including the design made by EFE, are reviewed in upcoming paragraphs.

Initially, the process started with thoroughly analysing the landscape and boundary conditions which apply to the construction of the bridge. This has been carried out in chapters 4 and 8. In addition, to ease decision making steps and references to the design, the longitudinal length of the bridge is separated into two segments, see figure 9.5, where the boundary conditions vary. One where the main river discharge is located and the other where no discharge is present under normal flow conditions.

Figure 9.5: Segregation lengths of two sections

For a variant the following characteristics are taken into account, a distinction can be made between structural characteristics, e.g. span length and project specific characteristics, e.g. aesthetics and costs.

- Structural characteristics
  - Largest span – Number of pillars required, the largest possible span for a bridge type is based upon the reference projects and Lin and Yoda (2017), figure 9.6
  - Hydraulic Performance
  - Load bearing capacity of the subsoil
- Project specific characteristics
  - Costs

- Building Time
- Maintenance
- Aesthetics

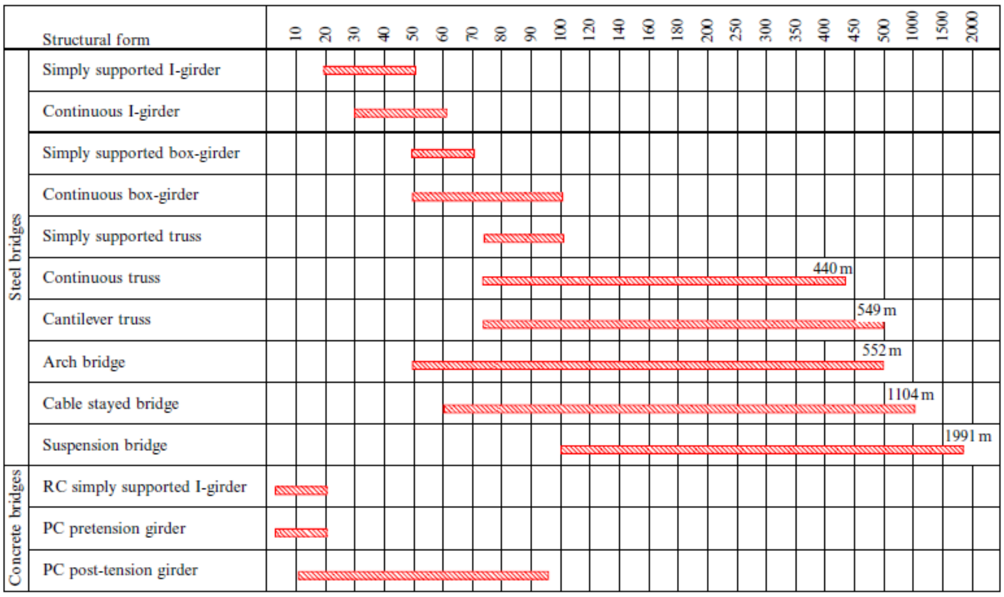

Figure 9.6: Appropriate span length according to Lin and Yoda (2017) and support by Pipinato A. (2016). Retrieved from Lin and Yoda (2017)[p. 28].

9.3 Considered Variants

The bridge can be a combination of different bridge types, most logically, the differences exists between the 'dry' and 'wet' segments, but this is not necessarily needed. In table 9.2 the possible combinations can be viewed. For the dry segment it is concluded that the most probable design is a beam bridge. As no real water discharge affects the foundation pillars in this segment, no reduction in the amount of pillars is necessarily needed, minimising costs and ease technical difficulty. However, it should be noted that, during high flood discharges, this 'dry' segment of the river is utilised as conveyance width as well. So these pillars should still be able to withstand the forces associated with these high flow conditions. A schematic overview of the different types of bridges can be found in appendix H.3.

Table 9.2: Design variants separated over a 'wet' and 'dry' segment.

Segment / Combination	**Dry**	**Wet**
0	Beam Bridge - Design EFE	
1	Beam Bridge - Alternative Design	
2	Beam Bridge	Bowstring Arch
3	Beam Bridge	Suspension
4	Beam Bridge	Truss with Arch
5	Beam Bridge	Cable Stayed

9.3.1 *Variant 0 - EFE*

A preliminary design supplied by the client. This design is quite simple and has been used regularly in Chile, the 'Chacabuco' bridge, figure H.3, has a similar design.

In order to correctly support the superstructure, EFE has proposed to construct a total of 61 foundation pillars, excluding two abutments, with a span of 30 metres. The structure is a combination of concrete beams/foundation pillars and steel I-profiles, supporting the railroad deck, these span the entire width of the river (1.9 km). A partial 3D model of the design can be seen in figure 9.7.

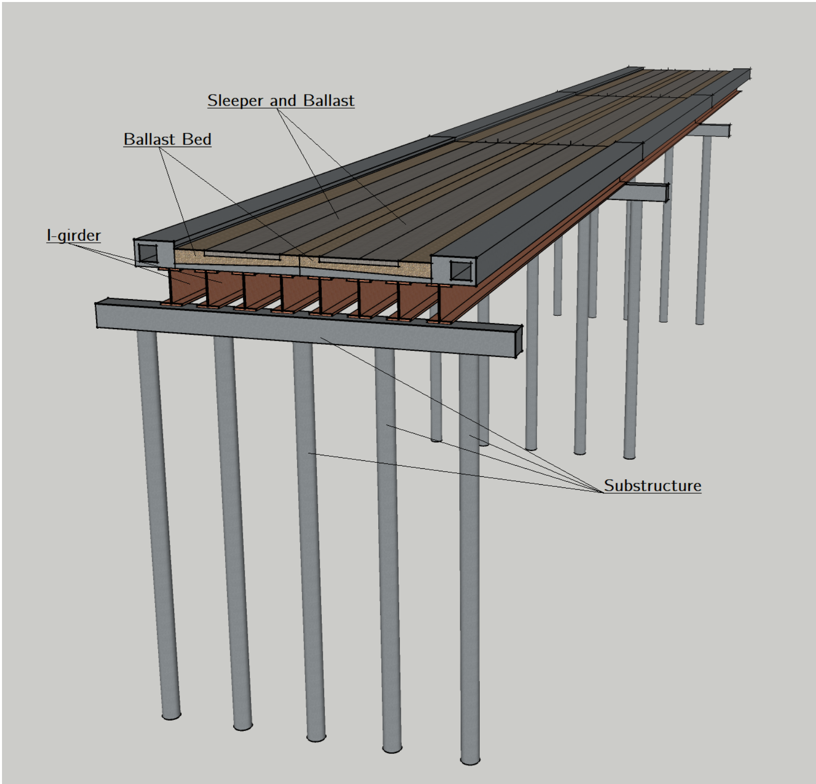

Figure 9.7: 3D sketch made from the technical drawings supplied by EFE, appendix H.4

(Dis)Advantages

- \+ Costs are deemed acceptable by EFE
- \+ Constructors have the knowledge and capacities to construct such bridges
- +/- Similar design as the 'Chacabuco'
- \- Hydraulic effects of the river could undermine the substructure over time
- \- Could prove costly to maintain
- \- Amount of foundation pillars over 'wet' and 'dry' segments are tremendous (≈33x in the 'wet' and 61 in total)

9.3.2 *Variant 1 - Alternative Beam Bridge*

An alternative beam bridge design looks similar to the aforementioned 'Hollandsch Diep' bridge, figure 9.1. A steel frame superstructure with supporting concrete foundation pillars which spans the entire width of the river (1.9 km). This type of frame allows for a larger main span than a regular concrete beam bridge. And thus, costs are likely to be higher. Additionally, it seemed that the steel frame of the bridge shows signs of corrosion earlier than expected according to Rijkswaterstaat, (Ad Tissink, 2018), pressing the need for a thorough maintenance round in 2024.

(Dis)Advantages

+ Achieves larger span than current bridges in the river (105 metres)
+ Potential to be aesthetically more attractive than current bridges in the river
+ Considerably reduces required pillars over 'wet' segment (11-12 number of pillars)
- Hydraulic effects of the river could undermine the substructure over time
- Costs are presumably somewhat higher than the proposed design from EFE
- Constructors might lack the ability to produce such a frame

9.3.3 *Variant 2 - Bowstring Arch*

This variant, and variants 3 to 5, include a different bridge type for the 'wet' segment; a beam bridge. This variant combines the beam bridge with a bowstring arch covering the 'wet' segment. Reducing the amount of foundation pillars needed in the river. This could reduce the potential effects of the river on the bridge.

(Dis)Advantages

+ Achieves larger span than current bridges in the river (250 - 550 metres)
+ Aesthetically more attractive than current bridges in the river
+ Considerably reduces required pillars over 'wet' segment (4-5 number of pillars)
- Costs are presumably higher than the proposed design from EFE
- Construction workers may lack technical expertise or experience for said type of construction

9.3.4 *Variant 3 - Suspension*

The suspension bridge greatly reduces the amount of foundation pillars required in the 'wet' segment. However, deeper and stiffer pilling in the subsoil is probably needed to support such a bridge. The geological properties of the subsoil should be taken into account.

Moreover, the Ministry of Public Works of Chile, is planning to construct the longest suspended bridge in Latin America (TheStructuralEngineer.info, 2018) in Los Lagos, crossing the Chacao channel, figure 9.8 This bridge has not been reviewed for the reference projects in section 9.1 as it is still under construction. The bridge will have a main span of 1,155 meters over a total length of 2,750 metres. The costs, however, are estimated at $740 million (=€658,000,000.-) Ministry of Public Works (nd).

(Dis)Advantages

+ Dwarfs the main span of a beam bridge (600 - 1,900 metres)
+ Could be an eye-catcher in the landscape
+ Greatly reduces required pillars over 'wet' segment (2-3 number of pillars)
+ Constructors have the ability to construct this type of bridge
- Costs are higher than the proposed design from EFE
- Geological properties of the subsoil might prove to be insufficient to anchor said structure, (Policy Advisory Group, 2007)

Figure 9.8: Rendered image of the Chacao bridge, connecting the mainland with the island of Chiloé. Retrieved from TheStructuralEngineer.info (2018)

9.3.5 *Variant 4 - Truss with Arch*

This type of bridge is partially similar to the bowstring arch bridge, but also integrates a truss in its superstructure. Reducing the stress in the arch but increases technical difficulty.

(Dis)Advantages

+ Achieves larger span than current bridges in the river (200 - 550 metres)
+ Aesthetically more attractive than current bridges in the river
+ Considerably reduces required pillars over 'wet' segment (3-6 number of pillars)
- Technical difficulty increases
- Costs are presumably higher than the proposed design from EFE

9.3.6 *Variant 5 - Cable Stayed*

A cable stayed bridge, like the Øresund bridge in figure H.4, greatly reduces the amount of foundation pillars required in the 'wet' segment. However, deeper and stiffer pilling in the subsoil is probably needed to support such a bridge. The geological properties of the subsoil could prove to be insufficient to support this type of structure.

(Dis)Advantages

+ Achieves larger span than current bridges in the river (230 - 1,100 metres)
+ Could be an eye-catcher in the landscape
+ Greatly reduces required pillars over 'wet' segment (2-4 number of pillars)
+ Easier to maintain than the proposed design from EFE
- Costs are presumably higher than the proposed design from EFE
- Constructors might lack the ability to produce such a frame

- Geological properties of the subsoil might prove to be insufficient to support said structure

9.3.7 *Summary Variants*

A short summary of the variants and their respective characteristics is given in table 9.3. In addition, a Probable Cost Index has been added. The index is based upon the costs of the reference projects, and these are compared to the initial estimated costs of the bridge design made by EFE, indicated as 0. An indexation of 1 means a small exceedance of costs compared to EFE's design and 2 indicates large exceedance of costs. However, the index is non-conclusive but act as an guide.

Table 9.3: Summary of the different possible variants

Variant Number	**Type**	**Span Allowance (m)**	**Estimated Req. Pillars (Wet Segment)**	**Probable Cost Index (0,1,2)**
0	Beam Bridge EFE	30 m	33x	0
1	Alternative Beam Bridge	≈ 100 m	11-12x	1
2	Bowstring Arch	250 - 550 m	4-5x	1
3	Suspension	600 - 1,900 m	2-3x	2
4	Truss with Arch	200 - 550 m	3-6x	1
5	Cable-Stayed	230 - 1,100 m	2-4x	2

10

Multi-Criteria Analysis

A multi-criteria analysis is an evaluation of different variants based on certain pre-specified criteria to come to the best design. It is a complex process with a solving procedure that implies different and specific challenges that originate from various sources (Clemen, 1991). According to Baris Yatsalo (2017, p.1) these challenges and difficulties include "its inherent complexity, the uncertainty of the decision situation, the choice of suitable preference structures, setting of expert judgements within decision analysis". Making the analysis prone to some subjectivity.

By weighing the different assessment criteria, a clear distinction can be made between the assessment criteria. Giving a higher value to those that are of more importance than the others.

10.1 Assessment criteria

To properly assess the different variants chosen in the chapter 9, the bridge characteristics are scored on criteria in order to compare the variants to one another. These criteria are based on the programme of requirements, described in chapter 8, and other important factors, according to Lin and Yoda (2017, p.27):

"The selection of the proper type of bridge is based on the results of the topographic survey, geological survey, traffic survey, geotechnical survey, hydro technical survey, seismic survey, and meteorological survey, etc., as well as the costs, environmental impact, and aesthetics."

The criteria taken into account for the MCA of the railway bridge are listed and elaborated in section 10.1.1.

10.1.1 *Criteria and Definitions*

In this section the different criteria are elaborated on which the bridge designs are scored.

- **Aesthetics:**
  A bridge has a certain aesthetical look and may appeal to certain people or not. The 'looks' of the bridge are mostly a subjective matter. However, a distinction between a bridge that would fit into its environment or has a more majestic appearance, can be made. The variants are evaluated accordingly, but are partly subjective to the scorers' opinion.
- **Costs:**
  Costs are important as the EFE only has a certain budget available to spend on the bridge. For most of the variants the constructions costs are unknown, therefore the costs are based on multiple reference projects where a similar bridge type has been constructed.
- **Hydraulic performance:**
  As the bridge has to pass over the river, the amount of pillars over the wet section, figure 9.5 of the river is best to be kept low. This could minimise scour holes and erosion near the foundation pillars, which could eventually compromise the foundation of the structure.

- **Building time:**
  As the EFE is on a quite tight schedule it is important to take the building time into account. This may ensure that the new railway bridge is ready on time as the old one is going to be at the end of its lifetime soon.

- **Maintenance:**
  The bridge is designed for a service lifetime of 100 years. For such a time span, the bridge undergoes several maintenance rounds, it is therefore wise to take this criteria into account. The amount of maintenance, and the accessibility to perform maintenance, is a factor which is taken into account.

- **Geological allowance:**
  Different bridges need different foundations to be able to cope with the forces it has to withstand. The ability to construct heavier foundations depend significantly on the conditions of the subsoil. Therefore the geological allowance is an important criteria to score the bridge designs on.

- **Complexity:**
  Every bridge is built differently, and thus it brings a certain complexity to the construction site and the workers. As some types of connections or constructions are more prone to faults than others, it is important to take the feasibility and complexity to build the bridge into account.

10.1.2 *Scoring Method & Weight Factors*

The bridge design types established in chapter 9 are multiplied with a certain scoring and weight scale. As both elevate the importance of the respective criteria, it is important to note that "A larger scale with more gradations increases the sensitivity of the evaluation process; shorter scales with fewer gradations reflect lower evaluation sensitivity." (Anil Mital, 2014, p. 30) and should therefore be chosen carefully. According to the same literature, the weights generally indicate the relative importance of the various criteria. It is common to use a 10-point or 100-point total, but other point totals are acceptable as well as long as the distribution over the various criteria is relative to each other (Anil Mital, 2014).

Scoring Method
The criteria for each individual variant are scored as followed:

1. Poor
2. Below average
3. Sufficient/Satisfactory
4. Above average/Good
5. Excellent

This means the criteria should be scored accordingly:

- **Aesthetic:** Not attractable (1) - Eye catching (5)
- **Costs:** Very expensive (1) - Very inexpensive (5)
- **Hydraulic Performance:** Very poor (1) - Very good (5)
- **Building Time:** Greatly exceeding proposed building time (1) - Within proposed building time (5)
- **Maintenance:** Difficult to maintain (1) - Easy accessible for maintenance (5)
- **Geological Allowance:** Subsoil not sufficient / Many foundation piles needed (1) - Minimal usage of piles (5)
- **Complexity:** Very complex (1) - Easy to construct (5)

Weight Factors
Determining the weights for the criteria, the weight factors, is a difficult process, as it is partly objective and subjective. The weights are determined in accordance with the programme of requirements, chapter 8, but the

scale and determination of importance per criteria is a partly subjective process. In order to achieve a sub-optimal weighing (as this process is not factual or mathematical, an optimal approach can not be established), different approaches have been reviewed, these are tallied in appendix H.5.1.

Conclusively, an approach with a 140-point total is chosen, with a scale ranging from [-13, -6, 0, +6, +13]. Reflecting the relative importance of the most prominent criteria, whilst not neglecting the least influencing factor, in accordance with Anil Mital (2014). This results in the following weight factors:

Table 10.1: Definitive weighing factors MCA criteria.

Criteria	**Importance [-13.-6,0,+6,+13]**	**Weight [140-point total]**
Aesthetic	0	20
Costs	+13	33
Hydraulic Performance	0	20
Building Time	+6	26
Maintenance	-6	14
Geological Allowance	0	20
Complexity	-13	7

10.2 Results

The MCA scoring table is filled in by the PPRB team members. Each of the variants has been scored whilst not knowing the respective weight of the different assessment criteria. The averaged non-weighed results are presented in section 10.2.1. These results are eventually multiplied with their respective weight and averaged over the group in section 10.2.2. The individual scores are elaborated in the appendix, section H.5.2.

10.2.1 *Non-Weighted Performance Alternatives*

The averaged non-weighted score, between the PPRB team members, is visible in table, 10.2. The highest scoring variant is 'Variant 1 - Alternative Beam Bridge' followed by 'Variant 2 - Bowstring Arch' and the design supplied by EFE (Variant 0).

- *Variant 1:* **Score: 22.25** - Criteria Max./Min.: Complexity (4.5)/ Hydraulic Performance (2.0)
- *Variant 2:* **Score: 20.75** - Criteria Max./Min.: Aesthetic (3.75)/ Costs & Building Time (2.5)
- *Variant 0:* **Score: 20.25** - Criteria Max./Min.: Complexity (4.5)/ Hydraulic Performance (1.0)

Table 10.2: Average (non-weighted) results of the MCA filled in by PPRB group members

Criteria	**Variant 0**	**Variant 1**	**Variant 2**	**Variant 3**	**Variant 4**	**Variant 5**
Name	*Beam Bridge EFE*	*Alternative Beam Bridge*	*Bowstring Arch*	*Suspension*	*Truss with Arch*	*Cable-Stayed*
Aesthetic	1.25	2.5	3.75	4.75	2.25	4.75
Costs	5	3.5	2.5	1	2.5	1
Hydraulic Performance	1	2	3.25	4.75	3.5	4.75
Building Time	4	3.75	2.5	1.75	2.5	1.75
Maintenance	1.75	2.75	2.75	2.75	2.25	3
Geological Allowance	2.75	3.25	3.25	2.5	3.25	2.5
Complexity	4.5	4.5	2.75	2	2.75	1.75
Total	**20.25**	**22.25**	**20.75**	**19.5**	**19**	**19.5**

Both beam bridges, variant 0 & 1, score very well on the complexity whilst receiving a poor hydraulic performance score. However, costs are considerably kept low compared to other bridge type designs. The design supplied by EFE shows some large deviations between the score of each respective criteria, whilst variant 1 & 2 show a more stable or average score overall.

10.2.2 *Weighted Performance Alternatives*

The averaged weighed score, between the PPRB team members, is visible in the table, 10.3. The highest scoring variant is the 'Variant 1 - Alternative Beam Bridge' followed by the 'Variant 0 - EFE' and 'Variant 2 - Bowstring Arch'.

- *Variant 1:* **Score: 431.5** - Criteria Max./Min.: Costs (115.5)/ Maintenance (38.5)
- *Variant 0:* **Score: 412** - Criteria Max./Min.: Costs (165)/ Hydraulic Performance (20)
- *Variant 2:* **Score: 410.25** - Criteria Max./Min.: Costs (82.5)/ Complexity (19.25)

Table 10.3: Weighted average score of the MCA populated by PPRB team members divided by four

Criteria	Weight	Variant 0	Variant 1	Variant 2	Variant 3	Variant 4	Variant 5
Name		*Beam Bridge EFE*	*Alternative Beam Bridge*	*Bowstring Arch*	*Suspension*	*Truss with Arch*	*Cable-Stayed*
Aesthetic	20	25	50	75	95	45	95
Costs	33	165	115.5	82.5	33	82.5	33
Hydraulic Performance	20	20	40	65	95	70	95
Building Time	26	91	91	65	45.5	65	45.5
Maintenance	14	24.5	38.5	38.5	38.5	31.5	42
Geological Allowance	20	55	65	65	50	65	50
Complexity	7	31.5	31.5	19.25	14	19.25	12.25
Total	140	**412**	**431.5**	**410.25**	**371**	**378.25**	**372.75**

From the averaged weighed results it can be concluded that the 'Alternative Beam Bridge' has the highest score. Outperforming the design made by EFE and the 'Bowstring Arch' by $\approx$ 20 points. Both beam bridges score above average on the costs, the most important criteria, whilst scoring low on the hydraulic performance. Additionally, the estimated gross building time also has a big influence. The beam bridges are considered to be easy and relatively fast to construct compared to the other variants.

Lastly, large differences between aesthetics, costs, hydraulic performance and building time are visible between variants 0,1,2 (referred to as left) and variants 3,4,5 (referred to as right). The score of the variants on the right side is higher considering the hydraulic performance and aesthetics. This is due to the possibility of larger spans, which can evade the channels in the river and a more attractive or 'special' kind of structure. However, the right variants score considerably lower on costs, the most heavy criteria, and building time, due to a more complex construction, resulting in an average difference between the left variants ($\approx$ 374) and right variants ($\approx$ 418) of 44 points.

10.3 Recommendation Bridge Type

In combination with the results obtained from the MCA, results from the hydraulic models (see chapter 7, and the programme of requirements in chapter 8, it can be concluded that the most preferred design is an alternative beam bridge design. Deviating from the original design proposed by EFE, but also keeping some aspects implemented from EFE's bridge design.

The alternative design scores better on hydraulic performance, which could be a key factor to fulfilling its service life, whilst also minimising costs, improving aesthetics, matching estimated building time and a higher geological allowance when comparing it to the beam bridge of EFE.

11

Preliminary Design

Following the multi-criteria analysis in the previous chapter, a preliminary design for the alternative is made. Firstly, the main span and locations for the foundation columns are determined in section 11.1. The location of the foundation columns is important to clearly clarify, as the position of the columns could be influenced by the morphological effects of the river, following from the hydraulic results in chapter 7.

As Concepción is situated in a region were high order magnitude earthquakes occurs, a load combination that includes earthquakes is most likely to be normative. However, other load combinations should be checked as well. As this is a preliminary study, not all load combinations are checked, but the most probable combinations, like earthquakes combined with train loading or tsunami's, are. The load combinations that are considered can be viewed in section 11.3.

This chapter shows the design process of the new railway bridge, where first, in section 11.1, the general dimensions are mentioned. Next in section 11.2, the acting loads are assessed on the longitudinal and transverse cross section. In section 11.3 the most important load combinations are evaluated. Subsequently, in section 11.4 the normative load combination is summarised. Thereafter in section 11.5 and 11.6 the design process of the column and foundation is described. Thereupon, the effects of the scour process are elaborated in section 11.7.

11.1 General Design Dimensions

The bridge deck design from EFE, visible in figure 11.3, is compared with the overall bridge design for the 'Hollandsch Diep' bridge, visible in figure 11.1. The most prominent difference between the two designs is the main span, EFE's main span is 30 metres whilst a span of 100 metres is assumed for the alternative design of this report. As a result much less columns are needed in the river, as can be seen in figure 11.2.

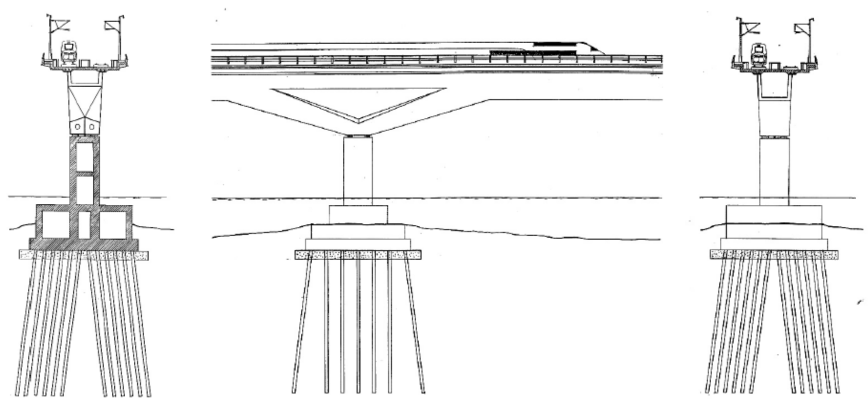

Figure 11.1: Conceptual design of the 'Hollandsch Diep' bridge. Retrieved from Benthem and Falbe-Hansen (2003, p. 5)

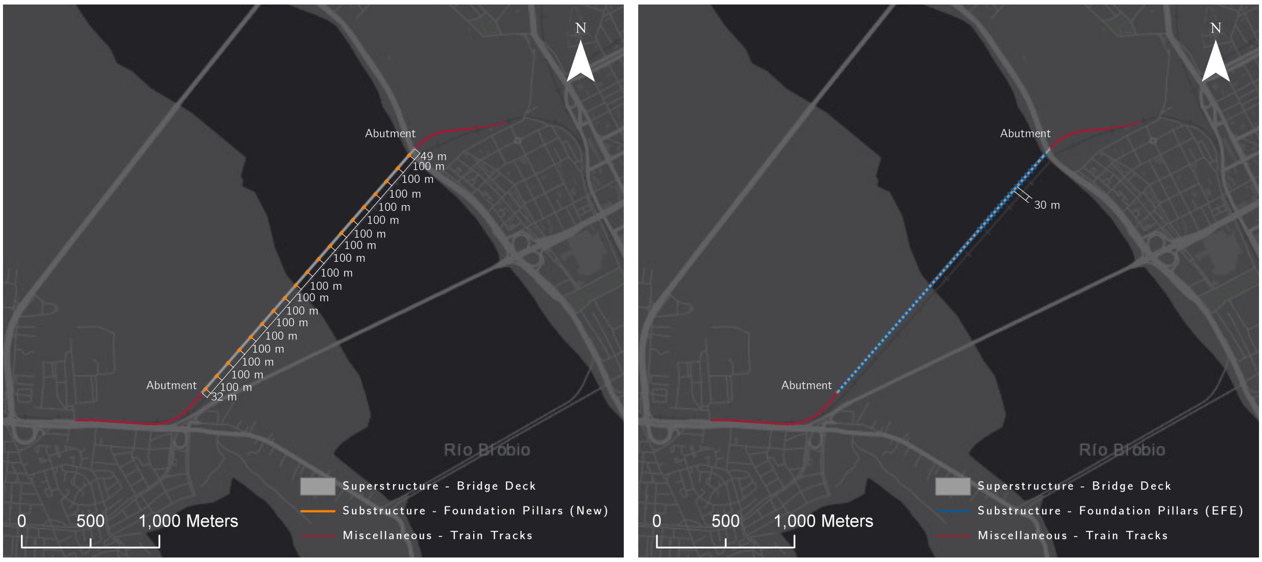

Figure 11.2: Placements of the columns, with on the left side the alternative design and on the right side EFE's design.

The positioning of the foundation columns for the alternative design are drawn using AutoCAD. These are combined with a longitudinal cross-section of the subsoil, supplied for by EFE, resulting in figure I.1 in appendix section I.1.

The super- and substructure of the bridge are a combination of a steel rigid frame and reinforced concrete foundation columns.

11.1.1 *Superstructure*

In accordance with section 11.1, assumptions for the superstructure are used. The superstructure is to be designed in a similar way as the reference project 'Hollandsch Diep', described in subsection 9.1.1. The cross-sectional design of the bridge deck is a combination between the Hollandsch Diep and EFE's design, visible in figure 11.3. The self weight of the superstructure is used in the calculations for the foundation of the bridge.

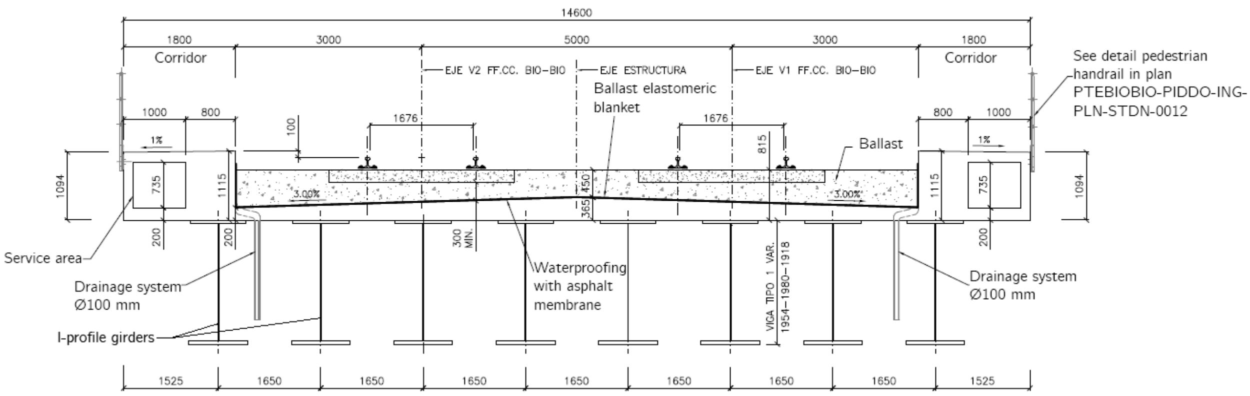

Figure 11.3: Cross-section of the deck of the bridge according the design by EFE. Retrieved and translated from P. Uribe, A. de Castro, R. Reginensi, P. Buguña, J. Piddo (2019a)

Contradictory to the bridge deck design made by EFE, figure 11.3, the alternative is made with a ballast-less track and without any I-girder profiles. The deduction of the ballast bed significantly reduces the self weight of the bridge, but more damping and elasticity have to be present in the connection between the supporting structure and the railway track, (Sectie Verkeersbouwkunde, 2015).

Concluding, the main elements of the superstructure of the bridge include:

- Railway tracks: UIC 60 for cargo trains, Agico Group (nd)
- Sleepers: It is assumed that a concrete two-block girder is used
- Overhead line: The weight of this element is neglected for the preliminary design
- Concrete Slab for the deck: The thickness of the slab is assumed to be 100 mm
- Steel V-frame: The weight of the frame according to Benthem and Falbe-Hansen (2003)

The cross-sectional view of the bridge can be seen in figure 11.4. The materials and their respective weights are listed in appendix section I.2.

11.1.2 *Supporting Column*

The substructure of the bridge consists of a straight rectangular reinforced concrete column, unlike visualised in figure 11.4 as 'foundation pillar', and the underlying foundation block with the foundation piles, defined in section 11.6. The design made in the figure is purely for visualisation purposes with dimensions for the column unknown as of yet.

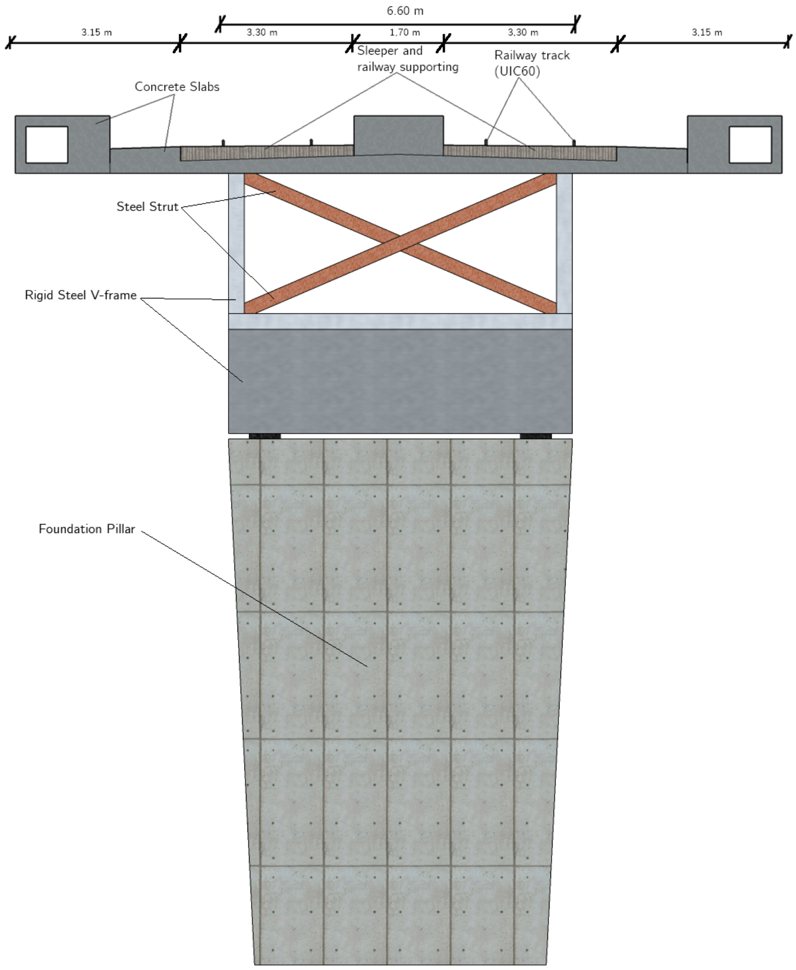

Figure 11.4: Cross-sectional view of the alternative bridge design.

11.2 Mechanical Schemes and Respective Loads

The loads that act on the bridge are segregated into two different directions, longitudinal loads and cross-sectional loads. However, they do no act independently from each other, but are combined according to the load combinations from section 11.3 and with their respective partial- and reduction factors, see table I.6.

11.2.1 *Longitudinal Cross-section*

The longitudinal cross-section of the bridge is visualised as a 1,881 metres long beam, supported by two abutments and 19 foundation columns, visualised in figure 11.5. One abutment is designed as a regular bearing and the other abutment as a roller bearing in order to compensate for any expansions as the result of thermal deviations. The columns that support the superstructure are designed as a resiliently clamped supports at the bottom, visible in figure 11.6, and a hinge where the column meets the superstructure. The columns have been measured from an AutoCAD drawing supplied by EFE and deviate in length. The respective length for each column can be viewed in appendix table I.1.

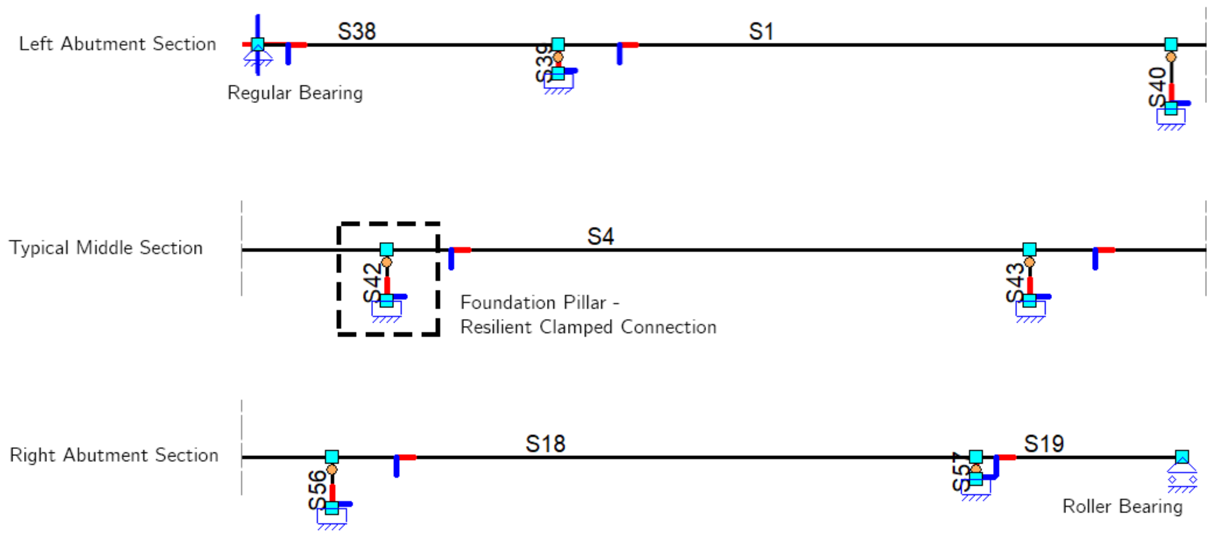

Figure 11.5: Mechanics scheme for the longitudinal cross-section of the bridge. The dotted square encircles a foundation column which mechanical scheme is further schematised in figure 11.6.

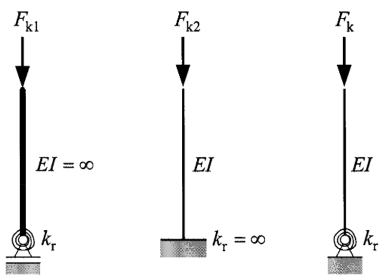

Figure 11.6: Mechanics scheme for a resiliently clamped column. Retrieved from C. Hartsuijker en J.W. Welleman (2016, p. 176).

11.2.2 *Loads on Longitudinal Cross-section*

The loads that are included in the longitudinal direction are the following and act on the columns according to figure 11.7:

- Self weight: q_g = 157.6 kN/m, appendix section I.2
- LM71: taken into account as both a point load and a distributed load, the magnitude of the load follows from the programme of requirements subsection 8.5.8 and appendix section I.4 figure I.2:
  - q_{vk} = 80 kN/m multiplied with $\Phi = 1.21$ and $\alpha = 1.21$, appendix I.4, = 117.1 kN/m
  - Q_{vk} = 250 kN multiplied with $\Phi = 1.21$ and $\alpha = 1.21$, appendix I.4, = 366.0 kN
- SW/2: Distributed over the entire length of the bridge as a distributed load, as shown in table 8.9 from the programme of requirements and figure I.3 in the appendix, q_{vk} = 150 kN/m multiplied with $\Phi = 1.21$, appendix I.4, = 181.5 kN/m

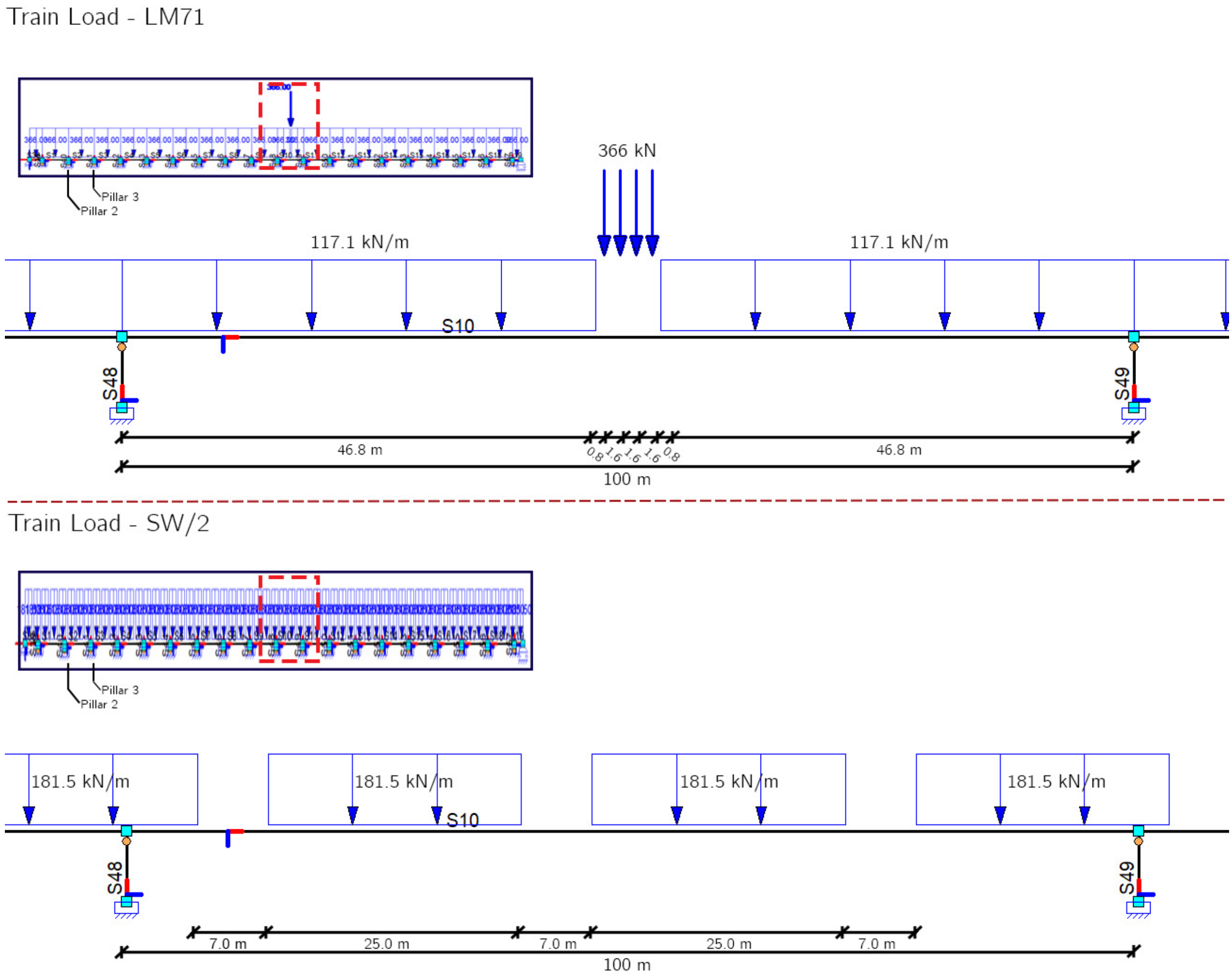

Figure 11.7: Visualisation of the acting trainloads on the bridge deck in longitudinal direction.

11.2.3 *Transverse Cross-section*

For the verification of the design in the transverse direction of the bridge components, a few loads need to be accounted for which deviate extensively from the longitudinal cross-section. These additional loads are, for example, the loads due to wind and a tsunami. Based on the cross-section shown in figure 11.4 a first mechanical scheme is derived. This scheme is shown in figure 11.8, in this situation a rigid scheme is visualised on top of the columns. Due to the fact that the rigid frame is constructed as one component, the substructure can be further simplified as scheme b. This is a rigid column supported by a bearing and a rotational spring, the latter to simulate a resiliently clamped support.

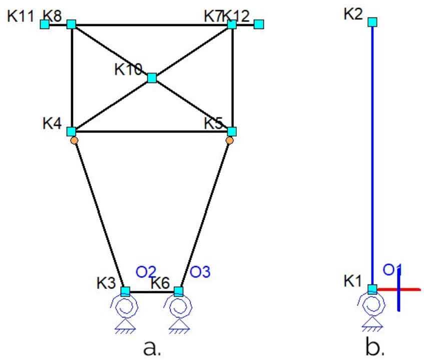

Figure 11.8: Mechanical schemes, in transverse cross-section, used for the design of the bridge

11.2.4 *Loads on Transverse Cross-section*

The loads that act in the transverse direction are listed below and are visible in figure 11.9:

- Hydrostatic Pressure = 207.9 kN/m, including the permanent loads, according to section 8.6.2, this force acts on all sides of the foundation column.
- Wind Loads: are determined according to subsection 8.5.7 and appendix I.5, the distributed load leads to a point load and bending moment of:
  - $F^{**}_{Wind,k}$ = 877.0 kN
  - $M_{Wind,k}$ = 1577.0 kNm,
- Earthquake = 25.4 MN, calculated in accordance with NEN-EN 1998 and NCh433, see appendix section I.3.
- Tsunami (Impact): as stated in 7.3 and I.7.2, for the wave impact situation three loads have to be taken into account, these forces still have to be multiplied with the width of the structure:
  - Impact Wave = 16.9 kN/m, applied at a height of 3.5 metres above, see 7.2, the bottom of the column, this results in a force of 67.6 kN.
  - Impact due to floating objects = 9.8 kN/m, applied at a height of 3.5 metres, above the bottom of the column, this results in a force of 39.2 kN.
  - Hydrostatic = 68.5 kN/m, this results in a force of 274 kN.
- Tsunami (Post-Impact): there are four types of post-impact forces resulting from a tsunami, according to 7.3, these forces still have to be multiplied with the width of the structure:
  - Drag Force = 11.2 kN/m, so a load of 44.8 kN.
  - Stacking impact force due to floating objects, though this load is neglected in this project due to the large distance in between the columns (≈ 100 metres).
  - Impact due to floating objects = 9.8 kN/m, applied at a height of 3.5 metres from the bottom of the column, resulting in a force of 39.2 kN.
  - Hydrostatic = 68.5 kN/m, thus resulting in a force of 274 kN.

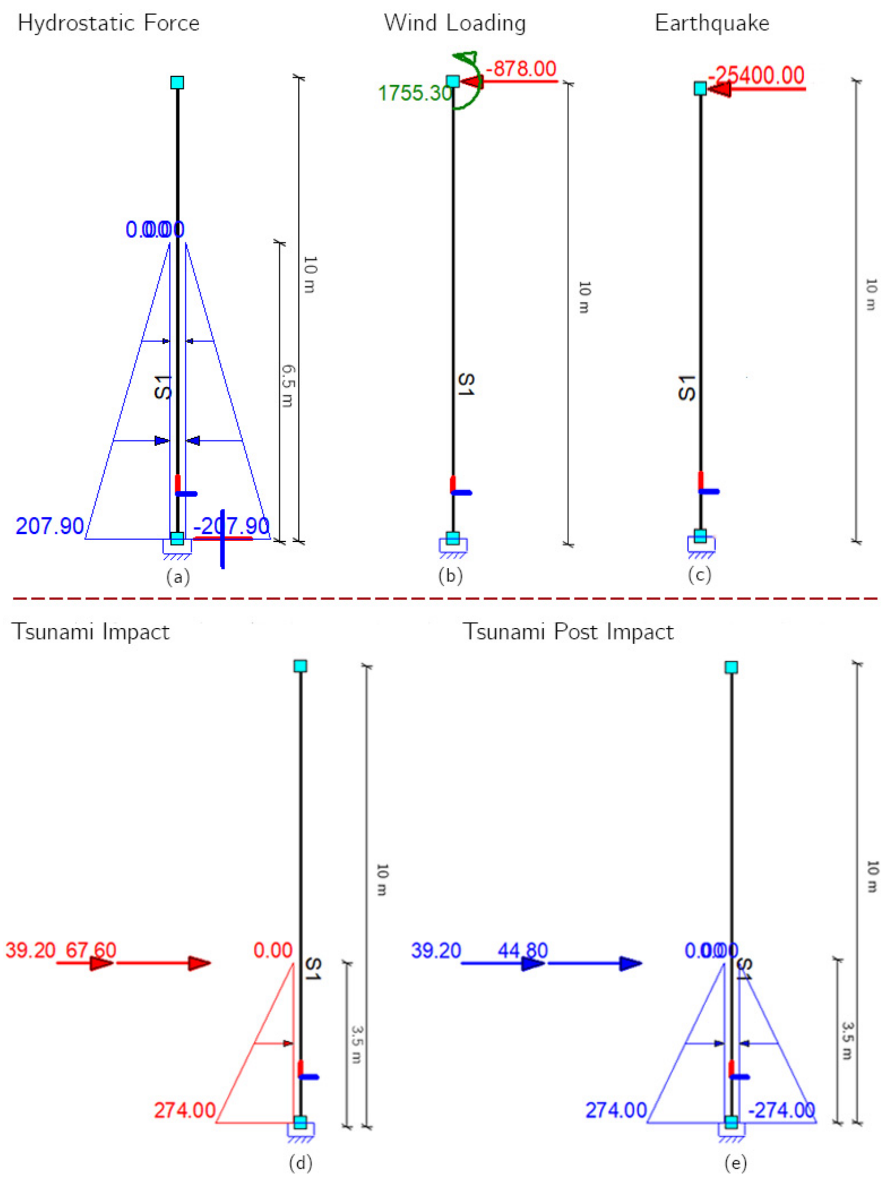

Figure 11.9: Visualisation of the acting loads on the column in transverse direction.

11.3 Considered Load Combinations

As stated in the introduction of this chapter, not all load combinations that can affect the bridge are checked. The most probable worst scenario load combinations, including load combinations with earthquakes, tsunami's, train loading and wind, are analysed. In any definitive design study, all load combinations should be checked. The load combinations that include loading due to an earthquake are taken into account according to NCH433-96-2010 (2003):

When designed with the method of load and resisting factors:

- 1.4 * (permanent loads + live loads + earthquake)
- 0.9 * permanent loads + 1.4 * earthquake)

Special load cases, such as tsunamis and earthquakes, are combined with the most probably variable load actions. The load combinations which are considered are visible in table 11.1. Train actions and a tsunami are not combined, in case of a tsunami, it is likely that a warning system prevents any train activity.

Table 11.1: Considered load combinations for the preliminary design.

-	Loading Source			
Type of loading	*Permanent*	*Leading Variable action*	*Other variable actions*	
LC0	Only Permanent	N.A.	N.A.	
LC1	Included	Earthquake	Wind	
LC2	Included	Earthquake	Train actions	Wind
LC3	Included	Tsunami	Wind	
LC4	Included	Train actions	Wind	

The load combinations are combined with the partial- and reduction factors as mentioned in sections 8.3 and G.1, respectively. The load combinations for earthquakes are listed at the start of this section. The combinations, with the responding factors, are listed in I.6

11.4 Normative Load Combination

20 load combinations have been checked in total. From the results, produced with MatrixFrame, the most prominent loads include an earthquake (FuC3 to FuC8 or LC1 to LC2), visible in figures I.9 and I.10. The normative loads are listed in table 11.2.

Table 11.2: Loads following from the normative load combination.

	N (kN)	V (kN)	M (kNm)
S40	36,763	36,789	370,349
S41	46,532	36,789	370,349

11.5 Design Column

Designing a column with an acting shear force of approximately 37 MN and a bending moment of 370 MN is challenging. To resist the shear large amounts of stirrups have to be applied and in order to resist the acting bending moment a large concrete surface area and reinforcement is required. Several iterations are conducted, with changing width and height dimensions but also adapting reinforcement percentages, the definitive calculations for the columns can be viewed in appendix section I.9. A cross-sectional view of the column is shown in figure 11.11.

For both columns 2 and 3 the same properties are applied. In short:

- Width = 3.2 metres
- Height = 2.5 metres
- Concrete class = C45/55

Although the maximum reinforcement percentage for C45/55 is 3.05%, 6% is used in the calculations for the bending moment capacity of the column. Otherwise it is impossible to gain enough capacity to resist the acting moment without getting immense dimensions for the column. This is further taken into account in the recommendations and conclusion. To reach a steel surface area of $A_{steel} = 0.06 \cdot A_{concrete} = 0.48\ m^2$ the following reinforcement bars are applied:

- 246 ϕ_{main}50 mm in total, with a concrete cover of 60 mm
- 170 ϕ_{main}60 mm in total, with a concrete cover of 70 mm

In order to withstand the acting shear force, double linking stirrups have to be applied, visible in figures 11.10 and 11.11. In addition, placing 123 ϕ50 reinforcement bars in one row would not fit in the column, as can be seen on the left side in figure 11.10. However, this asks for a recalculation of the bending moment capacity of the column, this is taken into account for the recommendations.

Concluding, with the acting shear force and bending moment on the columns, it is economical unviable or not possible to dimension such a column in accordance with the Eurocodes. Instead other measures should be taken, for instance installing dampening systems to reduce the acceleration of the bridge and the impact of an earthquake, calculate the force due to an earthquake based upon the entire system of the bridge instead of an individual pier model, optimise calculations and/or utilise different kinds of supporting structure.

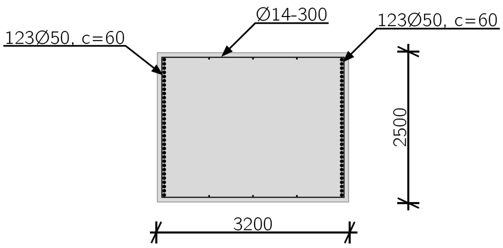

Figure 11.10: Side view and cross-sectional view of the column with respective reinforcement bards.

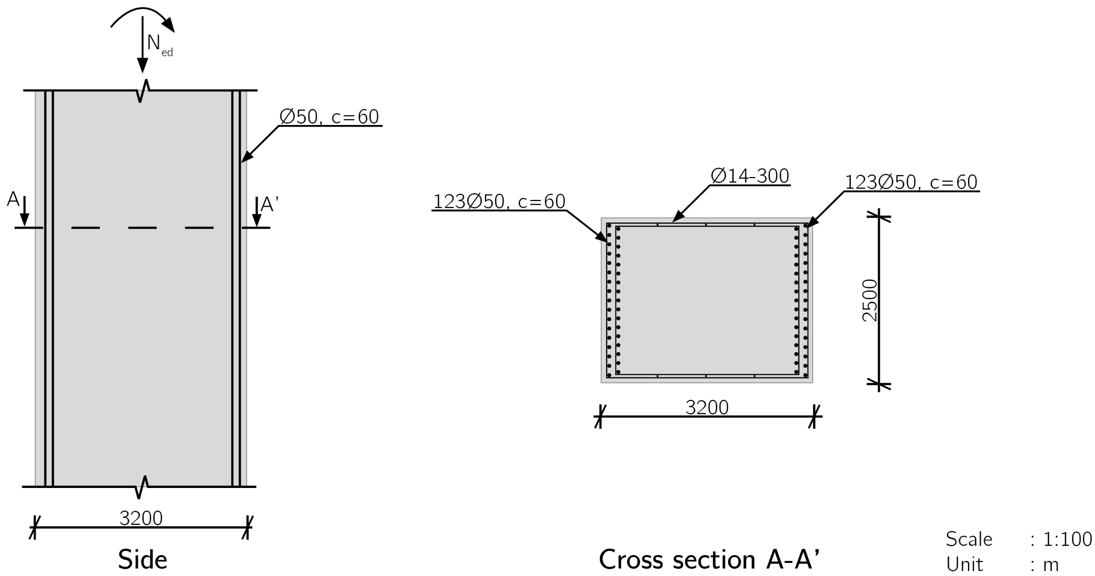

Figure 11.11: Side view and cross-sectional view of the column with respective reinforcement bards.

11.6 Design Foundation

Not all foundation columns are considered in this report, instead two normative, out of the total of 19, are considered. All the columns needed for this bridge type design have been numbered and are visible in appendix figure I.1.

Columns 2 and 3 are used for the normative design for all the columns, as for these locations the loads are the highest. The columns vary in length, 10 and 7.5 metres respectively (figure I.1), and the characteristic subsoil of each column is appropriated by SPT S4 and S7, respectively.

11.6.1 *CPT - S4 and S7*

The characteristic geotechnical information is retrieved from GC Geoconsult (2019c), GC Geoconsult (2019a) and GC Geoconsult (2019b). Based on the SPTs a conversion is made to CPT, see appendix I.10. Consequently, based on the derived CPT a calculation is performed with the Koppejan method to estimate the bearing capacities at these locations.

In figures 11.12 and 11.13 the characteristics of the subsoil for columns 2 and 3, respectively, can be viewed.

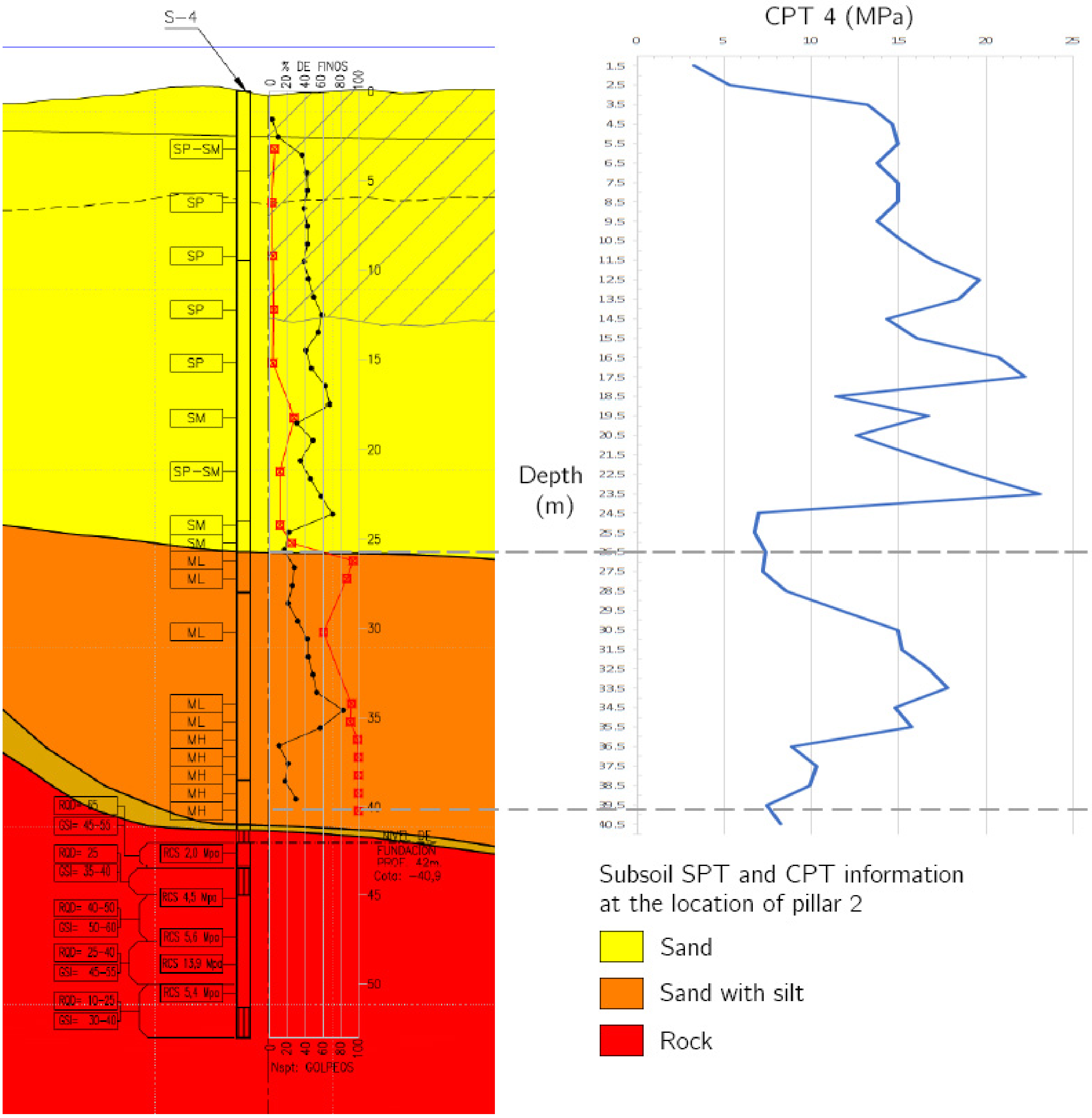

Figure 11.12: On the left the SPT, obtained at location 4 or column 2, on the right CPT values. Retrieved and revised from GC Geoconsult (2019c, p. 1) and GC Geoconsult (2019b, p. 3).

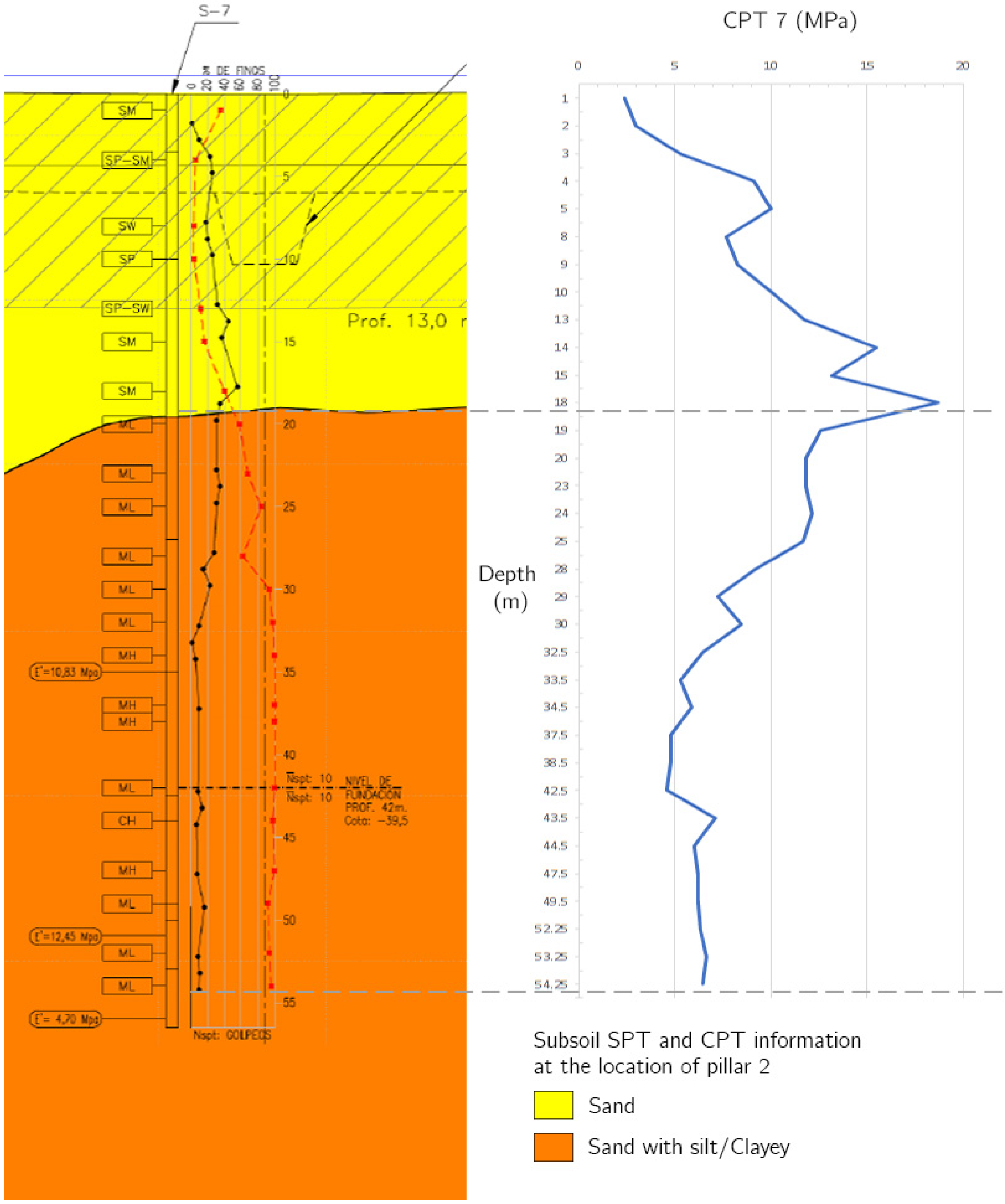

Figure 11.13: On the left the SPT, obtained at location 7 or column 3, on the right CPT values. Retrieved and revised from GC Geoconsult (2019c, p. 1) and GC Geoconsult (2019b, p. 3).

Based on these characteristics the bearing capacities are determined. The bearing capacity is determined with the Koppejan method, I.10. Using prefabricated square concrete piles of 450x450 mm results in a bearing capacity of 2958 kN and 2837 kN, for column 2 and 3 respectively. At column 2 the piles are driven into the soil to a depth of 21 metres, for column 3 this is 18 metres.

11.6.2 *Foundation of column 2*

To distribute the load from the column to the piles, a foundation block has to be constructed. This foundation block in turn carries 14 foundation piles, which are needed to resist the acting normal force and self weight of the column. According to NEN-EN 9997-1 (2017) one should consider the influence area of piles driven next to each other. To assure this influence area is as small as possible a minimum distance of approximately $3D_{eq}$ is used from center-to-center, this is 1.5 metres. To keep the dimensions of the foundation block manageable, the required number of foundation piles are divided into two rows. With a distance of roughly $6D_{eq}$, the two rows are completely outside of each other's influence area. This configuration is shown in figure 11.14

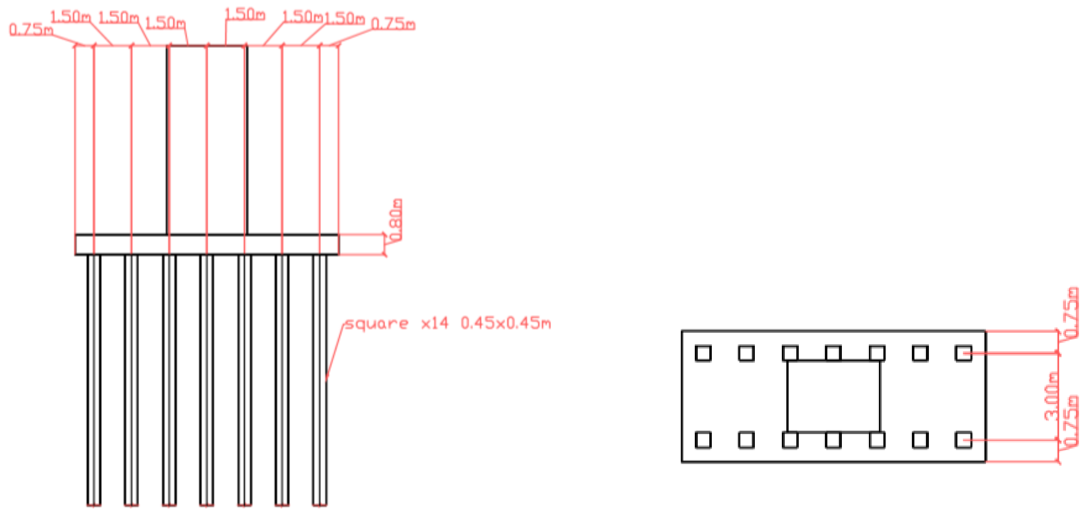

Figure 11.14: Configuration of the foundation block of column 2, with front view on the left and top view on the right

11.6.3 *Foundation of column 3*

The foundation of column 3 needs to be able to resist a higher acting normal force. In addition, the bearing capacity of the chosen driven piles at this location is slightly lower, and therefore this column requires 17 foundation piles. Initially, the same foundation block from column 2 is utilised. The grouping differs: 3 rows of foundation piles are applied instead 2. The two outer rows contain 6 piles each and the middle one 5. Even though an extra row is needed, the middle row is at a safe distance of approximately $3D_{eq}$, ensuring little interference of the piles and their influence areas. This configuration is shown in figure 11.15.

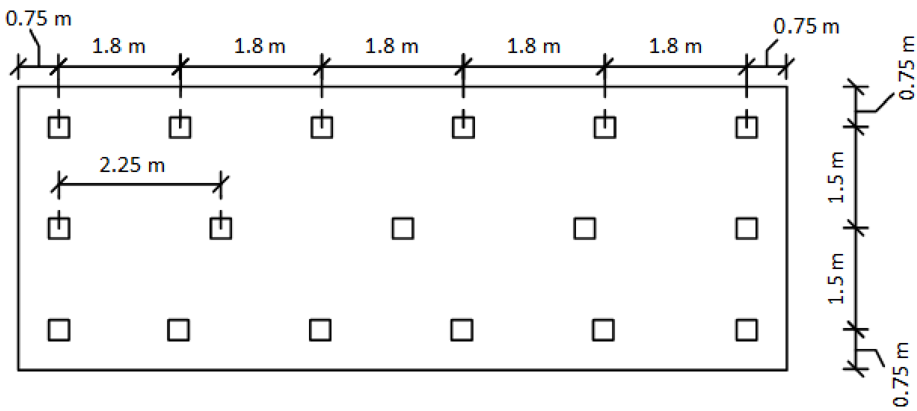

Figure 11.15: Configuration of piles for foundation block of column 3, top view

11.7 Scour

The number of foundation columns is kept to the possible minimum for this alternative beam bridge design. Since, as previously mentioned, the exact location of the channels in the Biobío river cannot be predicted with certainty, the columns should be able to withstand scour conditions as described in section 8.6.3. As described in that section the depth of a scour hole depends on the flow velocity, size and shape of the column.

The size and shape of the column are represented in equation 8.3 by the shape factor (K_S) and the angle of attack (K_α). In case of a rectangular or elliptic cross section the depth of a scour hole is large compared to a round cross section, since the K_S and K_α are both larger than 1, resulting in a deeper scour hole. Therefore, from a hydraulic point of view, the most optimal design for the column is a round profile. However, for the preliminary design a rectangular column is designed.

For a rectangular column with a length of 3.2 metres and a width of 2.5 metres, the shape factor is 1.44 and angle of attack factor is 1.2. These factors influence the depth of the scour hole quite severely. With a critical velocity of approximately 0.3 m/s and a flow velocity of 3.0 m/s, as found in the hydraulic analysis section 8.6, the velocity factor equals 1, indicating that there is live-bed scour. This results in a scour hole of about 8.90 metres with a water depth of 6.5 metres, which was found for the 100 year return period (figure 7.12). It is advisable to design bed protection in later design stages.

11.8 3D visualisations

The 3D model of the bridge is integrated into a landscape environment. A 3D- and side view are visible in figure 11.16. Figure 11.17 shows the bathymetry of 2020 integrated into the environment, where the differences between the old railroad bridge (yellow), EFE's column design (red) and PPRB's design are clearly visible.

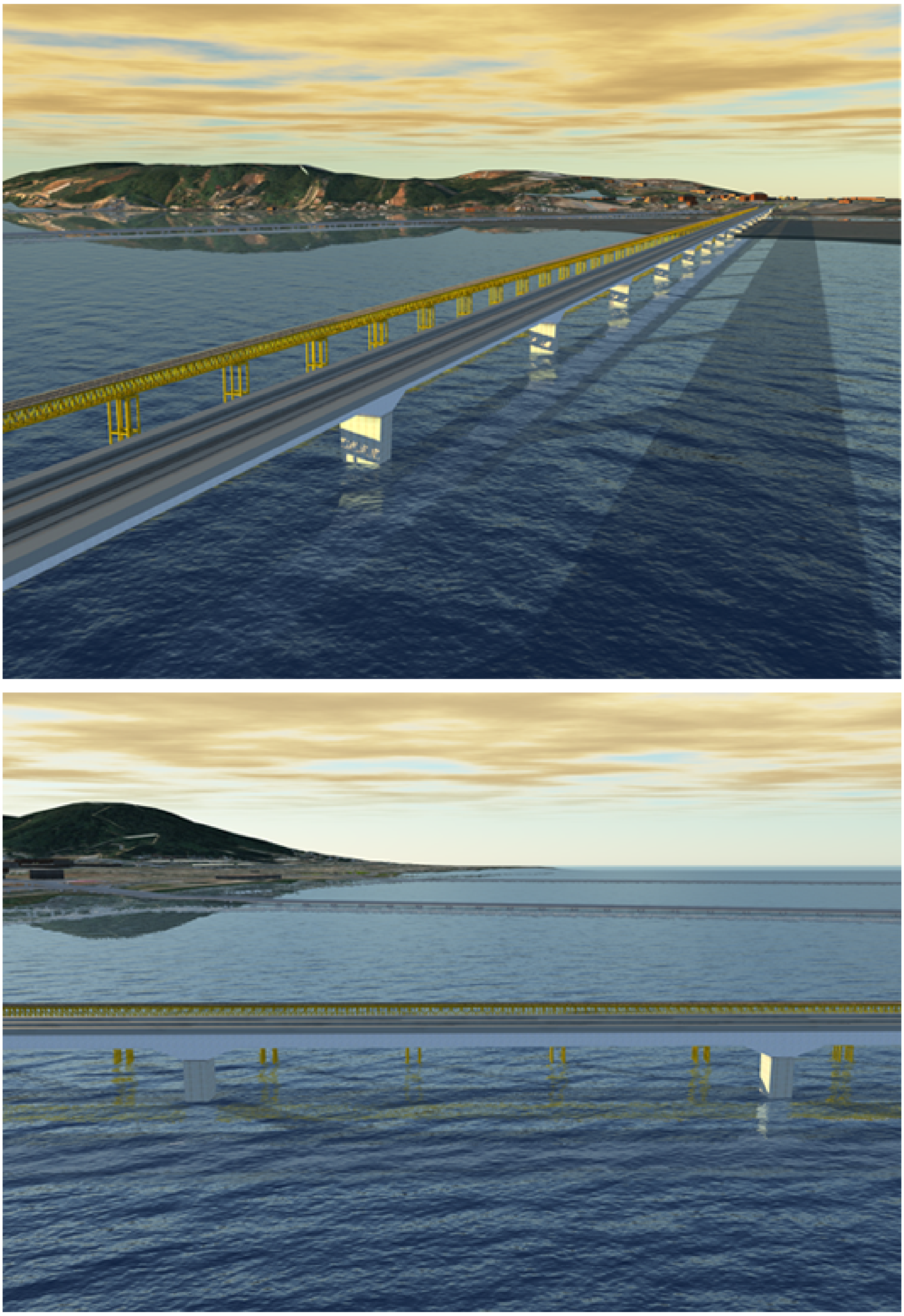

Figure 11.16: 3D model of the bridge integrated into the environment, using Infraworks.

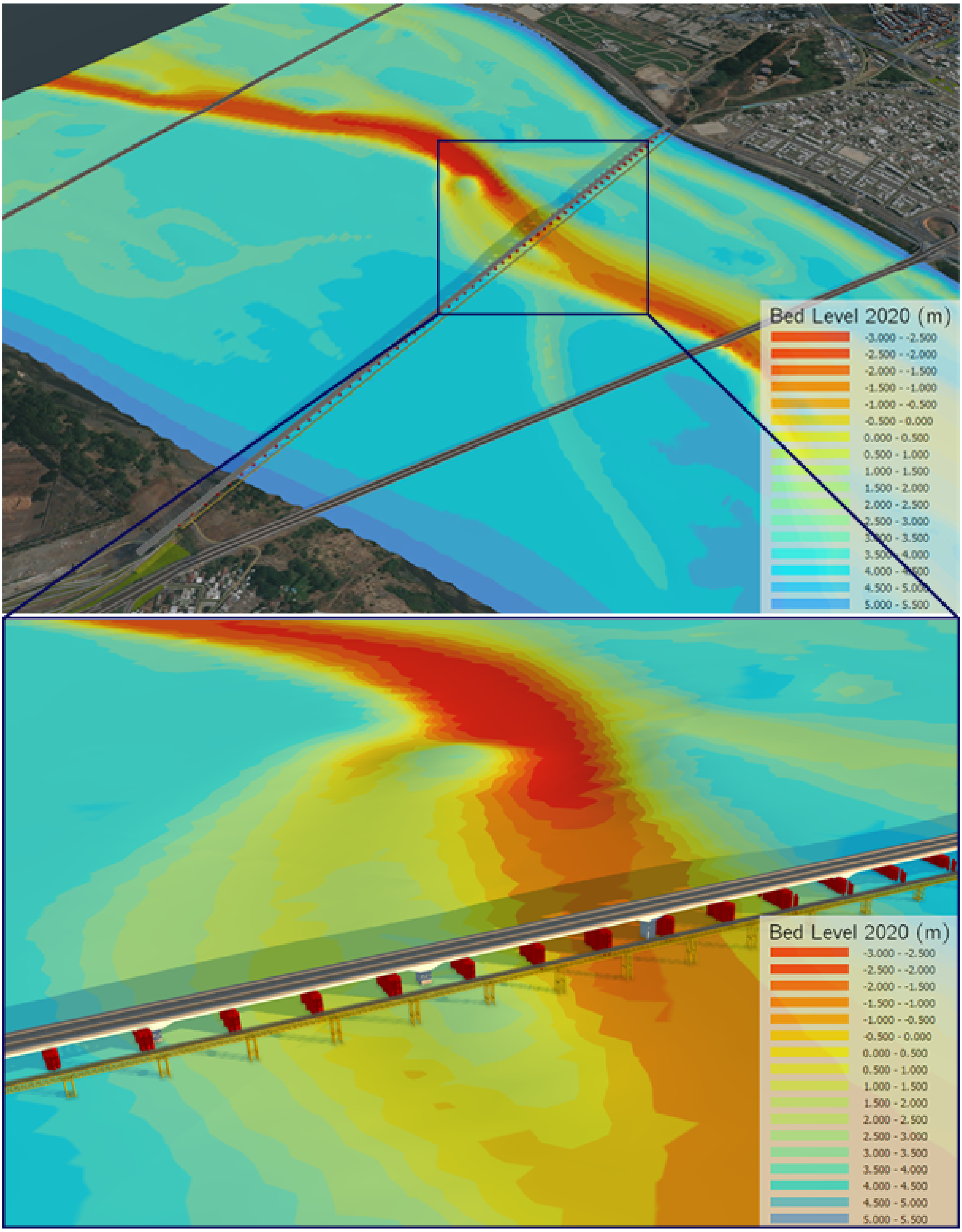

Figure 11.17: 3D model of the bridge integrated into the environment with the bathymetry of 2020, using Infraworks.

IV

Conclusions

12
Conclusion

In comparison with other Latin American countries Chile is a wealthy and growing nation. Especially the Biobío region, which is the second largest contributor to the country's GDP. This is due to the central location of the region which has created opportunities for the transport sector. This is due to the fact that goods coming from the north and south have to travel through the Biobío region. The communes of Concepción, San Pedro de la Paz and Hualpén have capitalised on this opportunity by developing industrial complexes and multiple harbours. This resulted in an increase wealth for these communes, which is evident from these communes' GDP, which is on average 10% higher than other communes in the region.

The transport of goods is currently facilitated by transport via road, water and rail. Transport by rail has experienced a growth of 162% between 1980 and 2008. If the freight tonnage is multiplied with the distance travelled it has even increased with 221%, indicating that more goods are transported to locations further away. The EFE itself estimates that the transport by rail is expected to increase even more with 60% by the year 2022, and that the passenger transport is tripled. To accommodate this growth, the current 130 year old railway bridge crossing the Biobío river between Concepción and San Pedro de la Paz is up for replacement. The existing single track bridge will be replaced by a bridge with two railway tracks, thus increasing the capacity which can be transported. Furthermore, the increased capacity reduces the load on the existing infrastructure as more can be transported by rail.

The coarse of the Biobío river has changed significantly during the last century. When comparing cross-sectional measurements from 1992 with those from 2010, it was found that the bed degradation equals 3.17 metres in the last 40 kilometres of the river. It can thus be concluded that the Biobío river is not in an equilibrium state. Furthermore, a sand bar is growing at the inner bend, constricting the flow to the northern bank of the river. This flow constriction results in a higher flow velocity, which increases the attack on the foundation pillars of the bridge causing an increase of erosion. Furthermore, the flow constriction leads to an increase in growth of vegetation over the past years on the sand bar, influencing the roughness of the bar and thus stabilising the location of the river bar. This has an effect on the erodability during a flood wave, as the bar is harder to erode due to the increased roughness. This river bar, as a result, has an effect on the flood wave. From the tidal analysis it can be concluded that the tide is not responsible for sediment transport, at least not averaged over the tidal cycle, as it was found that there is no skewness or asymmetry in the system. The main cause for sediment transport in the river is thus due to the discharge, which shows a clear seasonal variation with a higher discharge during winter, the result of an increase in precipitation.

When simulating a 10 year period to asses the morphological changes it was found that the bed levels do display significant changes over time. Although, when using the effective discharge, most changes occur during the first period, governing 5 years. Furthermore, it was observed that the location and dimensions of the channel do display the same variability as the Biobío river. However, due to simplifications in the model and natural disasters, the precise locations and dimensions cannot be predicted. For the design of the bridge the EFE uses the 100 year return period of the discharge with a flow velocity of 2.5 m/s. By running the short term simulation using the same 100 year return period discharge in the Delft3D model, it is found that the flow velocity set by EFE, has a probability of exceedance of 48.75%. This indicates that the EFE is using a flow velocity which is too low.

Due to the fact that the location of interest is in an earthquake prone area, the effects thereof need to be assessed. The event of an earthquake with a magnitude larger than 7.0 M_s and resulting tsunami is highly likely. In most cases the Biobío river is protected by the submarine canyon situated in front of the river mouth, mostly due to the horizontal dimensions of the canyon and in lesser extent to the depth. However, although protected in most cases, an earthquake causing a tsunami in front of the river which causes subsidence of the river mouth could reach the bridge. At the location of the bridge this would result in a water level increase of 3.5 metres. Therefore it can be concluded that the effect of a tsunami should be accounted for in the bridge design.

When comparing proposed variants for a railway bridge with the design of EFE using a multi-criteria analysis, it appears that variant 1, an alternative beam bridge, scores the highest, even higher than the current design of EFE. The alternative bridge design scores better on hydraulic performance, because this alternative reduces the amount of pillars required to cross the river by approximately 70%. Although, the other alternatives score even better on hydraulic performance, their costs are significantly higher and take longer to construct. These criteria are also part of the multi-criteria analysis.

In this report the focus remains on the preliminary design of the substructure, the superstructure is assumed similar to the design of the Hollandsch Diep bridge in the Netherlands. Considering the different load combinations it is found that the normative load combination includes loads due to an earthquake, wind on the longitudinal section of the bridge and loads due to train transportation SW/2. This load combination results in a very high shear force and bending moment. In order to withstand such a load, a non pre-stressed 3.2m by 2.5m (BxH) concrete C45/55 column is designed, with a reinforcement percentage of 6%, for the substructure. Although the upper boundary value for the reinforcement percentage is 3.05% for C45/55, 6% has been applied, to avoid immense column dimensions and thus withstand large bending moments. However, breaching this upper boundary value is not favourable or allowed according to the Eurocodes, it is therefore advisable to look into other mechanics to reduce the acting forces. Additionally, a scour hole of 8.90 metres is predicted, when using the 100 year return period discharge and rectangular shaped columns.

The soil beneath the respective column locations exist mostly of sand, sand with silt, clayey sand and, at the bridge bearing of Concepión, rock. The considered SPT's are converted to CPT values for S4 and S7. From which it can be concluded that the subsoil can yield a high bearing capacity for the foundation piles. For column 2 (location of SPT4), 14 prefab concrete piles of 0.45m by 0.45m to a depth of 21 metres are needed. Whilst for column 3 (location of SPT7), the amount of piles is increased to 17, with similar dimensions, 0.45m by 0.45m to a depth of 18 metres. These foundation piles are supported by a foundation block that is attached to the substructure. The foundation piles, located under the foundation block, are distributed in such manner that the interference between the piles is minimised.

13 Discussion

Different results have been obtained during the progress of analysing the Biobío river system, writing the programme of requirements and making a preliminary design for the railway bridge. The results are discussed in this chapter, starting with the river morphological hydraulic analysis in section 13.1, the hydraulic analysis considering tsunami's in section 13.2, the structural analysis in section 13.3 and lastly the discussion on the integral design tools in section 13.4.

13.1 Hydraulic Analysis - River Morphodynamics

Most importantly the results of this hydrodynamic and morphological model are only an approach to describe the real-life situation of the Biobío river. Therefore, the results of the model should be investigated more thoroughly and checked with field measurements.

Especially the calibration of the Delft3D model could be improved by having better and more detailed bathymetry measurements to compare the model outcomes with. The 2010 bathymetry is detailed enough to use as a starting point for model simulation. The 2015 bathymetry, however, is very coarse and therefore not optimal to use in the comparisons with the modelled updated bathymetry. When observing the 2015 bathymetry it is visible that the dry parts of the area are measured with a higher accuracy than the wet part, where the accuracy is lower and measurements are missing. For instance, there are no channels visible in the 2015 measurements, but Google Earth shows the obvious development of varying channels. Another bottleneck of the calibration process is the limited amount of time and the various calibration parameters at our disposal. For this analysis only some calibration parameters were used to find a better fit between the model and real-life measurements. The multiple calibration parameters and the aforementioned 2015 bathymetry both influence the reliability of the results.

Another thing to note when considering the morphological results of the model is the area of application. Due to the negligence of waves and salinity the model area downstream of the railway bridge does not represent the real situation correctly. Although this part is needed to run the model properly, the results of this area should not be taken as governing.

The used median sediment diameter is an approximation and, as the sensitivity analysis has shown, does influence the situation significantly. Also the extraction of sediment, in the form of sand by the sand mining companies, is not taken into consideration in this model, although this can prove to be the reason why the main channel of the Biobío river is situated at the outer band as opposed next the river bar as modelled in the Delft3D model.

The influence of a flood wave is, at this moment, limited to the situation of a smooth bed, using the 2010 bathymetry as a starting point. More interesting is to investigate the development of the river bed due to a flood wave in the presence of multiple channels.

13.2 Hydraulic Analysis - Tsunami

For the assessment of the effects of tsunami propagation into the Biobío river, only the worst case scenario of the initial hypothetical earthquake and resulting tsunami is used. The consequence is that the results derived from this simulation still contain a high level of uncertainty and are only applicable in the described situation. As the worst case scenario with a very high moment magnitude earthquake was chosen, the tsunami has a large run-up reaching the location of the new bridge and therefore influencing the bridge design. This scenario is not the most likely case and therefore, other more probable cases could be simulated and the effect on the bridge and river can be estimated.

Besides the raw impact of the tsunami on the bridge, it is interesting to see what the influence of a tsunami is on the sediment transport in the delta. However, NeoWave cannot implement sediment transport as for example Delft3D FLOW can. Therefore these additional effects, caused by a tsunami, on the morphological evolution of the river are not accounted for, though these may have a real impact. This impact can be expected as a lot of sand is imported with the tsunami waves.

As the latest highly detailed bathymetry is from 2010, this has a big influence on the propagation as well. The depth has changed a lot since then, as the Biobío river has a highly dynamic character. Meaning that the run-up in 2019 can be very different from the simulated one.

13.3 Structural Analysis

The different results of the hydraulic analysis are used as input for the preliminary design and further complemented with requirements, requisites and wishes. With this, a preliminary design for the railway bridge is created, with the focus on the substructure. As a result, the design is limited and multiple assumptions were used in the process. Outcomes of the preliminary design need to be verified.

The forces acting in the transverse direction of the bridge are based upon the individual pier model, whilst the forces should be considered for the entire system of the bridge. This will probably lead to lower acting forces leading to a reduction of the required dimensions and reinforcement of the columns. Consequently, a design for the columns 2 and 3 is created where the percentage of reinforcement breaches the upper boundary value of 3.05%, in order to provide enough bending moment resistance, which is not tolerable. To stay beneath upper boundary value for the reinforcement percentage other measures can be undertaken. Such as implementing dampening systems that reduce the acceleration of the columns due to an earthquake, reducing main span of the bridge, re-evaluate the impact of an earthquake and the individual pier model calculation by a more thorough analysis.

As concluded, it is inevitable that a local scour hole of about 8.90 metres is formed after the placements of the columns. The scour hole can undermine the foundation of the bridge, which can in turn lead to a destabilising situation which is highly unfavourable. Therefore, bed protection should be considered. Additionally, the shape of the columns can be altered, as a circular or elliptic shape reduces the formed scour hole.

In addition, it is advisable to consider different kinds of foundation piles other than the chosen prefab concrete piles as their bearing capacity is capped at 3000 kN whilst the subsoil might able to provide a sum greater than this value. That being said, only 2 columns and the underlying subsoil for their foundations along the span of the bridge are considered in this report. For a complete assessment of the bridge, the remaining columns and abutments should be analysed and designed, as the characteristics of soil types and their qualities, acting loads and bathymetry for each respective column location deviates from the columns considered.

13.4 Integral Design Management

The integration of the different (management) tools, used in this project, is visible in figure 13.1. From the figure it is clear that a lot of different programmes have been used throughout the project, each with its own advantages and disadvantages. The challenge therefore was to combine the programmes in such a way that the disadvantages are mitigated.

The biggest challenge governed the use of ArcGIS. In the project team only one member is skilled enough to work with ArcGIS. If this team member had other obligations, no work in ArcGIS could be done which occasionally caused delays or miscommunication, which is troublesome due to the fact that ArcGIS was one of the core programmes in the project.

This can be solved by having more than one team member being able to work in ArcGIS. However, this leads to another problem, as it is not possible to work in the same environment on two different PCs, which means that either two environments must be created or both team members must work on the same PC.

Another challenge involved the usage of both Python and Matlab, both are data processing tools. By rewriting the Matlab scripts into Python, Matlab can be omitted from the used programmes which somewhat simplifies the process and increasing the efficiency during the project. Additionally, it is clearer to the team members what software is used for data processing.

Before the start of the project there was a general consensus about the programmes which were to be utilised. However, during the project some additional programmes were added, for instance InDesign and Photoshop as post processing tools. While the use of this tools proved to be value adding it also caused some small scope creep which resulted in a small delays when creating figures. Mainly because only one team member was skilled enough to work in InDesign. Thus before a figure was finished, two team members had to process the data and edit the figure.

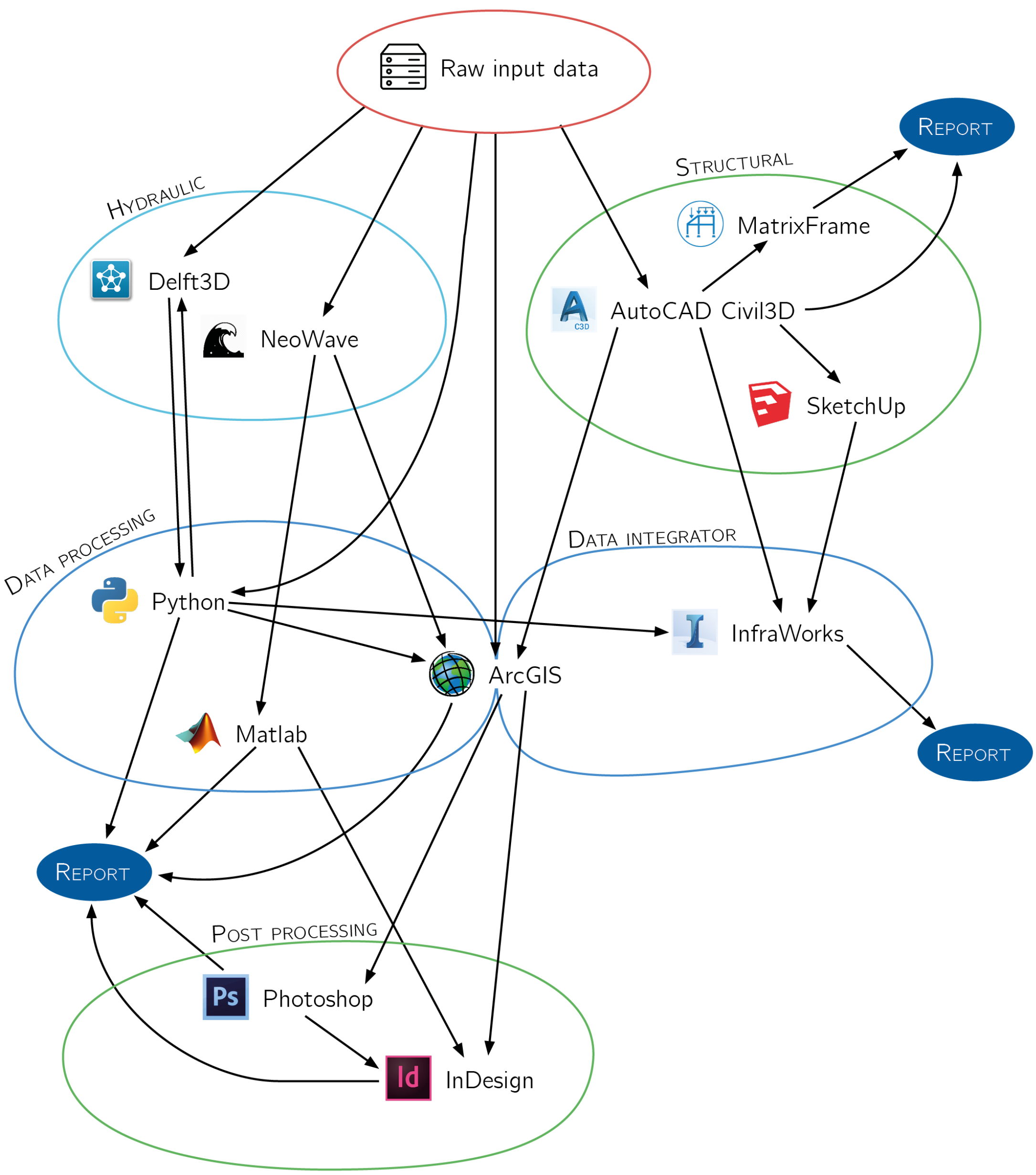

Figure 13.1: Integration of the different (management) tools in this project

14

Recommendations

This research is limited by our duration of two months in Concepción. A broader understanding of the Biobío river system can be established by instigating an ongoing research with this report as a basis. To provide possibilities and tools to continue the mentioned research with the help of this technical report and the used models, recommendations are collected throughout the project and summarised in this chapter.

The recommendations, in the form of bullet points, are split into separate topics to provide easy reference and general overview. The recommendations of the following topics are discussed:

- Recommendations Regional & Physical Analysis
- Recommendations Modelling River Morphodynamics with Delft3D
- Recommendations Modelling Tsunami Impact with NeoWave
- Recommendations Combining Hydraulic Results with Structural Analysis
- Recommendations Programme of Requirements
- Recommendations Preliminary Design
- Recommendations IDM Tools

14.1 Regional & Physical Analysis

- Investigate the options to make the railway network around Concepción more time and cost efficient.
- Investigate the means of how the railway bridge can contribute to the welfare of the Concepción municipality, by answering the question: how can the bridge add value other than a way of connecting North and South?
- Set interviews with the different stakeholders and further determine their wishes and concerns. This enables a more detailed project scope, but requires active stakeholder management.
- Investigate the role and influence of the different stakeholders in more detail and create a communication guide of how to work with the most prominent stakeholders.
- Investigate the role of the construction of different hydropower dams on the development of the Biobío river, as these dams have definitely influenced the river development (and morphodynamics) in the past.
- The obtained discharge data set at the Desembocadura gauge is limited. It is recommended to add another discharge gauge or ensure the Desembocadura gauge collects reliable data regularly.
- Conduct further research concerning the behaviour of flood waves in the Biobío river system, investigating diffusive and kinematic flood waves and their propagation.

- Conduct further research concerning the effect of the marine trench in front of the Biobío river mouth, on the propagation of tidal and tsunami waves

14.2 Modelling River Morphodynamics with Delft3D

- Include the waves module and salinity in the Delft3D model. This is especially of importance if the area of interest is extended to the river mouth and coastal area.
- Calibrate this model further by incorporating other calibration parameters, such as time dependent roughness factor, AlfaBs, spatially varying sediment characteristics, etc.
- Calibrate the model using a more detailed set of bathymetry data. Therefore, new and detailed LiDAR/Echo soundings measurements need to be obtained.
- Create a better understanding of the influence of AlfaBn and AlfaBs in this specific scenario.
- Obtain the detailed tidal information in front of the Biobío river mouth and incorporate this in the model.
- Investigate the use of the morphological scale factor (MorFac) by running a longterm simulation with a MorFac value of 1, to give precise results concerning the morphodynamics. Compare this to runs with an increased MorFac value to find the optimal MorFac value.
- Incorporate a time dependent roughness factor, as the vegetation on the river bar grows and develops over time.
- Investigate the influence of the D50 further as the performed sensitivity analysis proved the influence of the median sediment diameter.
- Incorporate the dredging quantities issued by the sand mining companies as this might influence the location of the channels.
- Refine the area of interest if more precise results are needed.,
- Investigate the possibility of creating a 3D model. The current model uses 2DH mode, meaning that there is 1 vertical layer resulting in depth-averaged properties. A 3D model could prove to give more reliable results regarding sediment transport.
- Explore the possibilities of incorporating a tsunami in Delft3D software. This might allow for a study on the effects that a tsunami can have on the river morphology.

14.3 Modelling Tsunami Impact with NeoWave

- Use probabilistic assessment of earthquake simulations to better assess the influence of a tsunami run up on the rive. When using this, more can be said about the (degree of) influence of the tsunamis.
- Investigate different models to be able to investigate the influence of a tsunami on sediment transport. NeoWave cannot be used for sediment transport as no active bed layer is used in the input file.
- Run the simulation with the non-depth integrated option, as in the current model the depth averaged option is used to shorten computing time.
- Obtain an up-to-date set of bathymetry data to be able to create more reliable results.

14.4 Combining Hydraulic Results with Structural Analysis

- Nearing the end of the research period, the EFE notified us they have been using the 200 year return period discharge for the flood wave scenario, contradictory to the 100 year return period used in our research.

Therefor, to verify the structural design criteria, the 200 year return period should be incorporated in the Delft3D model.

- Incorporate the foundation pillar into the models, in the form of dry point or thin dam, this shows the effects of a structure in the flow of the river. (For the tsunami, this means manually increasing the bathymetry, for Delft3D this means creating a dry point.)

14.5 Programme of Requirements

- The section requirements, 8.2, stated in the chapter 8, should be verified with the official programme of requirements produced by EFE. Unfortunately, this document has not been supplied for this study.
- The section *Wishes*, 8.4, is stated without any assessment from the client. In future studies, these should be discussed with the EFE.
- The programme of requirements in chapter 8 and the preliminary design in chapter 11 are based on the combination of the Eurocodes NEN-EN 1990 to NEN-EN 1998, NEN-EN 3215 and three Chilean building codes: NCh2369, NCh3363 and NCh433. For a continued study or bridge design, it is recommended that the Chilean building or American (AASTHO) building codes are utilised.
- In addition, the consequence class and accompanying exposure classes or other factors based on the design life are mentioned according to the Eurocodes. They should be altered towards Chilean standards.
- In subsection 8.5.2 the ultimate limit state is stated. The ULS of a bridge should be checked according to three sets, in this study, only set B relevant for the structural strength and geological properties, is checked.
- The load combinations that are utilised for the preliminary design of the substructure, are according to the Eurocodes. However, when the load combinations include earthquakes, the Chilean building codes are utilised. For a definitive design a consistent method should be used.
- The requirements in case of fire, have been stated quite rudimentary. In any definitive design, these should be reconsidered and matched to the design.
- The drainage system has not been designed in the preliminary design, this has to be done in a later stage.
- The rain loads are neglected for the preliminary design, these have to be accounted for in a latter design if the drainage system of the bridge does not meet the capacity of the 100 year return period for the rain intensity.
- Wind loads are accounted for by assuming a "simple" bridge deck, although in the later design process another situation might be possible. To account for this an updated verification for the wind loads is needed.
- The wind loads are applied without a dynamic assessment as the design is still in its preliminary stage. In a later design, a dynamic calculation might be required.
- The static train loads require an extra maintenance load of 5 kN/m, which has not been applied to the bridge deck as it has an almost negligible value, when comparing it to the current load models. For completeness, this has to be verified in a later design stage.
- The loading including an unloaded train has been neglected in the load combinations study. Although it is very likely that this type of loading is not normative, for completeness it should be checked nonetheless.
- The maximum seismic deformation has not been taken into account. For a final design, the structure should be checked for the allowable deformations.
- The vertical and horizontal deformations have not been taken into account in this study. For a final design, the maximal allowable deformations should be checked with the occurring deformations.

- Passenger comfort has been neglected in the preliminary design for the bridge. As the bridge will most likely be increasingly used for civilian transportation by train, it should therefore be taken into account in any final design.
- The accidental hazard of an impact load due to an accident with a crane or excavator has not been accounted for in the design, in a later design stage this has to be verified whether or not this load can be considered non-normative.
- In the preliminary design the loads due to a train accident, derailing, have not been accounted for. In a later design stage it has to be verified whether this load can can be neglected.
- Allowable settlements are mentioned quite rudimentary and should be thoroughly stated for any final design.
- Noise pollution due to train traffic has been neglected as the bridge is not situated in an urban area. However, a noise pollution study for the surrounding civilian area's should be conducted.
- The design for the abutments is outside of the scope of this study and should be designed for the final bridge design.

14.6 Multi-Criteria Analysis

- The results from the MCA have been averaged over the four team member of this study. It is advisable to broaden the pool in which the MCA score is averaged.
- The weights for each respective criteria are partly objective and subjective. It should be noted that the scores are therefore not exact science.
- Although six different bridge types have been considered, other designs, not thought of, could be included in a new MCA study.

14.7 Preliminary Design

- Perform a response spectrum procedure concerning the seismic loading, to receive more insight in the effect of an earthquake on the bridge and the response of the bridge.
- Replace the individual pier model calculation for the respective earthquake for by a calculation that takes the bridge into account as "one" system.
- Evaluate the value of applying dampening systems, to reduce the acceleration of the columns due to an earthquake.
- Consider a bridge system that is able to resist a high shear force and bending moment other than a solid concrete column.
- Bed protection should be considered as scour holes can form.
- Optimise calculations for the columns and foundation piles.
- Consider a circular or elliptic shape for the columns as this results in less scour.
- Calculate exact selfweight of the superstructure.
- Take into account the settlements of the entire bridge system, columns and foundation piles.
- Bridge should be designed according to Chilean building codes, this could lead to a economically more viable design.

14.8 IDM Tools

Different IDM (Integrated Design Management) tools were used during this project, including: sprint board, weekly progress reports, ArcGIS, Overleaf, Freedcamp and content management programs such as Google Drive or Dropbox. Part of the project is to evaluate these tools, using feedback from both team members and supervisors. The outcome is summarised below in the form of recommendations for future project and other project teams.

- The sprint board, showing the progress, and the stand-up, giving a summary of what has been done to the entire team, has to be kept short and efficient. Make a clear distinction of which tasks have to be presented on this board.
- Weekly progress reports are useful, it is recommended to draw this up on a set time every week. Incorporating the 'Grade of the week' prevents the very human romanticising in retrospection.
- More than one team member should be able to work with ArcGIS, to create an equal workload. Furthermore, it is recommended to include ArcGIS in the Civil Engineering curriculum.
- Overleaf is the best text processing system when multiple team members are working on a file at once. It is recommended to set formatting and editing rules together before the start of the project, to lower past processing time.
- Freedcamp was used frequently in the set-up of the project, but during the project itself it was neglected. It is important to keep the tasks in Freedcamp up-to-date and use this tool also during the course of and the finalising of the project.
- Content management programs can be useful, however one main program should be chosen to ensure easy content management.

Bibliography

1994bus (2017). https://en.wikipedia.org/wiki/Biotren#/media/File:Trazado_biotrén.png. [Online; Retrieved 13-06-2019].

Ad Tissink (2018). Hsl-brug moerdijk roest sneller dan gedacht. https://www.cobouw.nl/infra/nieuws/2018/05/hsl-brug-moerdijk-roest-sneller-dan-gedacht-101260738. [Online; Retrieved 04-06-2019].

Agico Group (n.d.). http://www.railroadpart.com/news/specifications-of-uic-60-steel-rail.html. [Online; Retrieved 18-06-2019].

Aguayo, M., Pauchard, A., Azocar, G., and Parra, O. (2009). Land use change in the south central Chile at the end of the 20 th century. understanding the spatio-temporal dynamics of the landscape [cambio del uso del suelo en el centro sur de Chile a fines del siglo xx. entendiendo la dinica espacial y temporal del paisaje]. *Revista Chilena de Historia Natural*, 82:361–374.

Aguirre, C., Pizarro, O., and Sobarzo, M. (2010). Observations of semidiurnal internal tidal currents off central Chile (36.6). *Continental Shelf Research*, 30:1562–1574.

Anil Mital, Anoop Desai, A. S. A. M. (2014). Product development: A structured approach to consumer product development, design, and manufacture. In *Developing Successful Products*, volume Second, chapter 2. Elsevier, second edition.

Aranguiz, R. (2012). The effect of a submarine canyon on tsunami propagation in the Gulf of Arauco, Chile. *Coastal Engineering Proceedings*, 1(33):5.

Aránguiz, R., González, G., González-Carrasco, J., Catalán, P., Cienfuegos, R., Yagi, Y., Okuwaki, R., Urra, L., Contreras, K., del Río, I., and Rojas-Orrego, C. (2015). The 16 september 2015 chile tsunami from the post-tsunami survey and numerical modeling perspectives. *Pure and Applied Geophysics*, 173.

Aránguiz, R. and Shibayama, T. (2013). Effect of submarine canyons on tsunami propagation: A case study of the Biobio canyon, Chile. *Coastal Engineering Journal*, 55(4):1350016–1–1350016–23.

Øresundsbro Konsortiet I/S (2018). Annual report 2018. Technical report, Øresundsbro Konsortiet I/S. https://data.oresundsbron.com/cms/download/%C3%85rsrapport%202018_EN.pdf.

Australian Government (n.d.). Infrastructure to Chile - trends and opportunities. https://www.austrade.gov.au/australian/export/export-markets/countries/chile/industries/infrastructure-to-chile.

Balachandran, A. (2012). The rail bridge to vallarpadam container transhipment terminal. kochi, kerala, india. https://www.iabse.org/IABSE/association/Award_files/Outstanding_Structure_Award/Viaduct_Spain.aspx. [Online; Retrieved 06-06-2019].

Baris Yatsalo, Alexander Korobovm, L. M. (2017). Fuzzy multi-criteria acceptability analysis: A new approach to multi-criteria decision analysis under fuzzy environment. *Elsevier*, page 10.

Battjes, J. and Labeur, R. (2017). *Unsteady flow in open channels*. Cambridge University Press, Delft, The Netherlands.

BBC (2012). Chile country profile. http://news.bbc.co.uk/2/hi/americas/country_profiles/1222764.stm.

Benthem, J. and Falbe-Hansen, K. (2003). Conceptual design of the new hsl bridge over hollandsch diep. *IABSE Symposium Report*, 87:7.

Bertran, C., Arenas, J., and Parraz, O. (2001). Macrofauna del curso inferior y estuario del r biob (Chile): cambios asociados a variabilidad estacional del caudal hrico. *Revista Chilena de Historia Natural*, 74(2):331–340.

Blom, A. (2018). River dynamics 1 - the river system. University Lecture.

Boroschek, R., Soto, P., and Leon, R. (2010). Registros del terremoto del maule mw = 8.8, 27 de febrero de 2010. Technical report, Universidad de Chile, Facultad de Ciencias Fisicas y Matematicas, Departamento de Ingenieria Civil.

Bosboom, J. and Stive, M. J. (2015). *Coastal Dynamics I*. Delft Academic Press, Delft, The Netherlands.

Bryant, E. (2014). *Tsunami - The Underrated Hazard*. Springer International Publishing, third edition. https://www.springer.com/gp/book/9783319061320.

C. Hartsuijker en J.W. Welleman (2016). Constructiemechanica 3: Stabiliteit van het evenwicht. lecture notes.

Caamaño, D. (2010). Sustainability of morphology features in alluvial rivers and coastal systems in Chile: The biob river as study case. Project Fondecyt Nº11100399.

Chiang, G., Munkittrick, K. R., McMaster, M. E., Barra, R., and Servos, M. (2014). Regional cumulative effects monitoring framework: Gaps and challenges for the biob river basin in south central Chile. *Gayana*, 78(2):109–119.

CIA (2019). The world factbook: Chile. `https://www.cia.gov/library/publications/resources/the-world-factbook/geos/ci.html`.

Clawpack (2019). Earthquake sources: Fault slip and the okada model. `https://www.clawpack.org/okada.html#fault-slip-on-rectangular-subfaults`. [Online; Retrieved 04-06-2019].

Clemen, R. (1991). Making hard decisions: an introduction to decision analysis. *Duxbury Press*.

Climate-Data.org (2018). `https://nl.climate-data.org/zuid-amerika/chili/viii-region-del-biobio/concepcion-3984/`. [Online; Retrieved 13-06-2019].

Climate-data.org (2019). Climate concepci. `https://en.climate-data.org/south-america/chile/viii-region-del-biobio/concepcion-3984/`.

Cobouw (1996). Thalys krijgt eigen moerdijkbrug (dutch). `https://www.cobouw.nl/bouwbreed/nieuws/1996/06/thalys-krijgt-eigen-moerdijkbrug-10139792`.

COPRI Chile Earthquake Investigation Team (2013). *Chile Earthquake and Tsunami of 2010*. American Society of Civil Engineers, Reston, Virginia, United States.

C.R. Braam, P. L. (2011). Constructieleer gewapend beton. AEneas.

Croquevielle, T. (2019). The renaissance of the train in Chile. `https://www.chiletoday.cl/the-train-in-chile/`.

Dee Lish (2012). `https://nl.pinterest.com/pin/505810601871320312/?lp=true`. [Online; Retrieved 01-06-2019].

Deltares (2008). Validation document delft3d-FLOW. Technical report, Deltares.

Deltares (2019a). D-Flow Flexible Mesh. `https://www.deltares.nl/en/software/module/d-flow-flexible-mesh/`.

Deltares (2019b). Delft3D-Flow, Simulation of multi-dimensional hydrodynamic flows and transport phenomena, including sediments, User Manual. Technical report, Deltares.

Deltares (2019c). QUICKIN: Generation and manipulation of grid-related parameters such as bathymetry, initial conditions and roughness, User Manual. Technical report, Deltares.

Deltares (2019d). RGFGRID: Generation and manipulation of structured and unstructured grids, suitable for Delft3D-Flow, Delft3D-Wave or D-Flow Flexible Mesh, User Manual. Technical report, Deltares.

Diego Caamaño Avendaño (2019). Personal communication.

Ecoronel, Observatorio ecológico de Coronel (2019). El r bio bio. `http://www.ecoronel.cl/espacios-verdes/ecologia-y-biodiversidad/patrimonios-naturales/rio-bio-bio/`.

EcuRed (2019). R bb (Chile). `https://www.ecured.cu/Río_Biobío_(Chile)`.

ENAP (n.d.). Enap. https://www.enap.cl/pag/338/1351/enap_refinerias.

Endmann, K. (1989). *Die Hammer Eisenbahnbrücke. Ein Zeugnis des Großbrückenbaus*. Darmstadt: Hestra-Verlag. ISBN 978-3777102207.

Engineering Discoveries (n.d.). What is difference between bridge and culvert? https://engineeringdiscoveries.com/2019/02/10/what-is-difference-between-bridge-and-culvert/. [Online; Retrieved 03-06-2019].

ESRI (2019). Motion of tectonic plates. https://www.arcgis.com/apps/MapJournal/index.html?appid=df5f94c0050b4075adfbba54fb13eaeb.

Federal Bridge Corporation (2016). Blue water bridge. http://www.bluewaterbridge.ca/docs/excel/Canada_US_Traffic1.xls. [Online; Retrieved 20-05-2019].

Fernández, O. (2019). Efe llega a rord de pasajeros, pero con proyectos clave a pendientes. https://www.latercera.com/nacional/noticia/efe-llega-record-pasajeros-proyectos-clave-aun-pendientes/471907/.

GC Geoconsult (2019a). Ptebiobio-geo-ing-ite-gopl-0001-anexo-b. Technical report, Grupo EFE. Confidential Document.

GC Geoconsult (2019b). Ptebiobio-geo-ing-ite-gopl-0001-anexo-d. Technical report, Grupo EFE. Confidential Document.

GC Geoconsult (2019c). Ptebiobio-geo-ing-pln-gopl-0001-anexo-a. Technical report, Grupo EFE. Confidential Document.

Gesche, A. S. (2018). El sistema ambiental de la cuenca del r biob (1990-2018). University Lecture.

Geyer, W., Hill, P., and Kineke, G. (2004). The transport, transformation and dispersal of sediment by buoyant coastal flows. *Continental Shelf Research*, 24(7–8):927–949.

Gobierno de Chile (2019). Biobio region. https://www.gob.cl/en/regions/biobio-region/.

Gobierno de Chile, Ministerio de Obras Publicas, D. G. d. A. (2019). Caudales medios diarios. data retrieved from DGA for the Rio Biobio En Desembocadura, 2006.

Goodwin, P. (2004). Analytical solutions for estimating effective discharge. *Journal of Hydraulic Engineering*, 130.

Gordon Wolman, M. and P. Miller, J. (1960). Magnitude & frequency of forces in geomorphic processes. *Journal of Geology - J GEOL*, 68:54–74.

GrupoEFE (2019). Construcci nuevo puente ferroviario biob. Technical report, GC Geoconsult.

Habit, E., Belk, M., Tuckfield, C., and Parra, O. (2006). Response of the fish community to human-induced changes in the Biobío River in Chile. *Freshwater Biology*, 51:1 – 11.

Hanks, T. C. and Kanamori, H. (1979). A moment magnitude scale. *Journal of Geophysical Research: Solid Earth*, 84(B5):2348–2350.

Hans Hendriksen (2017). https://www.flickr.com/photos/hanshendriksen/36249974916. [Online; Retrieved 01-06-2019].

Harry H. Barnes, J. (1967). Roughness characteristics of natural channels. Technical report, USGS, science for a changing world.

Heller, V. and Spinneken, J. (2013). Improved landslide-tsunami prediction: Effects of block model parameters and slide model. *Journal of Geophysical Research: Oceans*, 118(3):1489–1507.

Herrera, C. (2018). El poco conocido origen e historia del escudo de armas de concepci. https://www.diarioconcepcion.cl/ciudad/2018/10/16/el-poco-conocido-origen-e-historia-del-escudo-de-armas-de-concepcion.html.

Holthuijsen, L. H. (2007). *Waves in Oceanic and Coastal Waters*. Cambridge University Press.

IABSE (n.d.). Viaduct over river almonte, spain. https://www.iabse.org/IABSE/association/Award_files/Outstanding_Structure_Award/Viaduct_Spain.aspx. [Online; Retrieved 06-06-2019].

InfraCompass (n.d.). Chile - an overview of the infrastructure market. https://infracompass.gihub.org/ind_country_profile/CL.

Ingeniería Dolmen (2015). Informe final estudio hidrlico r b-b, cigo. Technical report, Grupo EFE. in Spanish.

International Federation of Red Cross And Red Crescent Societies (2006). Chile: Floods - situation map. https://reliefweb.int/map/chile/chile-floods-situation-map.

International Federation of Red Cross And Red Crescent Societies (2009). Situation report: Chile, floods - information bulletin n.1. Technical report, International Federation of Red Cross And Red Crescent Societies.

IOC Sea level monitoring (2019). Sea level at Coronel_CL station. http://www.ioc-sealevelmonitoring.org/station.php?code=crnl.

Isla, F. I., Flory, J. Q., Martínez, C., Fernández, A., and Jaque, E. (2012). The evolution of the b b delta and the coastal plains of the arauco gulf, b b region: the holocene sea-level curve of Chile. *Journal of Coastal Research*, 28(1):102–111.

ITIC (n.d.). Geologic hazards - tsunami. Technical report, International Tsunami Information Center (ITIC). Provided by Rafael Aránguiz.

Jarushi, F., AlKaabim, S., and Cosentino, P. (2015). A new correlation between spt and cpt for various soils. *International Journal of Geological and Environmental Engineering*, 9.

Kanamori, H. (1977). The energy release in great earthquakes. *Journal of Geophysical Research*, 82(20):2981–2987.

Kanamori, H. (1983). Magnitude scale and quantification of earthquakes. *Tectonophysics*, 93(3):185 – 199. Quantification of Earthquakes.

Karrasch, B., Parra, O., Cid, H., Mehrens, M., Pacheco, P., Urrutia, R., Valdovinos, C., and Zaror, C. (2006). Effects of pulp and paper mill effluents on the microplankton and microbial self-purification capabilities of the biob river, Chile. *Science of The Total Environment*, 359(1):194 – 208.

Kazezyilmaz-Alhan, C. and Medina, M. (2007). Kinematic and diffusion waves: Analytical and numerical solutions to overland and channel flow. *Journal of Hydraulic Engineering*, 133(2):217–228.

Khan, A. (2011). Seismogenic sources in the Bay of Bengal vis-a-vis potential for tsunami generation and its impact in the northern Bay of Bengal coast. *Natural Hazards*, 61.

Kowalik, Z., Knight, W., Logan, T., and Whitmore, P. (2005). Numerical modeling of the global tsunami: Indonesian tsunami of 26 december 2004. *Science of Tsunami Hazards*, 23(1):40–56.

Kruidhof, C. (2018). Hsl-brug mogelijk niet sterk genoeg voor windschermen. https://www.spoorpro.nl/spoorbouw/2018/01/22/hsl-brug-mogelijk-niet-sterk-genoeg-voor-windschermen/?gdpr=accept. [Online; Retrieved 04-06-2019].

Lamy, F.and Hebbeln, D. W. G. (1998). Terrigenous sediment supply along the Chilean continental margin: modern regional patterns of texture and composition. *Geologische Rundschau*, 87(3):477–494.

Langbein, W. B. and Leopold, L. B. (1970). *River Meanders and the Theory of Minimum Variance*, pages 238–263. Palgrave Macmillan UK, London.

Lüthi, M. P. and Vieli, A. (2016). Multi-method observation and analysis of a tsunami caused by glacier calving. *The Cryosphere*, 10:995–1002.

Latter, J. H. (1981). Tsunamis of volcanic origin: Summary of causes, with particular reference to krakatoa, 1883. *Bulletin Volcanologique*, 44(3):467–490.

Lin, W. and Yoda, T. (2017). Bridge engineering. *Chapter One: Introduction of Bridge Engineering*, page 30.

Lonely Planet (2019). History. https://www.lonelyplanet.com/chile/middle-chile/concepcion/history.

Lowe, D. J. and de Lange, W. P. (2000). Volcano-meteorological tsunamis, thec. AD 200 Taupo eruption (New Zealand) and the possibility of a global tsunami. *The Holocene*, 10(3):401–407.

Martínez, C. and Aránguiz, R. (2016). Riesgo de tsunami y planificación resiliente de la costa chilena: La localidad de Boca Sur, San Pedro de la Paz (37°S). *Revista de geografía Norte Grande*, pages 33 – 54. in Spanish.

Mary Bagley and Rachel Ross (2017). Krakatoa volcano: Facts about 1883 eruption. https://www.livescience.com/28186-krakatoa.html. [Online; Retrieved 03-06-2019].

McCarthy, C., Brown, C., Johanson, M., Raub, K., and Louis, R. S. (2018). *Chile & Easter Island*. Lonely Planet Global Limited.

McGuire, J. J. (2008). Seismic cycles and earthquake predictability on east pacific rise transform faults. *Bulletin of the Seismological Society of America*, 98(3):1067–1084.

MDOT (Michigan Department Of Transportation) (2018). Construction history of the blue water bridges. https://www.michigan.gov/documents/constrhistory_16062_7.pdf. [Online; Retrieved 20-05-2019].

Michael Bauer Research (2018). Chile purchasing power per capita.

Ministry of Public Works (2009). *Chile - Opportunities in Infrastructure 2009-2010*. Maval, first edition. https://www.mop.cl/Documents/chile%20opportunities%20in%20infrastructure.pdf.

Ministry of Public Works (2019). About MOP. https://www.mop.cl/Paginas/ingles.aspx.

Ministry of Public Works (n.d.). Descripci del proyecto - puente chacao. https://www.mop.cl/PuenteChacao/Paginas/descripcion_Proyecto.aspx. [Online; Retrieved 04-06-2019].

Moerman, E. (2011). Long-term morphological modelling of the mouth of the columbia river. Master thesis, Delft University of Technology.

Moerman, E. (2019). Personal communication.

Molenaar, W. and Voorendt, M. (2019). *Manual Hydraulic Engineering*. Faculty of Civil Engineering and Geosciences, TU Delft.

Montes, R. (2015). La tragedia en 2010. *El País*.

Mundal, H. (2006). Stord bridge. [Online; Retrieved 14-6-2019].

Murata, S., Imamura, F., Katoh, K., Kawata, Y., Takahashi, S., and Takayama, T. (2009). *Tsunami: To Survive from Tsunami*. WORLD SCIENTIFIC.

Murray-Webster, R. and Simon, P. (2007). Making sense of stakeholder mapping. *Project Management Practice*, 2007.

NASA, Earth Observatory (2019). Flooding in Chile. https://earthobservatory.nasa.gov/images/16990/flooding-in-chile.

National Geographic (2019). What caused the Chilean earthquake? Faults explained. https://news.nationalgeographic.com/news/2014/04/140402-earthquakes-usgs-chile-faults-science/. [Online; Retrieved 14-5-2019].

NCH2369-2003 (2003). Chilean standard nch2369.of2003: Earthquake-resistant design of industrial structures and facilities. Standard, Instituto Nacional de Normalizacion, Santiago, Chile.

NCh3363:2015 (2015). Structural design - buildings in risk areas of flooding due tsunami or seiche. Standard, Instituto Nacional de Normalizacion, Santiago de Chile. in Spanish.

NCH433-96 (1996). Chilean standard nch433.of96: Seismic design of buildings. Standard, Instituto Nacional de Normalizacion, Santiago, Chile.

NCH433-96-2010 (2003). Chilean emergency seismic design code for building after el maule 2010 earthquake. Standard, American Society of Civil Engineers, Reston, VA.

Nelson, M. (2013). Viewpoint – fifty years of hydroelectric development in Chile: A history of unlearned lessons. *Water Alternatives*, 6:195–206.

NEN 3215+C1+A1 (2018). Gebouwriolering en buitenriolering binnen de perceelgrenzen - Bepalingsmethoden voor de afvoercapaciteit, water- en luchtdichtheid en afstand van dakuitmondingen. Standard, Stichting Nederlandse Normalisatie Instituut, Delft.

NEN-EN 1990/A1 (1995). Eurocode: Basis of structural design. Standard, Stichting Nederlandse Normalisatie Instituut, Delft.

NEN-EN 1990+A1+A1/C2 (1990). Eurocode: Basis of structural design. Standard, Stichting Nederlandse Normalisatie Instituut, Delft.

NEN-EN 1991-1-4+A1+C2 (2011). Eurocode 1: Actions on structures - part 1-4: General actions - wind actions. Standard, Stichting Nederlandse Normalisatie Instituut, Delft.

NEN-EN 1991-1-7+C1+A1 (2015). Eurocode 1: Actions on structures - part 1-7: General actions - accidental actions. Standard, Stichting Nederlandse Normalisatie Instituut, Delft.

NEN-EN 1991-2+C1 (2015). Eurocode 1: Actions on structures - part 2: Traffic loads on bridges. Standard, Stichting Nederlandse Normalisatie Instituut, Delft.

NEN-EN 1997-1 (2005). Eurocode 7: Geotechnisch ontwerp - deel 1: Algemene regels. Standard, Stichting Nederlandse Normalisatie Instituut, Delft.

NEN-EN 1998-1 (2005). Eurocode 8: Design of structures for earthquake resistance - part 1: General rules, seismic actions and rules for buildings. Standard, Stichting Nederlandse Normalisatie Instituut, Delft.

NEN-EN 1998-2 (2006). Eurocode 8: Design of structures for earthquake resistance - part 2: Bridges. Standard, Stichting Nederlandse Normalisatie Instituut, Delft.

NEN-EN 9997-1 (2017). Geotechnical design of structures - part 1: General rules. Standard, Stichting Nederlandse Normalisatie Instituut, Delft.

NEN-EN1991-1-6 (2005). Eurocode 1: Actions on structures - Part 1-6: General actions - Actions during execution. Standard, Stichting Nederlandse Normalisatie Instituut, Delft.

NEN-EN:1992-1-1 (1997). Eurocode 2: Design of concrete structures - part 1-1: General rules and rules for buildings. Standard, Stichting Nederlandse Normalisatie Instituut, Delft.

NOAA Center for Tsunami Research (2019). Tsunami event - february 27, 2010 Chile. `https://nctr.pmel.noaa.gov/chile20100227/`.

NOAA Center for Tsunami Research and National Weather Service (2019a). National tsunami warning center, offshore maule, Chile tsunami of 27 february 2010. `https://www.tsunami.gov/previous.events/?p=Chile_02-27-10`.

NOAA Center for Tsunami Research and National Weather Service (2019b). Tsunami generation: Landslides. `https://www.weather.gov/jetstream/gen_slides`.

NOAA, National Centers for Environmental Information (2018). Ncei/wds global significant earthquake database, 2150 bc to present. `https://data.nodc.noaa.gov/cgi-bin/iso?id=gov.noaa.ngdc.mgg.hazards:G012153`.

Nordbø, I. (2001). *The destiny of the Biobío River. Hydro Development at any Cost*, page 6. Ñuke Mapuförlaget.

OECD and Bío Bío's Regional Steering Committee (2009). The b b region, Chile: Self-evaluation report. Technical report, OECD Reviews of Higher Education in Regional and City Development, IMHE.

OECD and The World Bank (2010). Higher education in regional and city development: The b b region, Chile. Technical report, OECD Reviews of Higher Education in Regional and City Development, IMHE.

Okada, Y. (1985). Surface deformation due to shear and tensile faults in a half-space. *Bulletin of the Seismological Society of America*, 75(4):1135–1154.

Okada, Y. (1992). Internal deformation due to shear and tensile faults in a half-space. *Bulletin of the Seismological Society of America*, 82(2):1018–1040.

P. Uribe, A. de Castro, R. Reginensi, P. Buguña, J. Piddo (2019a). Construcción Nuevo Puento Ferroviario Biobío - Disposicion General Tramo 1 al 8. Technical report, PIDDO Inteligencia Disponible.

P. Uribe, A. de Castro, R. Reginensi, P. Buguña, J. Piddo (2019b). Construcción Nuevo Puento Ferroviario Biobío - Cepas Tipo Cabezal de 2600 Armadura. Technical report, PIDDO Inteligencia Disponible.

Pelinovsky, E., Grue, J., and Karsten, T. (2006). *Hydrodynamics of Tsunami Waves*, pages 1–48. Springer Vienna, Vienna.

Pelinovsky, E., Talipova, T., Kurkin, A., and Kharif, C. (2001). Nonlinear mechanism of tsunami wave generation by atmospheric disturbances. *Natural Hazards and Earth System Sciences*, 1(4):243–250.

Pereda, H. B. (n.d.). Almonte hsr viaduct. `http://www.hectorbeade.com/bridge/almonte-hsr-viaduct/`. [Online; Retrieved 06-06-2019].

Pietrzak, J. (2016). *An Introduction to Stratified Flows for Civil and Offshore Engineers*. TU Delft, Delft, The Netherlands.

Pipinato A., P. R. (2016). *Innovative Bridge Design Handbook*. Butterworth-Heinemann, Boston.

Pirozzi, M. (2018). The stakeholder management perspective to increase the success rate of complex projects. *PM World Journal*, VII(1).

Pizarro, R., Valdés, R., García-Chevesich, P., Vallejos, C., Sangüesa, C., Morales, C., Balocchi, F., Abarza, A., and Fuentes, R. (2012). Latitudinal Analysis of Rainfall Intensity and Mean Annual Precipitation in Chile. *Chilean journal of agricultural research*, 72:252 – 261.

Policy Advisory Group (2007). Alternative refinement update. `http://www.sellwoodbridge.org/files/phase1/PAG_20071210_BridgeTypePresentation.pdf`. [Online; Retrieved 07-06-2019].

PorelDerechoalaCiudad (n.d.). `http://porelderechoalaciudad.cl/postales`. [Online; Retrieved 01-06-2019].

Project Management Institute (2013). *A Guide to the Project Management Body of Knowledge (PMBOK Guide) – Fifth Edition*, page 396. Project Management Institute, Inc., fifth edition.

PTI (2009). Longest railway bridge in kochi. `https://commons.wikimedia.org/wiki/File:The_Rail_Bridge_to_Vallarpadam_Is..jpg`. [Online; Retrieved 07-06-2019].

Puente Industrial (2019). Ruta. `http://www.puenteindustrial.cl/ruta/`.

Reniers, A. and Tissier, M. (2018). Linear wave theory - part 2/3: Chapter 5. University Lecture.

Road Traffic Technology (2018). Oresund bridge, sweden / denmark. `https://www.roadtraffic-technology.com/projects/oresund/`. [Online; Retrieved 20-05-2019].

Roelvink, D. J. (2006). Coastal morphodynamic evolution techniques. *Coastal Eng.*, 53.

Rojas, O., Mardones, M., Martínez, C., Flores, L., Sáez, K., and Araneda, A. (2018). Flooding in central Chile: Implications of tides and sea level increase in the 21st century. *Sustainability*, 10(12):4335.

Saldías, G. S., Sobarzo, M., Largier, J., Moffat, C., and Letelier, R. (2012). Seasonal variability of turbid river plumes off central Chile based on high-resolution modis imagery. *Remote Sensing of Environment*, 123:220 – 233.

Schiereck, G. J. and Verhagen, H. J. (2016). *Introduction to Bed, bank and shore protection*. Delft Academic Press, Delft, The Netherlands.

Schuurman, F., A. Marra, W., and Kleinhans, M. (2013). Physics-based modeling of large braided sand-bed rivers: Bar pattern formation, dynamics, and sensitivity. *Journal of Geophysical Research: Earth Surface*, 118.

Schuurman, F. and Kleinhans, M. (2013). Major bed slope effects affecting all river morphodynamics model. *10th International Conference on Fluvial Sedimentology*.

Schuurman, F., Shimizuc, Y., Iwasaki, T., and Kleinhans, M. (2016). Dynamic meandering in response to upstream perturbations and floodplain formation. *Geomorphology*, 253:94–109.

Scordilis, E. M. (2006). Empirical global relations converting m_s and m_b to moment magnitude. *Journal of Seismology*, 10(2):225–236.

Sectie Verkeersbouwkunde (2015). Bend and break: Railways. lecture notes.

Soto, R. (2008). Rail transport in Chile.

Starossek Engineering (n.d.). http://www.starossek.com/css/images/Duesseldorf-Neuss%20Railway%20Bridge/rheinbruecke_gallerie.html. [Online; Retrieved 01-06-2019].

Stelling, G. S. and Duinmeijer, S. P. A. (2003). A staggered conservative scheme for every froude number in rapidly varied shallow water flows. *International Journal for Numerical Methods in Fluids*, 43(12):1329–1354.

Strub, P. T., James, C., Montecino, V., Rutllant, J. A., and Blanco, J. L. (2019). Ocean circulation along the southern Chile transition region (3846): Mean, seasonal and interannual variability, with a focus on 2014–2016. *Progress in Oceanography*, 172:159 – 198.

Structurea (2018). Øresund bridge. https://structurae.net/structures/oresund-bridge. [Online; Retrieved 20-05-2019].

Stuhlmeier, R. (2009). KdV theory and the Chilean tsunami of 1960. *Discrete & Continuous Dynamical Systems - B*, 12(3):623.

Swabb, K. (2017). The global competitiveness report 2016-2017. Technical report, World Economic Forum. http://www3.weforum.org/docs/GCR2016-2017/05FullReport/TheGlobalCompetitivenessReport2016-2017_FINAL.pdf.

Taubenheim, H. E. (2010). Oresund bridge. https://structurae.net/structures/oresund-bridge. [Online; Retrieved 20-05-2019].

The Hindu (2010). A bridge over vembanad lake. https://www.thehindu.com/news/cities/Kochi/A-bridge-over-Vembanad-Lake/article16194216.ece. [Online; Retrieved 07-06-2019].

The World Bank (2017). Air transport estimations. https://data.worldbank.org/indicator/IS.AIR.GOOD.MT.K1?locations=CL.

TheStructuralEngineer.info (2018). Chile is building latin america's longest suspension bridge. https://www.thestructuralengineer.info/news-center/news/item/697-chile-is-building-latin-america-s-longest-suspension-bridge. [Online; Retrieved 04-06-2019].

Thiel, M., Macaya, E., Acuna, E., Arntz, W., Bastias, H., Brokordt, K., Camus, P., Carlos Castilla, J., Castro, L., Cortes, M., P. Dumont, C., Escribano, R., Fernandez, M., A. Gajardo, J., Gaymer, C., Gomez, I., E. Gonzalez, A., González, H., Haye, P., and Vega, J. M. A. (2007). The Humboldt Current System of Northern and Central Chile. *Oceanography and marine biology*, 45:195–345.

Truong, P. (2012). Wave-propagation velocity, tsunami speed, amplitudes, dynamic water-attenuation factors. *15th World Conference on Earthquake Engineering*.

UCSC (n.d.). UCSC. https://www.ucsc.cl/english-info/.

UNCTAD (2017). Container port traffic. https://data.worldbank.org/indicator/IS.SHP.GOOD.TU?locations=CL.

UPSeis (2007). How are earthquake magnitudes measured? http://www.geo.mtu.edu/UPSeis/intensity.html. [Online; Retrieved 22-05-2019].

USGC (2019). Google earth/kml files: Tectonic plate boundaries. https://earthquake.usgs.gov/learn/kml.php.

van Heemst, C., Willems, J., Weller, A., and van Verseveld, H. (2012). A flood defence strategy for the Greater Concepción - Analysing, modeling and finding engineering solutions for the Biobio floods. Technical report, University of Technology Delft.

Vila, I., Fuentes, L., and Contreras, M. (1999). Peces limnicos de Chile. *Boletin Museo Nacional de Historia Natural, Chile*, 48:61–75.

Vionnet, C., Tassi, P., and Vide, J. M. (2004). Estimates of flow resistance and eddy viscosity coefficients for 2d modelling on vegetated floodplains. *HYDROLOGICAL PROCESSES*, 18(15):2907–2926.

Walstra, D.-J., C. van Rijn, L., Ormondt, M., Briere, C., and Talmon, A. (2007). The effects of bed slope and wave skewness on sediment transport and morphology. *Coastal sediments*.

Welcome Chile (2019). History of concepci. https://www.welcomechile.com/concepcion/history.html.

Winch, G. (2007). *The Wiley Guide to Managing Projects*, chapter Managing Project Stakeholders, pages 321 – 339. John Wiley & Sons, Inc.

Wols, R. (2009). Derde moerdijkbrug. https://www.bhic.nl/ontdekken/verhalen/derde-moerdijkbrug. [Online; Retrieved 20-05-2019].

World Bank Group (n.d.). Concessions unit, ministry of public works, Chile. https://library.pppknowledgelab.org/documents/3833?ref_site=kl.

Ximena Valenzuela (2018). A fin de a puente chacabuco seronectado a costanera. https://www.diarioconcepcion.cl/ciudad/2018/09/23/a-fin-de-ano-puente-chacabuco-sera-conectado-a-costanera.html. [Online; Retrieved 20-05-2019].

Yamazaki, Y. and Cheung, K. F. (2011). Shelf resonance and impact of near-field tsunami generated by the 2010 chile earthquake. *Geophysical Research Letters*, 38(12).

Yamazaki, Y., Cheung, K. F., and Kowalik, Z. (2011). Depth-integrated, non-hydrostatic model with grid nesting for tsunami generation, propagation, and run-up. *International Journal for Numerical Methods in Fluids*, 67(12):2081–2107.

Yamazaki, Y., Kowalik, Z., and Cheung, K. F. (2009). Depth-integrated, non-hydrostatic model for wave breaking and run-up. *International Journal for Numerical Methods in Fluids*, 61(5):473–497.

Zöller, G., Hainzl, S., Ben-Zion, Y., and Holschneider, M. (2006). Earthquake activity related to seismic cycles in a model for a heterogeneous strike-slip fault. *Tectonophysics*, 423(1):137 – 145.

V

Appendices

A

Roles of stakeholders

In section 3.2 the technique of stakeholder mapping used in this report has been explained. Subsequently, this method has been used to map the stakeholders and identify which role each stakeholder has. For convenience the 3D stakeholder map is repeated in figure A.1, whereafter a description of the different roles is given.

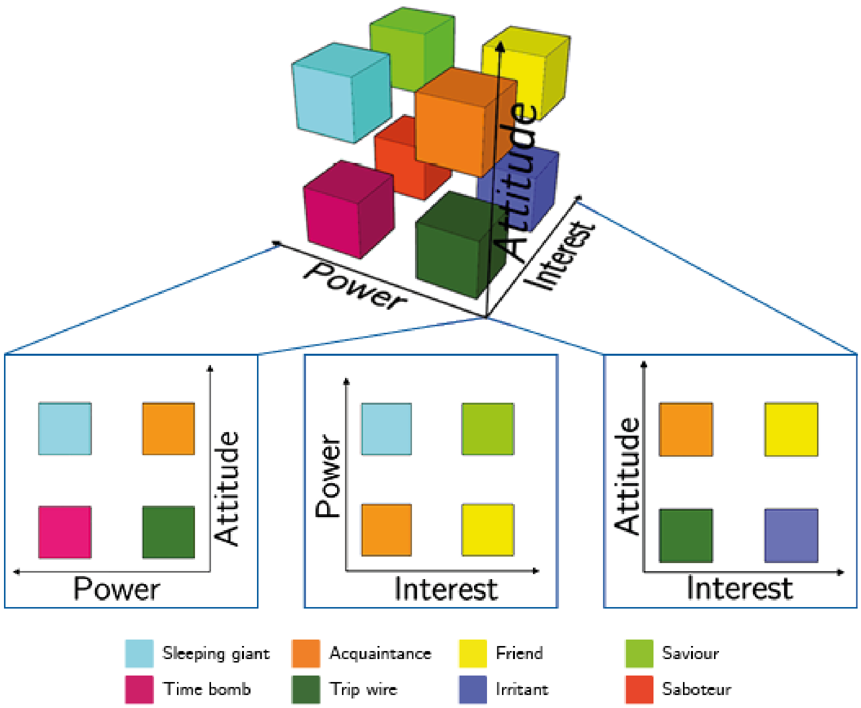

Figure A.1: 3d Stakeholder mapping technique, redrawn from (Murray-Webster and Simon, 2007)

Sleeping Giant
A sleeping giant is a powerful stakeholder with a positive attitude. However, the interest of a stakeholder classified as a sleeping giant is low, for instance because he or she is not directly involved in the project. The sleeping giant is an influential, passive backer of the project. The best method to manage this stakeholder is to engage them and increase their interest in the project in order to awaken them, the goal is to transform a sleeping giant into a saviour.

Time Bomb
The time bomb is comparable to the sleeping giant is terms of interest and power, i.e. powerful but rather low interest in the project. However, their attitude with regards to the project is different. Where the sleeping giant has a positive attitude the time bomb has a negative attitude towards the project. Hence the time bomb is a

influential, passive blocker of the project. Therefore the needs of a stakeholder classified as a time bomb must be understood, to make sure they will not become a saboteur.

Acquaintance
The acquaintance is a stakeholder who does not have a lot of power or interest in the project, but has a positive attitude towards the project. The best way to manage this stakeholder is to keep them informed and communicate relevant information towards this group.

Trip Wire
A stakeholder classified as trip wire has low power and a low interest in the project. However, their attitude towards the project is negative, he or she is an insignificant passive blocker of the project. The needs of a stakeholder in this group must be understood so that the project organisation can avoid the trip wire becoming an irritant.

Friend
If a stakeholder is classified as a friend they have a high interest and a positive attitude towards the project. However, a friend does not have a lot of power, they are an insignificant but active backer of the project. The friend should be used as a confidant or sounding board by the the project organisation.

Irritant
The irritant has a high interest in the project, but a negative attitude towards the project. Comparable to the friend they also have low power over the project organisation. The project organisation should engage these stakeholders so that they do not negatively promote the project, the main goal is to change their attitude towards the project so that they become a friend.

Saviour
The saviour is an important stakeholder to manage, because they have a high interest and positive attitude towards the project which is combined with have a lot of power. The saviour is thus an influential and active backer of the project. Therefore the project organisation must do whatever is necessary to keep them backing the project, and prevent them from becoming a saboteur.

Saboteur
Similarly to the saviour the saboteur is an important stakeholder to manage too, this because they too have power and a high interest in the project. The difference with the saviour is that the saboteur has a negative attitude towards the project and thus wants the project to fail, they are an influential active blocker. They should be engaged in the project to by changing their attitude towards the project or changing their interest in the project.

A.1 Visual Overview Political Structure

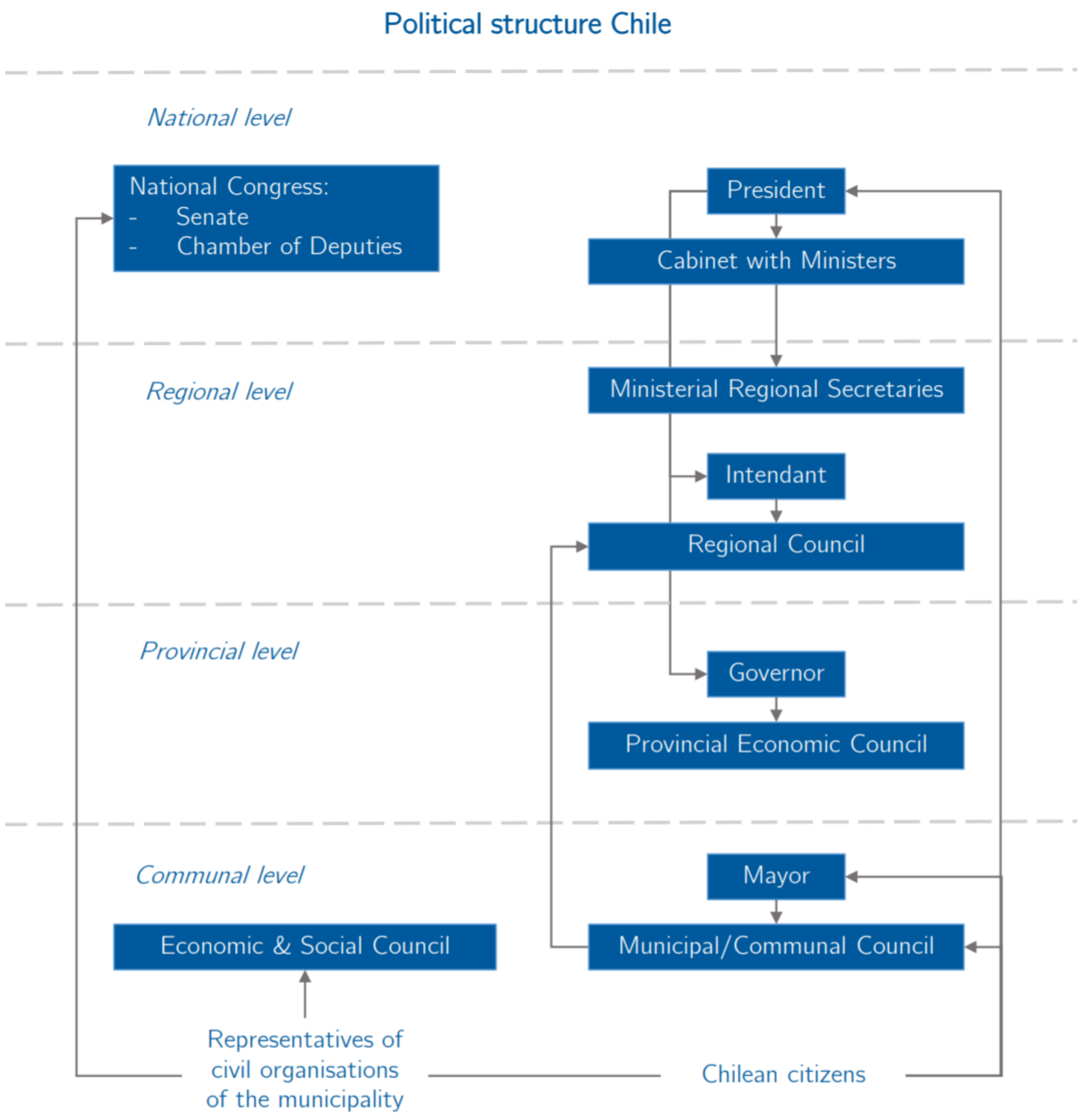

Figure A.2: Political structure of Chile

B

Theoretical Analysis Floodwave

A flood wave, or high water wave, in a river is driven downstream by the gravitational force, which is balanced by the resistance of the bed. Characteristics of a high water wave in a low-land river include, using the lecture slides of Battjes and Labeur (2017):

- Slow changes
- Inertia term in the momentum equation is negligible with respect to the friction term. However, inertia cannot be neglected in rivers with steep slopes or when wave phenomena are super-imposed.

When neglecting local and advective acceleration momentum equation for dynamic waves, the equation for the flood wave, simplifies to the kinematic wave model.

Momentum equation:

$$\frac{\partial Q}{\partial t} + \frac{\partial}{\partial s}\left(\frac{Q^2}{A_c}\right) + gA_c\frac{\partial h}{\partial s} + \frac{Q^2}{A_c R} = 0 \tag{B.1}$$

Reduced equation (neglecting local and advective acceleration), giving kinematic wave model:

$$gA_c\frac{\partial h}{\partial s} + \frac{Q^2}{A_c R} = 0 \tag{B.2}$$

When assuming uni-directional, steady and uniform flow the bed slope equals the slope of the free surface. When applying the quasi-uniform approximation: the depth gradient is small with respect to the bed slop and the flow is quasi-uniform, the propagation speed of the high-water wave is constant. In that case the discharge is only dependant on the water depth and not influenced by the depth gradient. The propagation speed of the high-water, kinematic, wave can be deducted from the Q-h relation or from:

Propagation speed of high-water wave:

$$c_{HW} = \frac{3}{2}\frac{B_c}{B}U_u \tag{B.3}$$

$$U_u = \sqrt{\frac{gRi_b}{c_f}} \quad \text{Using velocity uniform flow} \tag{B.4}$$

For the Biobío region the propagation speed of a flood wave can be of importance, if a flood wave is detected upstream, the time available for possible counter flooding measures or evacuation can be predicted.

The height of a kinematic flood wave does not change over time and the wave does not disperse, however it can change form. In steep rivers, slope > 0.002, natural flood waves behave almost similar to kinematic waves. In milder sloped rivers, slope $0.001 - 0.0001$, the natural flood wave behaves more according diffusive waves. (Kazezyilmaz-Alhan and Medina, 2007) In diffusive waves the curvature of the surface can no longer be neglected and the surface slope influences the discharge. This means that two points with equal depth in a diffusive wave have different velocities, the one in the leading edge of the wave increases the discharge at that location as the surface slope in the trailing edge of the slope decreases the discharge compared to the discharge in the leading edge. This means the front of the wave travels faster than the trailing edge and the diffusive wave diffuses (it's all in the name).

When neglecting friction, the total mass of the wave is preserved. As the wave diffuses, the wave length increases, to preserve the total mass the peak of the wave reduces. Using the diffusion model the height of a diffusive wave over distance and time can be calculated, this can also be of interest for Concepción. The flood wave might have an extreme height in an upstream location, but the height might reduce as effect of diffusion, meaning the height of counter flood measures can be lowered.

Using ArcGIS a first estimate of the river slope is obtained. With a height difference of 17.5 between the mouth of the river and a point 24.75 km upstream, the slope is equal to 0.00071. In this case this means the Biobío river is prone to diffusive flood waves instead of kinematic flood waves.

C

Setup Delft3D Model

In this appendix a more elaborate description of the model is presented. The goal of the description is that the steps are reproducible, and anyone with knowledge of Delft3D can reproduce the model of the Biobío river. This was one of the wishes of the client, so that the model can be used for further research in the future. The exact input data is summarised in appendix D.

The additional readings in this appendix include: section C.1 the description of an earlier Delft3D model by the UCSC, and the explanation of the decision for Delft3D compared to Delft3D or Delft3D Flexible Mesh Suite, section C.2. Furthermore, the exact creation of the grid (including DD-boundaries and running DD-boundaries) and coupling of the 2010 bathymetry to this grid are discussed in section C.3 and section C.3.2 respectively. Section C.4 discusses the initial conditions used to set up the model. Last but not least, section C.5 discusses the processes which are not taken into account in this model and the reason why.

C.1 Delft3D Model by the UCSC

The supervisor of the UCSC has created a Delft3D model of the Biobío once before. The model was created to see how the small channels in the Biobío river evolve over time, and with varying discharge. To achieve this goal a fine mesh, which increases the computational time and accuracy, was used. Furthermore, the model was used to get familiar with the Delft3D software. The mesh and bathymetry used in the model are presented in figure C.1. Note that the bathymetry of the river cannot be observed from this screenshot because of the deep canyon (about 180 m) in front of the river.

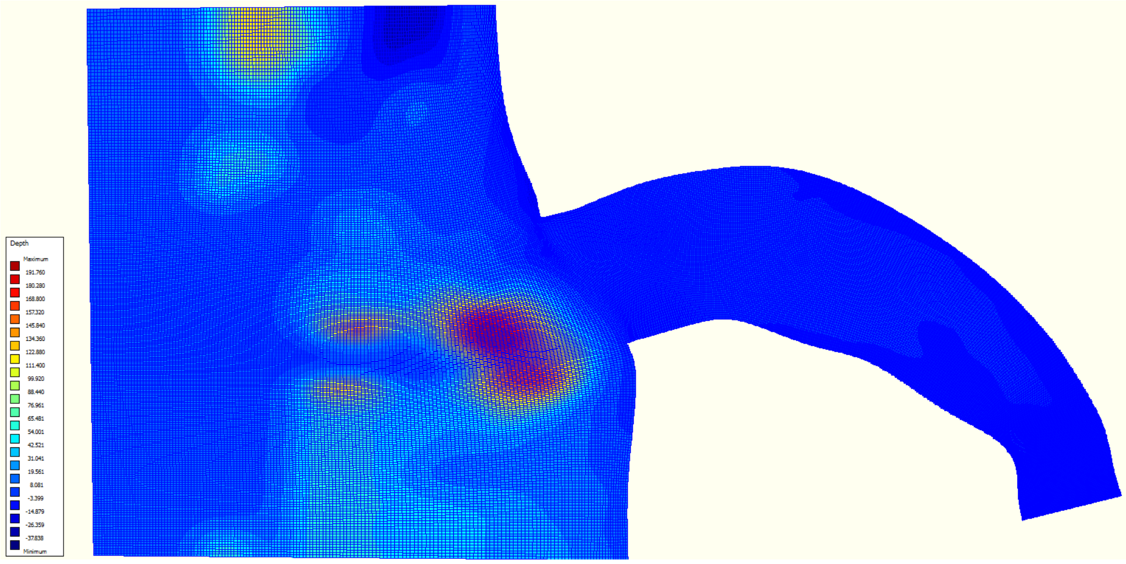

Figure C.1: Grid and depth of the earlier Delft3D model of the Biobío river

Two boundary conditions are implemented in the model, one upstream and the other one downstream. The upstream boundary condition is a time varying discharge, the values used are obtained from real measurements in the same time period. The downstream boundary condition of this model is located in the Pacific Ocean and is simplified to boundary with a constant water level of 0 m. This means no tidal data is used in the model. Most of the other input settings are still the default values of the programme. However, despite using mainly default settings the output is interesting. Two visuals of the output are shown below, figures C.2a and C.2b.

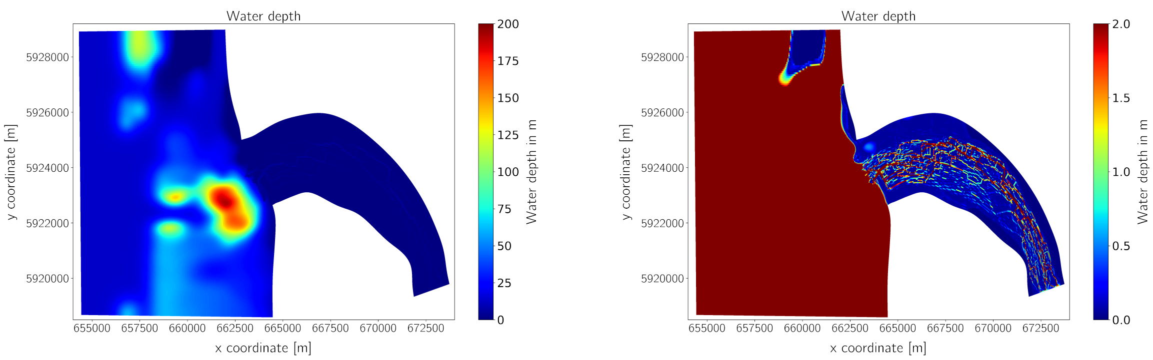

(a) Scale between 0 and 200 m water depth

(b) Scale between 0 and 2 m water depth

Figure C.2: Output result of Delft3D showing the waterdepth on the 12th of January 2010, 20:00.00

Figures C.2a and C.2b show the development of the channels in the river, visible as red or orange lines in the right figure. Which depict a larger water depth. Furthermore, the small channels do not develop in the inner bend of the river because of the presence of the river bar. The water will only flow over the river bar if the discharge increases significantly, for instance in case of the flood wave event discussed in section 4.3.1, but this is not simulated with this model and thus not visible in the figures. Another observation which can be made from these figures, and figure C.1, is that the small grid size is also used for the Pacific Ocean part of the model. Furthermore, the area is rather large resulting in an increase in computational time. Some other observations of the model are summarised below:

- Computation time of approximately 40 hours for the morphological data of four weeks. A morphological factor of 100 is used, which is rather large compared to the value of 25 used by Schuurman et al. (2016) in a similar river modelling exercise.

- The entire model has been refined to the same size, hence all grid cells have the same refinement. Especially for the area located in the Pacific Ocean, this is too fine since the focus of this research is primarily on the development of the river and the location of the new railway bridge.
- The northern and southern bank are not correctly interpreted in the model. They do not follow the actual river embankments, hence the landboundaries have to be modified.

However, some general ideas and data can be used to build a new model for the Biobío river. These includes:

- The general outline can be used to give an indication for the new model outlines
- The bathymetry in this model is a collection of precisely assembled field data, as described in section 4.2.1, which was combined with great care. The detailed bathymetry can be exported and interpolated to be used in a new grid/model.
- The initial input data of this model can be used in the set-up for the newer model.

C.2 Using Delft3D or Delft3D Flexible Mesh Suite

As mentioned in the introduction of the appendix, the Delft3D software is used to model the hydrodynamic and morphological development of the river. The reason Delft3D is chosen, and not another software package, is that the client prefers to work with Delft3D and wants to use the model for other research projects after this project is finished. Furthermore, during this project support is provided by Deltares which makes using Delft3D the preferred option.

The 'standard' Delft3D software consists of the Flow module, called Delft3D-FLOW. The Delft3D-FLOW module is a validated part of the software, and has proven its success in the description of river and coastal systems over the past years (Deltares, 2008). Besides the 'standard' Delft3D-FLOW software Deltares has worked on developing Delft3D Flexible Mesh Suite over the last couple of years, hereafter FM. The FM suite also has a FLOW module, which is called D-Flow Flexible Mesh (or D-Flow FM), and is the successor of Delft3D-FLOW. The advantage of the FM suite is that the user can create and implement irregular curvilinear grids, making the usage of triangles and polygons in a grid possible. This created an increase in flexibility in modelling river and coastal systems. Furthermore, the GUI, the Graphical User Interface, has improved significantly compared to the earlier versions. All differences between Delft3D-FLOW and D-FLOW FM are summarised in table C.1. For more information about D-Flow Flexible Mesh the reader is referred to Deltares (2019a).

Table C.1: Differences Delft3D-Flow and D-Flow Flexible Mesh

Delft3D-Flow	**D-Flow Flexible Mesh**
Structured, regular, linear grid	Unstructured, irregular, curvilinear grids
Standard flexibility	Increased flexibility
Standard GUI	Improved GUI

For this project a license to use both Delft3D-Flow and D-Flow FM was obtained from Deltares, for which we are grateful. The initial preference is to use the latest module, D-Flow FM, as this provides more flexibility in creating the grid resulting in a more accurate and efficient grid. Furthermore, the improved GUI of D-Flow FM would be beneficial for setting up the model.

However, the decision was made to use Delft3D-Flow and not D-Flow FM despite the advantages of using an unstructured grid. The decision was mainly based on communication with our contact at Deltares, Emiel Moerman, who stated the following: 'Morphology in FM is still heavily being developed. ... Considering you are new to the software and your project is just 2 months I would advise to go for the structured Delft3D-Flow.' (Moerman, 2019)

C.3 Creating and Running Composed Grid

In this section the steps followed to create the grid for the Biobío river model are elaborated. Firstly, the creation of land boundaries using Google Earth is explained after which the domain decomposition is elaborated in the second subsection. Finally in the third subsection attention is paid on how to run a Delft3D model with domain decomposition.

C.3.1 *Creating Landboundaries*

The creation of landboundaries can help with the creation of the grid as these boundaries can be used as reference. The landboundaries for this model were created with the help of Google Earth. This proves to be a perfect way of creating landboundaries if these are not readily available.

1. Create a 'path' in Google Earth and save the file for instance as L1.kml. It is important to save as a KML file, and not a KMZ file.
2. Convert the .kml file to .csv using an online converter, this creates the file L1.csv.
3. Import the .csv into a python script, which uses the Bidirectional UTM-WGS84 converter for Python. *Note: the Python script is not included in this report, but it can be send to the reader upon request by contacting Sander Winkel*
4. This creates .ldb files, for instance L1.ldb, with 3 columns: UTM Easting, UTM Northing and 0 (the z-coordinate).

The .ldb files can be loaded into RGFGRID, a submodule of Delft3D, as land boundaries which helps with the creation of splines.

C.3.2 *Coupling Bathymetry*

For the coupling of the created grids with the available bathymetry of 2010, the QUICKIN module of Delft3D is used. More specific: the steps 6.1 until 6.2 of QUICKIN manual were used (Deltares, 2019c).

For convenience the steps are summarised below:

1. Open grid and the .xyz file using the *'Open samples'* option.
2. Create polygon around grid.
3. Use *'Grid Cell Averaging'* and *'Triangular Interpolation'* to project the bathymetry data on the nodes of the grid/grid cell face centres.
4. Export the interpolated bathymetry data as a .dep file.
5. Repeat the steps mentioned above for the other grids, do not forget to export the .dep file for each grid separately.

Considerations when coupling the bathymetry:

- Check if all grid cells have a depth, if not, use 'Internal Diffusion' to fill in the depth of the missing points.
- Initial Courant numbers can be checked by using *Operations, 'Courant Numbers'*. These numbers are an approximation and the parameters for this, such as *Timestep for Courant Numbers* can be filled in at *Settings, 'General...'*
- Check for large variations in depth values between grid cells, if large variations are present either the grid can be refined or the depth file smoothened, in order to prevent 'Flow exited abnormally' (Courant) errors.

C.3.3 *Running the Model with DD-boundaries*

To run the Delft3D-Flow model with DD-boundaries the following steps need to be followed:

1. Create the different grids/domains using RGFGRID.
2. Where two domains need to be coupled draw a DD-boundary in RGFGRID, *Edit, DD boundaries, New*. The purple line now indicates the connection between the two domains.
3. Connect the two domains: *Operations, Attach Grids at DD Boundaries, Regular Grids*. The grids are now connected. One can orthogonalise the grids and connect the boundaries again, until the grid looks good to use. (Do not forget to check with *Views, Grid Property* the grid properties, such as orthogonality, every so often).
4. Once satisfied with the connected domains, the domains need to be saved as separate .grd files. The DD-boundaries need to be saved as well: *Operations, Compile DD boundaries*. The DD-boundaries are saved in a separate file, RGFGRID will give a pop-up: showing the number of DD-boundaries.
5. For every domain/grid a .mdf file has to be created and with the correct settings, keep in mind that several parameters have to be the same in all domains.
6. To run the model with multiple domains: open the .ddb file with notepad and change the name of the .grd files and to the name of the .mdf files. Furthermore, change the type of file from .grd to .ddb. For example change: *testgrid1.grd* to *test1.mdf*.
7. Return to the Delft3D main menu, click *Flow*, select the correct working directory containing the .ddb file and .mdf files and input of the domains. Click *Start DD* and select the .ddb file. The Flow simulation will start.

This information can also be found in paragraphs 5.2.9 and 5.3.17 of the Delft3D RGFGRID User Manual: (Deltares, 2019d) and Appendix B.14 of the Delft3D-Flow User Manual (Deltares, 2019b).

C.4 Initial Condition

The model was initially run with only the hydrodynamics (sedimentation and morphology inactive), this simulation included an initial water level of 5 metres. At the coastal boundary a constant water level of 5 metres was used, as the simulation progressed this constant water level was decreased to 0 metres in the course of days. The tide was not included in this simulation since this resulted in crashes due to instabilities.

Secondly, the model was run with the tide, as mentioned in section 5.3.2. The initial condition for this simulation is the last restart file from the previous simulation, since the water level was observed to be in equilibrium at the end of this simulation. The process of starting a new simulation from an old one is called a 'hot start'. In this simulation the sedimentation and morphological component were again inactive, so that a stable hydrodynamic situation could develop.

The restart file from the last simulation can be used in the morphological model. The morphological simulation can thus be hot started which has the advantages of minimising numerical errors, and no need to use a large smoothing time.

C.5 Neglected Processes

If desired and useful for the project, all of nature's processes can be included in the model. The inclusion of processes increases the computation time and the complexity of the system significantly. Therefore, the inclusion has to weigh up to the influence of the phenomenon in the area of interest. Furthermore, this is a first version of a Delft3D model for the Biobío river. The main focus was therefore on the grid, discharge and tidal data. However, other processes which could be included in future models are discussed below.

C.5.1 *Waves*

A sand bar is present in the mouth of the Biobío river, the development of this sand bar over time depends on the waves. However, the influence of the waves on the river system more upstream - near the location of the river - is small if not negligible. Therefore waves are not included in this model.

C.5.2 *Salinity*

The salinity is not taken into account as its influence in the river is rather small, according (Bertran et al., 2001) (also described in section 4.2). Diego Caamaño Avendaño (2019) has stated no corrosion due to salt of the current bridge foundation is observed. Secondly, there is no vegetation present on the foundation of the bridge, which is typical for a bridge close to the sea and in the area of salt water influence. Furthermore, for the same reason as the neglect of the waves, the area of interest (the area surrounding the new railway bridge) is located far away from the described phenomenon.

D

Input Parameters Delft3D Model

This appendix shows the input data for the Delft3D model, discussed in chapter 5, with this input data the model can be created or updated. The format is provided by Moerman (2019).

The mentioned time frame settings indicate a period of 10 weeks, which corresponds to a simulation time of 5 years.

Table D.1: Delft3D-MDF setting DD-Left.mdf

Data group	**Parameter**	**Description**	**Value**
Description			DD-LEFT BASE
Domain	Grid parameters	Grid	Left_grid.grd
		Enclosure	Left_grid.enc
		Grid points-M	242
		Grid points-N	162
		Latitude	-36.8 [deg]
		Orientation	0
		Layers	1
	Bathymetry	File	Left_bathymetry.dep
		Values specified at	Grid cell centres
	Dry points		n.a.
	Thin dams		n.a.
Time Frame		Reference date	01 06 2019
		Simulation start time	28 06 2019 00 00 00
		Simulation stop time	06 09 2019 00 00 00
		Time step	0.1 [min]
		Local time zone	0 (+GMT)
Processes	Sediments		Sediment-Sand
Initial conditions		File	tri-rst.DD-Left-RST_v2.20190628.000000
Boundaries	Tidal-Data	M1	1
		M2	1
		N1	161
		N2	2
		Type	Water level
		Reflection parameter	0 [s2]
		Forcing	Astronomic
		File	Tides-paper
	Tidal Constituents	Amplitude [m]	Phase [deg]
	M2	0.41	108.82
	S2	0.1274	100.75
	K1	0.2364	54.58
	O1	0.1596	33.23
		Thatcher-Harleman	0 [min]
Physical parameters	Hydrodynamic constants	Gravity	9.81 [m/s2]
		Water density	1000 [kg/m3]
	Roughness	Manning (file)	Left_vegetation.rgh
		Wall roughness	Free
	Viscosity	Background	

		Hor. eddy viscosity	0.4 [m2/s]
		Hor. eddy diffusivity	1.0 [m2/s]
	Sediment	File	Biobio_sediment.sed
	Morphology	File	Biobio_morphology.mor
Numerical parameters	Drying and flooding		Grid cell centres and faces
	Depth at grid cell faces		Mor
	Threshold depth		0.1 [m]
	Marginal depth		-999 [m]
	Smoothing time		60 [min]
	Advection scheme	Momentum	Cyclic
		Transport	Cyclic
	Forester filter	Horizontal	true
Operations			n.a.
Monitoring			n.a.
Additional parameters			n.a.
Output	Storage	Map results start	28 06 2019 00 00 00
		Map results stop	06 09 2019 00 00 00
		Interval	120 [min]
		History interval	1440 [min]
		Map results start	28 06 2019 00 00 00
		Map results stop	06 09 2019 00 00 00
		Interval	0 [min]
		Restart int.	40320 [min]

,

Table D.2: Delft3D-MDF setting DD-Middle.mdf

Data group	**Parameter**	**Description**	**Value**
Description			DD-MIDDLE BASE
Domain	Grid parameters	Grid	Middle_grid.grd
		Enclosure	Middle_grid.enc
		Grid points-M	162
		Grid points-N	162
		Latitude	-36.8 [deg]
		Orientation	0
		Layers	1
	Bathymetry	File	Middle_bathymetry.dep
		Values specified at	Grid cell centres
	Dry points		n.a.
	Thin dams		n.a.
Time Frame		Reference date	01 06 2019
		Simulation start time	28 06 2019 00 00 00
		Simulation stop time	06 09 2019 00 00 00
		Time step	0.1 [min]
		Local time zone	0 (+GMT)
Processes	Sediments		Sediment-Sand
Initial conditions		File	tri-rst.DD-Middle-RST_v2.20190628.000000
Boundaries	Tidal-Data		n.a.
Physical parameters	Hydrodynamic constants	Gravity	9.81 [m/s2]
		Water density	1000 [kg/m3]
	Roughness	Manning (file)	Middle_vegetation.rgh
		Wall roughness	Free
	Viscosity	Background	Uniform
		Hor. eddy viscosity	0.4 [m2/s]
		Hor. eddy diffusivity	1.0 [m2/s]
	Sediment	File	Biobio_sediment.sed
	Morphology	File	Biobio_morphology.mor
Numerical parameters	Drying and flooding		Grid cell centres and faces
	Depth at grid cell faces		Mor
	Threshold depth		0.1 [m]
	Marginal depth		-999 [m]

	Smoothing time		60 [min]
	Advection scheme	Momentum	Cyclic
		Transport	Cyclic
	Forester filter	horizontal	true
Operations			n.a.
Monitoring			n.a.
Additional parameters			n.a.
Output	Storage	Map results start	28 06 2019 00 00 00
		Map results stop	06 09 2019 00 00 00
		Interval	120 [min]
		History interval	1440 [min]
		Map results start	28 06 2019 00 00 00
		Map results stop	06 09 2019 00 00 00
		Interval	0 [min]
		Restart int.	40320 [min]

Table D.3: Delft3D-MDF setting DD-Right.mdf

Data group	**Parameter**	**Description**	**Value**
Description			DD-RIGHT BASE
Domain	Grid parameters	Grid	Right_grid.grd
		Enclosure	Right_grid.enc
		Grid points-M	32
		Grid points-N	162
		Latitude	-36.8 [deg]
		Orientation	0
		Layers	1
	Bathymetry	File	Right_bathymetry.dep
		Values specified at	Grid cell centres
	Dry points		n.a.
	Thin dams		n.a.
Time Frame		Reference date	01 06 2019
		Simulation start time	28 06 2019 00 00 00
		Simulation stop time	06 09 2019 00 00 00
		Time step	0.1 [min]
		Local time zone	0 (+GMT)
Processes	Sediments		Sediment-Sand
Initial conditions		File	tri-rst.DD-Right-RST_v2.20190628.000000
Boundaries	Tidal-Data	M1	32
		M2	32
		N1	2
		N2	161
		Type	Total discharge
		Reflection parameter	0 [s2]
		Forcing	Time-series
		File	Right_river-constant.bct
	Right_river-constant.bct	Time dd mm yyyy hh mm ss	Discharge [m3/s]
		28 06 2019 00 00 00	-1671
		06 09 2019 00 00 00	-1671
		Thatcher-Harleman	0 [min]
Physical parameters	Hydrodynamic constants	Gravity	9.81 [m/s2]
		Water density	1000 [kg/m3]
	Roughness	Manning (file)	U=0.03 V=0.03
		Wall roughness	Free
	Viscosity	Background	Uniform
		Hor. eddy viscosity	0.4 [m2/s]
		Hor. eddy diffusivity	1.0 [m2/s]
	Sediment	File	Biobio_sediment.sed
	Morphology	File	Biobio_morphology.mor
Numerical parameters	Drying and flooding		Grid cell centres and faces
	Depth at grid cell faces		Mor
	Threshold depth		0.1 [m]

	Marginal depth		-999 [m]
	Smoothing time		60 [min]
	Advection scheme	Momentum	Cyclic
		Transport	Cyclic
	Forester filter	horizontal	true
Operations			n.a.
Monitoring			n.a.
Additional parameters			n.a.
Output	Storage	Map results start	28 06 2019 00 00 00
		Map results stop	06 09 2019 00 00 00
		Interval	120 [min]
		History interval	1440 [min]
		Map results start	28 06 2019 00 00 00
		Map results stop	06 09 2019 00 00 00
		Interval	0 [min]
		Restart int.	40320 [min]

Table D.4: Delft3D Sediment parameter setting Biobio_sediment.sed

Data group	**Parameter**	**Description**	**Value**
Sediment Overall		Cref	1600 [kg/m3]
		IopSus	0 [-]
	Sediment-Sand	SedTyp	sand
		RhoSol	2650 [kg/m3]
		SedDia	1e-3 [m]
		CDryB	1600 [kg/m3]
		IniSedThick	5 [m]
		FacDSS	1 [-]

Table D.5: Delft3D Morphology input file Biobio_morphology.mor

Data group	**Parameter**	**Description**	**Value**
Mophology		EpsPar	false
		IopKCW	1
		RDC	0.01 [m]
		RDW	0.02 [m]
		MorFac	24 [-]
		MorStt	0 [min]
		Thresh	5e-2 [m]
		MorUpd	true
		EqmBc	true
		DensIn	false
		AksFac	1 [-]
		Rwave	2 [-]
		AlfaBs	1 [-]
		AlfaBn	10 [-]
		Sus	1 [-]
		Bed	1 [-]
		SusW	1 [-]
		BedW	1 [-]
		SedThr	0.1 [m]
		ThetSD	0 [-]
		HMaxTH	1.5 [m]
		FWFac	1 [-]

E

Results of calibration runs

In section 5.5 the calibration process has been discussed. Furthermore, the section included cross-sections at the location of the bridge together with boxplots to compare the variability of the Biobío system. As mentioned, the chosen set of parameters which has been used for the different scenarios in section 7.1 is the set for which the variability of the simulation best fits the variability of the measurements from 2015.

In section 5.5 only the results concerning the cross-section at the location of the bridge are shown. The other two cross-sections, one upstream and the other downstream: see figure 5.3, also contain valuable information. This appendix contains all data from these cross-sections. In table E.1 an overview of the simulation runs performed for the calibration are summarised.

Table E.1: Overview of simulations for calibration

Version	Roughness		Horizontal eddy viscosity	alfa,bn	alfa,bs
	In river	On the bar			
v1.3	n = 0.03	n = 0.03	0.4	10	1
v2.0	n = 0.03	n = 0.04	0.4	10	1
v2.1	n = 0.03	n = 0.04	0.6	10	1
v2.2	n = 0.03	n = 0.036	0.4	10	1
v2.3	n = 0.03	n = 0.036	0.6	10	1
v2.4	n = 0.03	n = 0.04	0.4	15	1
v3.0	n = 0.03	n = 0.04	0.4	15	10

E.1 Manning's Roughness Coefficient

To calibrate the Manning's roughness coefficient three simulations have been made:

- **v1.3** with a uniform roughness, so the roughness on the bar is the same as in the river flow
- **v2.0** with an increased roughness of n = 0.04 on the river bar
- **v2.2** with an increased roughness of n = 0.036 on the river bar

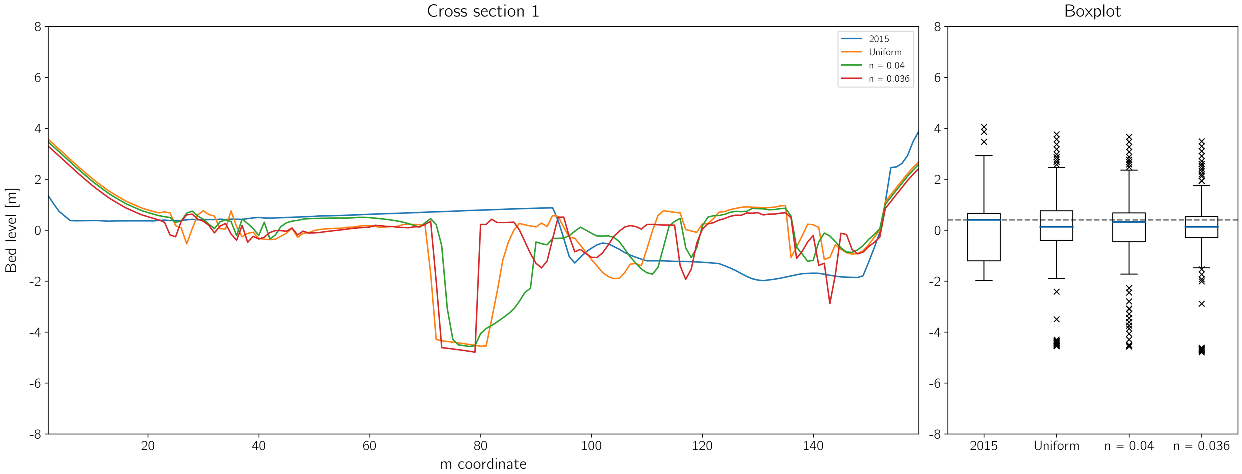

Figure E.1: Cross-section 1 with different values for the roughness

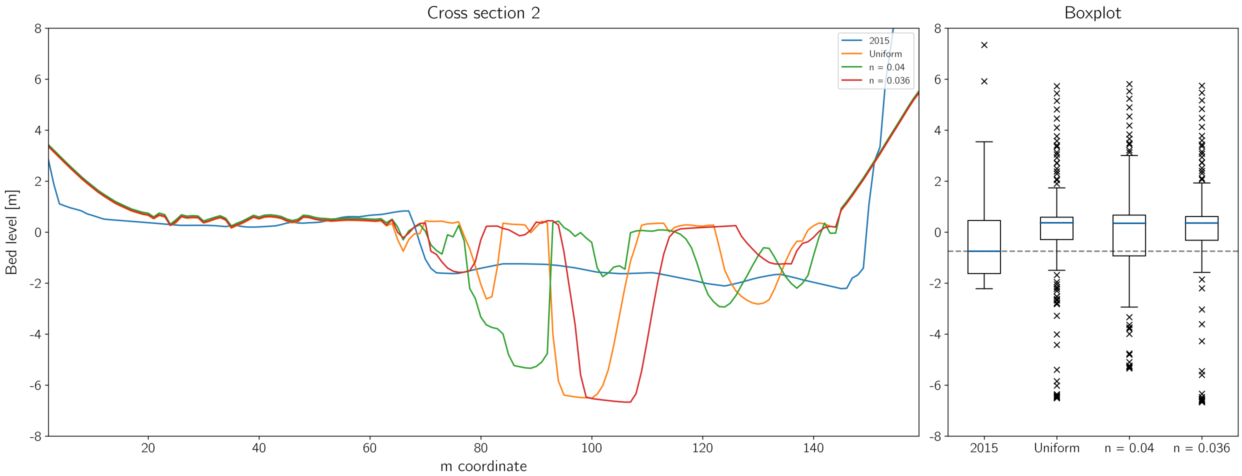

Figure E.2: Cross-section 2 with different values for the roughness

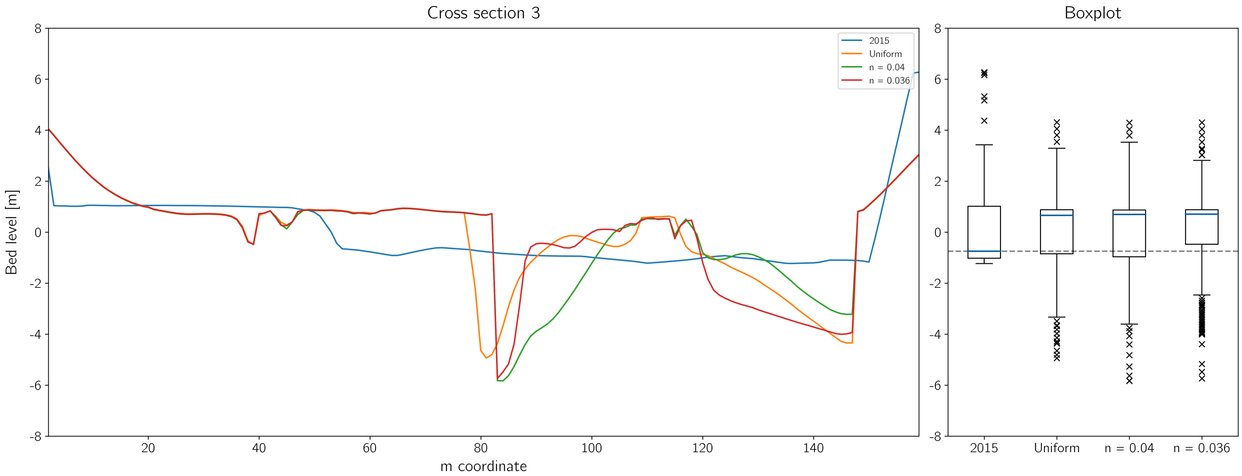

Figure E.3: Cross-section 3 with different values for the roughness

E.2 Horizontal Eddy Viscosity

For the calibration of the horizontal eddy viscosity the following simulations from table E.1 have been used:

- **v2.0** with a horizontal eddy viscosity of 0.4 m^2/s
- **v2.1** with a horizontal eddy viscosity of 0.6 m^2/s

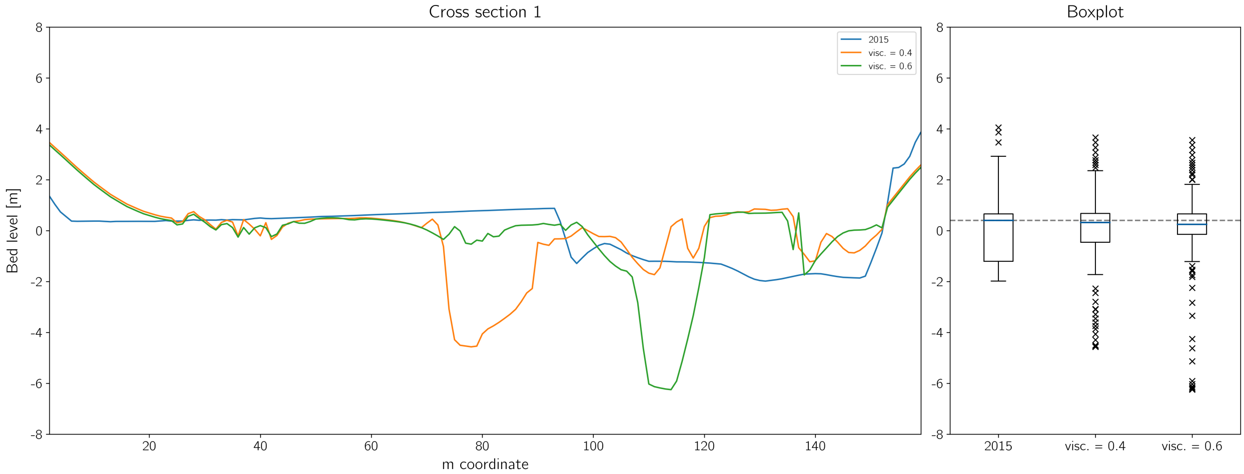

Figure E.4: Cross-section 1 with different values for the horizontal eddy viscosity

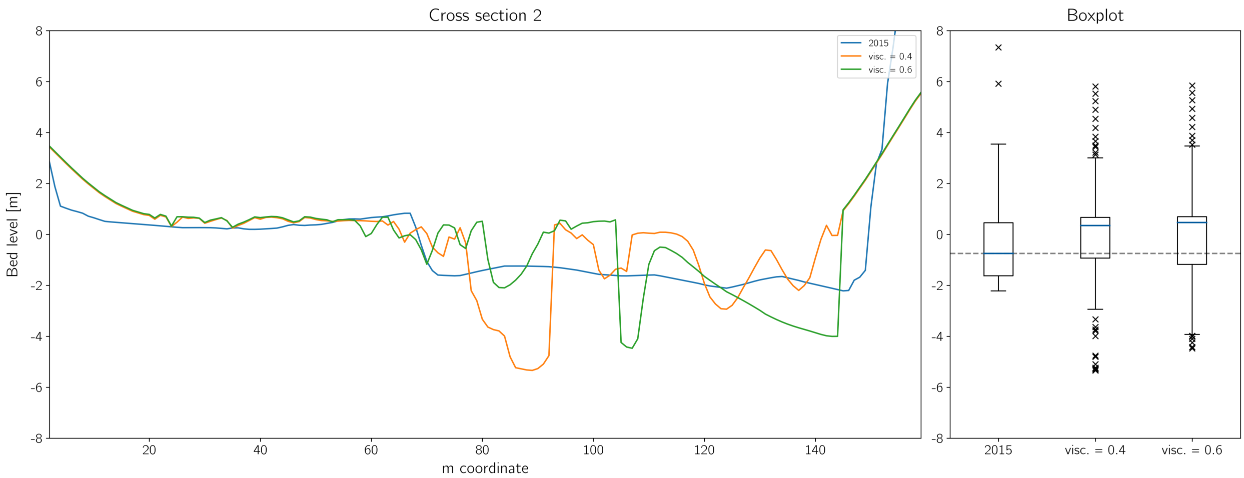

Figure E.5: Cross-section 2 with different values for the horizontal eddy viscosity

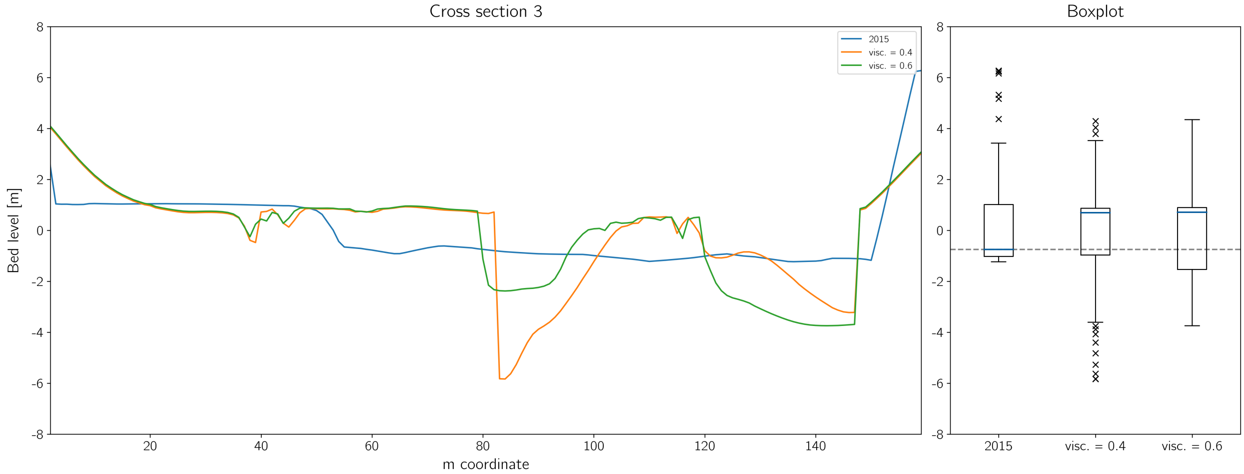

Figure E.6: Cross-section 3 with different values for the horizontal eddy viscosity

E.3 Transverse Bed Gradient Factor for Bed Load Transport

In the calibration of the transverse bed gradient factor for bed load transport, α_{bn}, the following simulations have been used:

- **v2.0** with an α_{bn} of 10
- **v2.4** with an α_{bn} of 15

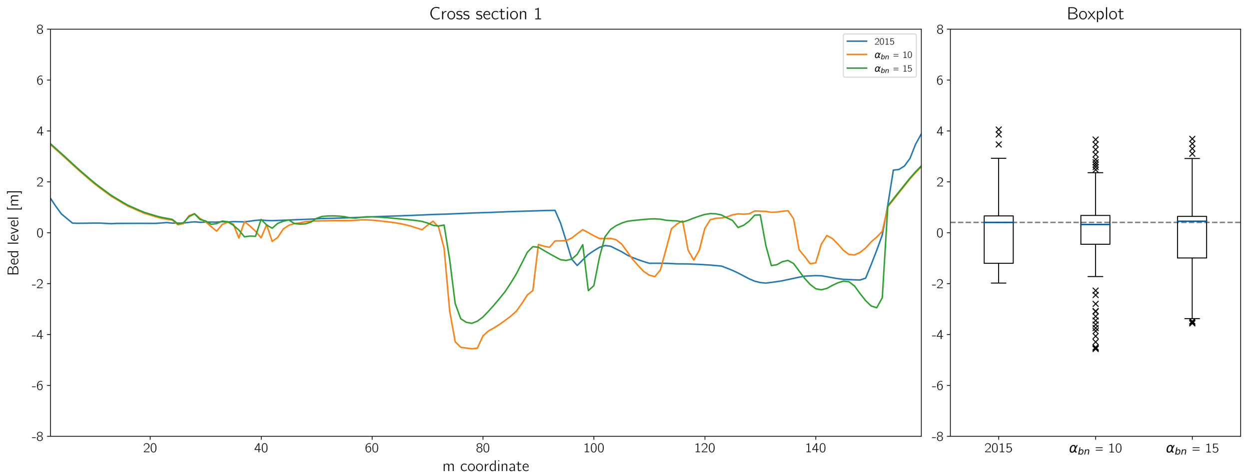

Figure E.7: Cross-section 1 with different values for α_{bn}

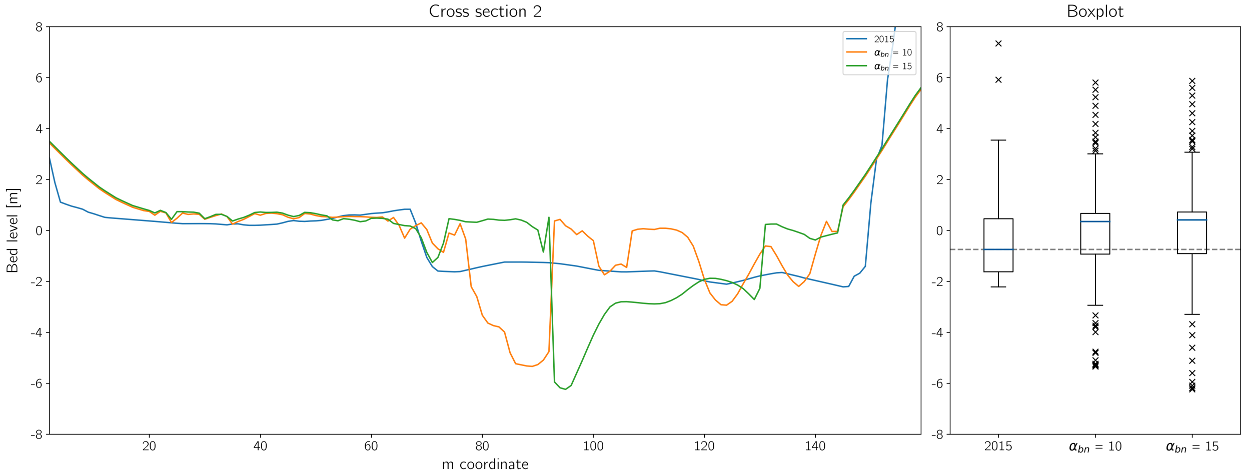

Figure E.8: Cross-section 2 with different values for α_{bn}

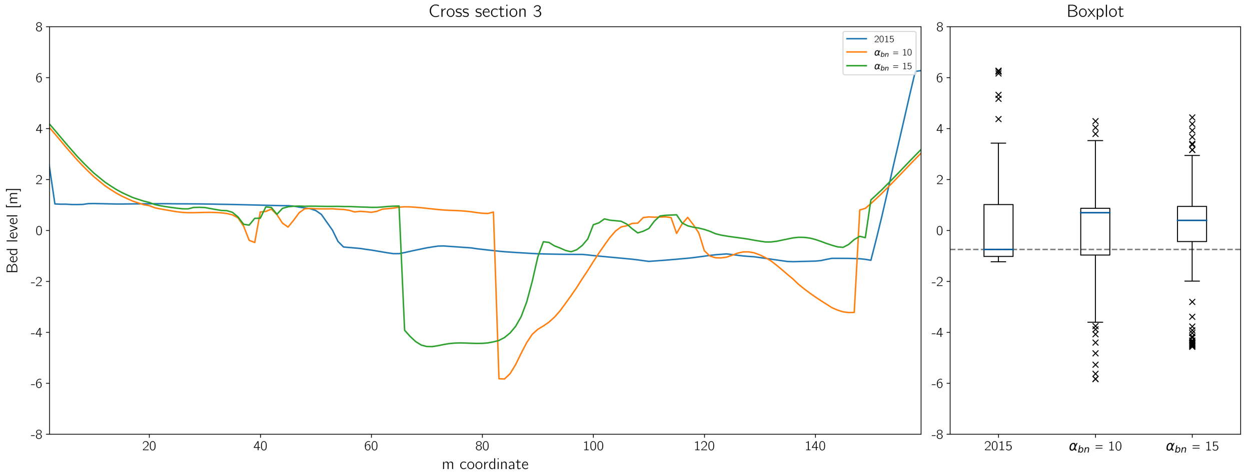

Figure E.9: Cross-section 3 with different values for α_{bn}

E.4 Streamwise Bed Gradient Factor for Bed Load Transport

For the calibration of the streamwise bed gradient factor for bed load transport, α_{bs}, the following simulations from table E.1 have been used:

- **v2.4** with an α_{bs} of 1
- **v3.0** with an α_{bs} of 10

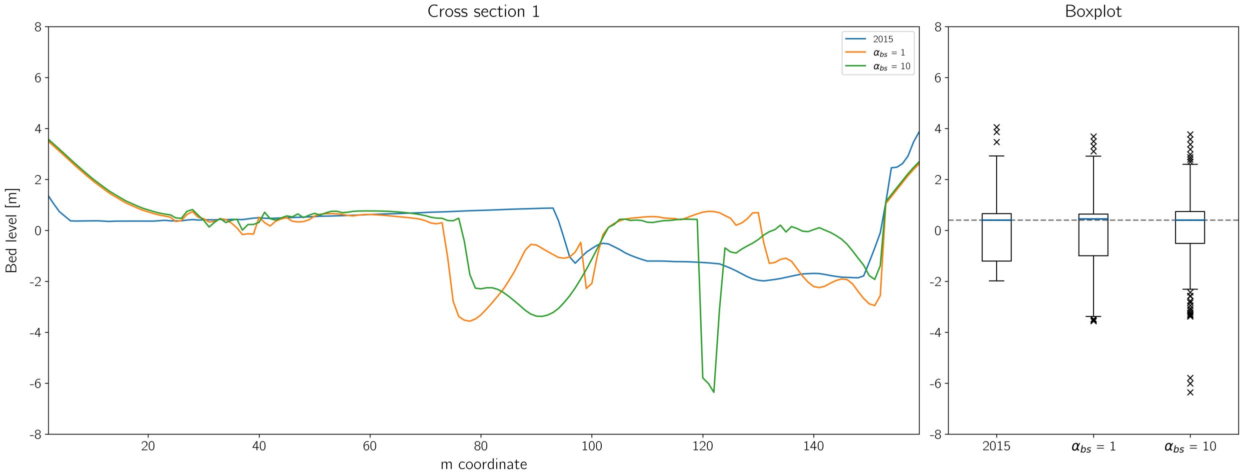

Figure E.10: Cross-section 1 with different values for α_{bs}

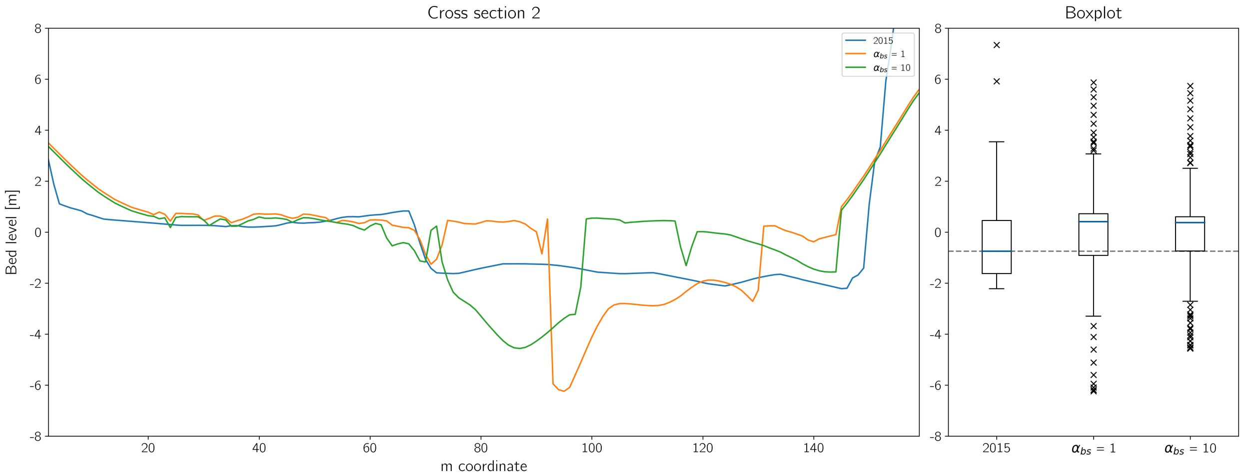

Figure E.11: Cross-section 2 with different values for α_{bs}

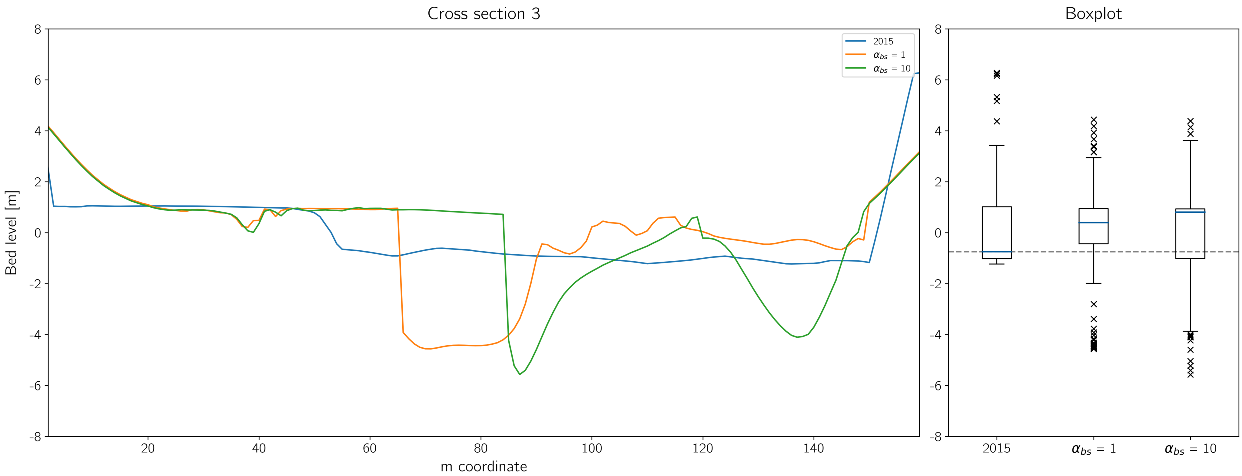

Figure E.12: Cross-section 3 with different values for α_{bs}

F
Tsunamis: Additional readings

Tsunamis are one of the most infamous natural disasters nowadays. The name comes from the Japanese word 'harbour wave' and are mostly caused by a fault event in the Earth's crust (Stuhlmeier, 2009). However, tsunamis can have other origins, e.g. landslides or volcanic activity.

Concepción, the Biobío river and the new railway bridge are all located near tectonic plates that show movements of about 72 mm/year, figure F.1. A tsunami can originate from moving tectonic plates and is likely to reach great height when entering the coastal zone, it is therefore necessary to assess the influence, e.g. hydraulic pressure and sedimentation/erosion, a tsunami could possibly have on the river and the bridge.

Figure F.1: Movement of the tectonic plates near Chile relatively to each other (USGC, 2019)

Properly modelling a tsunami is not an easy task. However, with the development of multiple numerical models over time this is becoming easier, one of this models is the NeoWave software, which can approximate tsunamis.

In section F.1 the different mechanisms which may cause a tsunami are described. Followed by the the dynamics and processes that take place for waves in the coastal and deep water zone in section F.2.

F.1 Sources of a Tsunami

It is well known that tsunamis mostly originate from earthquakes (see section 6.1, however, there are other sources as well. These sources or mechanisms are elaborated in this section. Additionally, the differences between the mechanisms are highlighted in each respective subsection.

F.1.1 *Volcanic Eruption*

A tsunami triggered by a volcanic eruption is the least common mechanism. A volcanic eruption can trigger a tsunami in two different ways. Either by the violent eruption of lava at the bottom of the ocean (pyroclastic flows) or by displacement of a large volume of air due to an eruption (Latter, 1981).

The latter generates a so-called gravity wave, which travels with the same speed as the tsunami wave. Causing the water to resonate and forming a volcano-meteorological tsunami (Lowe and de Lange, 2000).

Tsunamis triggered by volcanic eruptions are known to have a highly destructive character. Lowe and de Lange (2000) discusses the Krakatoa eruption of 1883 in Indonesia, causing a gravity-wave induced tsunami of 30 m. The natural disaster resulted in a loss of life of almost 30,000 people, both from the thermal effects and the resulting tsunami (Mary Bagley and Rachel Ross, 2017). An example of a tsunami caused by an volcanic eruption is shown in figure F.2

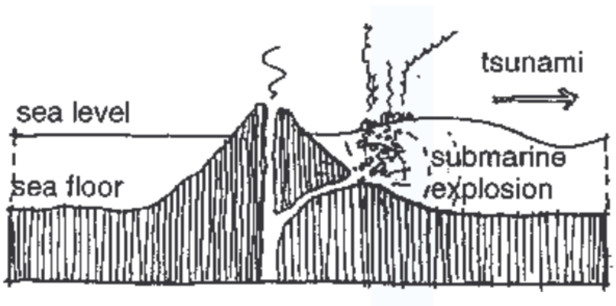

Figure F.2: Example of a tsunami caused by a volcanic eruption, from ITIC (nd)

F.1.2 *Landslide*

The second mechanism that is considered is the landslide (ITIC, nd). This can happen either above water or below the water. A tsunami which has its origin from a landslide is more common than a tsunami originating from a volcanic eruption. A landslide does not need to have a seismic cause. Although, a seismic activity far away may cause an instability of the soil and causing a landslide elsewhere. The landslide tsunami is predominantly triggered by mass movement of land, shore instabilities or glacier calvings (Heller and Spinneken, 2013; Lüthi and Vieli, 2016; NOAA Center for Tsunami Research and National Weather Service, 2019b), which then, in turn, impact an ocean, sea or lake, resulting in a tsunami. This process is shown in figure F.3.

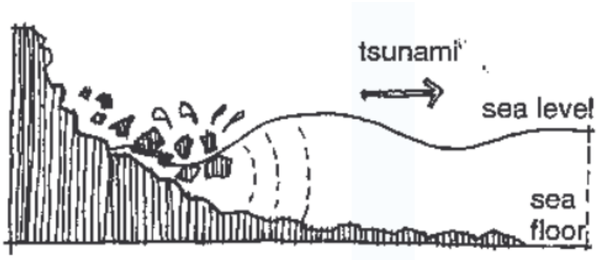

Figure F.3: Example of a tsunami caused by a landslide causing a tsunami, from ITIC (nd)

F.2 Tsunami Dynamics

The distinguished behaviour of a tsunami can be found in section 6.2. Below, the general wave processes are described.

F.2.1 *Waves in the Coastal Zone*

Waves in a coastal zone behave differently than waves in deep water. This is due to when a wave is in the transitional zone from deep to shallow water, the waves starts to "feel" the bottom. This phenomenon results in energy dissipation and the wave starts to deform. In this subsection the processes of wave transformation in coastal zones are discussed. For waves in shallow water the following governing equations are present (Bosboom and Stive, 2015):

Wave celerity:	$c = \sqrt{gd}$	[m/s]
Wave length:	$L = cT$	[m]
Specific wave energy:	$E_t = \frac{1}{8}\rho g H^2$	[J/m^2]
Wave power:	$U = E_t c$	[J/ms]

Another important relation for wave propagation is the dispersion relation, as for instance described by Reniers and Tissier (2018). This equation is visible below:

$$L = \frac{gT^2}{2\pi}\tanh\left(\frac{2\pi d}{L}\right)$$

The dispersion relation relates the wavelength to depth and is not dependent on whether it is in shallow or deep water. Although, it is an implicit relation, meaning that for a good computation of the wavelength, one needs to give an initial estimate, using for example $L_0 = \frac{gT_0^2}{2\pi}$, which is the wavelength in deep water (Bosboom and Stive, 2015) and start the iteration process to find the correct wave length.

Shoaling
To describe the phenomenon of shoaling one needs to consider a long-crested wave, with linear properties, that propagates into slowly adjusting shallow water. As the wave propagates in decreasing depth, the propagation speed is affected by the bottom. This corresponds with a ratio depth to wavelength of a half. According to the dispersion relation the decreasing water depth leads to a decrease in wave speed and wavelength (Bosboom and Stive, 2015).

Considering a domain with no dissipation of energy to relate the transformation to the depth gives a constant energy flux. The domain is limited by two wave rays and a distance Δx in between. In this domain the energy flux is thus given by:

$$
\begin{aligned}
E_1 n_1 c_1 &= E_2 n_2 c_2 \\
E &\propto H^2 \\
\frac{H_2^2}{H_1^2} &= \frac{c_1}{c_2}\frac{n_1}{n_2} \\
\frac{H_2}{H_1} &= \sqrt{\frac{c_1}{c_2}\frac{n_1}{n_2}} = \sqrt{\frac{1}{\tanh kd}\frac{1}{2n_2}} = K_{sh}
\end{aligned}
$$

This equation has been derived in the books of Holthuijsen (2007) and Bosboom and Stive (2015) and is also known as Green's law. Bosboom and Stive (2015) also mentions that a tsunami wave is subject to the process of shoaling and possibly tunnelling. This causes the wave to steepen and rise to great heights.

As the wave rises, it grows higher than ten times the water depth. From that point it is not possible to describe the amplitude of the tsunami using the Green's law. This is due to the fact that for shallower depths one should also consider advective terms (Truong, 2012).

Refraction

Refraction is the process that describes the turning movement of an oblique incident wave towards the beach. This is due to the fact that in shallow water, waves propagate with a celerity proportional to $\sqrt{gd}$. Therefore, an oblique incident wave has a part that is in shallower water and a part in deeper water. This difference in water depth causes the same wavecrest to travel with different celerities and thus causing the wave to turn towards the shore. This effect is in addition to shoaling. Again consider the domain of two wave rays and a width 'b'. Since the waves are now turning towards the coast, the width 'b' at greater depth is not the same as in the part of the wave travelling in more shallow water. Considering the same requirement as before: no dissipation of energy. The energy flux is now given by:

$$
\begin{aligned}
E_1 n_1 c_1 b_1 &= E_2 n_2 c_2 b_2 \\
E &\propto H^2 \\
\frac{H_2^2}{H_1^2} &= \frac{c_1}{c_2}\frac{n_1}{n_2}\frac{b_1}{b_2} \\
\frac{H_2}{H_1} &= \sqrt{\frac{c_1}{c_2}\frac{n_1}{n_2}}\sqrt{\frac{b_1}{b_2}} = \sqrt{\frac{1}{2n_2}\frac{c_1}{c_2}\frac{b_1}{b_2}} = K_{sh}K_r
\end{aligned}
$$

When a tsunami is generated in a large ocean many obstacles such as islands, seamounts and submarine canyons can refract a tsunami in such a way that the energy is concentrated on a shoreline far away, which is called 'focussing'. On the contrary, the bed topography can also lead to spreading of the wave energy over a larger area. Thus leading to defocussing (Bryant, 2014).

Diffraction

Diffraction is the phenomenon of wave transformation due to either sudden obstruction of the propagation of the wave or large differences in depth. This causes the wave train to be interrupted and creates a shadow zone behind the object or feature. The object/feature partly reflects the wave energy seawards, while the remainder will bend around the feature (Bosboom and Stive, 2015). Calculations on this matter are quite complex, as the wave height differs over the wave ray in the shadow zone. However, numerical models are quite efficient in modelling this phenomenon.

F.3 Post Processing of the Results

Used equations from NCh3363:2015 (2015):

- Drag force:

$$\begin{aligned} F_d &= \frac{1}{2}\rho C_d b \left(du^2\right)_{max} \\ \rho &= \text{density } = 1200kg/m^3 \\ C_d &= \text{drag coefficient } = 2 \\ b &= \text{width of structure} \\ d &= \text{depth} \\ u &= \text{Flow velocity} \end{aligned} \tag{F.1}$$

- Wave impact force:

$$F_I = 1.5 * F_d \tag{F.2}$$

- Impact force of floating objects:

$$\begin{aligned} F_{IF} &= 500 \cdot \left(\frac{Ub}{\Delta t}\right) \\ \Delta t &= 0.1 \text{ for concrete structures} \end{aligned} \tag{F.3}$$

- Drag force due to accumulation of floating objects:

$$\begin{aligned} F_d &= \frac{1}{2}\rho C_d B_d \left(du^2\right)_{max} \\ \rho &= \text{density } = 1200kg/m^3 \\ C_d &= \text{drag coefficient } = 2 \\ B_d &= \text{minimum accumulation width} \\ d &= \text{depth} \\ u &= \text{Flow velocity} \end{aligned} \tag{F.4}$$

- Hydrostatic force due to a tsunami:

$$\begin{aligned} F_{hydrostatic} &= \frac{1}{2}\rho g \zeta^2 \\ \rho &= \text{density } = 1200kg/m^3 \\ g &= \text{gravitational acceleration } = 9.81\ m/s^2 \\ \zeta &= \text{water level inundation} \end{aligned} \tag{F.5}$$

G

Programme of Requirements: Additional readings

G.1 Elaboration POI's

In addition to the map created in chapter 8, figure 8.1, 3D images with a short summary of the POI's are supplied.

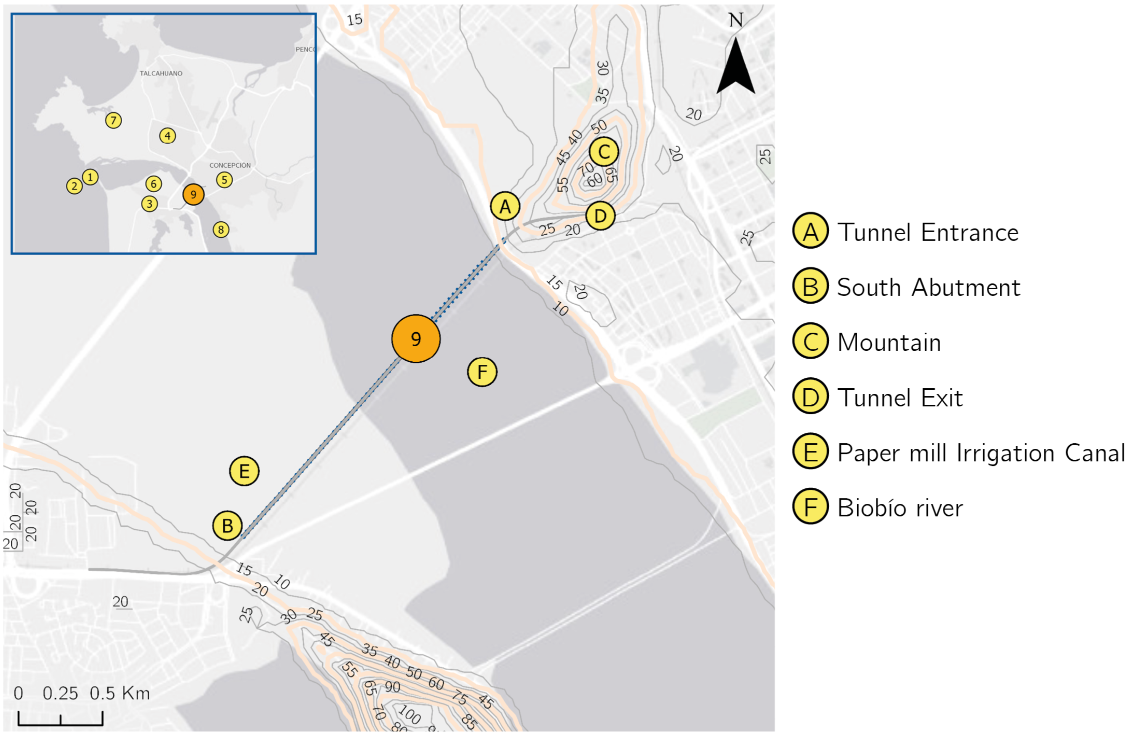

Figure G.1: Location of the railway bridge with additional points of interests (POI). The image in the top left corner refers to figure 4.1.

POI A – Tunnel Entrance & Northern Abutment
The bridge abutments are referred to as 'North Abutment' and 'South Abutment'. When taking a closer look at the northern abutment it can be seen that it is placed on a foot of a 'mountain' on which multiple water storage tanks are situated. A 2x2 highway is located in front of the abutment.

Figure G.2: 3D view of the northern or Concepción based abutment.

Figure G.3: 3D view of the northern or Concepción based abutment.

POI B – Southern Abutment

The Southern Abutment is less special, no real hindrances are in the vicinity.

Figure G.4: 3D view of the southern or San Pedro de la Paz based abutment.

Figure G.5: 3D view of the southern or San Pedro de la Paz based abutment.

POI C – Mountain

The old railway bridge goes through the mountain via a tunnel. As the new railway bridge is placed at a height of approximately 60 metres, a new tunnel has to be bored.

Figure G.6: 3D view of the mountain, located in Concepción, where the train tunnel passes through.

POI D – Tunnel Exit

Figure G.7: 3D view of the mountain, located in Concepción, where the train tunnel passes through.

Figure G.8: 3D view of the mountain, located in Concepción, where the train tunnel passes through.

POI E – Paper mill Irrigation Canal
The paper mill company needs an inflow of water in order to maintain its production. The irrigation canal intercepts the bridge at a southern point.

Figure G.9: Irrigation channel located at the river bank of San Pedro de la Paz

Figure G.10: Zoomed in view of the irrigation channel.

G.2 Geological Characteristics

In figure G.11 a cross-section, in longitudinal direction, of 42 soil penetration tests for the bridge can be seen. The different soil types have been listed in the legend in the bottom right. Most common soil types are:

- Sand
- Silt
- Granite

Figure G.11: Longitudinal cross-section of 42 soil penetration tests, data retrieved from (GrupoEFE, 2019)

G.3 Building Code Requirements

Ultimate Limit States
According to NEN-EN 1990:

1. "The design values of actions for ULS in the persistent and transient design situations (expressions 6.9a to 6.10b) should be in accordance with tables A2.4(A) to (C)
2. In applying tables A2.4(A) to (C) in cases when the limit state is very sensitive to variations in the magnitude of permanent actions, the upper and lower characteristic values of these actions should be taken according to 4.1.2(2)P
3. State equilibrium (EQU, 6.4.1 and 6.4.2(2)) for bridges should be verified using the design values of actions in table A2.4(A)
4. Design of structural members (STR, see 6.4.1) not involving geotechnical actions should be verified using the design values of action of table A2.4(B)
5. Design of structural members involving geotechnical actions and the resistance of the ground should be verified using one only of the following three approaches supplemented, for geotechnical actions and resistances: (...)
6. Site stability should be verified accordance with EN 1997
7. Hydraulic and buoyancy failure, if relevant, should be verified in accordance with EN 1997
8. The γ_P values to be used for pre-stressing actions should be specified for the relevant representative values of these actions in accordance with EN 1990 to EN 1999." (p. 69)

And with tables A2.4(A) to (C) - Design values of actions on pages 18 to 21.

Load Combination Factors - Railway Bridge Specific
According to NEN-EN 1990:

Table G.1: Recommended values of Ψ-factor for railway bridges. Retrieved and revised from NEN-EN 1990/A1 (1995, p. 15)

Actions			**Ψ0**	**Ψ1**	**Ψ2**
Individual components of traffic actions	LM 71		0.80	(1)	0
	SW/0		0.80	(1)	0
	SW/2		0	1.00	0
	Unloaded Train		1.00	-	-
	HSLM		1.00	1.00	0
	Traction and braking Centrifugal forces Interaction forces due to deformation under vertical traffic loads		Individual components of traffic actions in design situations where the traffic loads are considered as a single (multi-directional) leading action and not as groups of loads should use the same values of Ψ-factors as those adopted for the associated vertical loads		
	Nosing Forces		1.00	0.80	0
	Non public footpaths loads		0.80	0.50	0
	Real trains		1.00	1.00	0
	Horizontal earth pressure due to traffic load surcharge		0.80	(1)	0
	Aerodynamic effects		0.80	0.50	0
Main traffic actions	gr11 (LM71 + SW/0)	Max. vertical 1 with max. longitudinal	0.80	0.80	0
	gr12 (LM71 + SW/0)	Max. vertical 2 with max. transverse			
	gr13 (Braking/traction)	Max. longitudinal			
	gr14 (Centrifugal/nosing)	Max. lateral			
	gr15 (Unloaded train)	Lateral stability with "unloaded train"			
	gr16 (SW/2)	SW/2 with max. longitudinal			
	gr17 (SW/2)	SW/2 with max. transverse			
	gr21 (LM71 + SW/0)	Max. vertical 1 with max. longitudinal	0.80	0.70	0
	gr22 (LM71 + SW/0)	Max. vertical 2 with max transverse			
	gr23 (Braking/traction)	Max. longitudinal			
	gr24 (Centrifugal/nosing)	Max. lateral			
	gr26 (SW/2)	SW/2 with max. longitudinal			
	gr27 (SW2)	SW/2 with max. transverse			
	gr31 (LM71 + SW/0)	Additional load cases	0.80	0.60	0
Other operating actions	Aerodynamic effects		0.80	0.50	0
	General maintenance loading for non public footpaths		0.80	0.50	0
Wind forces (2)	F_{Wk}		0.75	0.50	0
	F^{**}_{Wk}		1.00	0	0
Thermal actions (3)	T_k		0.60	0.60	0.50
Construction loads	Q_c		1.00	-	1.00
Comments: **(1)**	0,8 if 1 track only is loaded 0,7 if 2 tracks are simultaneously loaded 0,6 if 3 or more tracks are simultaneously loaded.				
(2)	When wind forces act simultaneously with traffic actions, the wind force Ψ0 F_{Wk} should be taken as no greater than F^{**}_{Wk} (see EN 1991-1-4). See A2.2.4(4).				
(3)	See EN 1991-1-5.				
(4)	If deformation is being considered for Persistent and Transient design situations, Ψ2 should be taken equal to 1,00 for rail traffic actions. For seismic design situations, see Table A2.5.				
(5)	Minimum coexistent favourable vertical load with individual components of rail traffic actions (e.g. centrifugal, traction or braking) is 0,5LM71, etc				

Serviceability Limit State

For the serviceability limit states the design values of actions should be taken from table G.12 except if otherwise specified in EN 1991 to EN 1999. (NEN-EN 1990+A1+A1/C2, 1990, p.23)

Table A2.6 - Design values of actions for use in the combination of actions

Combination	Permanent actions G_d		Prestress	Variable actions Q_d	
	Unfavourable	Favourable		Leading	Others
Characteristic	$G_{kj,sup}$	$G_{kj,inf}$	P	$Q_{k,1}$	$\psi_{0,i}Q_{k,i}$
Frequent	$G_{kj,sup}$	$G_{kj,inf}$	P	$\psi_{1,1}Q_{k,1}$	$\psi_{2,i}Q_{k,i}$
Quasi-permanent	$G_{kj,sup}$	$G_{kj,inf}$	P	$\psi_{2,1}Q_{k,1}$	$\psi_{2,i}Q_{k,i}$

Figure G.12: Design values of actions for use in the combination of actions. Retrieved from NEN-EN 1990+A1+A1/C2 (1990)

Dynamic Train Loading

In the Dutch Building Code, NEN-EN 1991-2+C1 (2015), a distinction between static and dynamic calculations for train loading is made. This is determined in combination with the following figure (in Dutch).

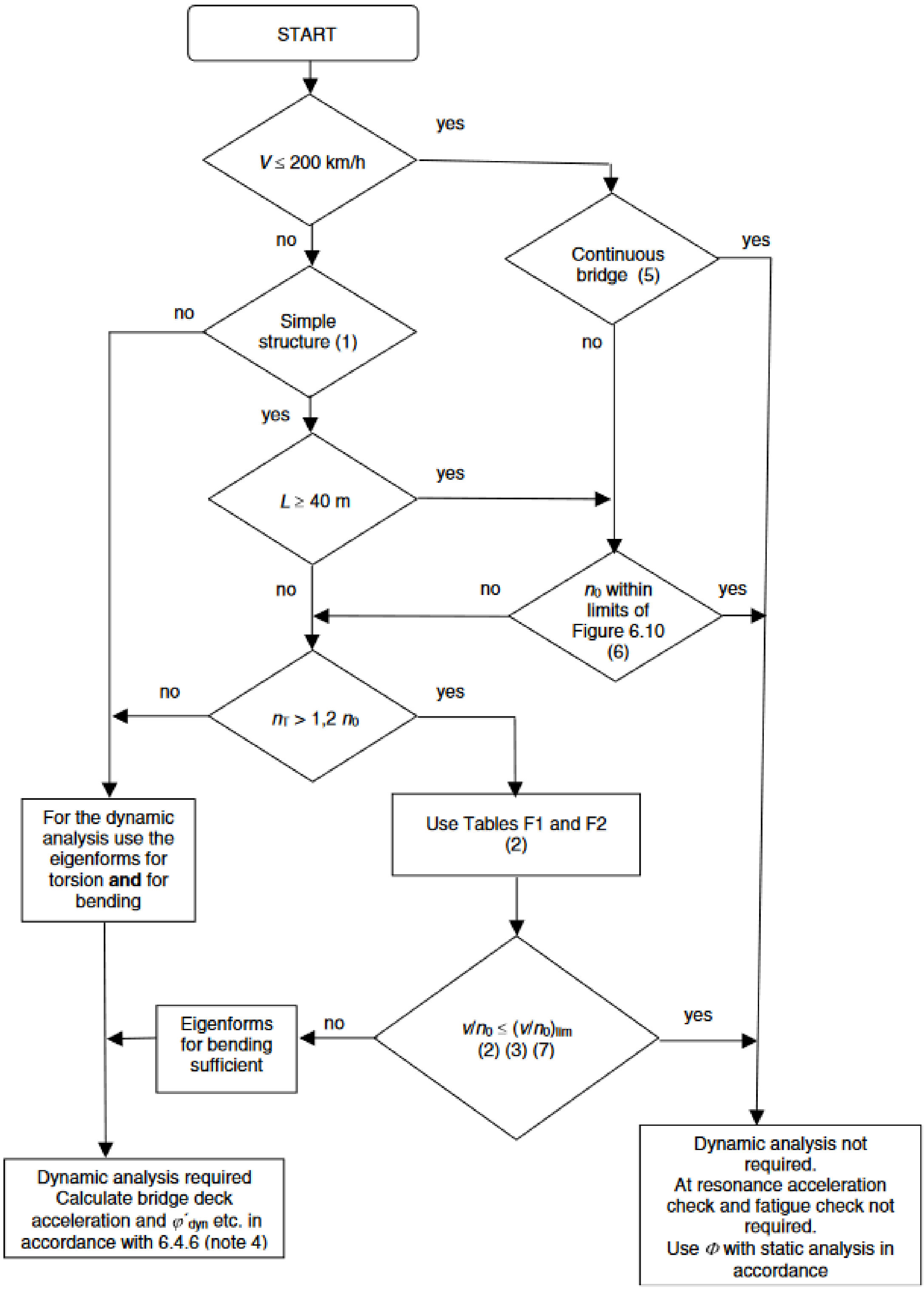

Figure G.13: Determination type of loading on a bridge. Retrieved from NEN-EN 1991-2+C1 (2015, p. 76)

H

Variants and MCA

H.1 Parameters

- **Total length:** 1,880 metres
- **Length 'wet' part:** 1,130 metres
- **Length 'dry' part:** 750 metres
- **Proposed width:** 14.6 metres
- **Clearance:** 12 metres (above sea-level)

H.2 Miscellaneous Bridge Projects

Bridges that are not necessarily railroad bridges can still serve as a basis for the design variance study. Therefor, (road)bridges that adhere to the criterion, stated in section 9.1, are listed below and taken into account.

Stord Bridge – Norway
The Stord Bridge, constructed in Norway, consists out of two lanes for traffic and a combined pedestrian and cyclists pathway. The construction of the bridge was finalised in 2000. The daily traffic is on average 6,600 vehicles.

Figure H.1: Stord Bridge, retrieved from: Mundal (2006)

- Type: Suspension
- Length: 1,077 m
- Width: 14 m
- Main span: 667 m
- Clearance: 18 m
- Costs: €45,000,000.- Mundal (2006)

Blue Water Bridges – USA and Canada
The 'Blue Water bridges' consists out of two bridges that connect Michigan, United States and Ontario, Canada, with each other. For the reference projects only the newer version is taken into account. The older version is a cantilever truss bridge and the newer version is bowstring arch type. The bowstring type opened in 1997, and daily traffic nowadays is nearly 15,000 vehicles. (Federal Bridge Corporation, 2016)

Figure H.2: Blue Water bridges, with on the left the bowstring type and on the right the older brother, a cantilever truss type, retrieved from Dee Lish (2012).

- Type: Bowstring Arch
- Length: 1,862 m
- Width: 16 m
- Main span: 281 m
- Clearance: 47 m
- Costs: €67,700,000.- (MDOT (Michigan Department Of Transportation), 2018)

Puente Chacabuco – Chile
The 'Chacabuco' is currently still under construction, although half of it is already open to traffic. The bridge is a common beam bridge, supported by 332 pillars. The total estimated costs are figured at $58,000 million Chilean pesos (€76 million euros) and the project should have finished back in 2018 (Ximena Valenzuela, 2018).

Figure H.3: Puente Chacabuco in Concepción, retrieved from PorelDerechoalaCiudad (nd)

- Type: Concrete beam bridge
- Length: 1,465 m
- Width: 14 m
- Main span: 40 m
- Clearance: Unknown
- Costs: €76,000,000.- (Ximena Valenzuela, 2018)

Øresund bridge – Denmark and Sweden
The Øresund bridge is a bridge connecting the city of Copenhagen and Sweden. The total structure exists of a tunnel and a bridge and was constructed to to decrease the travel time between the countries. As before the construction of the bridge the only a route was via a ferry. The bridge does not only provides a road for motor vehicles but has a railway section as well.

The beginning of the construction started at 1996 and took almost 4 years (Structurea, 2018). The costs for the construction of the bridge were over 12 billion DKK, which is around €1,600,000,000 (Road Traffic Technology, 2018). Though this includes the bridge and tunnel part of the construction. In 2018 the average of crossing vehicles per day around was 20,500 (Øresundsbro Konsortiet I/S, 2018).

Figure H.4: Øresund Bridge, retrieved and modified from: Taubenheim (2010)

- Type: Cable-stayed bridge with harp system
- Length: 7,845 m
- Width: 23.5 m
- Main span: 490 m
- Clearance: 57 m
- Costs: over €1,600,000,000.- for the entire project (Road Traffic Technology, 2018)

H.3 Types of Bridges

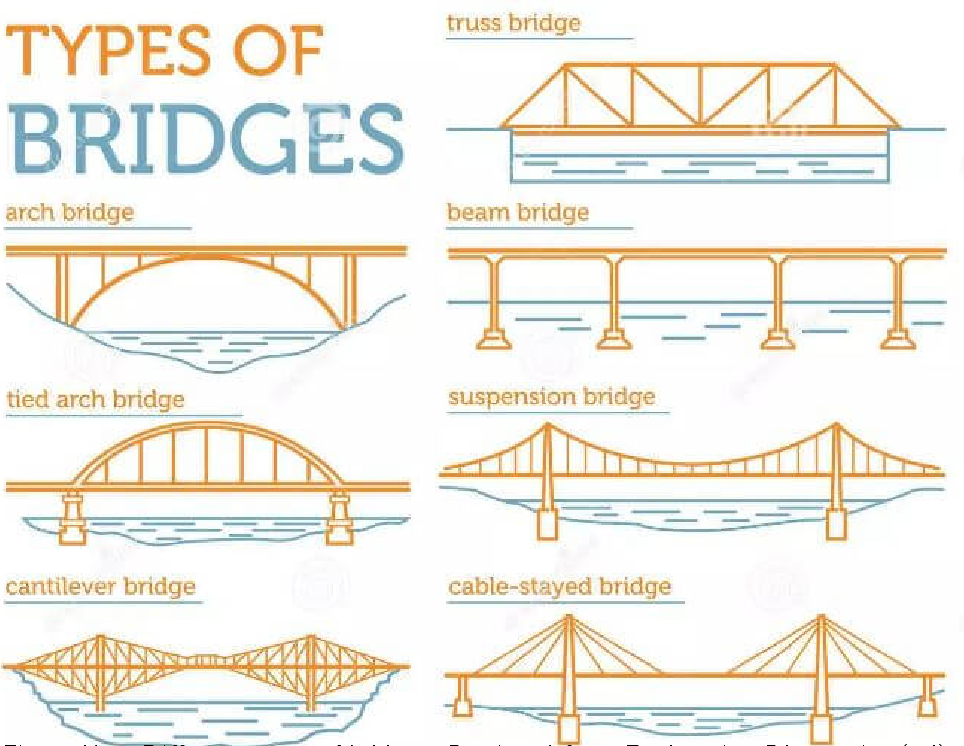

Figure H.5: Different types of bridges. Retrieved from Engineering Discoveries (nd)

H.4 Bridge Design Variants

H.4.1 *Variant 1 - EFE*

The 3D model from figure 9.7 has been created according to the technical drawings supplied by EFE. These drawings are visible in the figure below. It is worthwhile to mention that these design are, as of yet, not definitive.

Superstructure

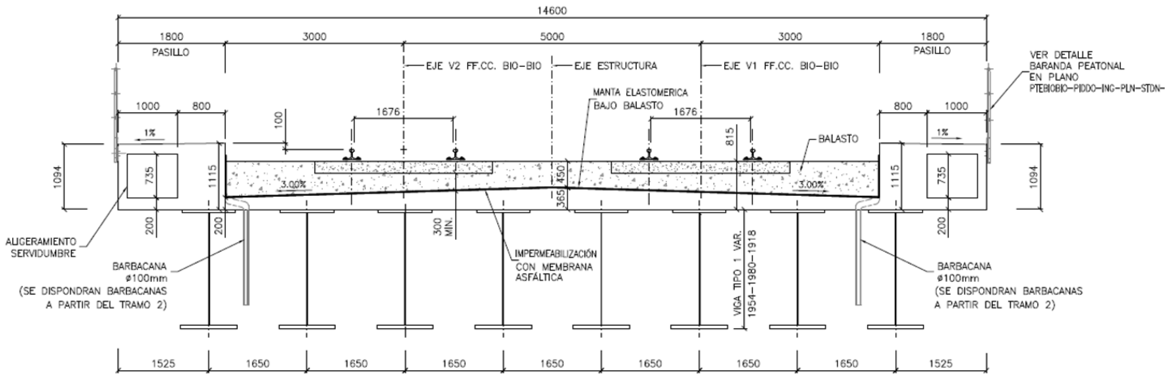

Substructure

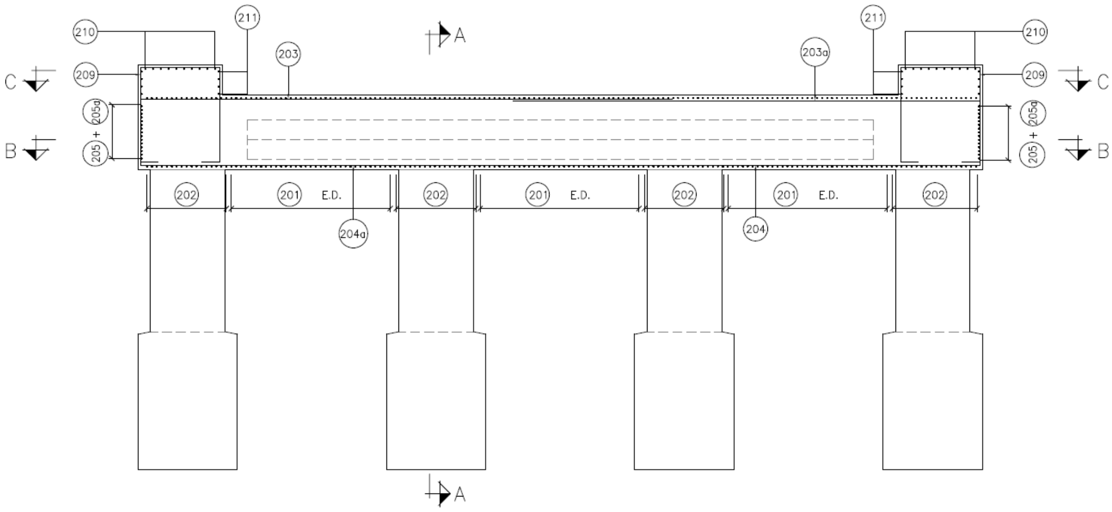

Figure H.6: In the top a technical drawing of the superstructure. Retrieved from P. Uribe, A. de Castro, R. Reginensi, P. Buguña, J. Piddo (2019a). And in the bottom a technical drawing of the substructure. Retrieved from P. Uribe, A. de Castro, R. Reginensi, P. Buguña, J. Piddo (2019b)

H.5 MCA

In addition to the explanation in the main document, some additional reading is added in this section. Providing the process towards the determination of the weights for the criteria and some additional information of the MCA scores.

H.5.1 *Criteria Weights Determination*

To achieve a sub-optimal weighing scale and point distribution method, different approach are examined. These approaches are listed and elaborated in this section. The initial steps undertaken for the first process are listed below.

- Initial start with a 70-point weighing total, averaging each criteria with 10-points each

- Creating a scale with five segments [-5, -2, 0, +2, +5], an uneven number of segments are chosen as an uneven number of criteria exist, creating a relative scale:
  - -5: Least relevant
  - -2: Less relevant
  - +0: Neutral
  - +2: More relevant
  - +5: Most relevant
- Weighing one criteria with a factor of +5 (15-point total) will lead to one criteria being rated with a factor of -5 (5-point weight)

The importance of a criteria is based upon the programme of requirements in chapter 8 and subjective importancy. Resulting in the importancy and weighing factor of the table H.1 below.

Table H.1: Initial approach for the weighing factors.

Criteria	**Importance [-5,-2,0,+2,+5]**	**Weight [70-point total]**
Aesthetic	0	10
Costs	+5	15
Hydraulic Performance	0	10
Building Time	+2	12
Maintenance	-5	5
Geological Allowance	0	10
Complexity	-2	8

Reviewing the citation, from Anil Mital (2014) in subsection 10.1.2, with the table and the respective weights, it is established that the differences between the criteria and their respective importance are not sensitive enough. Which would not lead to a sub-optimal approach.

Therefor, a second altered approach is created. At first a 100-point weighing total is considered, however, it is concluded that the distribution over seven criteria is inefficient and will not lead to a relative weighing of the criteria. Consequently, a 140-point weighing total is chosen and the scales are altered.

- Initial start with a 140-point weighing total, averaging each criteria with 20-points each
- Creating a scale with five segments [-15, -8, 0, +8, +15], an uneven number of segments are chosen as an uneven number of criteria exist, creating a relative scale:
  - -15: Least relevant
  - -8: Less relevant
  - +0: Neutral
  - +8: More relevant
  - +15: Most relevant
- Weighing one criteria with a factor of +15 (35-point total) will lead to one criteria being rated with a factor of -15 (5-point weight)

Table H.2: Second approach for the weighing factors.

Criteria	**Importance [-15.-8,0,+8,+15]**	**Weight [140-point total]**
Aesthetic	0	20
Costs	+15	35
Hydraulic Performance	0	20
Building Time	+8	28
Maintenance	-15	5
Geological Allowance	0	20
Complexity	-8	12

Although, this iterations emphasises the respective importance of the different criteria, it might be too sensitive. Comparing the weight factor of the 'Costs' (35x) and 'Maintenance' (5x), it can be concluded this is indeed too sensitive. A third iteration is made, with a 140-point total and the scale outliers are numbed down.

- Initial start with a 140-point weighing total, averaging each criteria with 20-points each
- Creating a scale with five segments [-13, -6, 0, +6, +13], an uneven number of segments are chosen as an u neven number of criteria exist, creating a relative scale:
  - -13: Least relevant
  - -6: Less relevant
  - +0: Neutral
  - +6: More relevant
  - +13: Most relevant
- Weighing one criteria with a factor of +13 (33-point total) will lead to one criteria being rated with a factor of -13 (7-point weight)

Resulting in the following weighing factors:

Table H.3: Third and final iteration for the weighing factors.

Criteria	**Importance [-13.-6,0,+6,+13]**	**Weight [140-point total]**
Aesthetic	0	20
Costs	+13	33
Hydraulic Performance	0	20
Building Time	+6	26
Maintenance	-13	7
Geological Allowance	0	20
Complexity	-6	14

Conclusively, these weighing are considered enough to emphasise the respective importance of the different criteria, whilst not neglecting or over-estimating any criteria. These factor are taken into account for the scoring of the different variants.

H.5.2 *Thoroughly Elaborated Results*

The results of the MCA are viewable in this subsection. In table H.4 the weighted averaged score between the group members of PPRB, divided by four, are displayed. This table is taken as guide for the recommendation in chapter 10. In addition, the individual scores for the team members and the MCA populated by both structural supervisors are shown.

Table H.4: Weighted average score of the MCA populated by PPRB team members divided by four

Criteria	Weight	Variant 0	Variant 1	Variant 2	Variant 3	Variant 4	Variant 5
Name		*Beam Bridge EFE*	*Alternative Beam Bridge*	*Bowstring Arch*	*Suspension*	*Truss with Arch*	*Cable-Stayed*
Aesthetic	20	25	50	75	95	45	95
Costs	33	165	115.5	82.5	33	82.5	33
Hydraulic Performance	20	20	40	65	95	70	95
Building Time	26	91	91	65	45.5	65	45.5
Maintenance	14	24.5	38.5	38.5	38.5	31.5	42
Geological Allowance	20	55	65	65	50	65	50
Complexity	7	31.5	31.5	19.25	14	19.25	12.25
Total	140	**412**	**431.5**	**410.25**	**371**	**378.25**	**372.75**

PPRB MCA Scores: I

Table H.5: Weighted score of the MCA by team member I

Criteria	Weight	Variant 0	Variant 1	Variant 2	Variant 3	Variant 4	Variant 5
Name		*Beam Bridge EFE*	*Alternative Beam Bridge*	*Bowstring Arch*	*Suspension*	*Truss with Arch*	*Cable-Stayed*
Aesthetic	20	20	60	80	100	40	100
Costs	33	165	99	99	33	99	33
Hydraulic Performance	20	20	40	60	100	60	100
Building Time	26	78	78	52	52	78	52
Maintenance	14	28	28	42	42	42	42
Geological Allowance	20	20	40	60	80	60	80
Complexity	7	28	28	21	14	21	14
Total	140	**359**	**373**	**414**	**421**	**400**	**421**

Preference bridge type for team member: **Bowstring Arch**.
The bowstring arch allows for larger spans, meaning it can 'evade' the channels in the river, resulting in a better hydraulic performance. In addition, it also provides a better aesthetic look than a regular composite beam bridge.

PPRB MCA Scores: II

Table H.6: Weighted score of the MCA by team member II

Criteria	Weight	Variant 0	Variant 1	Variant 2	Variant 3	Variant 4	Variant 5
Name		*Beam Bridge EFE*	*Alternative Beam Bridge*	*Bowstring Arch*	*Suspension*	*Truss with Arch*	*Cable-Stayed*
Aesthetic	20	20	60	80	80	40	100
Costs	33	165	132	66	33	66	33
Hydraulic Performance	20	20	40	60	100	80	100
Building Time	26	104	104	52	52	52	52
Maintenance	14	14	28	28	42	28	56
Geological Allowance	20	100	80	60	20	60	20
Complexity	7	35	35	21	7	21	7
Total	140	**458**	**479**	**367**	**334**	**347**	**368**

Preference bridge type for team member: **Alternative beam bridge**.
As this provides an easy, though more attracting design. Providing a more aesthetically pleasing view over the Biobío river. It also provides a more resilient hydraulic performance, requiring less pillars in the river. This may reduce the comparability of the foundation of the bridge.

PPRB MCA Scores: III

Table H.7: Weighted score of the MCA by team member III

Criteria	Weight	Variant 0	Variant 1	Variant 2	Variant 3	Variant 4	Variant 5
Name		*Beam Bridge EFE*	*Alternative Beam Bridge*	*Bowstring Arch*	*Suspension*	*Truss with Arch*	*Cable-Stayed*
Aesthetic	20	40	60	80	100	60	100
Costs	33	165	99	66	33	66	33
Hydraulic Performance	20	20	40	60	80	60	80
Building Time	26	78	78	52	52	52	52
Maintenance	14	28	42	42	42	28	42
Geological Allowance	20	40	40	60	80	60	80
Complexity	7	35	28	14	21	14	21
Total	140	**406**	**387**	**374**	**408**	**340**	**408**

Preference bridge type for team member: **Alternative Beam Bridge**
This relative simple bridge poses possibilities as there is experience with this kind of bridges, but compared to the traditional design multiple improvements can be made. The design is also cost effective and relatively easy to maintain. The Hollandsch Diep bridge is furthermore, I think, a very pretty design, it is elegant and simple. The hydraulic performance has to be optimised for this design as there are relatively more foundation pillars needed. Interesting to investigate the shape of the pillars in the flow. How does the shape of the foundation pillars affect the flow and thus the hydraulic performance of the bridge.

PPRB MCA Scores: IV

Table H.8: Weighted score of the MCA by team member IV

Criteria	Weight	Variant 0	Variant 1	Variant 2	Variant 3	Variant 4	Variant 5
Name		*Beam Bridge EFE*	*Alternative Beam Bridge*	*Bowstring Arch*	*Suspension*	*Truss with Arch*	*Cable-Stayed*
Aesthetic	20	20	20	60	100	40	80
Costs	33	165	132	99	33	99	33
Hydraulic Performance	20	20	40	80	100	80	100
Building Time	26	104	104	104	26	78	26
Maintenance	14	28	56	42	28	28	28
Geological Allowance	20	60	100	80	20	80	20
Complexity	7	28	35	21	14	21	7
Total	140	**425**	**487**	**486**	**321**	**426**	**294**

Preference bridge type for team member: **Bowstring arch**.
Good hydraulic performance, not the best but considering the other factors as time and cost this bridge is a good alternative. Scores average or above average on almost all the criteria

I

Preliminary Design

This appendix supplies additional information about the preliminary design and also governs the geotechnical information of the subsoil, respective loads taken into consideration in the preliminary design, variable loads that work on the structure and the load combinations that are considered in this report.

I.1 Geotechnical Information and Foundations

In the table below the respective length for each of the foundation pillars is shown. The length of the pillars have been measured from the bridge deck straight downward to the riverbed. The pillars and their location along the longitudinal cross section of the river are shown in figure I.1.

Table I.1: Respective length of the foundation pillars measured from the bridge deck downward to the river bed in drawings supplied by EFE.

	Height from deck to riverbed
Pillar 1	4.5 m
Pillar 2	10.0 m
Pillar 3	7.5 m
Pillar 4	8.0 m
Pillar 5	8.0 m
Pillar 6	7.5 m
Pillar 7	8.0 m
Pillar 8	7.5 m
Pillar 9	7.0 m
Pillar 10	7.0 m
Pillar 11	7.0 m
Pillar 12	7.0 m
Pillar 13	6.5 m
Pillar 14	6.5 m
Pillar 15	6.5 m
Pillar 16	6.5 m
Pillar 17	7.0 m
Pillar 18	8.0 m
Pillar 19	3.5 m

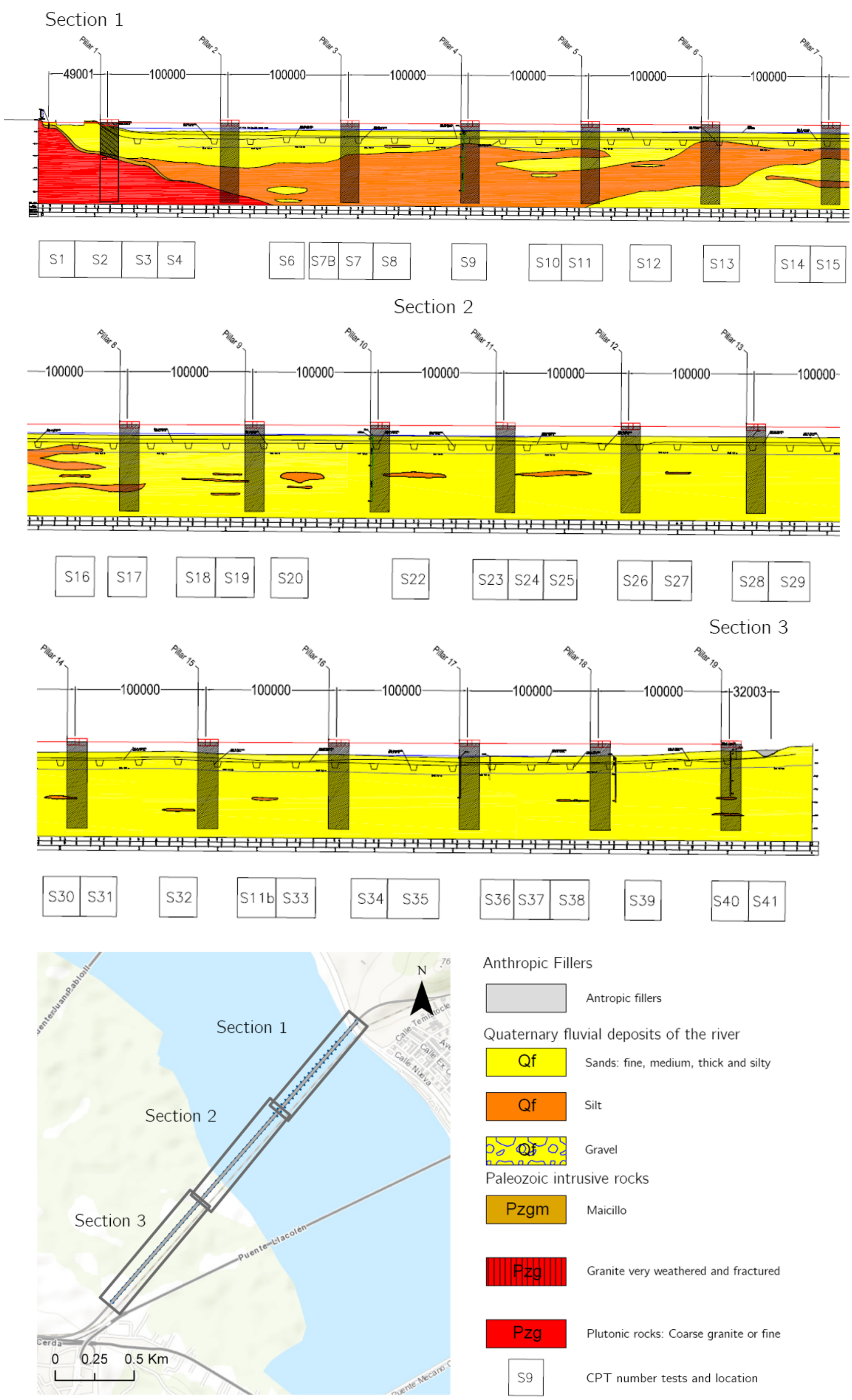

Figure I.1: The required foundation pillars placed above a longitudinal cross section of the river and the sub soil.

I.2 Self Weight of Superstructure

The self weight of the superstructure, with their respective elements, is listed below.

- The cross sectional surface of the concrete slabs is estimated in accordance with the cross section supplied by EFE, visible in figure 11.3.
- Sleepers are according to Sectie Verkeersbouwkunde (2015, p. 29).
- Railway tracks are initially designed for heavy train traffic, therefore the type UIC60 is chosen, Agico Group (nd).
- The total weight of the Rigid Steel V-frame is assumed to be roughly equal to, taken from the partnership that eventually won the tender for the 'Hollandsch Diep' bridge (Benthem and Falbe-Hansen, 2003), 900 tons over 105 metres (one span).

The self weight loads are summarised in the table I.2 below.

Table I.2: Elements/materials with their respective self weight

Material	ρ_g (kg/m^3)	**Surface** (m^2)	q_g (kN/m)
Concrete (Reinforced)	2,500	$\approx$2.9	71,0
Sleepers (Concrete)	200	$\approx$1.0	2.0
Railway Track (UIC60)	7,850	$76.7 \cdot 10^{-4}$	0.6
Rigid V-frame (Steel)	7.850	$\approx$1.1	84.0

I.3 Seismic Loads

For the seismic loading of the bridge, documents from both Chilean sources: NCH2369-2003 (2003); NCH433-96-2010 (2003) and Dutch building codes NEN-EN 1998-1 (2005); NEN-EN 1998-2 (2006) are used. These sources were introduced in chapter 8. In this report an initial approach to the seismic loading is performed. This analysis is very limited as it is for the preliminary bridge design, therefore it is recommended to continue this (seismic) research in the future.

The Chilean building codes, NCH2369-2003 (2003); NCH433-96-2010 (2003), do not include codes which can be used for the seismic design of bridges. As a result, designs solemnly based on these codes are not reliable, and therefore using the NEN-codes is the preferred alternative.

Note: The mostly used process in seismic design in Chile is the model response spectrum procedure, especially in the more earthquake prone area of Concepción. (Zone 3 according table 4.1 of NCH433-96-2010 (2003)) This procedure can be used for the design of the bridge, but is very time-consuming and needs more experienced knowledge concerning structural dynamics. This process can be looked into in a later design phase or additional research.

I.3.1 *Individual Pier Model*

For the preliminary design of the bridge the 'Individual pier model' can be used to approximate the seismic effects. According NEN-EN 1998-2 (2006) this method is described as follows: 'In some cases the seismic action in the transverse direction of the bridge is resisted mainly by the piers, without significant interaction between adjacent piers. In such cases the seismic action effects acting in the i-th pier may be approximated by applying on it an equivalent static force, F_i:'

$$F_i = M_i S_d(T_i) \tag{I.1}$$

With:

$$M_i = \text{Effective mass attributed to pier i}$$
$$T_i = \text{Fundamental period of pier i,}$$
$$\text{considered independently of the rest of the bridge}$$
$$T_i = 2\pi\sqrt{\frac{M_i}{K_i}}$$
where :
$$K_i = \text{the stiffness of the system, in this case: a individual foundation pillar}$$
$$S_d(T_i) = \text{Spectral acceleration of design Spectrum,}$$
$$\text{according paragraph 3.2.2.5 from NEN-EN 1998-1 (2005)}$$

The simplification is allowed for the initial analysis if the following condition is met (equation 4.19 from (NEN-EN 1998-2, 2006)):

$$0.90 \leq T_i/T_{i+1} \leq 1.10 \tag{I.2}$$

If this is not the case, a 'redistribution of the effective masses attributed to each pier is required, leading to the satisfaction of the above condition.'

In this case only the seismic action in the transverse direction of the bridge and its piers is considered. The effective weight on a random pillar 'i' and a pillar 'i+1' is considered to have the same mass, as both pillars carry the effective weight of 100 metres of the superstructure and their own self-weight. The condition I.2 is therefore valid. As a result the individual pier model can be used in this preliminary design and filling in equation I.1 results in the needed static force.

I.3.2 *Preliminary Seismic Calculations*

For filling in equation I.1 the following values and information are needed.

Fundamental period of pier, T_i:

$$T_i = 2\pi\sqrt{\frac{M_i}{K_i}} \tag{I.3}$$

Using the parameters as described in table I.3.

Table I.3: Parameters used for the fundamental period of pier T_i calculation

Parameter	**Abbreviation Parameter**	**Source**	**Value**
Measurements pillar, height	H	Own assumption	2.0 m
Measurements pillar, width	B	Own assumption	3.0 m
Concrete type		Own assumption	C55/67
E-modulus C55/67	E	NEN-EN:1992-1-1 (1997), Table 3.1	38000 N/mm^2
Moment of Inertia	I	Rectangular profile	$\frac{1}{12} \cdot H \cdot B^3$
Bending stiffness	K_i		$E \cdot I$
Length bridge attributed to pier i	L_i	11.1	100 m
Weight bridge	W	I.7.1	157.60 kN/m
Effective mass attributed to pier i	M_i		$L \cdot W/9.81$

Filling in equation I.3 with the information of table I.3, a fundamental period of pier i, T_i, of 0.61 seconds is found.

Design ground acceleration on type A ground, a_g:

$$a_g = \gamma_1 a_{gR} \tag{I.4}$$

And with T_i, is 0.61 seconds, the design spectrum for elastic analysis,S_d, according page 41 (equations 3.13 till 3.16) from NEN-EN 1998-2 (2006) is equal to:

With $T_B \leq T \leq T_C$:

$$S_d(T) = a_g S \frac{2.5}{q} \tag{I.5}$$

Using the parameters as described in tables I.4 and I.5.

Table I.4: Parameters for ground type D taken from table 3.2 of NEN-EN 1998-1 (2005)

Ground type	**S**	T_B **(s)**	T_C **(s)**	T_D **(s)**
D	1.35	0.2	0.8	2

Table I.5: Parameters used for design spectrum for elastic analysis $S_d(T)$ calculation

Parameter	**Abbreviation Parameter**	**Source**	**Value**
Seismic zone Chile	Zone	NCH433-96 (1996, p.11)	Zone 3
Category structure	Category	NCH433-96 (1996, p.6)	Category A (vital structure)
Ground type (based on Nspt)	Type	CPT S9, Nspt = 10	Type D
Gravitional constant	g		9.81
Ground acceleration	Mw > 5.5	NEN-EN 1998-1 (2005), Paragraph 3.2.2.2	Type 1
Reference peak ground acceleration on type A ground	a_{gR}	NCH433-96 (1996) Table 6.2	0.40 g
Importance factor	γ_1	NCH433-96 (1996) Table 6.1	1.2
Behaviour factor	q	NEN-EN 1998-1 (2005), Paragraph 3.2.2.5	1.0
Lower bound factor horizontal design spectrum	β	NEN-EN 1998-1 (2005), Paragraph 3.2.2.5	0.2

Filling in equations I.4 and I.5 with the information of tables I.4 and I.5 leads to a design spectrum for elastic analysis $S_d(T)$ of 15.89. Filling in this value for the design spectrum in equation I.1 the equivalent static force, F_i, on the pier due to seismic loading is approximately 25.4 MN.

I.4 Train Loads

For determining the loads due to the trains, several load models need to be considered. These models can be found in the NEN-EN 1990+A1+A1/C2 (1990). The load models that need to be accounted for are the LM71 and SW/2 model. In this preliminary design the additional loading due to eccentricity is not taken into account.

Additional to the train tracks there loads as the result of maintenance need to be taken into account, NEN-EN 1991-2+C1 (2015). This action has to be accounted for by using an additional distributed load of 5 kN/m over the length of the span.

I.4.1 *Static Loading Model: LM71*

The first static loading model that needs to be verified is LM71. In case the train loads are expected to be larger than "regular train traffic", one has to use an additional α value to multiply the characteristic values with. For this design an α value of 1.21 is assumed. The loading model can be schematised as shown in figure I.2. The length at section (1) in this figure is unlimited.

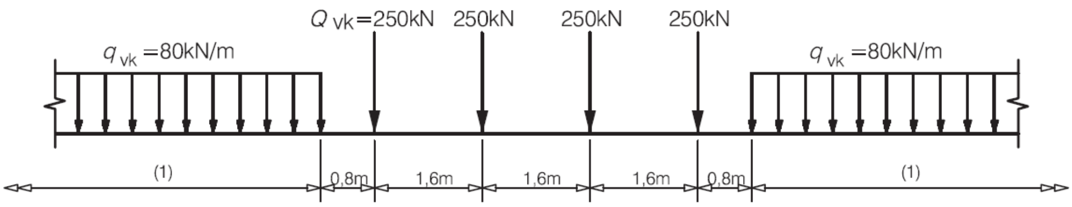

Figure I.2: Loading scheme according to LM71, from NEN-EN 1991-2+C1 (2015)

I.4.2 *Static Loading Model: SW/2*

The second static loading model that needs to be accounted for is the SW/2 model, the loading scheme is visualised in figure I.3. The loading scheme is used along the bridges' length. For this the loads summarised in table 8.9 are used. For SW2 this means:

- $q_{vk} = 150$ kN/m
- $a = 25$ m
- $c = 7$m

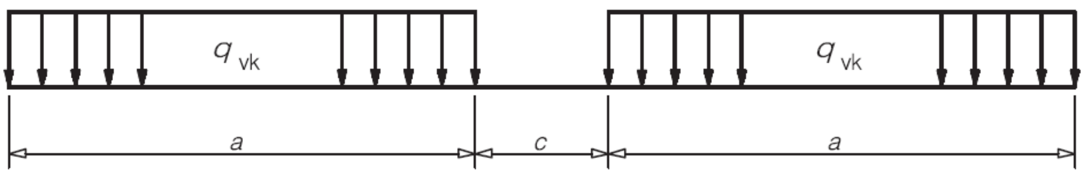

Figure I.3: Loading scheme according to SW/2, from NEN-EN 1991-2+C1 (2015)

I.4.3 *Dynamic Train Loads*

Following the flow chart for dynamic loading NEN-EN 1991-2+C1 (2015), p. 85, one can find that a check for the limits of $n_{0,lower/upper}$ needs to be performed. In this a span (L) of 100 metres is considered. The actual n_0 in Hertz can be estimated with equation I.6, from NEN-EN 1991-2+C1 (2015).

$$\begin{aligned} n_{0,upper} &= 94,76L^{-0,748} = 1.54 \\ n_{0,lower} &= 23,58L^{-0,592} = 3.02 \\ n_0 &= \frac{17.75}{\sqrt{\delta_0}} \end{aligned} \tag{I.6}$$

After rewriting this equation one can determine the upper and lower limit of the deflection, meaning $34.5 < \delta_0 < 132.2$ mm. It is assumed that for the preliminary stage of the design the superstructure suffices this requirement. Meaning that, for now, a simple dynamic calculation suffices which can be done by applying an additional dynamic factor on the aforementioned loading models.

The dynamic factor Φ can be calculated with equation I.7. In this equation the state of maintenance and the "determining length" (L_Φ) is taken into account. In the NEN-EN 1991-2+C1 (2015) a choice between two states of maintenance can be made. For now, as it is a preliminary design, the value that gives a higher dynamic factor is taken as governing.

$$\Phi = \frac{2.16}{\sqrt{L_\Phi} - 0.2} + 0.73 \tag{I.7}$$

With: $1.00 \leq \Phi \leq 2.00$, and using a length of 11 m, thus an L_Φ of 22 m, for the cross beams as shown in figure H.6. This gives a value of 1.21 for Φ.

I.5 Wind Loads

According to the NEN-EN 1991-1-4+A1+C2 (2011), wind loads need to be determined with an extra overheight of 4 metres above the tracks. The distributed load is computed using a Maple sheet, and assumes a total height of the bridge of 16 metres. The wind load can be computed with:

$$F_{wind} = \frac{1}{2}\rho_{air}(v_b^{**})^2 C A_{ref} \tag{I.8}$$

Where:

$v_b^{**} = 25$ m/s, according to NEN-EN 1991-1-4+A1+C2 (2011)

$\rho_{air} = 1.225$ kg/m^3

$C = c_e c_o$

$A_{ref} = d_{total} * L$

To determine c_e and c_o, other parameters need to be determined first. Using the equations from NEN-EN 1991-1-4+A1+C2 (2011) one can compute these parameters as shown in equations I.9 to I.14. The first variable that needs to be determined is I_v, which is computed with:

$$I_v = \frac{k_I}{c_o * \ln(z/z_0)} = 0.1355 \tag{I.9}$$

Where:

$k_I = 1$, defined as the turbulence factor

$c_0 = 1$, defined as the orography factor

$z_0 = 0.01$, defined as the roughness length

The second variable that is needed is the k_r, defined as the terrain factor. This can be determined with:

$$k_r = 0.19 \cdot \left(\frac{z_0}{z_{0,II}}\right)^{0.07} = 0.16975 \tag{I.10}$$

Where:

$z_{0,II} = 0.05$, terrain roughness for region II.

Next the roughness height needs to be calculated:

$$c_r = k_r \cdot \ln\left(\frac{z}{z_0}\right) \tag{I.11}$$

This gives a value of 1.25 for c_r. Using this value to compute the mean wind velocity:

$$v_m = 25 * c_r * c_o = 31.31\ m/s \tag{I.12}$$

This speed can be used to determine the pressure due to the wind on the bridge deck:

$$q_z = ((1 + 7I_v)0.5)\rho_{air} v_m^2 = 1170.18 \tag{I.13}$$

At last the exposure factor can be computed, which is needed for the drag coefficient.

$$c_e = \frac{q_z}{0.5\rho_{air} v_b^{**}} = 3.07 \tag{I.14}$$

The force coefficient (c_f) can be determined with the width to height ratio of the bridge deck. The total width of the bridge deck is 14.6 m. The height of the bridge deck is assumed to be 1 m. Adding the overheight of 4 metres to this value, gives a total height of 5 metres. So the ratio becomes: 2.92. Then using figure 8.3 from NEN-EN 1991-1-4+A1+C2 (2011) gives a value of 1.5 for c_f. This results in a C value of 4.6. Using equation I.8, this results in a load of 878 kN. This load is applied at 2 metres above the bridge deck. To properly attach this load to the bridge deck for the transverse scheme, a bending moment has to be applied. This bending moment has a value of 1755 kNm.

I.6 Load Combinations

In the table I.6, all the load combinations and their respective partial- and reduction factors are listed. It is important to notice that LC1, LC2.1 and LC2.2 are according to the Chilean building code NCH433-96-2010 (2003).

I.6.1 *Loads, Partial- and Reduction Factors*

Table I.6: Load combinations utilised for the preliminary design of the bridge pillars.

LC0	Permanent + Floodwave load (subsection 8.6.2)	
	ξ/ψ	γ,gj,sup
Eq. 6.10	NA	1.35
Eq. 6.10a	NA	1.35
Eq. 6.10b	0.85	1.35

LC1	Permanent + Floodwave load	Earthquake	Wind (main)
A	1.4	1.4	1.4
B	0.9	1.4	0

LC2.1	Permanent + Floodwave load	Earthquake	LM71	Wind (main)
A	1.4	1.4	1.4	1.4
B	0.9	1.4	0	0

LC2.2	Permanent + Floodwave load	Earthquake	SW/2	Wind (main)
A	1.4	1.4	1.4	1.4
B	0.9	1.4	0	0

LC3.1	Permanent + Floodwave load		Tsunami (Impact)	Wind (main)	
	ξ/ψ	γ,gj,sup	γ,Q,1	γ,Q,1	ψ_0
Eq. 6.10	NA	1.35	1.5	NA	NA
Eq. 6.10a	NA	1.35	NA	1.5	0.75
Eq. 6.10b	0.85	1.35	1.5	NA	NA

LC3.2	Permanent + Floodwave load		Tsunami (Post-Impact)	Wind (main)	
	ξ/ψ	γ,gj,sup	γ,Q,1	γ,Q,1	ψ_0
Eq. 6.10	NA	1.35	1.5	NA	NA
Eq. 6.10a	NA	1.35	NA	1.5	0.75
Eq. 6.10b	0.85	1.35	1.5	NA	NA

LC4.1	Permanent + Floodwave load		LM71	Wind (main)	
	ξ/ψ	γ,gj,sup	γ,Q,1	γ,Q,1	ψ_0
Eq. 6.10	NA	1.35	1.45	NA	NA
Eq. 6.10a	NA	1.35	NA	1.5	0.75
Eq. 6.10b	0.85	1.35	1.45	NA	NA

LC4.2	Permanent + Floodwave load		SW/2	Wind (main)	
	ξ/ψ	γ,gj,sup	γ,Q,1	γ,Q,1	ψ_0
Eq. 6.10	NA	1.35	1.2	NA	NA
Eq. 6.10a	NA	1.35	NA	1.5	0.75
Eq. 6.10b	0.85	1.35	1.2	NA	NA

I.6.2 *Application of Factors within MatrixFrame*

In order to maintain the overview of all factor with their respective load combinations, two table have been created. In table I.7 the load combinations, defined as FuC#, are visible with their calculated factors. In table I.8, each of the load combinations FuC# has been matched with their respective load combinations from table I.6.

Table I.7: The load combinations (FuC#) as input for MatrixFrame.

	Permanent Superstructure	**LM71**	**SW/2**	**Wind Loads**	**Tsunami**	**Earthquake**	**Tsunami Post impact**
Number	*B.G.1*	*B.G.2*	*B.G.3*	*B.G.4*	*B.G.5*	*B.G.6*	*B.G.7*
FuC1	1.35						
FuC2	1.15						
FuC3	1.4			1.4		1.4	
FuC4	0.9					1.4	
FuC5	1.4	1.4		1.4		1.4	
FuC6	0.9					1.4	
FuC7	1.4		1.4	1.4		1.4	
FuC8	0.9					1.4	
FuC9	1.35				1.5		
FuC10	1.35			1.13			
FuC11	1.15				1.5		
FuC12	1.35						1.5
FuC13	1.35			1.13			
FuC14	1.15						
FuC15	1.35	1.45					1.5
FuC16	1.35			1.13			
FuC17	1.15	1.45					
FuC18	1.35		1.2				
FuC19	1.35			1.13			
FuC20	1.35		1.2				

Table I.8: The load combinations (FuC#) referenced with their respective equations according to table I.6.

Number	Load Combination	Type
FuC1	LC0 - Eq. 6.10 & 6.10a	Only permanent
FuC2	LC0 - Eq. 6.10b	
FuC3	LC1 - A	Earthquake and wind
FuC4	LC1 - B	
FuC5	LC2.1 - A	Earthquake, LM71 and wind
FuC6	LC2.1 - B	
FuC7	LC2.2 - A	Earthquake, SW/2 and wind
FuC8	LC2.2 - B	
FuC9	LC3.1 - Eq. 6.10	Tsunami (Impact) and wind
FuC10	LC3.1 - Eq. 6.10a	
FuC11	LC3.1 - Eq. 6.10b	
FuC12	LC3.2 - Eq. 6.10	Tsunami (Post) and wind
FuC13	LC3.2 - Eq. 6.10a	
FuC14	LC3.2 - Eq. 6.10b	
FuC15	LC4.1 - Eq. 6.10	LM71 and wind
FuC16	LC4.1 - Eq. 6.10a	
FuC17	LC4.1 - Eq. 6.10b	
FuC18	LC4.2 - Eq. 6.10	SW/2 and wind
FuC19	LC4.2 - Eq. 6.10a	
FuC20	LC4.2 - Eq. 6.10b	

I.7 Application of Loads

The loads are applied in longitudinal and transverse cross-sections. They are represented separately in the subsections below, but are eventually combined according to the load combinations set up in section I.6.

I.7.1 *Longitudinal Application*

Self weight - Superstructure
The self weight is an equally distributed load over the entire length of the bridge, in accordance with table I.2.

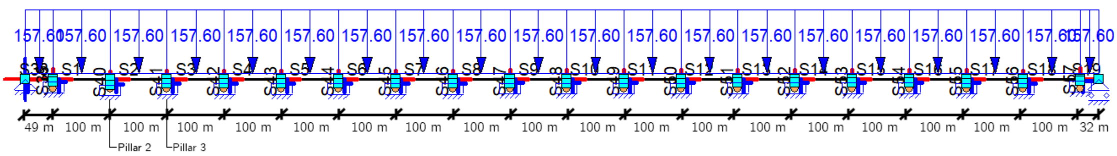

Figure I.4: Self weight of the superstructure.

Train Load - LM71
This train load is placed along the entire length of the bridge, see reference figure I.2. It includes four point loads, Q_{vk}, and two equally distributed loads, q_{vk}, in accordance with I.4.1.

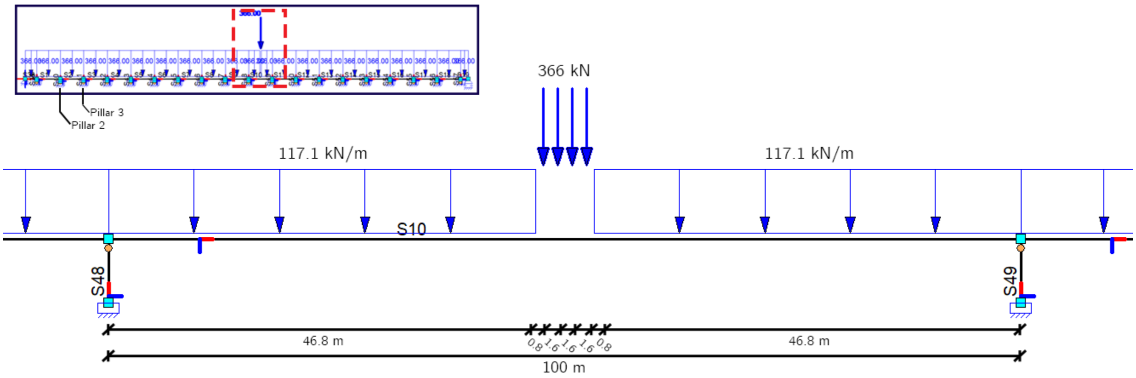

Figure I.5: Visualisation of the application of the train load LM71 placed on a segment of the bridge. In the top left corner the entire bridge is shown.

Train Load - Heavy SW/2

This train load is placed along the entire length of the bridge, see reference figure I.3. It only includes a distributed load, q_{vk}, segmented into 25 metres with a spacing of 7 metres, in accordance with table I.4.2.

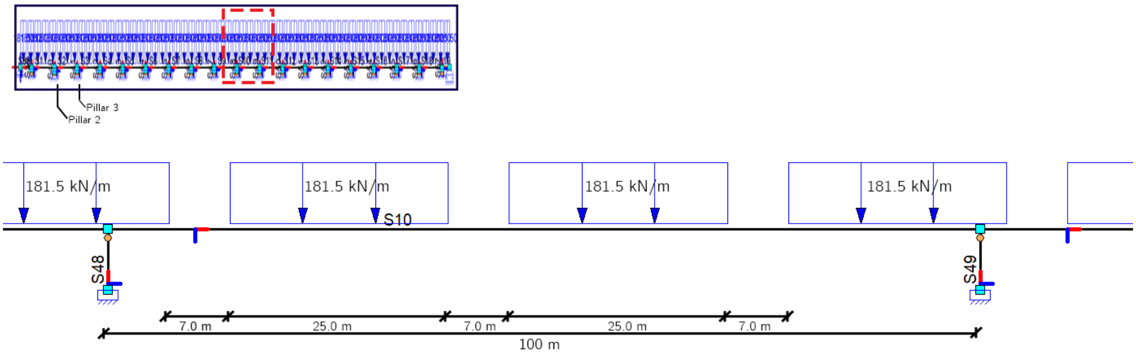

Figure I.6: Visualisation of the application of the train load SW/2 placed on a segment of the bridge. In the top left corner the entire bridge is shown.

I.7.2 *Transverse Application*

A pillar with the most probable highest loading, pillar 2 (length of 10 m), is taken as normative for the load combinations. The loads that apply to the transverse cross-section are listed below and visualised in figures I.7 and I.8.

Hydrostatic Force

This force is applied as a pressure with the highest pressure at the deepest part. Due to the flood wave this results in a total depth of 6.5 metres, also visible in figure 7.12. Thus the length over which the hydrostatic pressure is present, is equal to 6.5 metres. This is shown in figure (a) of I.7.

Wind load

The wind load has to be applied at an overheight of 4 metres above the train tracks. Although these are not shown in this mechanical scheme, the forces have to be translated towards the tip of the pillar. This is done by adding a bending moment at the tip to account for the bending moment due to the wind loads. This is shown in figure (b) of I.7.

Earthquake

The force of an earthquake has the most impact if the bending moment is the largest, thus requiring the biggest moment arm. By applying the force of the earthquake at the tip of the pillar, one has sufficed in this requirement. This is shown in figure (c) of I.7.

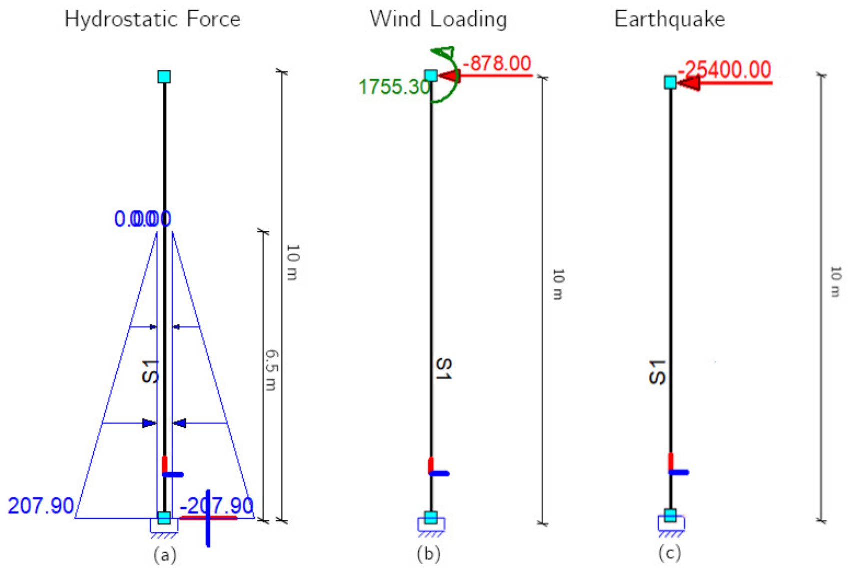

Figure I.7: Loads, in kN, on the structure due to the hydrostatic force (a), wind (b) and earthquake (c) loading.

Tsunami - Impact
At wave impact due to a tsunami, the following loads should be applied: hydrostatic force, the impact force due to a wave and the impact force due to floating objects. Both the impact forces are applied at 3.5 metres, to ensure that their impact is the highest on the structure. The hydrostatic force is only applied at one side, since the initial wave, when reaching the bridge, is only present at one side. This is shown in figure (d) of I.8.

Tsunami - Post impact
The post impact forces of a tsunami include the hydrostatic pressure, drag force and the impact force due to floating objects. The latter two are applied at a height of 3.5 metres above the bottom of the pillar, as this is the top of the water level inundation (see 7.2). In this manner these loads have the biggest influence. The hydrostatic pressure is applied at both sides as the water is flows around the structure. This is shown in figure (e) of I.8.

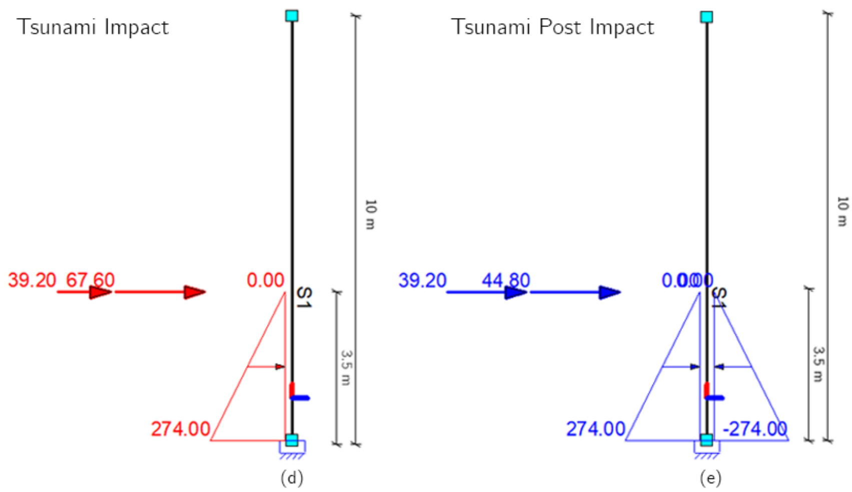

Figure I.8: Loads due to a tsunami wave, at impact (d) and post impact (e)

I.8 Normative Load Combinations

The three most prominent load combinations for column 2 and 3 are shown in figures I.9 and I.10.

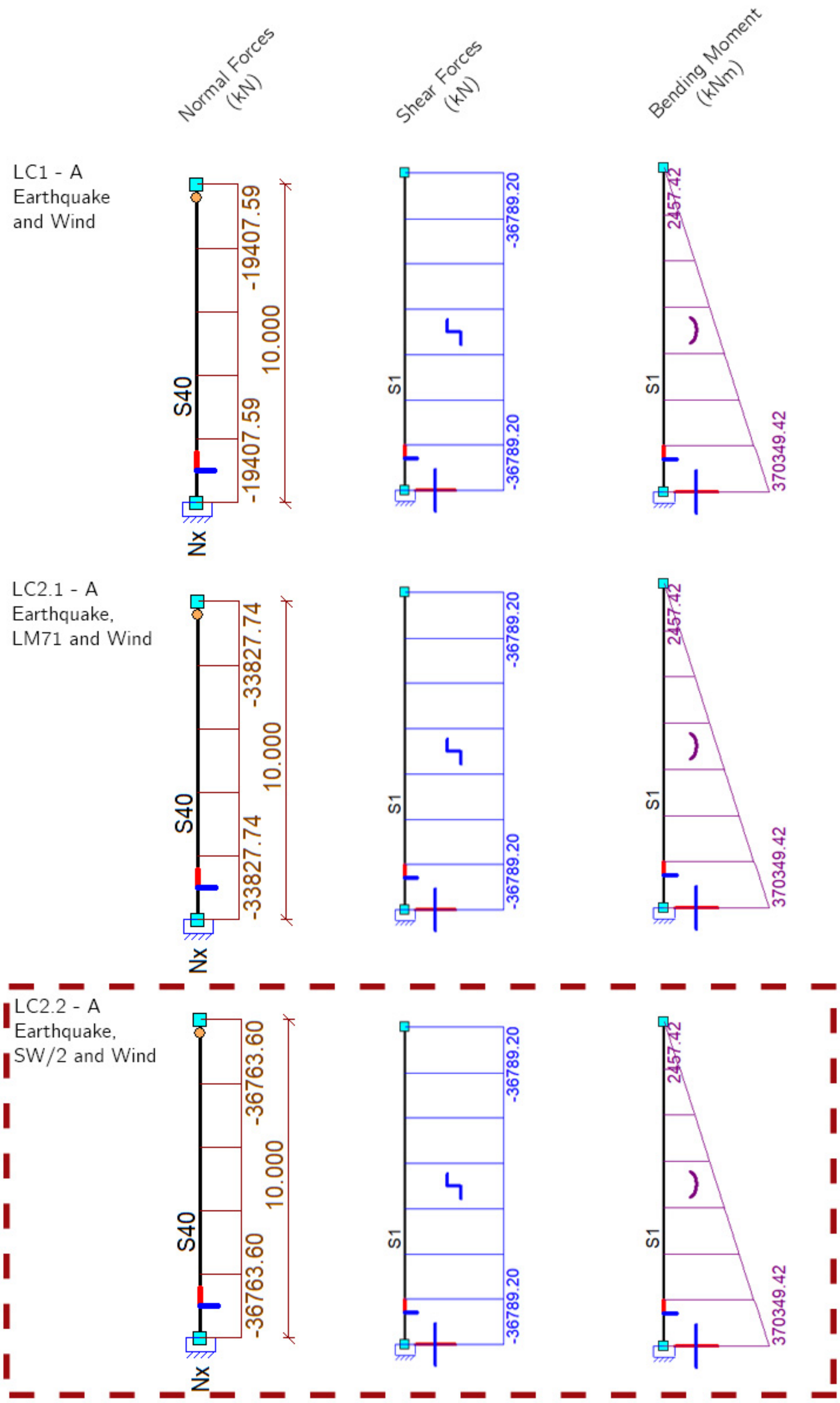

Figure I.9: FuC3/5/7 or LC1-A, LC2.1-A, LC2.2-A with the respective loads for pillar 2.

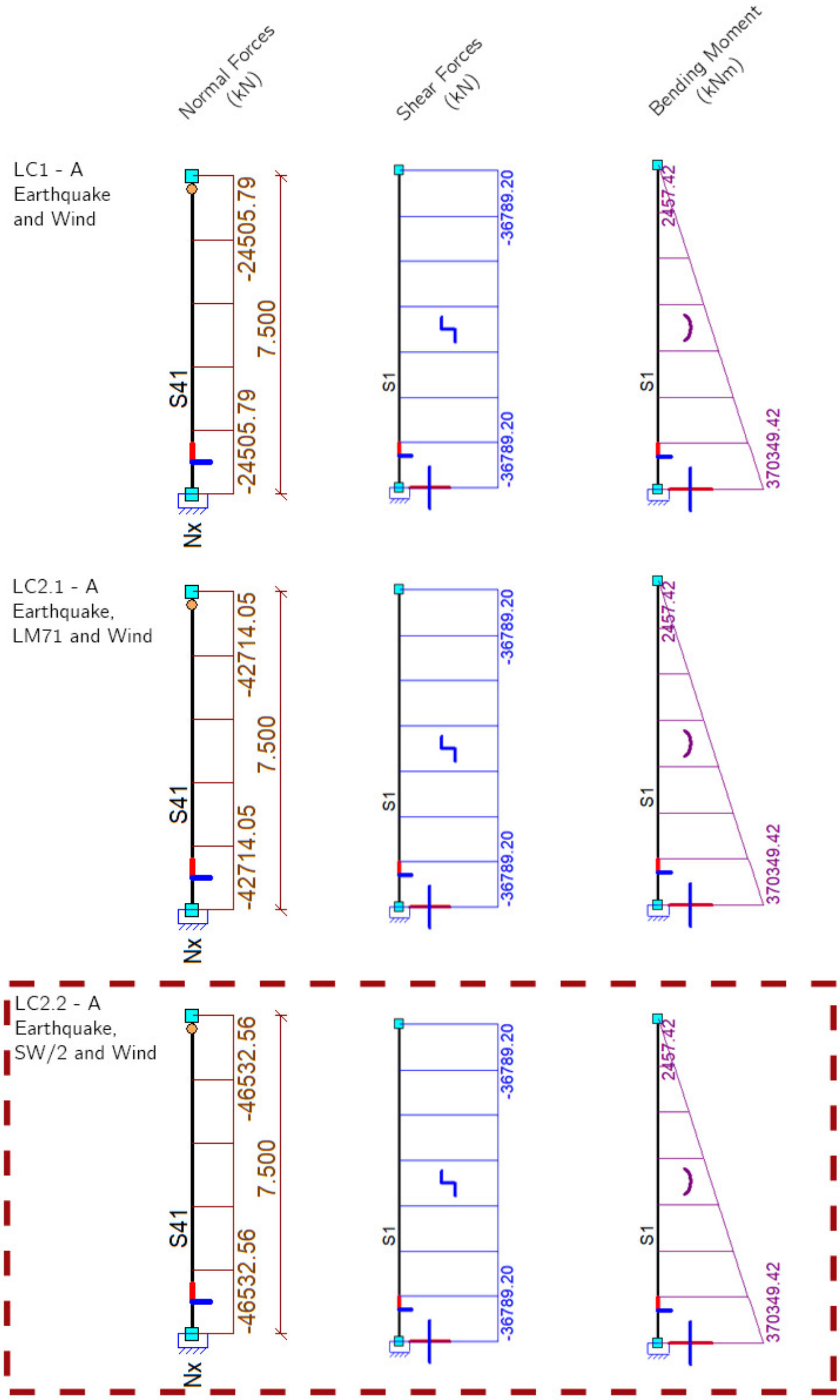

Figure I.10: FuC3/5/7 or LC1-A, LC2.1-A, LC2.2-A with the respective loads for pillar 3.

Concluding, load combination FuC7 leads to the highest forces within the structure. These forces are summarised in table I.9.

Table I.9: Summary of the loads due to load combination FuC7

	N (kN)	**V (kN)**	**M (kN)**
Pillar 2	36,764	36,789	370,349
Pillar 3	46,533	36,789	370,349

I.9 Dimensions Column

Using concrete class C45/55 results, and its respective characteristics according to Molenaar and Voorendt (2019), in the following information:

- Consequence Class is CC2, 8
- Exposure Classes are XC1, XC2 and XS1 8
- f_{ck} = 45 MPa
- f_{cm} = 53 MPa
- f_{ctm} = 3.8 MPa
- $f_{ctk,0.05}$ = 2.66 MPa
- E_{cm} = 36,000 MPa

And steel:

- f_{yk} = 500 N/mm^2
- f_{yd} = 435 N/mm^2
- E_s = 200,000 N/mm^2

With the factors:

- $\alpha_{cc} = 1.0$, according Molenaar and Voorendt (2019)
- $\gamma_c = 1.5$ considering persistent and transient loads and $\gamma_c = 1.2$ for accidental loads, according Molenaar and Voorendt (2019)
- $\gamma_s = 1.15$ for reinforcement steel, considering persistent and transient loads and $\gamma_s = 1.0$ for accidental loads, according Molenaar and Voorendt (2019)

$$f_{cd} = \frac{\alpha_{cc} f_{ck}}{\gamma_c} \tag{I.15}$$

Filling in equation I.15 gives $f_{cd} = 30\ MPa$.

I.9.1 *Dimensions & Reinforcement - Column 2*

Ultimately, after several rough optimisations, a width of 3.2 metres and height of 2.5 metres has been verified. Initially, for further calculations below, the upper boundary of the percentage of reinforcement, 3.05%, for concrete class C45/55 is assumed. In short:

- Width (b) = 3.2 [m]
- Height (h) = 2.5 [m]
- Length (l) = 10.0 [m]
- Reinforcement (ρ_{max}) = 3.05 [-]
- Reinforcement surface A_{steel} = 0.236 [m^2]
- Concrete Class C45/55

Second order moment
Firstly, it is checked whether a second order moment should be taken into account. If the slenderness, λ, is larger than the limit value for the slenderness, λ_{lim}, a second order moment is included in the total loading. In order to determine both λ and λ_{lim}, a few steps have to be taken. Firstly, the buckling force N_{buck}:

$$N_{buck} = \pi^2 \cdot \frac{EI}{l_0^2}$$

The buckling length, l_0, equals 0.7 times the length of the column, 7 meters. The moment of inertia 'I' can be calculated with the dimensions of the column:

$$I = \frac{1}{12} \cdot b \cdot h^3 = \frac{1}{12} \cdot 3.2 \cdot 2.5^3 = 4.17\ m^4$$

The buckling force then becomes:

$$N_{buck} = \pi^2 \cdot \frac{3.6 \cdot 10^4\ [N/mm^2] \cdot 4.17 \cdot 10^{12}\ [mm^4]}{7000^2\ [mm]} = 3.02 \cdot 10^7\ kN$$

To calculate the limit value of the slenderness, the relative normal force, n, is needed:

$$n = \frac{N_{Ed}}{A_c \cdot f_{cd}}$$

With:

- $N_{Ed} = 36,763$ kN
- $A_c = b \cdot h = 3.2 \cdot 2.5 = 8\ m^2$

The relative normal force then becomes $n = 0.153[-]$. Now that this factor is determined, the limit value of the slenderness can be calculated:

$$\lambda_{lim} = \frac{20 \cdot A \cdot B \cdot C}{\sqrt{n}}$$

With the following factors, according to C.R. Braam (2011, p.359):

- A = 0.7
- B = 1.1
- C = 0.7
- n = 0.153

This results in $\lambda_{lim} = 27.54\ [-]$. To determine the slenderness. The following equation is used:

$$\lambda = \frac{l_0}{i}$$

Where 'i' is calculated by:

$$i = \frac{h}{3.46} = \frac{2.5}{3.46} = 0.723\ [-]$$

Then λ becomes:

$$\lambda = \frac{7}{0.723} = 9.688\ [-]$$

A calculation for the second order moment is not required as $\lambda < \lambda_{lim}$.

Normal force capacity
The normal resisting capacity of the column, N_{Rd}, can be calculated with the following equation:

$$N_{Rd} = A_{c,eff} \cdot f_{cd} = 8.0\ [m^2] \cdot 30\ [N/mm^2] = 240,00kN$$

With the effective acting normal force, this results in a unity check (UC) of:

$$UC = \frac{N_{Ed}}{N_{Rd}} = \frac{36,763}{240,000} = 0.15$$

Reinforcement
As mentioned before, a reinforcement area of 0.244 m^2 is assumed. To achieve this steel area, 125 bars with a diameter of 50 mm are applied. With this diameter the concrete cover can be calculated, in accordance with Molenaar and Voorendt (2019, p.223) and to Eurocode 2, the concrete cover c_{nom} is determined as follows:

$$c_{nom} = c_{min} + \Delta c_{dev}$$

Where the minimum cover, c_{min}, is the highest value of:

- $c_{min,dur}$ = 35 mm, table 35-11 of Molenaar and Voorendt (2019, p.224), with 'structural class' S4 and exposure class XS1.
- $c_{min,b}$
  - $\phi_{bar} = 50$ mm
  - $c_{min,b} > \phi_{bar}$ or;
  - $c_{min,b} > \phi_{bar} + 5$ mm
- 10 mm

The tolerance for Δc_{dev} equals 5 mm. This results in a concrete cover $c_{nom} = 60$ mm.

Moment resisting capacity and reinforcement
With the predefined steel reinforcement area, A_{steel}, concrete cover, c_{nom} and main dimensions, 2.5 m x 3.2 m, the moment resisting capacity is calculated. This is done by approximating the yield strength of the reinforced concrete column in accordance with C.R. Braam (2011, p.350).

Assuming that the $\sigma_{s,compression} \leq f_{yd}$ and $1.75‰ < \epsilon_c < 3.50‰$. Where ϵ_c is the extension of concrete in a percentage value. The reinforcement bars will reach yielding strength when the deformation ϵ_{sy} equals the yielding strength of steel (f_{yd}) divided by the E-modules of steel (E_s):

$$\epsilon_{sy} = \frac{f_{yd}}{E_s} = \frac{435\ [N/mm^2]}{200,000\ [N/mm^2]} = 2.17‰$$

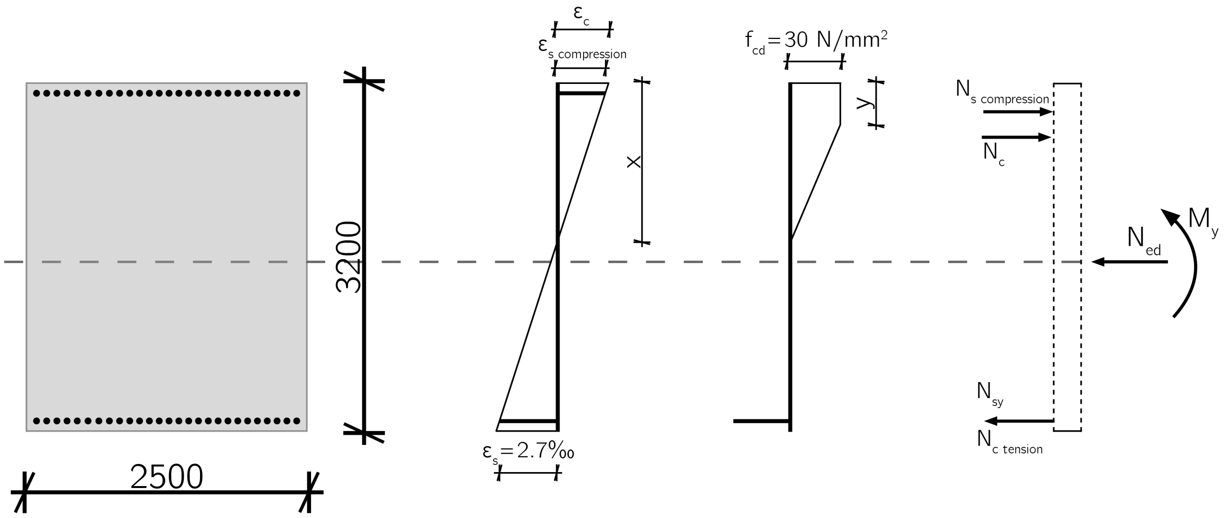

Figure I.11: Deformation -and stress diagram if ϵ_s *equals* 2.17‰.

Assuming a polygon like shape in accordance with C.R. Braam (2011, p.349), visible in figure I.11 first from the right, for the stress diagram. In combination with the locations of the reinforcement bars ($N_{s,compression}$ and $N_{s,tension}$), acting normal force (N_{Ed}) and concrete compression force (N_c) a equilibrium for the normal force can be set:

$$\sum H = 0 \text{ follows: } N_c + N_{s,compression} - N_{s,tension} - N_{Ed} = 0 \tag{I.16}$$

From which N_{Ed} is the only known force as of yet. N_c, $N_{s,compression}$ & $N_{s,tension}$ are determined:

$$N_c = \frac{1}{2} \cdot h \cdot (x - y) \cdot f_{cd} + h \cdot y \cdot f_{cd} = 37,500 \cdot x + 37,500 \cdot y \tag{I.17}$$

$$N_{s,compression} = A_{s,compression} \cdot \sigma_{s,compression}$$

$$N_{s,tension} = A_{s,tension} \cdot f_{yd}$$

$$N_{Ed} = 36,764 \; [kN]$$

Where:

$$A_{s,compression} = A_{s,tension} = \frac{125 \cdot \frac{1}{4}\pi \cdot 50^2}{2} = 0.122 \; [m^2]$$

Then $N_{s,tension}$ becomes:

$$N_{s,tension} = 0.122 \cdot 10^6 \; [mm^2] \cdot 435 \; [N/mm^2] = 53.1 \cdot 10^6 \; [N] \tag{I.18}$$

To determine N_c and $N_{s,compression}$ the stress diagram from figure I.11 is utilised. With $\epsilon_{s,compression}$ and $\sigma_{s,compression}$ being:

$$\epsilon_{s,compression} = \frac{x-a}{b-a-x} \cdot 2.17 \cdot 10^{-3}$$

Where:

- a = 60 [mm], symbolises the concrete cover
- x = unknown as of yet [mm], the compression height of the concrete
- b = 3,200 [mm], width of the column

And thus:

$$\epsilon_{s,compression} = \frac{x-60}{3,200-60-x} \cdot 2.17 \cdot 10^{-3}$$

Substituting $\epsilon_{s,compression}$ into $\sigma_{s,compression}$ results in:

$$\sigma_{s,compression} = E_s \cdot \epsilon_{s,compression} = \frac{x-60}{3,200-60-x} \cdot 2.17 \cdot 10^{-3} \cdot 2 \cdot 10^{5} = \frac{x-60}{3,140-x} \cdot 435 \; [N/mm^2] \quad (I.19)$$

Additionally, it is given that:

$$\frac{x-y}{b-a-x} = \frac{\epsilon_{c3}}{\epsilon_s} == x-y = \frac{1.75‰}{3.50‰} \cdot (3,140-x) \quad (I.20)$$

This equation contains two unknowns, that both can be substituted into equation I.17. In this calculation the equation, I.20, is substituted with the x as the unknown into equation I.17:

$$y = 1.8 \cdot x - 2532 \; [mm]$$

$$N_c = 37,500 \cdot x + 37,500 \cdot (1.8 \cdot x - 2532) = 105,000 \cdot x - 18.5 \cdot 10^7 \; [N] \quad (I.21)$$

Now all normal forces from equations I.18, I.19, I.21 and N_{Ed} can be substituted into equation I.16:

$$N_c + N_{s,compression} - N_{s,tension} - N_{Ed} = 0$$

$$[105,000 \cdot x - 18.5 \cdot 10^7] + [122 \cdot 10^3 \cdot \frac{x-60}{3140-x} \cdot 435] - [53.1 \cdot 10^6] - [36.8 \cdot 10^6]$$

$$105,000 \cdot x + 5.31 \cdot 10^7 \cdot \frac{x-60}{3140-x} = 1.85 \cdot 10^8 \; [N]$$

Solving this equation results in a value of 1380.5 mm for the concrete compressing zone x, and a negative value of -47.4 mm for y, which is not favourable. Conclusively, the bending moment capacity, $M_{Rd,yield}$, is calculated:

$$M_{Rd,yield} = \frac{1}{2} \cdot h \cdot (x-y) \cdot f_{cd} \cdot [\frac{1}{2} \cdot b - (y + \frac{1}{3} \cdot (x-y))] + h \cdot y \cdot f_{cd} \cdot (\frac{1}{2} \cdot b - \frac{1}{2} \cdot y) + A_{s,compression} \cdot f_{yd} \cdot (\frac{1}{2} \cdot b - a) + A_s \cdot f_{yd} \cdot (\frac{1}{2} \cdot b - a)$$

$$M_{Rd,yield} = \frac{1}{2} \cdot 2,500 \cdot (1,380.5 - (-47.4)) \cdot 30 \cdot [\frac{1}{2} \cdot 3,200 - ((-47.4) + \frac{1}{3} \cdot (1,380.5 - (-47.4)))] +$$

$$2,500 \cdot (-47.4) \cdot 30 \cdot (\frac{1}{2} \cdot 3,200 - \frac{1}{2} \cdot 2,500) + 122,000 \cdot 435 \cdot (\frac{1}{2} \cdot 3,200 - 60) +$$

$$122,000 \cdot 435 \cdot (\frac{1}{2} \cdot 3,200 - 60) = 2.20 \cdot 10^{11}\ [Nmm] = 220,411\ [kNm]$$

This is checked against the acting bending moment:

$$UC = \frac{M_{Ed}}{M_{Rd,yield}} = \frac{370,349}{220,411} = 1.68$$

As can be seen the column is not able to resist the acting bending moment. After several alterations of the dimensions and reinforcement percentage in the column, avoiding a significant larger column, the reinforcement percentage has to be increased to 6% of the concrete area, $A_{steel,total} = 0.48\ m^2$. Repeating the method above yields a bending moment capacity of $M_{Rd,yield} = 384,708$ kNm and UC follows:

$$UC = \frac{370,349}{384,708} = 0.96$$

Which is satisfactory. The same is repeated for column 3 and the results for each respective segment are summarised below.

Shear reinforcement
To determine whether stirrups are needed the concrete shear capacity is checked against the acting shear force. This is done with the following equation:

$$V_{Rd;c} = [C_{Rd,c} \cdot k \cdot (100 \cdot \rho_1 \cdot f_{ck})^{\frac{1}{3}} + k_1 \cdot \sigma_{cp}] \cdot b_w \cdot d$$

With a minimum of:

$$V_{Rd,c} = (v_{min} + k_1 \cdot \sigma_{cp}) \cdot b_w \cdot d$$

Where the following factors are needed:

- $d_{eff} = 3,200 - (c_{nom} + 0.5 \cdot \Phi_{main}) = 3115\ mm$
- $b_w = 2,500\ mm$
- $k = 1 + \sqrt{\frac{200}{d_{eff}}} = 1.253 < 2.0$
- $k_1 = 0.15$, Molenaar and Voorendt (2019, p.217)
- $C_{Rd,c} = 0.12$, Molenaar and Voorendt (2019, p.217)
- $f_{ck} = 45\ N/mm^2$
- $n1 = 1$, reinforcements with good attachment, C.R. Braam (2011, p.98)
- $n2 = 0.82$, reinforcements with diameter larger than 32 mm, C.R. Braam (2011, p.98)
- $f_{bd} = 2.25 \cdot n1 \cdot n2 \cdot f_{ctm} = 2.25 \cdot 1 \cdot 0.82 \cdot 3.8 = 7.01\ [N/mm^2]$
- $l_{b,rqd} = \frac{\Phi_{main}}{4} \cdot \frac{x - c_{nom}}{b - c_{nom} - x} \cdot \frac{f_{yd}}{f_{bd}} = \frac{50}{4} \cdot \frac{1,487-60}{3,200-60-1,487} \cdot \frac{435}{7.01} = 669.5\ [mm]$
- $l_{bd} = MAX(0.6 \cdot l_{b,rqd}; 10 \cdot \Phi_{main}; 100) = MAX(401.4; 500; 100) = 500\ [mm]$
- $A_{sl} = h + MAX(l_{b,rqd}; l_{bd}) = 3170\ [mm]$
- $\rho_1 = \frac{A_{sl}}{b_w \cdot d_{eff}} = \frac{3,170}{2,500 \cdot 3,115} = 4 \cdot 10^{-4}\ [-]$
- $\sigma_{cp} = \frac{N_{Ed}}{A_{c,eff}} = \frac{36,763}{7.52 \cdot 10^6} = 6.19\ [N/mm^2]$
- $v_{min} = 0.035 \cdot k^1.5 \cdot \sqrt{f_{ck}} = 0.035 \cdot 1.253^{1.5} \cdot \sqrt{45} = 0.329\ [N/mm^2]$

This results in capacity of:

$$V_{Rd,c} = [0.12 \cdot 1.253 \cdot (100 \cdot 4 \cdot 10^{-4} \cdot 45)^{1/3} + 0.15 \cdot 6.19] \cdot 2,500 \cdot 3,115 = 8,661\ kN$$

With a minimum of:

$$V_{Rd,c,min} = (0.329 + 0.15 \cdot 6.19) \cdot 2,500 \cdot 3,115 = 9,794\ kN$$

The bearing capacity for shear forces of the concrete column is not sufficient. Therefor, shear reinforcement is needed.

Horizontal shear reinforcement
The shear resistance, V_{Rd}, is determined by two equations, in accordance with Molenaar and Voorendt (2019, p.218), $V_{Rd,s}$&$V_{Rd,max}$ where the minimum value is governing.

$$V_{Rd,s} = n \cdot \frac{A_{sw}}{s} \cdot z \cdot f_{ywd} \cdot \cot(\theta) \tag{I.22}$$

Where:

- $A_{sw} = \frac{1}{2} \cdot \pi \cdot \phi^2_{stirrups}$ is the cross-sectional area of the shear reinforcement
- 'n' = 2 [-] (initially), is the number of stirrups links
- 's' = 32 mm (largest grain in concrete) + 5 mm (work ability factor) = 37 [mm], is the spacing of the stirrups
- $f_{ywd} = 435$ $[N/mm^2]$, is the design yield strength of the shear reinforcement
- $z = 0.9 \cdot d_{c,eff} = 2,804$ $[mm]$
- $\theta = 45°$, is the angle of the pressure diagonal

And $V_{Rd,max}$:

$$V_{Rd,max} = \frac{\alpha_{cw} \cdot b_w \cdot z \cdot v_1 \cdot f_{cd}}{\cot(\theta) + \tan(\theta)} \tag{I.23}$$

Where:

- $v_1 = 0.6 \cdot (1 - \frac{f_{ck}}{250} = 0.492$ $[-]$, is the strength reduction factor for concrete cracked in shear
- $\alpha_{cw} = 1$ $[-]$, for non pre-stressed structures
- $\sigma_{cp} = 6.18$ $[N/mm^2]$, the mean compressive stress
- $\theta = 45°$, is the angle of the pressure diagonal

A single linking, n = 1, stirrup of $\phi 14$ is applied initially. Now equations I.22 and I.23 become:

$$V_{Rd,s} = 2 \cdot \frac{\frac{1}{2} \cdot \pi \cdot 14^2}{s} \cdot 2,804 \cdot 435 \cdot \cot(45) = 20,295\ [kN]$$

$$V_{Rd,max} = \frac{1 \cdot 2,500 \cdot 2,804 \cdot 0.492 \cdot 30}{\cot(1) + \tan(1)} = 51,725\ [kN]$$

In this case the minimum value is that of $V_{Rd,s} = 20,295\ kN$, which is less than the acting shear force and therefor insufficient. Now 4 stirrups links are applied, increasing 'n' from 2 to 4, resulting in a shear force capacity of $V_{Rd,s} = 40,591\ kN$.

$$UC = \frac{V_{Ed}}{V_{Rd,s}} = \frac{36,789}{40,591} = 0.91$$

Which is satisfactory. In short, double linking stirrups of $\phi 14$ mm are needed. A cross-sectional view of the column is visible in figure I.12.

I.9.2 *Dimensions & reinforcement - Column 3*

Column 3 has a smaller length compared to column 2. However, the acting normal force on the column is higher, $N_{Ed} = 46,533$ kN.

- Width (b) = 3.2 [m]
- Height (h) = 2.5 [m]
- Length (l) = 7.5 [m]
- Reinforcement (ρ_{max}) = 3.05 [-]
- Reinforcement surface A_{steel} = 0.236 [m^2]
- Concrete Class C45/55

Seconder order moment

- $\lambda_{min} = 24.48$
- $\lambda = 7.27$

$\lambda < \lambda_{min}$ no seconder order moment calculation needed.

Normal force capacity

$$N_{Rd} = A_{c,eff} \cdot f_{cd} = 240,000[kN]$$

$$UC = \frac{N_{Ed}}{N_{Rd}} = \frac{46,533}{240,000} = 0.19$$

Moment resisting capacity and reinforcement
Due to a higher acting normal force, the concrete compression zone increases to x = 1487 mm. Then the bending moment capacity becomes:

$$M_{Rd,yield} = 388,850[kNm]$$

$$UC = \frac{M_{Ed}}{M_{Rd,yield}} = \frac{370,349}{388,850} = 0.95$$

Which is nearly the same as for column 2. It is therefor safe to assume that the dimensions of the column 2 and reinforcement can be applied to column 3. A cross-sectional view of the columns is visible in figure I.12.

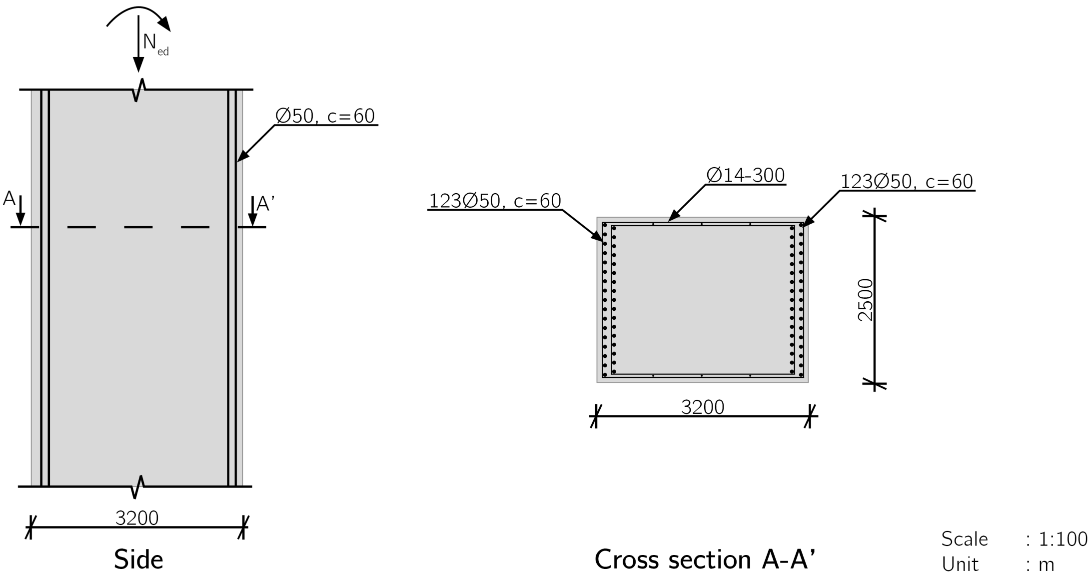

Figure I.12: Side view and cross-sectional view of the column with respective reinforcement bards.

I.10 Foundation Piles

Based on NEN-EN 9997-1 (2017) the total bearing capacity of the piles is computed. Any information about the subsoil has been obtained through a Standard Penetration Test (SPT). To determine the type and the amount of piles required to suspend the superstructure, the SPT data is converted to a Conus Penetration Test value (CPT). This is done accordingly with Jarushi et al. (2015), which gives translating formulas for the different soil types, for now only the linear conversions are used. These formulas are listed below and used to form the CPT values for S4 and S7 in figure I.13.

- Silty fine sand: $q_c = 0.15 * N + 5$
- Fine sand: $q_c = 0.291 * N + 2.43$
- Fine sand with silt: $q_c = 0.15 * N + 7.2$
- Clayey fine sand: $q_c = 0.06 * N + 5.7$
- Silty clayey fine sand: $q_c = 0.22 * N + 2.6$
- q_c in MPa

Initially, a square 300x300mm reinforced concrete prefab piles is chosen. The bearing capacity of a single pile is then calculated according to the Koppejan method, in accordance with Molenaar and Voorendt (2019, p.284-287). Which combines the maximum tip resistance, maximum pile shaft friction and the maximum negative shaft friction of a pile. However, this 300 by 300 mm pile is unsatisfactory as it provided a low bearing capacity, which eventually leads to the need of many foundation piles in order to support the column.

Consequently, a larger square 500x500mm reinforced concrete piles is used. The methodology is repeated to compute the bearing capacity. Ultimately, this pile will breach the upper boundary value for the bearing capacity of 3000 kN, according to figure 38-4 in Molenaar and Voorendt (2019), and can be considered economical not preferred. Therefore, two more iterations are done to find the optimum between depth and profile dimensions. In which a profile of 450x450 mm appeared to be the best option, depth and dimension wise.

Maximum tip resistance
The maximum tip resistance is calculated with the formula below:

$$p_{r;max;tip} = \frac{1}{2} \cdot \alpha \cdot \beta \cdot s \cdot (\frac{q_{c;I;avg} + q_{c;II;avg}}{2} + q_{c;III;avg})$$

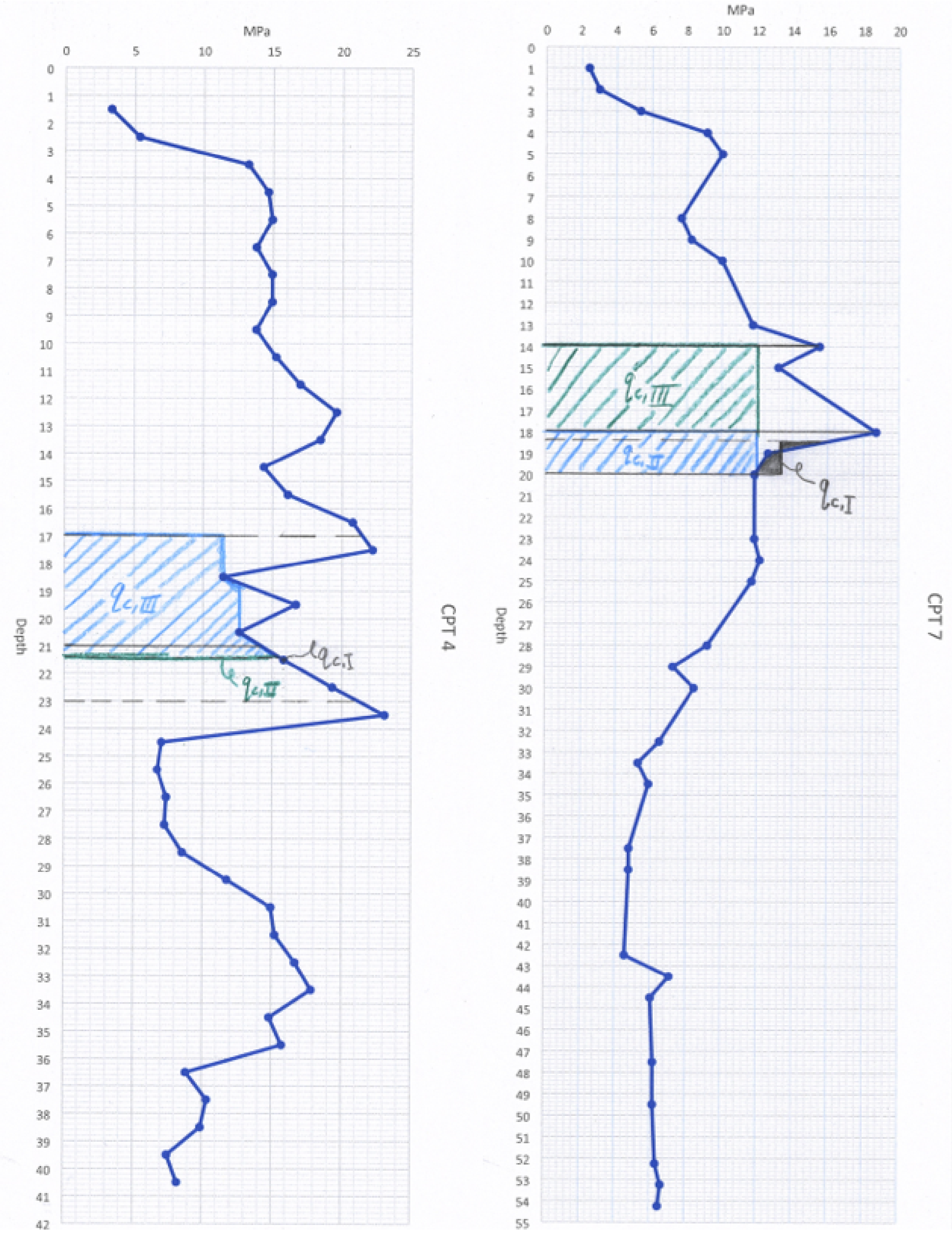

Figure I.13: CPT values for location 4 and 7, utilised to calculated the bearing capacity of the foundation piles.

In which:

- $q_{c;I;avg}$, $q_{c;II;avg}$ and $q_{c;III;avg}$ acquired via Koppejan method on I.13
- $D_{eq} = \sqrt{\frac{4}{\pi}} \cdot a \cdot \sqrt{\frac{b}{a}}$
  - a = 500 mm, width of the pile, shortest side
  - b = 500 mm, width of the pile, longest side
  - This results in a D_{eq} of 0.56 m
- $\alpha_p = 0.7$ for driven piles, according to table 38-1 Molenaar and Voorendt (2019, p.285)
- $\beta = 1.0$ influence factor according to figure 38-5 Molenaar and Voorendt (2019, p.285)
- $s = 1.0$ factor accompanying the shape of the cross-section of the foot, according to figure 38-6 Molenaar and Voorendt (2019, p.285)

For the Koppejan method the soil around the tip can be divided into three sections. These sections named I, II and III are dependent on the D_{eq}.

$$p_{r;max;tip} = \frac{1}{2} \cdot 0.7 \cdot 1.0 \cdot 1.0 \cdot \left(\frac{q_{c;I;avg} + q_{c;II;avg}}{2} + q_{c;III;avg}\right) \tag{I.24}$$

Since the soil in the river is very different throughout the cross-sections, multiple bearing capacities need to be calculated. For the preliminary design column 2 and 3 appeared to be normative. It is important to check whether the piles have the desired bearing capacity for the loads. First the calculation for CPT 4 is performed, followed by the calculation for CPT 7.

At the location of column 2 a pile of 33.5 m deep is assumed. This pile reaches the second layer of sand and minimising the possible setting.

- $q_{c;I;avg}$: The first section starts at depth of $0.7D_{eq}$ (21.4 m) from the base of the pile till $4D_{eq}$ (23 m), so that the lowest value for the average for $q_{c;I;avg}$ can be found. This is at a depth of 21.4 m and gives a value of 15 MPa.
- $q_{c;II;avg}$: The second section starts from the end of section one and up to the base of the pile while maintaining the lowest value in that section. This results in a value of 15 MPa.
- $q_{c;III;avg}$: The third section starts from the base of the pile up to $8D_{eq}$ above, this is at depth of 16.9 m. Using the value of section II when going up in the CPT chart as lowest starting value, a lower value can be found at a depth of 20.6 and 18.5 m, following the CPT results in a value of 11.5 MPa.
- Using the above values and equation I.24 a $p_{r;max;tip}$ of 9.3 MPa is found.

At the location of column 3 the soil consists out of more sand/silt based soil, this can be seen in the resulting CPT, as a lower cone resistance is found. Main difference is that in the CPT 7 a thick sand layer is found at a lower depth. Below this layer no soil layers are found to be sufficiently strong to resist the loads acting on the bridge. The choice is then made to drive a pile to a depth of 18 meters. Using the same methodology as for CPT 4 one can find the characteristic values for the tip resistance.

- $q_{c;I;avg}$: The first section starts at depth of $0.7D_{eq}$ (18.4 m) from the base of the pile till $4D_{eq}$ (20.3 m), so that the lowest value for the average for $q_{c;I;avg}$ can be found. This is at a depth of 20.3 m and gives a value of 13.6 MPa.
- $q_{c;II;avg}$: The second section starts from the end of section one and up to the base of the pile while maintaining the lowest value in that section. This results in a value of 12 MPa.
- $q_{c;III;avg}$: The third section starts from the base of the pile up to $8D_{eq}$ above, this is at a depth of 13.9 m. Using the value of section II when going up in the CPT chart as lowest starting value, since no value is lower than 12 MPa, this is the representative value for section III as well.
- Using the above values and equation I.24 a $p_{r;max;tip}$ of 8.7 MPa is found.

Maximum pile shaft friction
The maximum pile shaft friction can be found using:

$$p_{r;max;shaft;z} = \alpha_s \cdot q_{c;z;a}$$

- α_s = 0.010, for driven smooth prefab concrete piles, according to table 38-2 Molenaar and Voorendt (2019, p.286)
- CPT4: the lowest value for $q_{c;z;a}$ = 12 MPa in the sand layer. This is then used to compute the maximum shaft friction at this location
- CPT7: the lowest value for $q_{c;z;a}$ = 12 MPa in the sand layer. This is then used to compute the maximum shaft friction at this location

This results in the value of $p_{r;max;shaft;z}$ = 0.12 MPa at the location of column 2 and a $p_{r;max;shaft;z}$ of 0.12 MPa at the location of column 3.

Bearing capacity
The design value of driven prefab piles can not be more than 3000 kN. The bearing capacity can be accumulated by summing the tip resistance and shaft friction.

$$F_{r;max} = F_{r;max;tip} + F_{r;max;shaft}$$

Where:

- $F_{r;max;tip} = A_{tip} \cdot p_{r;max;tip}$, maximum tip resistance force
- $F_{r;max;shaft} = O_{p;avg} \cdot \int_0^{\Delta L} p_{r;max;shaft} \cdot dz$, maximum shaft friction force
- $O_{p;avg}$, is the average circumference of the pile shaft

For shaft friction only the friction of the sand layer is accounted for, this gives a less accurate estimation of the total bearing capacity, though the reality is not overestimated in this way. Filling in the tip resistance and shaft friction results in a bearing capacity for the foundation piles at column 2 of:

$$F_{r;max} = 0.45 \cdot 0.45 \cdot 9.3 + (2 \cdot 0.50 + 2 \cdot 0.50) \cdot \int_0^{\Delta L} 0.12 dL = 2958\ kN$$

Using the same equation for the foundation piles at column 3, this results in a bearing capacity $F_{r;max}$ of 2837 kN.

Table I.10: Summary of iterations for CPT4

Depth (m)	Dimensions (mm)	$F_{r;max}$ (kN)
33.5	300x300	1526
33.5	500x500	3022
21	500x500	3460
21	450x450	2958

Table I.11: Summary of iterations for CPT7

Depth	Dimensions (mm)	$F_{r;max}$ (kN)
18	300x300	1526
18	500x500	3370
18	400x400	2348
18	450x450	2837

From tables I.10 and I.11 it can be concluded that when using piles of a dimension of 450x450 mm the same amount of piles is needed. This is a benefit as smaller dimensions are less expensive.